Filtered multicarrier waveforms in the context of 5G : novel algorithms and architecture optimizations

Jérémy Nadal

IMT Atlantique
Bretagne-Pays de la Loire
École Mines-Télécom

UNIVERSITE BRETAGNE LOIRE

THÈSE / IMT Atlantique

sous le sceau de l'Université Bretagne Loire

pour obtenir le grade de

DOCTEUR D'IMT Atlantique

Spécialité : Télécommunications

École Doctorale Mathématiques et STIC

Présentée par

Jérémy Nadal

Préparée dans le département Electronique

Laboratoire Labsticc

Filtered Multicarrier Waveforms in the Context of 5G: Novel Algorithms and Architecture Optimizations

Thèse soutenue le 15 décembre 2017

devant le jury composé de :

Ghaya Rekaya-Ben Othman
Professeur, Télécom ParisTech / présidente

Didier Le Ruyet
Professeur, CNAM – Paris / rapporteur

Christoph Studer
Assistant Professor, Cornell University / rapporteur

Hao Lin
Ingénieur R&D, Orange Labs – Cesson Sévigné / examinateur

Charbel Abdel Nour
Maître de conférences, IMT Atlantique / examinateur

Amer Baghdadi
Professeur, IMT Atlantique / directeur de thèse

Acknowledgements

This PhD thesis would not have been accomplished without the valuable encouragements, availability and patience of my advisors Amer and Charbel. They have both made considerable efforts to help me provide the means to complete my work, beyond what could be expected. I consider myself to be really fortunate to have had the opportunity to work with such talented persons. I take this opportunity to also thank all my colleagues and friends, at the electronic department of IMT Atlantique, for the fruitfull discussions and the excellent working atmosphere.

I would like to express my gratitude for all the members of the jury and particularly my reviewers Prof. Didier Le Ruyet and Prof. Christoph Studer for dedicating part of their valuable time to evaluate my work. I appreciate their insightful remarks and motivating comments.

Finally, I would like to express my appreciation towards all partners within the METIS and FANTASTIC-5G Europeans projects as well as France Brevet. Particularly, I would like to thank Hao Lin, Pierre Siohan and Bruno Jahan from Orange Labs for the enriching cooperation in the METIS and FANSTACTIC-5G projects. All the technical exchanges that we had during exhibition events and project meetings where very fruitful and give me several ideas that considerably contribute to accomplish this work. For this reason, I express my deepest gratitude to you, hoping to be able to work with you again in the near future.

I would like to thank my parents, Christine and Michel and my sister Jessica for their total and unlimited support and for being always there for me. I particularly dedicate this PhD thesis to my late grandfather, which unfortunately couldn't have witnessed the fruit of my labour although he always believed in me.

Finally, I warmly thanks all the people not mentioned above who have supported me, directly or indirectly, during these few years.

Contents

List of Figures

List of Tables

Résumé long

Depuis l'introduction de la 4e génération de réseaux mobiles (4G), la demande en débit augmente significativement chaque année avec l'émergence de nouvelles applications et services. Il est par exemple prédit que dans un future proche, le volume de données à transmettre sera multiplié par 1000, nécessitant des débits 10 à 100 fois plus élevés. Pour des applications de type objets connectés, le nombre d'équipements communicant avec une seule cellule peut atteindre les 300 000. Ces nouvelles tendances poussent la 4G dans ses limites. Ainsi, la 5e génération de réseaux mobiles (5G), actuellement en cours de standardisation, devra apporter des solutions efficaces à ces nouveaux défis. Cette nouvelle génération prévoit d'introduire de nouveaux types de services pour ces applications émergentes, tout en améliorant le service conventionnel de communications mobiles en termes de débit, latence et couverture réseaux.

Pour les applications de type objets connectés, le service de communications massives entre machines (MMC) est introduit. Ce service correspond aux cas où un nombre important de capteurs est déployé et doit accéder à un réseau sans fils. Un des principaux défis de ce service est que les batteries de ces capteurs, disposant de ressources matérielles limitées, doivent avoir une longue durée de vie. D'autres applications émergentes de type usine du future et internet tactile demandent quant à elles des latences très faibles, inférieures à la milliseconde, et une communication très fiable (disponible 99.999% du temps). Le service *Mission Critical Communication* (MCC) est considéré pour ce type d'applications. Dans un contexte de communication entre véhicules, le service *Vehicular-to-Anything* (V2X) est également introduit. De plus, tous ces services doivent coexister dans un environnement radio unique.

Cela introduit alors de nouvelles contraintes, appelant à concevoir de nouvelles briques technologiques de la couche applicative jusqu'à la couche physique. Pour cette dernière, la forme d'onde *Orthogonal Frequency-Division Multiplexing* (OFDM) actuellement utilisée en 4G n'est pas adaptée pour supporter toutes ses exigeantes contraintes. En effet, celle-ci souffre d'une fuite de puissance hors-bande importante qui peut introduire de l'interférence entre différents services. De plus, le bon fonctionnement de l'OFDM nécessite une synchronisation stricte en temps et en fréquence avec la station de base, ce qui introduit une augmentation significative du volume de trafic de la partie signalisation. Par conséquent, la latence et la consommation énergétique sont grandement impactées. Ainsi, de nouvelles formes d'ondes candidates à la 5G ont été proposées, comme :

- Filter-Bank-Multi-Carrier with Offset Quadrature Amplitude Modulation (FBMC/OQAM),
- Universal-Filtered OFDM (UF-OFDM),
- Filtered-OFDM (F-OFDM),
- Zero-Tail OFDM (ZT-OFDM),
- Flexible-Configured OFDM (FC-OFDM),
- Block-Filtered OFDM (BF-OFDM)

Ces formes d'ondes sont des modulations multi-porteuses, et consistent à appliquer un filtrage spécifique à l'OFDM, par exemple en filtrant par sous-porteuse ou par sous-bande. Dans ce travail de thèse, nous avons considéré les modulations FBMC/OQAM et UF-OFDM. Une description technique de ces formes d'ondes est donnée dans la suite de ce résumé.

La forme d'onde FBMC/OQAM

FBMC (Filter-Bank-Multi-Carrier) est un système de transmission multi-porteuses qui introduit un banc de filtres pour permettre d'appliquer sur chaque sous-porteuse individuelle un filtre commun, appelé le filtre prototype (PF). La réponse de ce filtre dans le domaine temporel discret (réponse impulsionnelle), est composée de L échantillons. Le processus de décomposition effectué par le banc de filtres est appelé synthèse, ce qui signifie la construction d'un signal complet résultant du processus de filtrage. Tandis que les sous-porteuses en OFDM portent une forme d'onde fixe en sinus cardinale, le filtrage introduit dans FBMC permet d'avoir un meilleur contrôle sur les lobes secondaires de la forme d'onde, ce qui à son tour permet d'avoir une fuite de puissance hors-bande sous contrôle.

Le signal FBMC n'est pas composé de symboles en blocs successifs et séparés comme pour OFDM. En effet, les symboles FBMC transmis se chevauchent dans le domaine temporel. Chaque symbole FBMC, composé de L échantillons, porte jusqu'à M sous-porteuses filtrées. Le nombre de symboles qui se chevauchent est défini par le facteur de chevauchement K qui correspond au rapport entre la longueur du filtre prototype L et le nombre total de sous-porteuses M ($K = L/M$).

Le processus de reconstruction au niveau du récepteur est appelé analyse, c'est-à-dire la reconstitution du signal complet résultant du processus de filtrage. Une telle structure d'émetteur-récepteur nécessite généralement une complexité d'implémentation plus élevée que celle prévue pour OFDM, liée non seulement aux étapes de filtrage, mais aussi aux modifications appliquées à l'architecture modulateur/démodulateur. Cependant, l'utilisation de structures en *PolyPhase Network* (PPN) et la croissance rapide des capacités de traitement numérique au cours des dernières années ont fait de FBMC une approche réalisable en pratique.

D'après le théorème de Balian-low, les trois propriétés suivantes ne peuvent pas être obtenues en même temps, quel que soit le système de communications considéré :

1. L'orthogonalité dans le domaine des complexes.
2. La localisation en temps et en fréquence (filtrage).
3. L'efficacité spectrale maximale.

Pour OFDM, l'orthogonalité complexe est obtenue en sacrifiant la localisation fréquentielle. Le non-respect de la deuxième propriété ci-dessus attribue à OFDM une fuite de puissance hors-bande élevée. De plus, OFDM sacrifie également son efficacité spectrale (troisième propriété) pour éviter l'interférence entre symboles causé par les canaux multi-trajets, grâce à l'usage d'un préfixe cyclique. Pour rétablir la seconde propriété, les modulations en banc de filtre appliquent un filtrage par sous-porteuse. Par conséquent, l'efficacité spectrale ou l'orthogonalité dans le domaine des complexes doit être abandonnée d'après le théorème de Balian-low.

Ainsi, une variante des modulations en banc de filtres, appelée FBMC/OQAM (pour *Offset-QAM*), a été proposée comme alternative prometteuse à OFDM. Cette dernière permet d'atteindre théoriquement une meilleure efficacité spectrale qu'OFDM (pas de préfixe cyclique), tout en maintenant la propriété d'orthogonalité. L'introduction de la technique OQAM permet de préserver la propriété d'orthogonalité dans le domaine des nombres réels. Cette technique consiste à séparer la partie réelle et imaginaire des symboles QAM, pour obtenir des symboles en *Pulse Amplitude Modulation* (PAM). Ainsi, le nombre de symboles FBMC à transmettre est doublé, car deux fois plus de symboles de données doivent être transmises pour conserver le débit. Par conséquent, le nombre de symboles FBMC qui se chevauchent est également doublé, et $M/2$ échantillons séparent deux symboles FBMC successifs. Le facteur de chevauchement K garde cependant sa définition originale, c'est-à-dire $K = L/M$, même lorsque la technique de l'OQAM est utilisée.

Les symboles PAM doivent être multipliés par un terme de rotation en quadrature de phase avant d'être transmis. Cela permet d'assurer que les symboles PAM tournés situés aux sous-porteuses et symboles FBMC adjacents sont toujours en quadrature de phase. Cette opération est cruciale pour préserver l'orthogonalité. Côté récepteur, la partie réelle du signal démodulé est extraite, et les symboles QAM sont ensuite reconstitués. La partie imaginaire écartée du signal contient uniquement de l'interférence. Elle est généralement appelée interférence intrinsèque.

Grâce à la technique de l'OQAM, FBMC devient maintenant :

1. Orthogonale dans le domaine des réels,
2. Mieux localisée en temps et en fréquence que l'OFDM, grâce au filtrage par sous-porteuse,
3. Permet théoriquement d'atteindre une meilleure efficacité spectrale qu'OFDM puisqu'aucun préfixe cyclique n'est transmis.

En plus de ces avantages, FBMC est plus robuste face aux synchronisations temps/fréquence imparfaites en sélectionnant le filtre prototype approprié. Par conséquent, FBMC/OQAM constitue une technologie prometteuse pour plusieurs services 5G car

elle améliore la robustesse des systèmes de communications à différents types de déficiences. Par exemple, la robustesse de FBMC/OQAM par rapport au décalage/étalement Doppler peut être exploitée afin de prendre en charge le service V2X. De plus, un support efficace de la synchronisation relaxée peut être envisagé avec FBMC/OQAM pour les services MMC, grâce à sa faible fuite de puissance hors bande et sa robustesse contre le décalage temporel.

Cependant, l'introduction de l'OQAM n'est pas sans conséquence. En effet, cela complexifie l'utilisation des techniques d'estimation de canal et de multi-antennes MIMO. De plus, l'absence de préfixe cyclique peut être un problème, plutôt qu'un avantage, si le délai d'étalement du canal multi trajet est long comparé à la durée symbole.

La forme d'onde UF-OFDM

Le principe de la modulation UF-OFDM est de grouper les symboles QAM en plusieurs sous-bandes, chaque sous-bande étant composée de Q sous-porteuses. Ainsi, un maximum de $K = N/Q$ sous-bandes peuvent être utilisées, où N est le nombre total de sous-porteurses. Les lobes secondaires de chaque sous-bande sont atténués en filtrant chaque sous-bande indépendamment via un filtre composé de L échantillons. Ensuite, toutes les sous-bandes filtrées sont sommées, et le symbole UF-OFDM est ainsi formé, composé de $N + L - 1$ échantillons.

Les blocs constituant un émetteur UF-OFDM typique sont les suivants :

- Un *mapper* de sous-bande qui insert les symboles QAM dans les sous-bandes et sous-porteuses allouées,
- Une IFFT de taille N pour chaque sous-bande allouée,
- Un étage de filtrage pour chaque sous-bande, qui utilise une opération de convolution linéaire. Le filtre généralement considéré dans la littérature est le filtre de Dolph-Chebyshev,
- Une opération qui additionne tous les signaux filtrés à l'étape précédente, pour obtenir le symbole UF-OFDM.

Les étapes décrites ci-dessus doivent être répétées pour chaque symbole UF-OFDM à transmettre. Dans la version typique de l'UF-OFDM, les symboles ne se chevauchent pas entre eux, ce qui constitue une première différence fondamentale par rapport à FBMC/OQAM. Ces symboles constituent des blocs d'échantillons indépendants les uns des autres, comme OFDM. Dans ce cas, une légère perte en débit est introduite par la transition de montée et descente en puissance, en début et fin de symbole, à cause de l'opération de filtrage. Généralement, la taille du filtre L est fixée à $L = L_{CP} + 1$ pour obtenir le même débit qu'un système de communication OFDM, où L_{CP} est la taille de son préfixe cyclique.

La deuxième différence fondamentale avec FBMC est le type de filtrage utilisé. Cette dernière utilise un filtrage par sous-porteuses via un PPN, qui s'apparente à un fenêtrage. Dans le cas de l'UF-OFDM, le filtrage est réalisé sur un ensemble de sous-porteuses, via

une convolution linéaire. Une dernière différence importante est que l'UF-OFDM transmet des symboles QAM complexes et garde l'orthogonalité dans le domaine des complexes, alors que la modulation FBMC/OQAM relaxe l'orthogonalité dans le domaine des réels. De ce fait, la majorité des techniques de traitement de signal utilisées par l'OFDM peuvent être facilement adaptées à l'UF-OFDM. A noter que le théorème de Balian-Low présenté est toujours valide pour la modulation UF-OFDM : la localisation temps/fréquence est obtenue en sacrifiant du débit comme précisé dans le paragraphe précédent.

L'implémentation de l'émetteur UF-OFDM a une complexité calculatoire acceptable si le nombre de sous-bandes allouées est faible. Cependant, sa complexité devient prohibitive si plusieurs sous-bandes doivent être traitées. Ainsi, plusieurs implémentations alternatives ont été proposées dans la littérature pour réduire sa complexité.

L'implémentation du récepteur UF-OFDM est différente de son émetteur. En effet, les étapes suivantes pour démoduler un symbole UF-OFDM :

- Isoler les $N + L - 1$ échantillons constituant le symbole UF-OFDM reçu.
- Ajouter $N - L + 1$ zéros à la fin de la séquence isolée. Après cette étape, le signal contient $2N$ échantillons.
- Appliquer une FFT de taille 2N sur les échantillons obtenus à l'étape précédente, pour obtenir le signal dans le domaine fréquentiel.
- Retirer les échantillons aux positions impaires sortant de la FFT. Les échantillons aux positions paires sont gardés, où le lobe principal de chaque sous-porteuse est concentré.

Le signal obtenu en fréquence peut être traité avec les mêmes techniques utilisées dans un récepteur OFDM conventionnel, comme l'égaliseur. Optionnellement, une opération de fenêtrage peut être appliquée sur le signal dans le domaine temporel, avant d'appliquer la FFT à la troisième étape. Cette opération est tout de même recommandée car elle permet d'améliorer les performances du récepteur face aux erreurs de synchronisation en temps.

Comparée à celle du récepteur OFDM, la complexité du récepteur UF-OFDM est augmentée à cause de l'utilisation d'une FFT de taille doublée. Cependant, il est intéressant de noter qu'une large partie des échantillons en entrée de la FFT est nulle, et que la moitié des sorties est éliminée. Ainsi, une large partie des opérations effectuées sont inutiles, et peuvent être évitées : la taille de la FFT peut être divisée par 2, pour retrouver la même taille de FFT utilisée dans un récepteur OFDM. A la place d'insérer des zéros lors de la seconde étape, les $L-1$ derniers échantillons du symbole UF-OFDM sont additionnés aux $L-1$ premiers. Si l'opération de fenêtrage est considérée, elle doit être réalisée avant cette nouvelle étape. Enfin, les N échantillons obtenus sont traités via une FFT de taille N, comme pour OFDM. Ainsi, la complexité du récepteur UF-OFDM est comparable à celle du récepteur OFDM.

Objectifs de la thèse et contributions

Les nouvelles formes d'ondes candidates de la 5G sont des modulations multi-porteuses, et consistent à appliquer un filtrage spécifique à l'OFDM, par exemple en filtrant par sous-porteuses ou par sous-bandes. Ce filtrage permet d'améliorer le confinement spectral et relaxer les contraintes de synchronisations. Cependant, ces formes d'ondes ont également des désavantages et peuvent demander de nouvelles techniques pour améliorer la qualité de la communication. De plus, les techniques de filtrage avancées peuvent être une dizaine de fois plus complexe que l'OFDM. Cela demande donc des optimisations algorithmiques et architecturales pour réduire cette complexité. Finalement, ces formes d'ondes sont évaluées d'un point de vue théorique, mais les résultats ne sont pas toujours validés sur des plateformes matérielles de preuve de concept émulant tous les scénarios de la 5G.

Dans ce contexte, l'objectif de cette thèse est donc de proposer de nouveaux algorithmes et architectures matérielles pour les formes d'ondes FBMC/OQAM et UF-OFDM afin d'améliorer la qualité de la communication radio, de réduire leur complexité calculatoire et de valider les performances de ces formes d'ondes sur plateforme matérielle de preuve de concept pour chaque service prévu en 5G. Plusieurs contributions originales ont été proposées dans le cadre de cette thèse, dans le domaine algorithmique et conception matérielle. Dans le domaine algorithmique, les travaux réalisés durant cette thèse ont mené aux contributions suivantes :

1. Un nouveau filtre prototype court est proposé pour la forme d'onde FBMC/OQAM. Des études analytiques, complétées par simulation, montrent que le filtre proposé permet d'améliorer la résistance aux erreurs de synchronisation temporelle et de réduire la complexité du récepteur FBMC de type *Frequency-Spread* (FS) comparé aux autres filtres de la littérature.
2. Un nouveau type de récepteur FBMC adapté pour les filtres courts est proposé. Ce récepteur a la particularité d'améliorer sensiblement la résistance aux canaux doublement dispersifs pour des filtres courts, et de supporter les communications asynchrones.
3. Un émetteur UF-OFDM original de complexité significativement réduite par rapport à la littérature est proposé. Contrairement aux techniques existantes, l'émetteur proposé n'introduit aucune approximation dans le signal généré, et préserve ainsi le confinement spectral de la forme d'onde.

Dans le domaine de la conception matérielle, les travaux réalisés durant cette thèse ont mené aux contributions suivantes :

1. Une architecture matérielle optimisée des émetteurs FBMC et UF-OFDM de complexité comparable à OFDM.
2. Une architecture matérielle optimisée de l'étage de filtrage du récepteur FBMC avec l'implémentation FS (FS-FBMC), avec une complexité comparable à celle d'un récepteur PPN.
3. Une des premières plateformes matérielles de preuve de concept de la 5G, pouvant évaluer les performances des formes d'ondes pour les différents services de la 5G.

Structure du manuscrit et résumé des chapitres

Le manuscrit de thèse est composé de cinq chapitres, qui sont résumé dans les paragraphes suivants.

Chapitre 1 : La 5G et les formes d'ondes candidates

Ce premier chapitre présente le contexte scientifique de base permettant d'appréhender les contributions présentées dans les chapitres suivants. Dans une première section, les différents services émergeant de la 5G sont présentés plus en détails. En particulier, il est montré que la forme d'onde OFDM n'est pas adaptée pour supporter tous ces services. Ainsi, de nouvelles formes d'ondes ont été investigué dans la littérature, et une description technique de ses candidates est présentée, incluant FBMC/OQAM et UF-OFDM. Une brève introduction aux autres formes d'ondes prometteuses est également présentée. Ce chapitre se termine par une présentation des motivations qui ont conduit à étudier l'utilisation de filtres prototypes courts pour FBMC/OQAM. Particulièrement, les défauts de la forme d'onde FBMC/OQAM sont présentés, et il est montré que les filtres courts peuvent offrir des solutions adéquates pour une majeure partie des problèmes posés.

Chapitre 2 : Nouveau filtre prototype court pour FBMC/OQAM

Le choix du filtre prototype FBMC/OQAM peut significativement impacter les performances et la structure (taille de trame...) du système de communication. Ainsi, concevoir un nouveau filtre prototype est une tâche importante, et c'est pour cette raison qu'un nouveau filtre court est proposé dans ce chapitre. Ce chapitre présente dans une première section les deux types d'implémentations existantes des émetteurs et récepteurs FBMC/OQAM, basées sur les techniques de PPN et de FS. Dans une seconde section, la méthode de conception du filtre prototype est présentée, précédée par une description des filtres existants dans la littérature. Enfin, une dernière section est dédiée à l'analyse des performances et à la comparaison des filtres courts, en considérant différentes métriques. Différents types de perturbation de canal sont considérés, comme les erreurs de synchronisation en temps, en fréquence, et des canaux multi-trajet avec différents étalements de canal. Dans cette section, il est montré que de meilleures performances sont obtenues pour le filtre court proposé comparé aux filtres existants pour tous les types de perturbations considérées, si le récepteur FBMC basé sur le FS est utilisé. Cependant, les performances en taux d'erreur binaire sont dégradées par rapport à l'OFDM pour les modèles de canaux ayant un long étalement de canal. Cela montre la principale faiblesse des filtres courts, traitée dans la chapitre suivant.

Chapitre 3 : Nouveaux récepteurs FBMC/OQAM pour les filtres courts

Les deux chapitres précédents ont montré les avantages à utiliser des filtres courts pour FBMC. Cependant, l'absence de préfixe cyclique est pénalisante, car les canaux ayant une longue durée d'étalement dégradent les performances du récepteur FBMC. De plus,

le support des communications asynchrones est difficilement réalisable avec les récepteurs actuels lorsque des filtres courts sont considérés, contrairement aux filtres longs. Pour résoudre ces problèmes, un nouveau type de récepteur FBMC est présenté dans ce chapitre. L'idée est d'utiliser un égaliseur dans le domaine temporel, basé sur l'algorithme *Overlap-Save* (OS), avant la démodulation FBMC. Une première version de ce récepteur, nommé OS-FBMC, est présentée dans la seconde section de ce chapitre. L'égaliseur OS et le récepteur FBMC typique sont tous les deux fusionnés dans une unique structure, ce qui permet de réduire drastiquement la complexité calculatoire. Ceci est possible grâce à la localisation fréquentielle du filtre prototype. De plus, des techniques supplémentaires sont introduites pour réduire cette complexité. En particulier, une deuxième version du récepteur est proposée, dont le principe est d'appliquer l'OS sur un bloc de symbole FBMC (nommé OSB-FBMC). Ce chapitre se termine par une analyse détaillé de la complexité, de la latence, du débit, et de la résistance aux décalages temporels et aux canaux multi-trajets. Il est montré que l'OS-FBMC améliore significativement les performances sur canal multi-trajet, permettant d'être plus robuste qu'OFDM et autant que les filtres long. De plus, il permet de supporter les communications asynchrones, comme pour les filtres long.

Chapitre 4 : Un nouvel émetteur de faible complexité pour l'UF-OFDM

La forme d'onde UF-OFDM est une autre modulation multi-porteuse prometteuse pour la 5G, car elle combine les avantages de l'OFDM avec un meilleur confinement spectral et une résistance améliorée contre les décalages temps/fréquence. Cependant, son principal défaut réside dans sa complexité calculatoire coté émetteur, qui peut atteindre 200 fois la complexité d'un émetteur OFDM, si aucune simplification n'est appliquée. Des techniques ont été proposées dans la littérature, mais celles-ci reposent sur un compromis entre la complexité et le niveau de dégradation du confinement spectral à cause des erreurs d'approximation du signal généré. Dans ce contexte, un nouvel émetteur UF-OFDM de faible complexe et sans approximation du signal est proposé. Pour des tailles de sous-bande faibles, la complexité devient comparable à OFDM, indépendamment du nombre de sous-bandes alloués. De plus, l'architecture de l'émetteur proposée est flexible et peut être facilement adaptée pour supporter la modulation OFDM. Ce chapitre est organisé comme suit. Une première section présente l'émetteur proposé dans la littérature. L'émetteur UF-OFDM proposé est ensuite détaillé dans une seconde section, et les résultats obtenus en complexité sont finalement présentés dans une troisième et dernière section. Différentes configurations de taille et nombre de sous-bandes sont étudié, pour réaliser une comparaison complète entre les émetteurs UF-OFDM.

Chapitre 5 : Implémentation matérielle et prototypage sur carte

Ce chapitre détaille les contributions apportées dans le domaine de la conception matérielle. Dans un premier temps, une architecture matérielle de l'émetteur UF-OFDM proposée dans le chapitre précédent est détaillée. Les résultats de synthèse sur cible FPGA valident la faible complexité matérielle de cet émetteur. La deuxième section

de ce chapitre présente une architecture de complexité réduite pour l'émetteur FBMC/OQAM. Cette architecture *pipelinée* est basée sur l'algorithme de la IFFT élagué, et permet de n'utiliser qu'une seule IFFT (de taille réduite) au lieu de deux à cause de l'OQAM. Si des filtres courts sont utilisés, les résultats de synthèse montrent que la complexité devient comparable à OFDM. De plus, la consommation énergique est significativement réduite comparé à une architecture typique ou à un émetteur utilisant un filtre long. La troisième section propose une architecture pour l'étage de filtrage du récepteur FS-FBMC. Les résultats de synthèse montrent que la complexité de cet étage est comparable à celle d'un PPN, alors que l'implémentation FS est plus robuste aux erreurs de synchronisations et aux canaux multi-trajets. Dans une quatrième et dernière section, les performances des émetteurs et récepteurs implémentés sont évalués sur une nouvelle plateforme matérielle de preuve de concept pour la 5G, capable d'émuler plusieurs scénarios clefs de la 5G. Cette plateforme constitue un environnement matériel/logiciel complet, utilisant des cartes radio-fréquence et des interfaces pour le contrôle, la communication, et l'affichage des résultats. Les résultats montrent que les avantages théoriques des nouvelles formes d'onde sont également obtenus dans un système matériel réel.

Conclusion et perspectives

Les nouvelles formes d'ondes étudiées présentent d'importants avantages par rapport à l'OFDM, comme une fuite de puissance hors-bande plus faible, et une meilleure résistance aux erreurs de synchronisation. Cependant, l'ajout d'un filtrage a pour inconvénient d'augmenter la complexité calculatoire et matérielle de l'émetteur et du récepteur. Grâce aux nouveaux algorithmes et architectures matérielles proposés dans ce manuscrit, la complexité des émetteurs UF-OFDM et FBMC a été significativement réduite, pour être maintenant comparable à un émetteur OFDM.

L'utilisation de filtre court pour FBMC présente des avantages intéressants par rapport aux filtres longs, comme le support de trames courtes, ou bien leur plus faible complexité calculatoire et matérielle. En revanche, ils sont plus sensibles aux décalages temporels et aux canaux multi-trajets. Ainsi, deux solutions ont été apportées dans cette thèse pour résoudre ces problèmes : concevoir un nouveau filtre court plus robuste contre ces perturbations et proposer un nouveau type de récepteur FBMC. Cette deuxième contribution permet de considérer l'utilisation de communication asynchrone avec des filtres courts. Celà est intéressant pour les services de communications massives entre machines où une faible complexité et consommation énergique est souhaitée pour les émetteurs.

Pour finir, les résultats obtenues via la plateforme matérielle 5G développée durant cette thèse sont conforment aux attentes. Ceci constitue un premier pas pour valider les performances de ces formes d'ondes sur des systèmes réels, avant qu'elles soit déployées à plus grande échelle.

Des pistes d'améliorations peuvent être envisagées pour la suite des travaux de cette thèse. Dans un premier temps, la plateforme matérielle peut être enrichie en intégrant un émulateur de canal réaliste et en implémentant le récepteur OS-FBMC. De plus,

cette plateforme considère des communications avec une seule antenne en émission et réception, alors que les systèmes modernes tendent à utiliser plusieurs antennes pour améliorer le débit et/ou la fiabilité (mécanisme de diversité). Il est cependant important de noter que le support de techniques multi-antennes peut poser problèmes avec FBMC/OQAM, et demande des études plus approfondies. Par exemple, le récepteur OS-FBMC en bloc pourrait être exploité pour supporter des techniques de diversité de type Alamouti. De plus, un nouveau champ de recherche prometteur a vu le jour récemment, et consiste à utiliser un nombre très important d'antenne coté station de base pour servir un grand nombre d'utilisateurs. Ce type de système est majoritairement étudié avec OFDM. Cependant, peu de contributions ont été réalisées avec FBMC, et encore moins avec des filtres courts. Il pourrait donc être intéressant d'étudier les avantages que pourrait apporter FBMC dans ce contexte.

Introduction

Context of the 5G – next generation communication networks and services

Since the introduction of the 4th Generation mobile networks / Long Term Evolution (4G/LTE), the data traffic increases significantly each year and new wireless applications and services are continuously emerging. It is predicted that, in a near future, the wireless traffic will increase exponentially resulting in 1000x higher mobile data volumes and 10-100x higher end-user data rates [1]. In addition, the number of User equipment (UE) will massively increase with up to 300 000 devices needing to communicate with a single Base Station (BS) for Internet-of-things applications. The emergence of new services may also require extremely reliable connections, with an availability of 99.999%. The latency also will become a crucial constraint for emerging applications such as tactile Internet or factory automation. Finally, efficiency in terms of resources utilization, such as energy and radio spectrum, is becoming more and more critical.

These new trends push the 4G/LTE to its limit. It will no longer be able to ensure an efficient traffic in a near future. Therefore, the 5th generation of wireless communication networks, in standardization process nowadays, is foreseen to provide an efficient solution to these trends. It is expected that this new generation will support new emerging services, while extending the support of the conventional Mobile BroadBand (MBB) service of 4G/LTE with improved data rates, capacity, and coverage.

For Internet-of-things applications, Masse Machine Communication (MMC) service is introduced. This new service corresponds to the case where a massive amount of actors and/or sensors are deployed and need to access the wireless network. Contrary to the conventional MBB service, the demand in data rate per device is relatively low. Furthermore, the transmission is sporadic and typically involves relatively small packets per connection. One of the main challenges of MMC service concerns the requirement of long battery life for low power devices with limited hardware resources. Consequently, the energy consumption should be highly reduced, by reducing the signalling overhead and optimizing the hardware implementation.

Other emerging applications require low latency communications with high reliability, such as tactile Internet, factory automation, and vital sign monitoring. In order to support this kind of applications, the Mission Critical Communication (MCC) service is introduced.

Another service foreseen in 5th Generation mobile networks (5G) concerns vehicular-based communications, referred to as Vehicular-to-Anything (V2X) service. It corresponds to communications between two vehicles, referred to as Vehicular-to-Vehicular (V2V), or between a vehicle and the infrastructure, referred to as Vehicular-to-Infrastructure (V2I). Today, also known as Intelligent Transportation Systems [1], V2X consists of use cases where other core services involve nodes with high speeds. In addition to the support of high speeds, the related technical requirements are often combined to those encountered in the other 5G services. For instance, collision avoidance systems may require low latency with high reliability, and can be included in both MCC and V2X services, allowing composite services [1].

All these services must coexist in a unique wireless environment. This introduces new challenges, requiring investigation on new techniques to fulfil network constraints, from the application layer to the physical layer. For the latter, the current Orthogonal Frequency-Division Multiplexing (OFDM) waveform used in 4G/LTE may not be adapted to support all these demanding constraints. In fact, OFDM was an attractive solution in 4G/LTE due to its high robustness against multipath channel thanks to its Cyclic Prefix (CP), its orthogonality in both the time and frequency plane, its straightforward implementation with a Fast Fourier Transform (FFT), and the simple per-subcarrier equalizer. OFDM is also known to efficiently support multiple Multiple-Input Multiple-Ouput (MIMO) schemes [2], such as spatial multiplexing and MIMO diversity scheme employing Alamouti code [3].

However, the high Out-Of-Band Power Leakage (OOBPL) of OFDM compromises the coexistence of multiple services in the same carrier as foreseen in 5G. In addition, it requires strict synchronization with the BS in time and frequency for each user, which adds important signalling overhead. Consequently, the latency and the energy consumption are highly impacted.

In this context, multiple candidate waveforms for 5G have been investigated, such as Filter Bank Multi-Carrier (FBMC)/Offset Quadrature Amplitude Modulation (OQAM), Universal-Filtered Orthogonal Frequency-Division Multiplexing (UF-OFDM), Filtered-Orthogonal Frequency-Division Multiplexing (F-OFDM), Flexible-Configuration Orthogonal Frequency-Division Multiplexing (FC-OFDM), Zero-Tail Orthogonal Frequency-Division Multiplexing (ZT-OFDM), Generalized Frequency Division Multiplexing (GFDM), and Block-Filtered-Orthogonal Frequency-Division Multiplexing (BS). These candidate waveforms are mainly based on multicarrier modulation with specific filtering scheme used on the top of the OFDM basis. The filtering operation is applied in digital domain, before transmitting the baseband discrete signal to the Digital-to-Analog Converter (DAC). This filtering step enables to greatly reduce the OOBPL, increasing the coexistence capability and relaxing the synchronization constraint.

The difference between these waveforms mainly lies in the type of the filtering operation, per subcarrier or per group of subcarriers (subband), and in the orthogonality feature. For example, FBMC/OQAM applies per subcarrier filtering and it preserves the orthogonality in the real field. GFDM also applies per subcarrier filtering, however it is not orthogonal. Both UF-OFDM and F-OFDM propose subband filtering, however the latter is not orthogonal.

Objectives of the thesis

Most of the proposed new waveforms are often studied and analyzed at the algorithmic level considering mainly the quality of the communication link. Although this remains as one of the main performance indicators, the related hardware complexity and energy efficiency are becoming increasingly crucial requirements for future mobile terminals and networks. Therefore, the investigation of low-complexity implementations and the availability of real hardware prototypes are of high interest for performance validation and proof-of-concept of the diverse proposed communication techniques.

In this context, the typical transmitters of 5G candidate waveforms such as FBMC/OQAM and UF-OFDM are considered several times more complex than state-of-the-art OFDM. Particularly, a straightforward implementation of the UF-OFDM transmitter is estimated to be up to 200 times more computationally complex than OFDM [4]. Some recent techniques have been proposed to reduce this computational complexity [4] [5]. However, these techniques still require up to 10 times the complexity of OFDM [4] while calling for an approximated signal implying a penalty in bit error rate and in spectral confinement. Concerning FBMC, the use of the OQAM scheme requires to duplicate the processing units (or to double the processing rate) when compared to OFDM. In addition, the filtering stage may introduce a non-negligible complexity increase. Therefore, it is of high interest to investigate novel algorithms and hardware optimizations in order to reduce the complexity and the energy consumption of these waveforms.

While FBMC offers several interesting advantages with respect to OFDM, it has few important issues that need to be addressed. For instance, the filtering operation introduces a ramp-up and ramp-down transitions at the beginning and the end of each transmitted frame. To avoid significant spectral efficiency loss, the frame duration must be increased. However, 5G aims to use short frame sizes for several communication scenarios in order to reduce the latency. In addition, certain techniques designed for OFDM are not directly applicable to FBMC due to the OQAM scheme. Among these techniques, there are the pilot structure for channel estimation, the FFT-spread to reduce Peak-to-Average Power Ratio (PAPR), and the compatibility with MIMO Alamouti scheme [3]. Finding appropriate solutions to these technical issues is crucial if FBMC is adopted for certain services in future communication systems. It is worth noting in this regard that UF-OFDM is compliant with most of the techniques designed for OFDM, which can be re-used with minimal adaptations.

In this context, the objectives of this thesis work can be summarized in the following points:

- Algorithms analysis and simplification for FBMC and UF-OFDM waveforms from an implementation perspective towards low complexity and efficient transceiver design.
- Hardware architecture exploration for the devised low-complexity algorithms. The target objective is to propose a hardware implementation comparable in complexity to OFDM.

- Implementation and integration of the proposed transceiver architectures in a real hardware platform with RF interface. This platform should serve as a proof-of-concept with realistic conditions for the proposed hardware architectures. It should also illustrate the waveform performance in relevant 5G scenarios.

Thesis contributions

Towards these objectives, several original contributions have been proposed in the framework of this PhD thesis. These contributions, related to both algorithmic domain and hardware design domain, are summarized below.

Contributions in algorithmic domain

- A novel short Prototype Filter (PF) for FBMC allowing for near perfect reconstruction and having the same size as one OFDM symbol is proposed. Using Frequency Spread (FS) implementation for the FBMC receiver, analytical analysis and simulation results show that the proposed filter exhibits better robustness to several types of channel impairments when compared to state-of-the-art short PFs and OFDM modulation.
- A novel FBMC receiver technique suitable for short filters is proposed. It is based on the idea proposed in [6] where a time-domain equalizer based on a Overlap-Save (OS) algorithm (for fast convolution operation) is employed before the FBMC demodulation. We show that both the time-domain equalizer and the FBMC receiver can be merged in a unique structure due to the frequency localization of the filter, enabling to greatly reduce the computational complexity. An alternative OS-FBMC scheme is derived, where FBMC symbols are transmitted by block and demodulated all at once in the frequency domain, which further reduces the complexity.
- A novel low-complexity UF-OFDM transmitter without any signal quality loss is proposed. For small subband sizes, the complexity becomes comparable to OFDM regardless of the number of allocated subbands. Furthermore, the proposed transmitter architecture is flexible and can be easily adapted to support OFDM modulation.

Contributions in hardware design domain

- An efficient pipelined hardware architecture of the FBMC/OQAM transmitter capable of supporting several filter lengths and targeting low complexity is proposed and compared to typical FBMC/OQAM and OFDM implementations.
- FS-based hardware architecture of the filtering stage is proposed for the designed short PF, showing lower complexity than the classical PolyPhase Network (PPN)-based implementation.
- One of the first flexible and efficient hardware platforms for 5G waveform design and proof-of-concept is proposed. This platform allows the support of several

communication scenarios as foreseen in 5G. The proposed platform constitutes a complete hardware/software development environment, with digital processing, radio frequency boards, and all associated interfaces for control, communication, and results display.

Manuscript Organization

This manuscript is divided into five chapters. In the first Chapter, the emerging services foreseen in 5G are presented in more details. It is shown that OFDM is not adapted to support all these services. Therefore, new candidate waveforms has been investigated, and a technical description of some of these candidates, including FBMC/OQAM and UF-OFDM, are presented in the next section. This chapter end by presenting the motivation for investigating FBMC/OQAM with short PFs. Particularly, the several issues of FBMC/OQAM are presented, and it is shown that short PFs can offers an appropriate solution for FBMC/OQAM.

Based on this motivation, a novel short PF is presented in Chapter 2. The chapter starts by presenting the existing two implementations in the literature for FBMC/OQAM transceivers, PPN and FS based implementations. Then, the proposed novel short prototype filter is presented together with relevant state-of-the-art filters for FBMC/OQAM. Finally, several performance metrics are evaluated and compared to illustrate the benefits of the proposed contribution. In this regard, several channel impairments are considered such as timing offset, frequency offset, and multipath channel conditions. It is shown that, when using a FS-FBMC receiver, the proposed PF outperforms the existing short PFs for all the above considered impairments. However, when compared to OFDM, performance degradation is observed with channel models having long delay spread. This highlights the main weakness of FBMC with short PFs.

Therefore, an original FBMC receiver technique that addresses this issue is presented in Chapter 3. In addition, the proposed receiver further improves the robustness of FBMC with short PFs against timing offset, enabling the support of asynchronous communications. The main idea is to employ a time-domain equalizer based on an OS algorithm before the FBMC demodulation. A first version of this receiver, referred to as OS-FBMC, is presented after a short review of existing FBMC/OQAM equalization techniques. Both the time-domain equalizer and the FBMC receiver are merged in a unique structure due to the frequency localization of the PF, enabling to greatly reduce the computational complexity. Then, several additional complexity reduction techniques are devised and another block-based receiver is proposed, referred to as Overlap-Save-Block (OSB)-FBMC. In this receiver, FBMC symbols are transmitted in blocks and demodulated all at once in the frequency domain, which further reduces the complexity. The chapter ends by in-depth analysis of the complexity, latency, data rate, and robustness against timing offset and multipath channel impairments of the proposed FBMC receivers. Performance results are compared with OFDM and with a FBMC/OQAM system using a reference long PF.

Chapter 4 focuses on the second considered waveform of this PhD work: the UF-

OFDM waveform. The first section of this chapter presents a review on existing recent UF-OFDM transmitter implementations. The high complexity of these techniques is highlighted. The need to explore low complexity techniques without degrading the signal quality leads us to propose a novel UF-OFDM transmitter. The idea and the architecture of this transmitter are detailed. It is also shown that the proposed UF-OFDM transmitter can be easily adapted to support OFDM transmission. Analytical complexity comparison is provided for several configurations, corresponding to the extreme cases where a user occupies all the available bandwidth to achieve high date rates.

Chapter 5 is dedicated to the presentation of the contributions related to hardware design domain. The chapter starts by presenting the hardware architectures of OFDM and UF-OFDM transceivers. Then, the hardware architectures of the proposed FBMC/OQAM transceivers are presented. In this regard, a novel pipelined FBMC transmitter with reduced complexity is detailed. Finally, the chapter ends by describing the proposed proof-of-concept hardware platform. The performance of UF-OFDM and FBMC/OQAM waveforms are presented for the MMC, MCC, and V2X related scenarios. The results in these scenarios are also compared to OFDM.

The manuscript ends by summarizing the main PhD contributions and the proposal of new work perspectives.

Patents, publications, and demonstrations:

The results of this thesis work have been disseminated in patents, journal/conference publications, and demonstration events. Four patents have been filled, and others are planned. Two journal papers have been published in IEEE Trans. on Circuits and Systems II and IEEE Trans. on Vehicular Technology. One journal paper submitted to IEEE Access. Three international conference papers was published and one submitted to ICC'2018, in addition to one presentation in a national workshop. The integration of the proposed technical contributions in a proof-of-concept hardware platform have been presented in 9 exhibition events, including Mobile World Congress 2015.
Finally, during this PhD work I have actively participated in two European research projects, METIS and FANTASTIC-5G. I have participated in several technical meetings and contributed to several internal reports and deliverables.

Patents

P1. Patent on the proposed design of short filter for FBMC.

P2. Patent on the half frequency shift technique for FBMC.

P3. Patent on the proposed Overlap-Save FBMC receiver.

P4. Patent on the proposed technique for reducing the complexity of the UF-OFDM transmitter.

Journal papers

J1. J. Nadal, C. Nour, and A. Baghdadi, "Low-complexity pipelined architecture for FBMC/OQAM transmitter," in *IEEE Transactions on Circuits and Systems II: Express Briefs*, vol. 63, no. 1, pp. 19-23, Jan. 2016.

J2. J. Nadal, C. Abdel Nour, and A. Baghdadi, "Novel UF-OFDM transmitter: significant complexity reduction without signal approximation," in *IEEE Transactions on Vehicular Technology*, vol. 67, no. 3, pp. 2141–2154, 2017.

J3. J. Nadal, C. Abdel Nour, and A. Baghdadi, "Design and Evaluation of a Novel Short Prototype Filter for FBMC/OQAM Modulation," in *IEEE Access*, vol. 6, pp. 19610–19625, 2018.

Conference papers

C1. J. Nadal, C. Abdel Nour, A. Baghdadi, and H. Lin, "Hardware prototyping of FBMC/OQAM baseband for 5G mobile communication systems," in *IEEE Int. Symp. Rapid Syst. Prototyping (RSP)*, Delhi, India, Oct. 2014, pp. 135–141.

C2. J. Nadal, C. Abdel Nour, A. Baghdadi, and H. Lin, "FBMC/OQAM baseband for 5G mobile communication systems: hardware design and on-board prototyping," in *GDR ISIS workshop 2014 – 5G & Beyond: Promises and Challenges*, Paris, France, Oct. 2014.

C3. S. Medjkouh, J. Nadal, C. Abdel Nour, and A. Baghdadi, "Reduced complexity FPGA implementation for UF-OFDM frequency domain transmitter," in *IEEE Workshop on Signal Processing Systems (SiPS)*, Lorient, France, Sep. 2017.

C4. J. Nadal, C. Abdel Nour, and A. Baghdadi, "Flexible hardware platform for demonstrating new 5G waveform candidates," in *29th IEEE International Conference on Microelectronics (ICM)*, Beirut, Lebanon, Dec. 2017.

C5. J. Nadal, F. Leduc-Primeau, C. Abdel Nour, and A. Baghdadi, "A block FBMC receiver designed for short filters," in *IEEE International Conference on Communications (ICC)*, Kansas City, MO, USA, May 2018.

Demonstrations

D1. J. Nadal, C. Abdel Nour, A. Baghdadi, and H. Lin, "FBMC/OQAM-related new waveform," METIS exhibition stand at the *European Conference on Networks and Communications (EuCNC)*, Bologna, Italy, 2014.

D2. J. Nadal, C. Abdel Nour, A. Baghdadi, L. Hao, B. Jahan, and P. Siohan, "Flexible FBMC air interface for 5G," EU 5G Research/5G-PPP METIS exhibition stand at *Mobile World Congress (MWG)*, Barcelona, Spain, 2015.

D3. J. Nadal, C. Abdel Nour, A. Baghdadi, L. Hao, B. Jahan, and P. Siohan, "New candidate waveform for 5G," Exhibition stand at *Orange Labs Research Fair* , Paris, France, 2015.

D4. J. Nadal, C. Abdel Nour, A. Baghdadi, L. Hao, B. Jahan, and P. Siohan, "Flexible FBMC air interface for 5G," Exhibition stand at the *3rd International MiWEBA workshop – Green 5G networks*, Rennes, France, 2015.

D5. J. Nadal, C. Abdel Nour, and A. Baghdadi, "Enabling 5G new services – Post-OFDM waveforms," Exhibition stand at the *European Researchers night*, Brest, France, 2016.

D6. J. Nadal, C. Abdel Nour, and A. Baghdadi, "Flexible PoC for Post-OFDM waveforms," FANTASTIC-5G exhibition stand at the *2nd Global 5G Event*, Rome, Italy, 2016.

D7. J. Nadal, C. Abdel Nour, and A. Baghdadi, "Flexible PoC platform for post-OFDM waveforms," Exhibition stand at the *IEEE International Symposium on Turbo Codes & Iterative Information Processing (ISTC)*, Brest, France, 2016.

D8. J. Nadal, C. Abdel Nour, and A. Baghdadi, "Proof-of-concept for post-OFDM waveforms as candidates for 5G," Exhibition stand at the *IEEE International Workshop on Signal Processing Systems (SiPS)*, Lorient, France, 2017.

D9. J. Nadal, C. Abdel Nour, and A. Baghdadi, "Hardware demonstration of post-OFDM waveforms," FANTASTIC-5G exhibition stand at the *European Conference on Networks and Communications (EuCNC)*, Oulu, Finland, 2017.

CHAPTER

1 5G and post-OFDM waveform candidates

5th generation mobile communication standard is foreseen to cope with a high degree of heterogeneity in terms of services: mobile broadband, massive machine and mission critical communications, broad-/multicast services and vehicular communications. Consequently, diverse and often contradicting key performance indicators need to be supported, such as high capacity/user-rates, low latency, high reliability, ubiquitous coverage, high mobility, massive number of devices, low cost/energy consumption. 4G is not designed to meet such a high degree of heterogeneity efficiently. Moreover, having multiple radio access technologies for multi-service support below 6 GHz will be too costly.

Waveform design is considered as one of the key technology components in this regard. OFDM waveform, adopted in 4G, exhibits several limitations in terms of spectrum usage and robustness to frequency and timing synchronization errors. In order to overcome these limitations and to cope with the new 5G requirements, several research initiatives have been conducted to design new waveforms. Proposed candidates, referred to as post-OFDM waveforms, are mainly based on multicarrier modulation with specific filtering scheme used on the top of the OFDM basis.

This chapter provides the basic scientific background related to the presented PhD contributions in subsequent chapters. It starts by a brief background on OFDM as used in the conventional mobile broadband service in 4G. Then, the specific requirements of massive machine communications, mission critical communications, and vehicular-to-anything communications scenarios foreseen in 5G are introduced. In this context, the limitations of the OFDM modulation are highlighted. This introduction is followed then by a technical description of FBMC/OQAM and UF-OFDM; the two main waveforms addressed in this thesis work. A brief introduction to few other promising candidate waveforms is also provided. Finally, the chapter ends by motivating the use of short prototype filters for FBMC/OQAM waveform.

1.1 OFDM and considered 5G scenarios

Three main 5G communication scenarios have been considered in the framework of this thesis: (1) massive machine communications, (2) mission critical communications, and (3) vehicular-to-anything communications. This section provides a brief description of these scenarios, together with a background on OFDM as used in the conventional mobile broadband service in 4G.

1.1.1 Mobile broadband service and OFDM in 4G

MBB communications scenario refers to the traditional mobile Internet access service. It became available for the first time in 1991 as part of the 2nd Generation mobile networks (2G). Higher speeds have then been specified in 2001 and 2006 as part of the third (3G) and fourth (4G) generations. In 5G, this scenario is referred to as enhanced Mobile BroadBand (eMBB). It extends the support of conventional MBB through improved data rates, capacity, and coverage. Typical use cases are multimedia streaming, voice-over-IP, internet browsing, videoconferencing, file downloads, etc.

OFDM, with data transmitted on a large number of parallel narrow-band subcarriers, is the core of the 4G/LTE downlink radio transmission. Due to the use of relatively narrowband subcarriers in combination with a cyclic prefix, OFDM transmission is inherently robust to time dispersion on the radio channel without a requirement to resort to advanced and potentially complex receiver-side channel equalization. For the uplink, where the available transmission power is significantly lower than for the downlink, single-carrier transmission, based on Discrete Fourier transform (DFT)-precoded OFDM, referred to as Single-Carrier Orthogonal Frequency-Division Multiplexing (SC-OFDM), is used. SC-FDMA has a smaller peak-to-average power ratio than regular OFDM, thus enabling less complex and/or higher-power terminals.

OFDM modulation: Originally proposed by Weinstein and Ebert in 1971 [7], OFDM has been widely used in wireless communication systems [2], such as Digital Video Broadcasting - Terrestrial standard and IEEE 802.11 standard (Wi-fi), in addition to 4G/LTE standard. OFDM is a multi-carrier modulation that divides the available bandwidth into multiple elementary narrow-band signals, called subcarriers.

These subcarriers are modulated by complex valued symbols issued from a conventional digital modulation scheme (such as Quadrature Amplitude Modulation (QAM)), carrying the data to transmit. In frequency domain, each transmitted subcarrier results in a cardinal sine function spectrum with side lobes that produce overlapping spectra between subcarriers The subcarriers are equally spaced in frequency domain, so that the individual peaks of subcarriers all line up with the nulls of the other subcarriers as illustrated in Figure 1.1, where subcarrier frequency spacing is denoted by ΔF. The resulting orthogonality allows to receive the symbols without interference in both time and frequency.

The implementation of the OFDM transmitter is based on an Inverse Fast Fourier Transform (IFFT) of size N [8], where N is the total number of subcarriers which can be transmitted. From these N subcarriers, a subset are selected to carry N_C QAM symbols

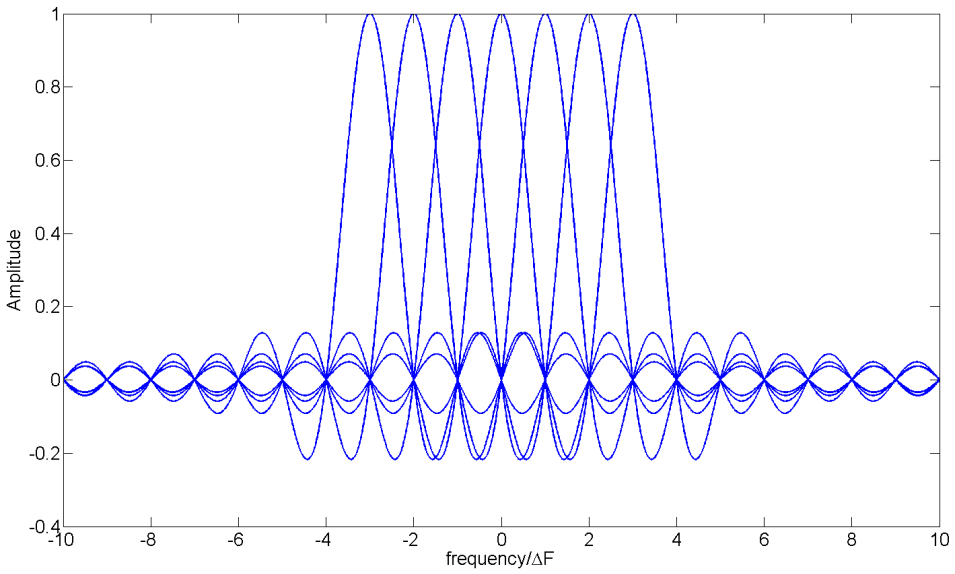

Figure 1.1 — OFDM: cardinal sine function spectrum and orthogonal subcarriers.

to transmit. These latter are the allocated subcarriers. The input indexes of the IFFT are directly related to the subcarrier indexes. The N_C QAM symbols are therefore feed to the corresponding input of the IFFT, while the remaining ones at set to zero. At the output of the IFFT, a time domain signal composed of N samples is obtained. Lastly, a CP of length L_{CP} is inserted [9] before the first samples, by copying the last L_{CP} samples of the obtained time domain signal. The time domain signal is therefore composed of $L_{CP} + N$ samples, corresponding to the OFDM symbol. These steps are repeated for each OFDM symbol to transmit.

Each sample composing the OFDM symbol is transmitted at the frequency sampling F_s. Therefore, the time duration of one OFDM symbol is $T = (N + L_{CP})/F_s$ seconds, assuming that F_s is expressed in Hz. The subcarrier frequency spacing is equal to $\Delta F = N/F_s$ Hz. If N_C subcarriers are transmitted, the used bandwidth is therefore $N_C \Delta F$ Hz. The 4G/LTE set of parameters are presented in Table 1.1 for all available bandwidth configurations [10]. The subcarrier spacing is always equal to $\Delta F = 15$ kHz. Similarly, the OFDM symbol duration is always equal to ≈ 71.35 μs. The minimum resource size which can be allocated for a user in 4G/LTE is one Resource Block (RB). It corresponds to the transmission of 7 OFDM symbols, each carrying 12 subcarriers, for a duration of 0.5 ms and a bandwidth of 180 kHz. It is worth noting that, the CP of the first OFDM symbol in a RB is slightly increased to obtain this exact duration of 0.5 ms.

From Table 1.1, the effective bandwidth is calculated using the expression $N_C \Delta F = 12 N_{\mathrm{RB}} \Delta F$, where N_{RB} being the number of allocated RB. In fact, the bandwidth configuration only indicates the OFDM parameters which must be chosen for the transmission into the available bandwidth. In 4G/LTE, the effective bandwidth obtained is always less that the available bandwidth, since a guard-band is introduced to limit the out-of-band radiation. This guard-band represents 10% of the available bandwidth for a configuration with a bandwidth larger than 2.5 MHz. For instance, if the 5 MHz bandwidth configuration is considered, a maximum of 25 RBs are allocated (i.e. 300 subcarriers). Since

Table 1.1 — 4G/LTE set of parameters for all available configurations.

Bandwidth configuration (MHz)	1.25	2.5	5.0	10.0	15.0	20.0
Frequency sampling (MHz)	1.92	3.84	7.68	15.36	23.04	30.72
IFFT size M	128	256	512	1024	1536	2048
Number of available RB	6	12	25	50	75	100
CP length L_{CP}	9	18	36	72	108	144
Effective bandwidth (MHz)	1.08	2.16	4.5	9.0	13.5	18.0

subcarriers are spaced by 15 kHz, the effective bandwidth is 4.5 MHz.

When the OFDM symbol is generated, the obtained baseband signal is fed to the Radio Frequency (RF) interface, comprising the following components:

- DAC, to convert the digital baseband signal to the analog domain.
- Analog filter, to reduce the OOBPL.
- High Power Amplifier (HPA), to amplify the power of the signal.
- Frequency mixer, to shift the baseband signal to the desired carrier frequency.
- Antenna, to convert the electrical signal into radio waves.

The radio signals then propagate though the channel. The ideal channel propagation corresponds to the line-of-sight, where the radio signal directly travels from the transmitter antenna to the receiver antenna. However, the channel environment is more complex in practice, and particularly for wireless communications where the signal is reflected or diffracted by several obstacles such as buildings, trees, and vehicles. Due to this effect, multiple paths are created. Each path has its own propagation delay, amplitude, and phase distortion. At the receiver antenna, the received signal r at time instant t, denoted by $r(t)$, corresponds to the summation of the signals carried by each path:

$$r(t) = \int_0^{\tau_{DS}} h(\tau)s(t-\tau)d\tau, \tag{1.1}$$

where s is the transmitted OFDM signal, h is the channel impulse response, τ_{DS} is the difference between the arrival time of the earliest and the latest significant multipath component, referred to as delay spread. After the RF interface, the sample number k of the signal r, denoted by $r(k)$, can be expressed in discrete domain as follows:

$$r(k) = \sum_{l=0}^{L_{DS}-1} h(lT_s)s((k-l)T_s) + w(k), \tag{1.2}$$

where $T_s = 1/F_s$ is the sampling period and L_{DS} is the duration (in number of samples) of the delay spread. To simplify the notation, we consider T_s as implicit in the related expressions. Due to the imperfection of the electronic components and the RF residual interferences, a noise term w is added. The multipath channel can introduce Inter-Symbol Interference (ISI), since the last samples from an OFDM symbol are delayed and summed to the first samples of the next OFDM symbol. However, the CP acts as a guard-interval and ISI is avoided if the delay spread of the channel is shorter than the CP duration. This point is obviously considered in the design of the CP duration. Furthermore, the CP eases

the equalization, i.e. the processing technique which reverses the distortion introduced by the channel. In fact, the received OFDM symbol is demodulated by applying the dual operation of the transmitter: removing the CP and applying a FFT of size N. At the FFT input, the linear convolution introduced by the channel is equivalent to a circular convolution due to the CP. Recalling the following property of the FFT:

$$\mathrm{FFT}(s \circledast h) = \mathrm{FFT}(s)\mathrm{FFT}(h) \tag{1.3}$$

where $\circledast$ is the circular convolution operator. Therefore, the received frequency domain signal Y, after FFT, at the subcarrier index k can be expressed as follows:

$$Y(m) = H(m)X(m) + W(m), \tag{1.4}$$

where H is the frequency response of the channel, X is the transmitted QAM symbols, and W is the noise term. Then, the estimated QAM symbols $\hat{X}(k)$ are obtained by using a simple per-subcarrier equalizer on the received frequency domain signal Y. This yields the following:

$$\hat{X}(m) = C(m)Y(m), \tag{1.5}$$

where $C(m)$ is the equalizer coefficient at the subcarrier index m. We have $C(m) = 1/H(m)$ if the Zero-Forcing (ZF) equalizer is used. Alternatively, Minimum Mean Square Error (MMSE) equalizer coefficients can be considered to minimize the square mean of the error introduced by the noise. In this case, we have:

$$C(m) = \frac{H^*(m)}{||H(m)||^2 + \eta}, \tag{1.6}$$

where $||H(m)||^2 = H(m)H^*(m)$ is the absolute value of H and η is the inverse of the Signal-to-Noise Ratio (SNR) when additive white Gaussian noise is considered. However, the computation of the MMSE equalizer coefficients requires to first estimate the SNR, which adds complexity and which is subject to approximation errors that may limit its performance.

The orthogonality in both time and frequency planes, its high robustness against multipath channel conditions, its straightforward implementation using FFT, and the per-subcarrier equalizer are key features that make OFDM an attractive solution for eMBB scenario. This is in addition to the efficient support of multiple MIMO schemes [2], such as spatial multiplexing and MIMO diversity scheme employing Alamouti code [3]. However, considering the multiple new services and requirements foreseen in 5G a question arises: *is OFDM capable to face all the challenges brought by the 5G?*

1.1.2 Massive machine communications

Massive machine communications can be considered as one part of Machine Type Communications (MTC) [11]. The respective 3rd Generation Partnership Project (3GPP) term is massive MTC (mMTC). This scenario corresponds to the case where a massive amount of actors and/or sensors are deployed anywhere in the landscape and that need to access the wireless network. Today, this is also known as Internet-of-Things (IoT).

Typical use cases are smart metering, natural ecosystem monitoring, remote maintenance/control, flock/fleet tracking/tracing, remote diagnostics etc. A common assumption is that the communication in MMC is mostly unidirectional: uplink is the dominant communication [12] [13]. Furthermore, the transmission is sporadic and typically involves relatively small packets per connection. Consequently, the required data rate is typically low, with around 1 kb/s to 10 kb/s for each device. On the other hand, the user density is much higher than what is generally assumed for MBB services. In this regard, it is estimated that up to 300000 devices must be able to communicate inside a single cell [12]. Such user density is clearly not supported in the current 4G/LTE systems. Finally, one of the most important aspects of MMC is that the sensors have generally limited available hardware resources and should operate for long battery life. Therefore, the complexity and the energy consumption related to the hardware implementation of the modulation techniques must be kept as low as possible.

In order to reduce the energy-consumption in this scenario which implies a huge number of devices, the signalling overhead introduced by the synchronization procedure must be minimized. Therefore, the ideal transmission scheme for MMC should be as follows:

1. the sensor/UE wakes-up from sleep mode,
2. it transmits the data to the BS,
3. it returns again in sleep mode.

This is in practice difficult to achieve since it requires the support of asynchronous communications. In this case, there is no prior synchronization with the BS. From the physical layer point of view, this means that the relative delays between the received user signals are random and can be higher than the symbol duration. As the OFDM modulation assumes strict orthogonality between users, such scenario of communications cannot be supported by OFDM. An alternative solution is to synchronize each sensor in time with the BS. This time synchronization can be obtained, for instance, through the downlink reference signals transmitted by the BS [14]. However, since the users are localized at different distances from the BS, each one can have different propagation delay. Therefore, at the BS, the received signals sharing the same time base overlap. Consequently, a time misalignment is created which may introduce undesirable interference across all users.

An example is illustrated in Figure 1.2. Two devices, identified as UE1 and UE2, transmit an OFDM signal through their corresponding channel respectively having a propagation delay of τ_1 and τ_2. Thanks to the use of a CP, the received data of each device can be perfectly recovered if the timing offset between devices $\Delta\tau$ is lower than the CP duration T_{CP}, i.e. when $T_{CP} < |\tau_1 - \tau_2|$. This requires to apply a circular shift operation on the OFDM symbol for each device. Such operation is efficiently implemented after the FFT, in frequency domain, thanks to a simple linear phase rotation operation. However, if $\Delta\tau > T_{CP}$ then for some devices the receiver processing window at the BS will not be aligned with the OFDM symbol (including CP) to demodulate. Part of the next (or previous) OFDM symbol is therefore included in the processing window.

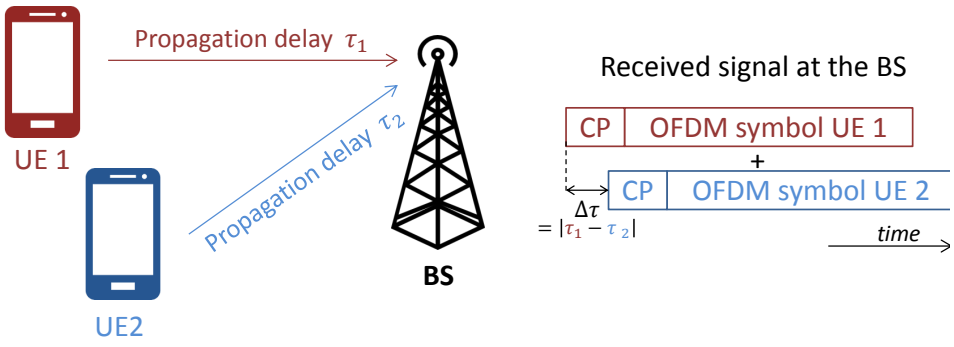

Figure 1.2 — Example of a wireless environment involving MMC service.

Therefore, the devices having a timing offset higher than the CP duration suffer from severe performance loss. In addition, the orthogonality is lost with the devices occupying the adjacent subcarriers, introducing Inter-User Interference (IUI) even if these devices are perfectly synchronized.

In 4G/LTE, this issue is resolved by using the Timing Advance (TA) mechanism [14]. The BS estimates the relative propagation delay of each device and transmits this information back to the corresponding device. Then, at the next uplink transmission, each device applies a delay such that all the signals received by the BS are correctly aligned in time. Since a feedback transmission is employed, this corresponds to a closed-loop synchronization technique.

The major issue of this TA mechanism is related to the corresponding high signalling overhead. Particularity, if the device is moving, the TA value must be refreshed. Therefore, the TA value must be periodically re-transmitted using the downlink channel, leading to significant increase in power consumption. Furthermore, the uplink transmission being pre-dominant for MMC, it is unreasonable to reserve radio resources in downlink for only transmitting the TA. Therefore, the synchronization procedure must be relaxed for MMC. For this reason, open-loop synchronization is considered where each device is synchronized in time with the base station, but no feedback information is transmitted to the device. Consequently, the relative timing offset between devices must be mitigated directly at the base station.

A straightforward solution for OFDM could be to increase the CP duration so that $\Delta\tau$ is always greater than the CP duration for any distance within the power range of the BS. However, the data rate and the energy efficiency are reduced since the transmission of the CP signal costs additional energy. Therefore, alternative modulation techniques may be required to support open-loop synchronization.

1.1.3 Mission critical communications

Mission critical communications is another type of MTC which implies a wireless connectivity, where sensor and actor messages need to be transmitted between the respective communication partners with very low latency and very high reliability [1] [11]. The respective 3GPP term is Ultra Reliable Low Latency Communications (URLLC). Typical

use cases of MCC are factory automation [15], vital sign monitoring, safety and security applications (e.g. video surveillance, intrusion detection) [1]. It is expected that the achieved latency can be lower than 1 ms [16] and the Packet Error Rate (PER) inferior to 10^{-5} [16], down to 10^{-9} for specific applications [15]. The latency is directly related to the Time Transmission Interval (TTI) which refers to the duration of a transmission on the radio link. In 4G/LTE, the TTI is considered to be equal to 1 ms [17] [14], corresponding to the transmission of 14 OFDM symbols and the duration of 2 RBs. Without considering propagation delay, hardware latency, and retransmission mechanisms, the minimal achievable latency in 4G/LTE is therefore 1 ms. This implies that the overall end-to-end communication latency is higher than 1 ms. Consequently, the MCC latency requirement is not fulfilled in 4G/LTE. Therefore, solutions have been investigated to reduce the latency.

A first approach is to reduce the number of OFDM symbols transmitted in a RB. One of the major issues of this solution is that it imposes a constraint on the pilot structure for channel estimation. The transmission of these pilots are crucial to receive the signal as they are used at the receiver side to estimate the channel response and compensate the introduced distortion. In 4G/LTE, a RB is composed of 7 OFDM symbols and the pilots are transmitted in the 4^{th} OFDM symbol for the uplink case. This unavoidable signalling overhead introduces a data rate loss of 14.3%. If the number of OFDM symbols is reduced to reduce the latency then the data rate loss becomes worse. As an example, if a RB contains 4 OFDM symbols for low-latency communication, the data rate loss introduced by the pilot signalling becomes 25%. This is clearly a significant drawback for applications requiring high data rate communication.

Therefore, a second solution is envisaged in 5G. It consists of directly reducing the OFDM symbol duration while keeping the same number of OFDM symbols in a RB [18] [19]. A simple way to do this is to reduce the number of samples contained in an OFDM symbol by changing the IFFT size M, while keeping the same frequency sampling F_s [18]. This is advantageous since the same RF front-end configuration can be kept for all type of services. It only requires an IFFT size which can be re-configured dynamically, which is already the case in 4G/LTE in order to support multiple bandwidth configurations. As a consequence, the subcarrier frequency spacing is increased since we have $\Delta F = F_s/M$. Therefore, services using different subcarrier frequency spacing may coexist in the same carrier. For instance, some frequency resources can be used for typical MBB services while the adjacent ones can be employed for MCC, as illustrated in Figure 1.3.

However, the orthogonality condition of the OFDM modulation is rather strict since it requires that the same modulation numerology (parameters) must be employed for each user in the same carrier, such as the IFFT size and the CP size. Since it is not the case for a mixed-numerology system, IUI is expected. Due to its low spectral confinement, a large number of subcarriers must be used as guard-band to avoid severe interference level, leading to capacity loss. For instance, reference [20] shows that up to 300 kHz of guard-band (20 subcarriers) must be inserted between two users to obtain a PER of 10^{-9}. This corresponds to the case where one user has a typical subcarrier frequency spacing of $\Delta F = 15$ kHz, while the second has $\Delta F = 60$ kHz, both using a convolutional Forward Error Correction (FEC) code with 1/2 code rate and a 64-QAM constellation. Therefore,

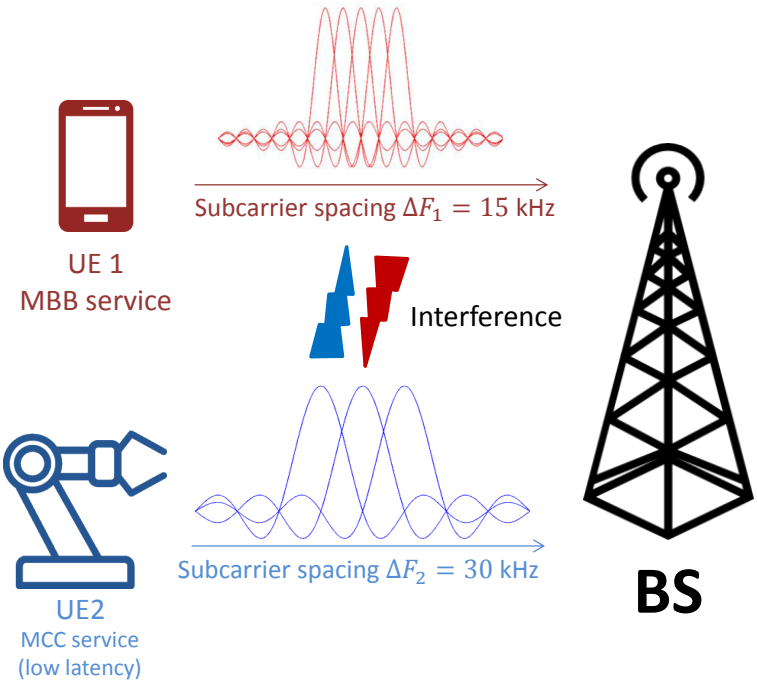

Figure 1.3 — MBB and MCC services transmitting data with different subcarrier frequency spacing.

alternative modulation techniques may be required to support mixed-numerology system for low-latency communications in MCC.

1.1.4 Vehicular-to-anything communications

V2X service corresponds to communications between two vehicles, referred to as V2V, or between a vehicle and the infrastructure, referred to as V2I. Today, also known as Intelligent Transportation Systems [1], V2X consists of use cases where other core services involve nodes with high speeds. In addition to the support of high speeds, the related technical requirements are often combined to those encountered in the other 5G services. For instance, collision avoidance systems may require low latency with high reliability, and can be included in both MCC and V2X services. Other examples are pay-as-you-drive which is the combination of V2X with MMC, and infotainment which can correspond to the combination of V2X with MBB. Such combination of more than one core service may also be called as composite services [1]. Figure 1.4 provides an example of a wireless environment involving V2X service.

The cellular V2I service is closely related to the MBB service, where users communicate through a BS.In the scenario foreseen in 5G, the user is located in a vehicle moving at speed ranging from 70 km/h for a car in an urban environment, to more than 500 km/h for high-speed railway [21]. Such high speed is theoretically not supported by the current 4G/LTE standard, where the mobility speed limit is considered to be 300 km/h [22]. In 5G, this speed limit has been increased up to 500 km/h [22].
The time variation of the channel impulse response generates Inter-Carier Interference (ICI) due to the Doppler spread effect, and must be compensated. Consequently, the

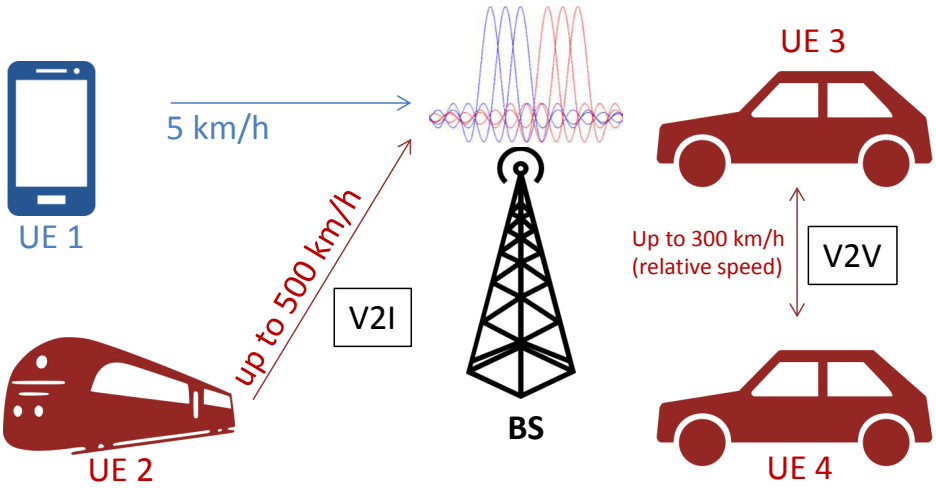

Figure 1.4 — Example of a wireless environment involving V2X service.

OFDM receiver complexity is greatly increased. In addition, the orthogonality between users is compromised since the amplitude peaks and the zeros of the cardinal sine pulse conveyed by each subcarrier are frequency shifted. In order to address these issues, a straightforward solution is to reduce the symbol duration. However, this raises the issue of coexistence between services as encountered in MCC scenario, described above in Section 1.1.3.

Regarding the V2V service, it requires Device-to-Device (D2D) communications raising the issue of spectrum sharing. Indeed, if the UEs are not synchronized with the BS, packet collisions can arise between the D2D users and the other MBB users located at proximity. This results in IUI and performance loss even if these users occupy adjacent frequency resources in the same carrier, since OFDM requires strict time synchronization to ensure the orthogonality between users. Again, alternative modulation techniques are required to overcome these scenario-specific limitations.

1.2 Post-OFDM waveforms

Different waveform proposals have been investigated these last years as an alternative to OFDM in the context of 5G. FBMC/OQAM, UF-OFDM, FC-OFDM, ZT-OFDM, F-OFDM, and BS are examples of such recently proposed waveforms. In this PhD work, we have mainly investigated FBMC/OQAM which introduces subcarrier filtering stage on top of OFDM and UF-OFDM where subband-wise filtering is applied. Therefore, this section provides a technical description of these considered two waveforms. Furthermore, a brief introduction to few other promising candidate waveforms is provided.

1.2.1 FBMC/OQAM waveform

FBMC is a multicarrier transmission scheme that introduces a filter-bank to enable efficient pulse shaping of the signal conveyed on each individual subcarrier. Therefore, each subcarrier is filtered by a common filter called the PF. The PF time-domain response,

or impulse response, is composed of L samples in discrete domain. The process of decomposition performed by the filter-bank is called synthesis, meaning construction of a complete signal resulting from the filtering process.

While the subcarriers in OFDM carry a fixed cardinal sine pulse shape, the subcarrier-wise filtering introduced in FBMC enables to have more control about the secondary lobes of the transmitted pulse, which in turn offers more flexibility about the resulting OOBPL. The FBMC signal is not composed of successive and separate block-symbols as in OFDM, since the transmitted FBMC symbols overlap in time-domain. Each FBMC symbol carries up to M filtered subcarriers and is composed of L samples. The number of overlapping symbols is defined by the overlapping factor K, which corresponds to the ratio between the PF length L and the total number of subcarriers M ($K = L/M$).

The reconstruction process at the receiver is called analysis, meaning reconstitution of a complete signal resulting from the filtering process. Such a transceiver structure usually requires a higher implementation complexity related not only to the filtering steps but also to the applied modifications to the modulator/demodulator architecture. However, the usage of digital polyphase filter bank structures [23] [24], together with the rapid growth of digital processing capabilities in recent years have made FBMC a practically feasible approach.

According to Balian-low theorem [25], one of the following statements cannot be achieved for any communication system:

1. Orthogonality in the complex domain.
2. Localization in time and frequency.
3. Maximum spectral efficiency.

For OFDM, the complex orthogonality comes at the sacrifice of the localization in frequency. The absence of property 2) usually attributes to a OFDM system a high OOBPL. Furthermore, OFDM must also slightly sacrifice property 3) to combat multipath channel through the use of CP. To overcome the shortcoming 2) of OFDM, filter-bank modulations apply a subcarrier wise filtering. Consequently, the spectral efficiency or the complex orthogonality must be abandoned, according to the Balian-low theorem.

As a promising variant of filtered modulation schemes, FBMC/OQAM can usually achieve a higher spectral efficiency than OFDM while maintaining the orthogonality. FBMC/OQAM was originally proposed in [26], also called OFDM/OQAM [24]. The function of the OQAM scheme is to preserve the orthogonality in the real field. It consists of first separating the real and imaginary parts of the QAM symbols to transmit, so that Pulse-Amplitude Modulation (PAM) symbols are obtained. Then, the number of FBMC symbols to transmit are doubled, so that the data rate is not reduced. Therefore, the number of overlapped FBMC symbols is also doubled and there is now a delay of $M/2$ samples between two successive FBMC symbols. Note that the overlapping factor K is still defined as $K = L/M$, even when using the OQAM scheme.

Before being transmitted, the PAM symbols are multiplied by a quadrature phase rotation term. This enables to ensure that all phase-rotated PAM symbols, located at

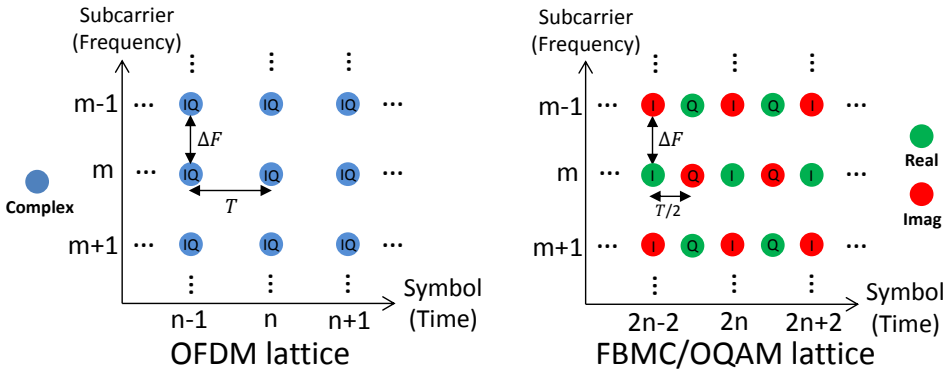

Figure 1.5 — Time and frequency transmission scheme (lattice) for OFDM and FBMC/O-QAM.

adjacent subcarriers and adjacent FBMC symbol positions, are in quadrature phase as illustrated in Figure 1.5. This is crucial to preserve the orthogonality. At the receiver side, the real part of the demodulated samples are extracted and the QAM symbols are reconstructed. The discarded imaginary samples correspond to interferences, referred to as intrinsic interference [27].

With the OQAM scheme, FBMC becomes:

1. Orthogonal in the real field due to the OQAM scheme.
2. Better localized than OFDM in time and frequency due to the subcarrier-wise filtering.
3. Theoretically having higher spectral efficiency than OFDM as it does not include a CP.

Additional advantages include the robustness against imperfect synchronizations and highly variant fading channel conditions by selecting the appropriate prototype filter type and coefficients [28] [29]. Therefore, FBMC/OQAM constitutes an enabler to several 5G services as it enhances system robustness to different types of impairments. For instance, the robustness of FBMC/OQAM against Doppler shift and spread can be exploited to support V2X services. Furthermore, efficient support of relaxed synchronization can be envisaged with FBMC/OQAM thanks to its low OOBPL and its robustness against timing offset [28], enabling MMC services.

However, the introduction of the OQAM scheme complicates the support of certain techniques, such as channel estimation and MIMO techniques. Moreover, the absence of a CP is an issue, rather than an advantage, when facing multipath channel with long delay spread.

In the literature, typical implementation of FBMC/OQAM employs a PPN based structure [30], enabling a low complexity implementation of the FBMC/OQAM transceiver. At the transmitter side, the typical implementation is composed of one IFFT, as in OFDM, followed by one PPN for the filtering stage as shown in Figure 1.6. Receiver side implementation of the PPN applies dual operations with respect to the ones performed by the constituent blocks of the transmitter [30]. The IFFT size is always equal to M (maximum number of allocated subcarriers) independently of the

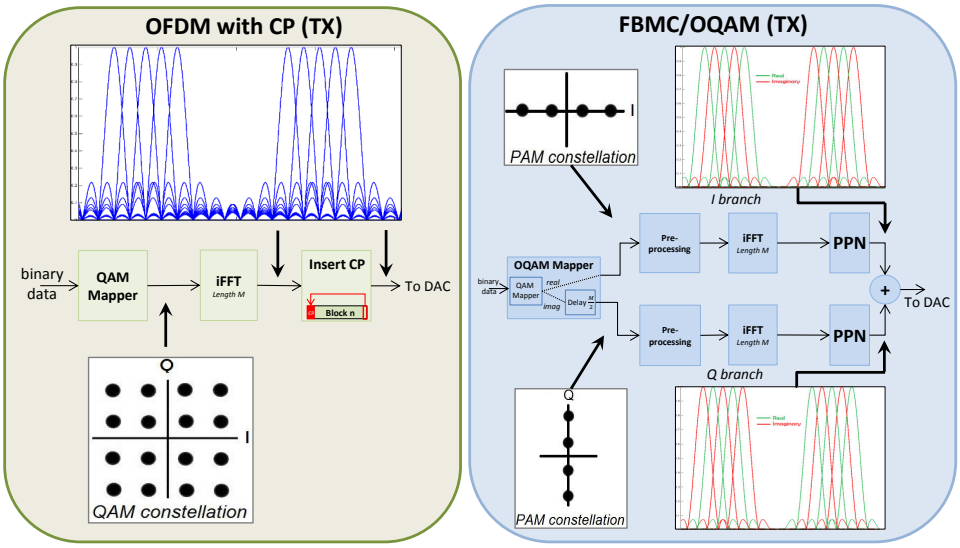

Figure 1.6 — PPN implementation of the FBMC/OQAM transmitter.

chosen PF. On the other hand, the PPN processing depends on the PF length, since this is the processing unit where the filtering stage is performed. Indeed, the PPN processing steps at the transmitter side can be summarized as follows [31]:

Step 1) Duplicating the M samples at the IFFT output $K-1$ times.
Step 2) Applying a windowing operation, where the window is the impulse response of the PF, composed of KM samples.
Step 3) Applying a delay of $M/2$ samples.
Step 4) Summation with the generated signal at the previous iteration (overlapping).

Due to the OQAM scheme, the IFFT and PPN processing units must be duplicated to achieve the same processing rate as OFDM, as shown in Figure 1.6. It is however possible to avoid the use of two IFFT blocks at the transmitter side through the use of pruned FFT algorithm. This leads to a reduced-complexity implementation as detailed in [32]. From the above described steps, it can be inferred that the complexity of the PPN processing highly depends on the overlapping factor K. The windowing operation requires $2KM$ real multiplications per FBMC symbol, assuming that the impulse response of the PF is generally real-valued. Furthermore, the summation operation requires $2KM$ real additions. The overlapping factor K being related to the PF length, it can be advantageous to use short PFs with $K = 1$ to reduce the complexity. In addition, the PPN processing step 1) is avoided for this type of PF. Otherwise, this step may require the use of at least a memory able to store $M(K-1)$ complex samples [31].

The obtained time-domain FBMC/OQAM signal is represented in Figure 1.7. Due to the periodic property of the IFFT, the duplication in step 1) preserves the continuity of the signal, and the widowing operation in step 2) smooths the transition at the beginning and end of the FBMC symbol. Therefore, the discontinuity between successive symbols are limited, contrary to OFDM. Furthermore, this windowing operation in time domain is equivalent to a circular convolution in frequency domain, which explains why the

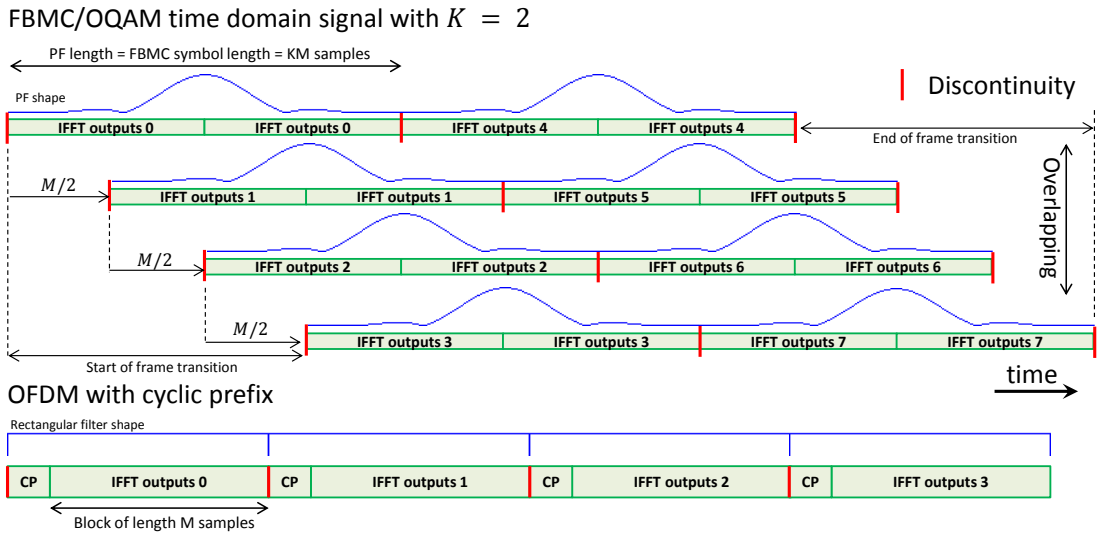

Figure 1.7 — FBMC/OQAM overlapping structure with $K = 2$.

pulse shape of each subcarrier corresponds to the frequency response of the PF. This observation leads to the FS implementation of FBMC/OQAM [33], which will be detailed in Chapter 2.

1.2.2 UF-OFDM waveform

The UF-OFDM modulation was first proposed through the name of Universal Filtered Multi-Carrier (UFMC). The principle of the UF-OFDM modulation [34] is to group the complex samples carrying information into several subbands, each composed of Q subcarriers. These complex samples can be, for instance, issued from a QAM constellation. Therefore, a maximum of $\lfloor N/Q \rfloor$ subbands can be used, where N is the total number of subcarriers, and $\lfloor x \rfloor$ represents the largest integer less than or equal to x (floor operator). The secondary lobes of each subband are attenuated by filtering each subband independently using a corresponding filter of length L samples. Then, all filtered subbands are summed together. This forms the UF-OFDM symbol, composed of $N + L - 1$ samples.

The principle of the UF-OFDM transmitter is illustrated in Figure 1.8. It consists of the following steps:

Step 1) A subband mapping which inserts the complex samples carrying information into the corresponding subcarrier indexes for each subband.
Step 2) An IFFT of size N for each allocated subband.
Step 3) A filtering stage for each subband, which can be implemented using a linear convolution operation.
Step 4) A final summation operation where all filtered subband signals are summed together to form an UF-OFDM symbol.

The above steps must be repeated for each UF-OFDM symbol to transmit. It is worth noting that while a UF-OFDM symbol does not have a CP, a slight data rate loss is introduced due to the ramp-up and ramp-down transition of the subband filtering. If

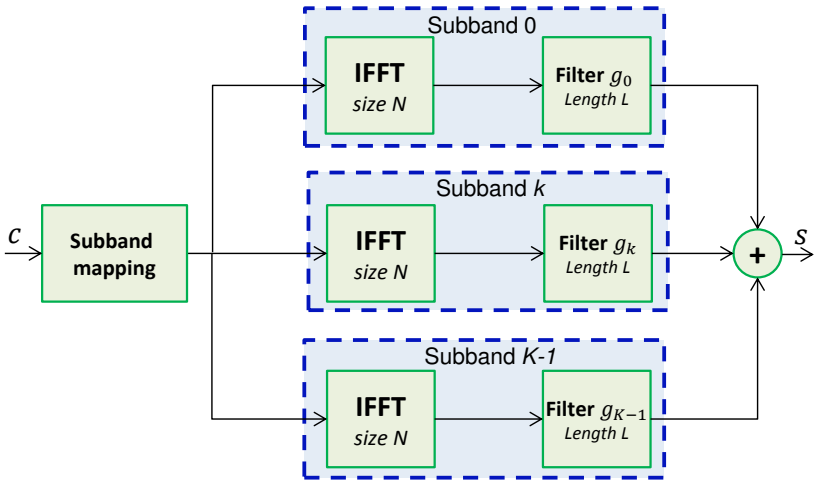

Figure 1.8 — Principle of the UF-OFDM transmitter.

the subband filter is of length L, then $L-1$ additional samples are appended to the N time-domain samples carrying information.

Generally, the length of the subband filter is designed such as the introduced data rate loss is equivalent to the one introduced by the CP in OFDM. If L_{CP} is the CP length, then we have $L = L_{CP}+1$. The UF-OFDM receiver implementation is completely different from its transmitter implementation. It was described in [35], and consists of the following steps:

Step 1) Isolating the $N+L-1$ samples constituting the received UF-OFDM symbol.
Step 2) Appending $N-L+1$ zeros at the end of the isolated samples. The obtained signal contains $2N$ samples.
Step 3) Applying an FFT of size $2N$ on the zero-padded signal to obtain the frequency domain signal.
Step 4) Discarding the odd FFT output indexes (down-sampling by 2) to keep the even indexes where the main lobe of each transmitted subcarrier is concentrated.

The obtained frequency-domain signal can be processed using same type of techniques as for OFDM, such as equalization. This equalization aims to compensate the effect of the channel impairments and the distortion caused by the subband filtering.

Before computing the FFT, a windowing operation can be applied on the time-domain samples between step 2) and step 3). This windowing operation is presented as optional in [35]. It is however highly recommended since it improves the performance of the UF-OFDM receiver when relaxed synchronization is considered [36]. The UF-OFDM receiver complexity is slightly increased when compared to the typical OFDM receiver implementation, due to the use of a FFT of larger size. However, $N-L+1$ input samples of the FFT are zero-valued and half of its outputs are discarded, which results in redundant operations. In fact, it is shown in [37] that the FFT size can be reduced down to N, the same FFT size as used in the OFDM receiver. Instead of applying a zero-padding operation on the $N+L-1$ samples of the received UF-OFDM symbol,

the last $L-1$ samples are added to the first $L-1$ samples. If a windowing operation is performed, it has to be applied before this step. Then, the obtained N samples are directly computed by a FFT of size N. Therefore, the UF-OFDM receiver has almost the same complexity as the OFDM receiver.

1.2.3 Other 5G waveform candidates

FC-OFDM:

FC-OFDM waveform [38] was proposed in the context of the FANTASTIC-5G European research project [39] [37]. In fact, an ideal modulation scheme should be flexibly adaptable when the requested service changes. Therefore, the idea of this modulation is to select different types of waveform in the same carrier, such as OFDM or FBMC/OQAM, depending on the channel condition or the type of service in a multi-service environment. Consequently, each RB can be configured with 4G/LTE based waveform for MBB service or with filtered waveform for emergent 5G services such as V2X or MMC. Depending on the uplink or downlink transmissions, the FC-OFDM modulation specifies different configuration modes [38] [40]. For instance, three configuration modes which can coexist within the same bandwidth are proposed for the downlink transmission:

1. **Configuration mode 1** corresponds to a classical OFDM modulation with insertion of a CP. Thus, it is fully compatible with MBB service currently provided in 4G/LTE standard. In addition, a postfix and a windowing operation is added to reduce the OOBPL.
2. **Configuration mode 2** can be seen as an FBMC/OQAM modulation using a half-sine shaped filter with overlapping factor equal to 1. The major difference is the introduction of post-processing stage after the IFFT which inserts a prefix, a postfix, and a windowing operation. This mode conserves some advantages of FBMC/OQAM. For instance, it can be used to improve the robustness against Doppler shift/spread in case of high mobility for V2X service, or for MMC service due to its capability to support relaxed synchronization.
3. **Configuration mode 3** uses the same modulation and processing technique as described for mode 2, but at half data rate. Only PAM symbols are sent through the channel instead of OQAM symbols. The principal advantage of this mode is its orthogonality to both mode 1 and mode 2. Thus, instead of inserting a guard band (composed of null subcarriers), FC-OFDM with configuration mode 3 can be used between two subbands respectively configured in mode 1 and 2 to avoid important loss in spectral efficiency [38].

Table 1.2 summarizes the properties of these configuration modes for FC-OFDM in downlink. In this case, the implementation of the FC-OFDM modulator is based on two IFFTs as shown in Figure 1.9. First, a QAM mapper is used for mode 1, and a PAM mapper followed by a quadrature phase rotator is used for mode 2 and mode 3.

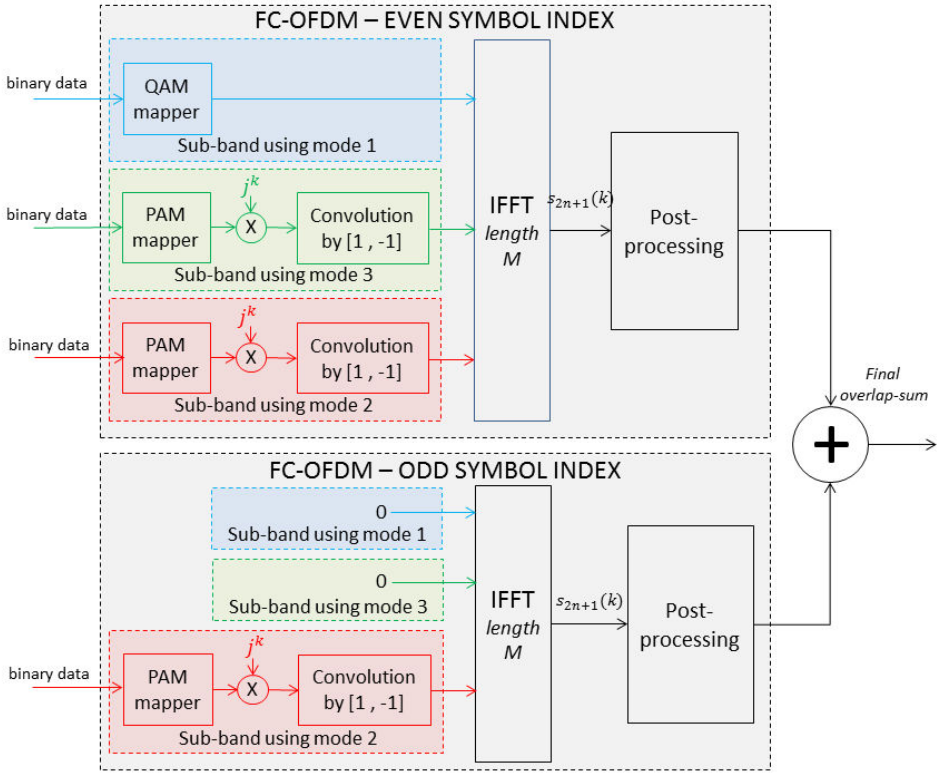

Figure 1.9 — FC-OFDM downlink transmitter.

Then, for these two last modes, a filtering operation is realized in frequency domain. It consists of a trivial convolution operation with coefficients $[1, -1]$, which corresponds to a half-sine shape in time domain. It can be simply implemented with a shift register as mentioned in [38]. The advantage of using a frequency representation is that only one IFFT can be used to compute the 3 modes at the same time (instead of 3 IFFTs), since each mode generates a set of subcarriers which can be mapped directly to the IFFT. However, to support mode 2, a second IFFT must be used to generate the staggered path due to the OQAM processing, at odd symbol indexes.

The FC-OFDM solution for uplink [37] is naturally different from that of the downlink as it targets different use cases. In this context, 3 other different configuration modes are proposed:

1. **Configuration mode 1** is based on the OFDM modulation.
2. **Configuration mode 2** is based on the SC-OFDM modulation, as currently used in the 4G/LTE uplink.

Table 1.2 — Characteristics of the three FC-OFDM downlink configuration modes.

Mode	Filter shape	Coefficients	Even symbol index	Odd symbol index	Orthogonality
1	Rectangular	[1]	QAM	0	Complex, with mode 1 and 3
2	Half-sine	$[1, -1]$	PAM	PAM	Real, with mode 2 and 3
3	Half-sine	$[1, -1]$	PAM	0	Real, with mode 1, 2 and 3

3. **Configuration mode 3** corresponds to the ZT-OFDM modulation [41]. It consists of inserting zero-valued samples at the beginning and the end of the FFT pre-coder used for the SC-OFDM modulation.

Similarly to the FC-OFDM downlink, a cyclic prefix and postfix are inserted, followed by a windowing operation to reduce the OOBPL. Furthermore, the last samples of the symbol number n overlap with the first samples of the symbol number $n+1$.

ZT-OFDM: Another candidate waveform proposed in the context of the 5G is the ZT-OFDM [41]. This waveform is based on the SC-OFDM modulation scheme, where a FFT pre-coder is inserted between the IFFT of size M and the QAM mapper [42]. This pre-coder aims to reduce the PAPR. However, there is 2 fundamental differences between ZT-OFDM and SC-OFDM modulations:

1. No CP is inserted.
2. Zero-valued samples are inserted at the beginning and the end of the FFT pre-coder.

The insertion of these zeros enables to smooth the signal transition between successive ZT-OFDM symbols in time domain, hence the term *zero-tail* in ZT-OFDM. Consequently, the OOBPL is reduced. This zero-tail also helps to mitigate the ISI introduced by multipath channels. In addition, the insertion of zeros implies no overhead in power consumption, contrary to the CP. Therefore, compared to OFDM, the saved power can be used for the data, improving the Bit-Error Rate (BER) performance of the system over Additive White Gaussian Noise (AWGN) channels. On the other hand, the data rate is slightly reduced due to the zero-tail. However, its length can be adapted to the channel conditions and the acceptable OOBPL level, without changing the symbol duration. Therefore, the data rate can be controlled. This feature makes ZT-OFDM modulation more flexible than OFDM. Its robustness against multipath channel with high delay spread is however questionable.

F-OFDM: F-OFDM waveform [43] is also a promising candidate for 5G. This waveform is based on a subband-filtering, similarly to UF-OFDM. However, there is several notable differences when compared to the latter. First, F-OFDM inserts a CP of length L_{CP}. Second, the subband filter length (L) is superior to the CP length. The impulse response coefficients of this filter are designed so that most of the energy is concentrated on L_{CP} samples, in order to avoid severe ISI. In addition, this filter is designed so that its frequency response is flat over the supported subband bandwidth. The third difference concerns the use of a matched filter at the receiver side. Promising results have been demonstrated for relaxed synchronization. However, one of the current issues of this waveform concerns its complexity, particularly at the transmitted side.

BF-OFDM: The investigation of advanced modulation techniques is still on-going. For instance, the BF-OFDM waveform has been recently proposed in [44]. It is presented as an improved version of the FFT-FBMC technique proposed in [45]. The particularity of the FFT-FBMC scheme lies in the application of several FFT pre-coders before the FBMC transmitter. If N_C subcarriers are allocated and N_s FBMC symbols transmitted,

then N_C FFTs of size N_s are performed on the transmitted data symbols across the time axis. Additionally, a CP can be inserted at the output of the FFT pre-coders to isolate 2 successive blocks of pre-coded FBMC symbols in order to limit the interference level.

For this transceiver, the OQAM scheme is not used. Instead, a particular transmission scheme is proposed where half of the FFT pre-coder inputs are fed by QAM symbols and the second half inputs are fed by zero-valued samples. Such scheme contributes to limit the intrinsic interference level. In fact, the distortion caused by the intrinsic interference is compensated at the receiver, after the IFFT pre-coder.

In BF-OFDM, a pre-distortion stage is added before the FFT pre-coder at the transmitter side. Then, it is shown that the receiver can simply be implemented using a CP removal operation followed by a FFT and a per-subcarrier equalizer, similarly to OFDM. Therefore, such waveform is very interesting for downlink communication where the receiver complexity at the UE side must be minimal. In this case, the increased transmitter complexity at the BS side can be considered acceptable.

1.3 Motivation for using short PF with FBMC

Current literature often focuses on FBMC/OQAM using a PF with a duration $K = 4$ times higher than an OFDM symbol. However, it is worth noting that other overlapping factors such as $K = 8$ or $K = 2$ can be considered. Nevertheless, having K as low as possible, i.e. $K = 1$, can be highly advantageous. Among others, it enables particularly to support short frame sizes for low-latency communication and to reduce the transmitter power consumption, as detailed in the next sub-sections. In the rest of this chapter, PFs with $K > 1$ will be referred to as *long filters*, and the ones with a duration equal to one OFDM symbol as *short filters*.

1.3.1 Support of short frame sizes for low-latency communication

A major issue of FBMC/OQAM employing long PFs is that it implies large ramp-up and the ramp-down at the beginning and the end of each transmitted frame [46]. Therefore, FBMC/OQAM has been judged inadequate in the literature to support 5G scenario requiring low-latency communications such as MCC. For instance, reference [20] shows that FBMC/OQAM has higher coexistence capability than UF-OFDM when mixed numerology must be supported in the same carrier, where 45 kHz of guard-band is sufficient to avoid any IUI. Nevertheless, the article concludes that the extended symbol duration of FBMC/OQAM is a serious drawback for low-latency requirement.

To overcome this concern, few solutions have been investigated in the literature. The first proposed one is to simply truncate the PF impulse response for the first and last transmitted symbols [47]. This technique is extremely simple to implement and implies no complexity overhead. However, a first undesirable effect of the PF impulse response truncation is the increase of OOBPL due to the sharp transition introduced by the truncation. Thankfully, this issue can be efficiently addressed by applying a windowing operation instead of a hard-truncation, so that the transition is smoothed. The window

coefficients can be obtained, for instance, from a raised-cosine function as considered in [48]. The second drawback of this technique concerns the orthogonality which is partially lost, implying the introduction of interference. The more filter coefficients are truncated, the higher the interference level is. To achieve a Signal-to-Interference Ratio (SIR) level higher than 30 dB for any FBMC symbol, only 320 coefficients from a typical long PF of length 1024 samples can be truncated [47]. For comparison, an OFDM symbol is composed of 256 samples using the same set of parameters considered in the above article (neglecting the CP length). When the PF impulse response is truncated, the last FBMC symbol is composed of 704 samples. In other words, almost two time more OFDM symbols can be transmitted during the remaining filter transition, and without taking into account the OQAM scheme. This also applies for the first FBMC symbol. Therefore, the data rate loss may not be negligible for short frame sizes.

More recently, a technique based on transmitting virtual symbols to reduce the filter transition has been proposed [49]. The idea is to transmit an additional FBMC symbol before the first and after the last ones normally transmitted in a frame. These symbols do not contain any information. They are constructed in such a way that the the ramp-up and ramp-down transitions of the PF are suppressed. Finally, the first and last samples of the frame, now almost zero-valued, are truncated or windowed. The additional symbols are called virtual symbols since they are not fully transmitted and their only function is to shorten the filter transition. The different steps of this technique can be summarized as follows [49]:

Step 1) Generate the typical FBMC/OQAM frame signal.
Step 2) Isolate the last (or first) samples of the frame to obtain the tail signal.
Step 3) Find the virtual PAM symbols to transmit so that the obtained time-domain signal is close to the previously isolated tail signal.
Step 4) Generate the virtual tail signal using the virtual PAM symbols previously found.
Step 5) Subtract the samples of the virtual tail signal from the last (or first) samples of the frame.
Step 6) Apply a windowing operation.

From the above steps, it can be inferred that the complexity of the transmitter will be increased. Indeed, the construction of virtual symbols depends on the data being sent at each frame, requiring on-line computation. In [50], a matrix based computation is derived. It is evaluated that at least 36% more real addition operations and 14% more real multiplication operations are required. These results are obtained assuming a total number of subcarriers equal to $M = 256$, with $N_C = 192$ allocated subcarriers. In 4G/LTE, the ratio between the total number of subcarriers and the maximum number of allocated subcarriers is $N_C/M \approx 0.586$ for any bandwidth configuration. A typical FBMC/OQAM transmitter scales in $\mathcal{O}(M\log_2(M))$, whereas the virtual symbol computation scales in $\mathcal{O}(0.586)^2M^2$. Therefore, for higher M values than what are considered in [50], large complexity increases are expected. Moreover, it is assumed in [50] that all the matrix coefficients are pre-computed and stored in a Look-Up-Table (LUT), which

introduces an additional complexity overhead. The matrix dimension depends on the number of allocated subcarriers N_C. Therefore, it must be designed and stored for each possible allocation size, further increasing the memory requirement.

In conclusion, an efficient support of short frame sizes with long PFs remains an open issue. Thankfully, this is not the case for short PFs, since their duration is divided by 4 when compared to long PFs with $K = 4$. The FBMC symbol duration becomes equal to the duration of one OFDM symbol. The filtering transition is only due to the OQAM scheme in this case, which only introduces an overhead of $M/2$ samples. In addition, truncation can be applied without introducing interference [51]. However, it still requires the use of a cyclic prefix and a cyclic suffix at the beginning and the end of the frame, and the application of a window function (raised-cosine or Dolph-Chebyshev window for instance) to keep low OOBPL due to the absence of signal continuity at the edges of the frame.

1.3.2 Low computational complexity

FBMC symbols are typically generated by applying an IFFT on the transmitted PAM symbols, followed by a PPN stage. The IFFT size only depends on M (maximum number of allocated subcarriers) which does not depend on the PF length L. On the other hand, the PPN processing highly depends on the PF length since this is the processing unit where the filtering stage is performed. The PPN processing steps have already been presented above in Section 1.2.1. We recall them again here in order to discuss in more details the related computational complexity:

Step 1) Duplicating the M samples at the IFFT output $K - 1$ times.
Step 2) Applying a windowing operation, where the window is the impulse response of the PF, composed of KM samples.
Step 3) Applying a delay of $M/2$ samples.
Step 4) Summation with the generated signal at the previous iteration (overlapping).

These steps are executed for each FBMC symbol. Note that step 1) can be seen as a long cyclic-prefix insertion, performed in a similar way as for OFDM. From the above algorithm steps, it can be inferred that the windowing operation requires $2KM$ real multiplications per FBMC symbols, assuming that the impulse response of the PF is generally real-valued. Furthermore, the summation operation requires $2KM$ real additions. As a reminder, the overlapping factor of the PF is $K = L/M$, with $K = 4$ for long PFs and $K = 1$ for short PFs. It becomes clear that for short PFs, the computational complexity is highly reduced when compared to long PFs. Particularly, the number of real multiplications is divided by 4. From this lower computational complexity, it can be expected that lower power consumption can be obtained.

In addition, the step 1) of the above algorithm is avoided for short PFs. This step may requires, in practice, the use of at least a memory able to store $M(K-1)$ complex samples. For comparison, the minimum memory depth of an IFFT is M complex samples. Therefore, the memory resources are at least tripled for long PFs when compared to short

PFs. Again, this leads not only to a larger complexity increase, but also to a higher power consumption due to memory accesses.

The same conclusion is obtained for the complexity of the PPN stage at the side receiver. However, comparing the complexity of the receiver without taking into account other necessary processing units such as the equalizer is not fair. Particularly, the complexity comparison at the receiver side only has meaning if the performance level of both short and long PF systems are evaluated.

1.3.3 High energy efficiency

Multi-carrier modulations are generally highly sensitive to non-linearity distortions due to their high PAPR [52]. For instance, the non-linearity of the HPA generates distortion on the transmitted signal which degrades the BER performance. FBMC/OQAM has similar PAPR than OFDM, assuming that an infinite number of symbols are transmitted in a frame. In practice, the ramp-up and ramp-down of the PF at the beginning and the end of each frame introduce a slight increase in PAPR [50].

A straightforward solution to address this non-linearity issue is to simply reduce the average signal power so that the peaks remain in the linear zone of the HPA. Alternatively, HPA with high amplification gain can be used to extend the linear zone. However, these two techniques are not the most energy efficient solutions. Therefore, PAPR reduction techniques has been widely investigated in the literature for OFDM [53], and most of these techniques have been adapted for FBMC/OQAM [54]. In 4G/LTE uplink transmission, PAPR reduction is achieved by applying a FFT on the QAM symbols, before being assigned to the allocated subcarriers [42]. For FBMC/OQAM, a different pre-coder must be employed since real-valued samples must be transmitted before the IFFT. For instance, a Discrete Cosine Transform (DCT) pre-coder can be considered.

Figure 1.10 shows the Complementary Cumulative Distribution Function (CCDF) of the OFDM and FBMC/OQAM signals with and without the pre-coder, obtained by simulation. For FBMC/OQAM, transmissions using a short and a long PF are considered. The employed short PF is the one designed in [55], which corresponds to a simple half sinus shape. The long PF is the one proposed in [33], which is the PF generally considered in the literature. The simulation parameters are set to the typical 5 MHz bandwidth ($M = 512$) with 300 allocated subcarriers and a 16-QAM constellation. Without the pre-coder, the FBMC/OQAM signal using the short PF has similar PAPR when compared to the long PF. In fact, the PF choice has almost no impact on the signal PAPR. When compared to OFDM, the PAPR is however slightly increased. As stated above, this is due to the presence of a ramp-up and a ramp-down transitions at the beginning and the end of the FBMC/OQAM frame.

All the pre-coded signals achieve significant peak-power reduction when compared to their non-pre-coded versions. For FBMC/OQAM, the efficiency of the pre-coding technique depends on the PF choice. As shown in Figure 1.10, the long PF implies higher PAPR than the short PF, although the same pre-coder is employed. Such result was observed in [56], where multiple PAPR reduction techniques were tested for different PFs. This can be explained by the fact that the pre-coding techniques are typically

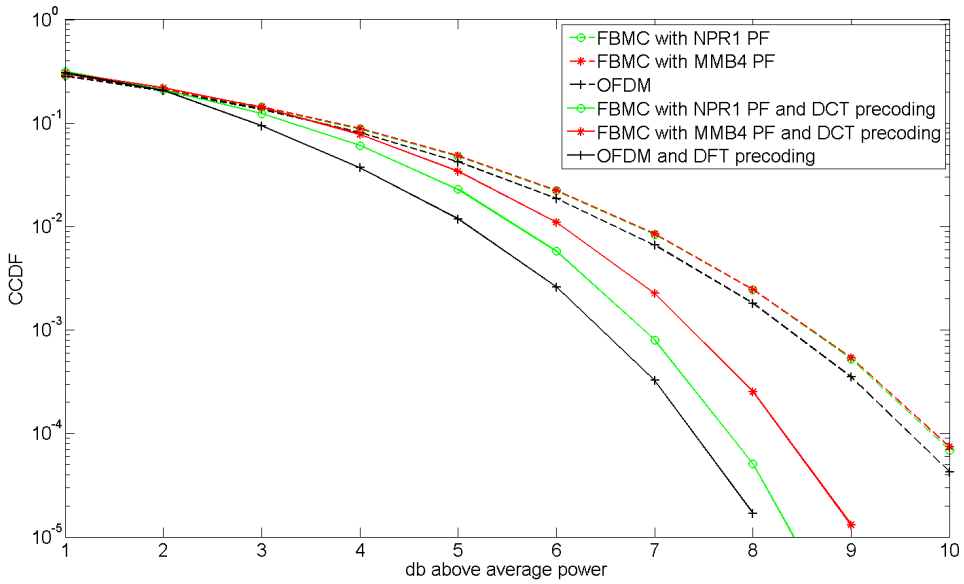

Figure 1.10 — CCDF comparison between OFDM and FBMC/OQAM using a short and a long PF with and without pre-coder.

employed for each FBMC symbol independently, whereas the FBMC symbols overlap before being sent through the channel. Since short PFs can achieve lower PAPR, higher power efficiency can be obtained when compared to long PFs.

In addition, the support of short frame duration, enabled by short PF, can potentially lead to further reduction in energy consumption [57]. Lastly, we have highlighted in the previous section the fact that short PFs have lower computational complexity than long PFs. Therefore, it is expected that additional reduction in power consumption can be obtained from the hardware processing when compared to long PFs.

1.3.4 Efficient block-based channel estimation

The estimation of the Channel Impulse Response (CIR) or the Channel Frequency Response (CFR) is a crucial aspect in communication systems. A failure to estimate the channel response results in high degradation of the system performance. By transmitting reference signals called pilots, known to both transmitter and receiver sides, the channel response can be estimated. Particularly, the orthogonality property of OFDM, preserved due to the CP even when facing multipath channel, enables to avoid any interference between the pilots and the data if transmitted in the same carrier.

Therefore, the channel estimation problem is simplified since at subcarrier m we have the following:

$$Y(m) = H(m)Z(m) + W(m), \tag{1.7}$$

where Y is the received signal, H the frequency response of the channel, Z the reference pilot and W the noise term. The pilots can be distributed in the time (symbol) and frequency (subcarrier) lattice into 3 types of structures [58] [59], as shown in Figure 1.11:

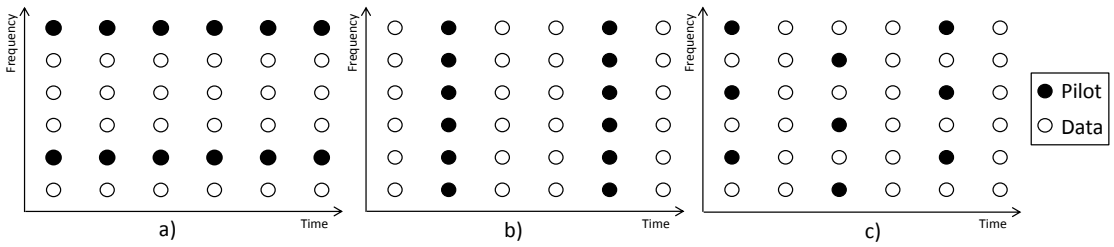

Figure 1.11 — Different types of pilots distribution: a) comb-type structure, b) block-type structure, c) scatter-type structure.

- Comb-type structure, where pilots are transmitted at each symbol index.
- Block-type structure, where pilots are transmitted at each allocated subcarrier index.
- Scatter-type structure, where pilots are transmitted at different subcarrier and symbol indexes.

Note that the channel estimation at the data positions can be obtained through interpolation. In 4G/LTE uplink scenario, the FFT pre-coding makes it difficult to use comb-type and scatter-type pilot structures, since it is applied to all the allocated subcarriers. Therefore, block-type pilot structure is chosen where the pilots are located at the 4^{th} OFDM symbol for each transmitted RB. The transmitted pilots are generated from a Zadoff-Chu sequence [60] which has a constant amplitude zero autocorrelation property. When this sequence is processed by an IFFT, the samples obtained at its outputs remain a Zadoff-Chu sequence. Therefore, the above property is preserved. At the receiver side, the CFR can be estimated through a least square estimation, which gives:

$$\hat{H}(m) = \frac{Y(m)}{Z(m)}. \tag{1.8}$$

While being simple and of low complexity, the estimation accuracy of this technique is rather poor at low SNR since the noise contribution is neglected. More efficient channel estimation techniques can be considered. For instance, the MMSE based estimation yields [61]:

$$\hat{\boldsymbol{H}}_{\boldsymbol{MMSE}} = \boldsymbol{R}_{\boldsymbol{H}}\Big(\boldsymbol{R}_{\boldsymbol{H}} + \sigma^2(\boldsymbol{Z}\boldsymbol{Z}^{\dagger})^{-1}\Big)^{-1}\hat{\boldsymbol{H}}_{\boldsymbol{LS}}, \tag{1.9}$$

where † is the Hermitian transpose operator and

- $\hat{\boldsymbol{H}}_{\boldsymbol{LS}}$ is the vector composed of the least square estimation of the CFR,
- $\boldsymbol{Z}$ is the vector composed of the transmitted pilot values,
- $\boldsymbol{R}_{\boldsymbol{H}}$ is the channel autocorrelation matrix,
- σ^2 is the noise variance.

The implied several matrix inversions make this technique quite complex to implement. Although complexity reduction techniques have been proposed [62], the channel autocorrelation matrix is not directly available and must be estimated.

FBMC with real-valued pilots: In FBMC/OQAM, channel estimation is a more complex task due to the absence of complex orthogonality. To avoid interference with

the transmitted data, the transmitted pilots must be real valued. However, the received signal is still corrupted by imaginary-valued interference terms (the intrinsic interference) resulting from the adjacent transmitted data. Assuming that the PF is well localized in time and frequency [63], (1.7) becomes:

$$Y(m) = H(m)\Big(Z(m) + iJ(m)\Big) + W(m) \tag{1.10}$$

where J is the unknown intrinsic interference signal. Successive interference cancellation techniques such as [64] can be employed to estimate the CFR. However, the complexity is highly increased since it requires to successively estimate the data values through FEC decoding.

A more simple technique can be employed, relying on the use of pairs of pilots [65]. This technique consists of transmitting 2 pilots at an adjacent time and frequency localization. If a block-type pilot structure is considered, the pilots can be transmitted at 2 adjacent subcarrier indexes. Then, by assuming that the channel response is the same over these 2 pilots positions, we obtain 4 equations with 4 unknown terms which can be resolved. The estimation accuracy is however rather poor, leading to important BER degradation [65].

Alternatively, [65] proposes a more robust technique called Interference Approximation Method (IAM), based on block-type pilot structure. The originality of this technique lies in transforming the inconvenient intrinsic interference into an advantage. Indeed, if the value of the interference terms can be controlled, additional power can be recovered increasing the accuracy of the estimation. This can be obtained if the sequence vector $[1, 1, -1, -1]$ is repeated across all the allocated subcarriers serving as pilots. To avoid uncontrollable intrinsic interference from the previous and the next FBMC symbols, all the subcarriers values are set to zeros. In other words, they are not transmitted through the channel and only act as guard-interval.

This technique was further improved in [66], where the transmission of purely real and imaginary pilot values are considered. In this case, the IAM sequence vector becomes $[1, i, -1, -i]$. Such techniques are particularly interesting for short PFs, since their short duration enables to completely isolate the pilots from the data. It is shown in [67] that when using an IAM-based channel estimation technique, FBMC/OQAM using a short PF outperforms OFDM by 2.3 dB and outperforms FBMC/OQAM using a long PF by 0.3 dB. Similar results are obtained in [65]. However, these outstanding results must be put into perspective. Indeed, the IAM technique suffers from a high PAPR making it subject to the non-linearity distortions of the HPA [68].

FBMC with complex-valued pilots: In fact, complex-valued pilots can be employed for FBMC. For instance, when using a half sinus short PF, it can be shown that the filtering effect of the transceiver is equivalent to applying circular convolution by the coefficients $[-1/2, 1, -1/2]$ on the transmitted pilot values. This supposes that the adjacent FBMC symbols are not transmitted. Then, assuming that the variation of the CFR over adjacent subcarriers is negligible, (1.7) can be rewritten as follows:

$$Y(m) \approx H(m)\Big(\frac{-Z(m-1) + 2Z(m) - Z(m+1)}{2}\Big) + W(m) \tag{1.11}$$

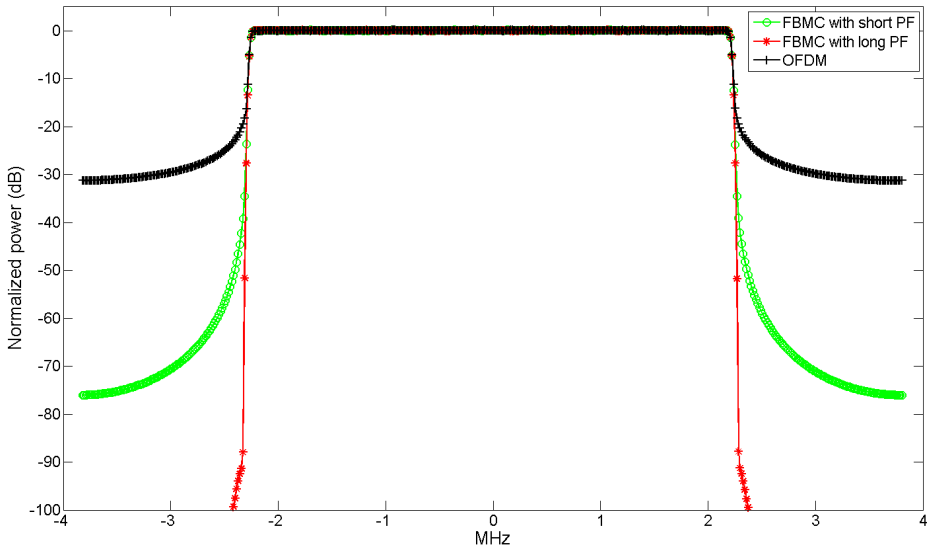

Figure 1.12 — PSD comparison of OFDM and FBMC/OQAM using a short and a long PF.

Therefore, by setting $Z(2m+1) = 0$, we have $Y(2m) = H(2m)Z(2m) + W(2m)$, where $Z(2m)$ can be a complex-valued pilot. The CFR at even subcarrier indexes can be estimated, and the CFR at odd subcarrier indexes can be obtained through interpolation. Consequently, Zadoff-Chu sequences can still be employed for FBMC/OQAM, along with the channel estimation techniques considered for OFDM. This assumes that the pilots are isolated from the data, introducing a data rate loss. However, the data rate loss is minimal for short PFs where only 1 FBMC symbol is necessary as guard-interval to perfectly isolate the pilots. This makes short PFs more suitable than long PFs for channel estimation techniques employing block-type pilot structure, as it is the case in 4G/LTE uplink communications.

1.3.5 Limitations of short PFs

Besides the many advantages presented above, FBMC/OQAM using short PFs encounters some limitations. Since short PFs have lower time duration than long PFs, the frequency confinement is slightly degraded. This is illustrated in Figure 1.12 which shows the simulated Power Spectral Density (PSD) for OFDM and FBMC/OQAM using the short PF of [55] and the long PF of [33]. The simulation parameters are set to a typical 5 MHz bandwidth ($M = 512$) with 300 allocated subcarriers. In a multi-user uplink context, a guard-band must be inserted between users to avoid interference. In practice, between 2 and 3 subcarriers used as guard-band can be sufficient for short filters, while long filters require only 1 subcarrier [69] [70]. Thankfully, the OOBPL obtained with short PF is still highly reduced when compared to OFDM.

It is however worth noting that the OOBPL inferior to -100 dB obtained with the long PF is only theoretical, assuming the floating-point precision of a 64-bit computer processor. In practice, the signal has to be at least quantized before being transmitted through the DAC of the RF interface. Furthermore, considering floating-point preci-

sion for hardware implementations is highly complex and energy consuming. Therefore, fixed-point precision must be considered, particularly at the transmitter side for uplink communications. The quantization errors introduce distortions on the resulting PSD [71]. In addition, the non-linearity of the HPA also introduces a spectral regrowth distortion [72] [73].

While being robust against Carrier Frequency Offset (CFO) or Doppler spread [74] [28], one of the major drawbacks of FBMC/OQAM using short PF is its sensitivity to multipath channel with long delay spread. In fact, the performance of FBMC/OQAM over multipath mainly depends on the ratio between the delay spread and the filter length.

Short PFs are also sensitive to timing offset impairments [28]. In fact, long PFs can support higher timing offset than short PFs and they are currently more adapted to support relaxed synchronization.

Furthermore, more advanced receiver techniques are considered when long PFs are employed, such as the frequency-spread based receiver. Such receiver relies on typical FFT and a low-complexity one-tap equalizer, as for OFDM, making it relatively attractive. Particularly, it enables the support of asynchronous communications [75], which may be one the reasons that long PFs are extensively employed in the literature.

In order to overcome these limitations and improve the robustness of FBMC/OQAM using short PFs, original contributions are presented in the next two chapters.

1.4 Summary

In this chapter we have provided the basic scientific background related to the presented PhD contributions in subsequent chapters. First we have presented the principles of OFDM multicarrier modulation as used in the conventional MBB service in 4G. Then, the specific new requirements of MMC, MCC, and V2X scenarios foreseen in 5G have been introduced. In this context, the limitations of the OFDM modulation to meet these requirements are highlighted. In MMC, where the uplink is the dominant communication, the synchronization procedure must be relaxed in order to reduce the signalling overhead. Such feature cannot be supported by OFDM if the resulting timing offsets are higher than the CP duration. In MCC, reducing the symbol duration while keeping the same number of symbols in a RB is considered as the most suitable solution to reduce the communication latency. Therefore, the support of mixed-numerology in the same carrier is mandatory. Again, OFDM is limited in this regard due to its low spectral confinement which implies the use of large number of subcarriers as guard-band to avoid severe interference level. In V2X, the high mobility is the main requirement to fulfil. High vehicle speeds, beyond the currently supported by OFDM in 4G/LTE, are foreseen in 5G. In this scenario, ICI becomes significant when using OFDM compromising the orthogonality between users. Therefore, alternative modulation techniques are required to overcome all these scenario-specific limitations.

This introduction is followed then by a technical description of FBMC/OQAM and UF-OFDM waveforms. The contributions of this PhD thesis, presented in subsequent

chapters, are mainly related to these two waveforms. FBMC/OQAM introduces subcarrier filtering stage on top of OFDM and preserves the orthogonality in the real field thanks to the OQAM scheme. The typical low-complexity PPN implementation is detailed. Regarding UF-OFDM, subband-wise filtering is applied. The principles of the transmetter and receiver structres are presented and discussed. For these two waveforms, the key features and differences with respect to OFDM are analyzed. In addition, a brief introduction to other promising candidate waveforms (FC-OFDM, ZT-OFDM, F-OFDM, and BF-OFDM) was provided.

Finally, the chapter has ended by a detailed analysis in order to motivate the use of short prototype filters for FBMC/OQAM waveform. This analysis was supported by relevant recent state-of-the-art techniques. Compared to long PFs, the chapter illustrated how the use of short PFs can bring key advantages in terms of: (1) support of short frame sizes for low-latency communications, (2) low computational complexity, (3) high energy efficiency, and (4) efficient block-based channel estimation. On the other hand, the encountered limitations have been summarized. FBMC/OQAM using short PFs has slightly degraded frequency confinement and it is more sensitive to multipath channel with long delay spread and to timing offset impairments. Nevertheless, original contributions are proposed in the next two chapters to overcome these limitations and improve the robustness of FBMC/OQAM using short PFs.

CHAPTER

2 Novel short prototype filter for FBMC

FBMC/OQAM has been considered in recent research projects as one of the most promising waveform candidates to cope with the new 5G air interface requirements. It exhibits better spectral shape and improves mobility support compared to OFDM thanks to the use of a time and frequency localized PF. In fact, the choice of this filter can impact significantly the different performance levels in addition to the frame structure of the communication system. Furthermore, the length of the prototype filter impacts considerably the transceiver complexity and the latency. Therefore, careful design of new prototype filters is of high interest to improve the robustness of FBMC/OQAM against channel impairments and to support the new requirements introduced by 5G scenarios. In this context, a novel short prototype filter is proposed and presented in this chapter. The proposed filter allows for near perfect reconstruction and having the same size as one OFDM symbol.

The chapter starts by presenting the existing two implementations in the literature for FBMC/OQAM transceivers, PPN and FS based implementations. Then, the proposed novel short prototype filter is presented together with relevant state-of-the-art filters for FBMC/OQAM. Finally, several performance metrics are evaluated and compared to illustrate the benefits of the proposed contribution.

2.1 FBMC/OQAM transceivers

FBMC is a multicarrier transmission scheme that introduces a filter-bank to enable efficient pulse shaping for the signal conveyed on each individual subcarrier. This additional element represents an array of band-pass filters that separate the input signal into multiple components or subcarriers, each one carrying a single frequency sub-band of the original signal. As a promising variant of filtered modulation schemes, FBMC, originally proposed in [26] and also called OFDM/OQAM [24] or Staggered Modulated Multitone (SMT) [76], can potentially achieve a higher spectral efficiency than OFDM since it does not require the insertion of a CP. Additional advantages include the robustness against highly variant fading channel conditions and imperfect synchronization by selecting the appropriate PF type and coefficients [28].

The usage of digital polyphase filter bank structures [23] [24], together with the rapid growth of digital processing capabilities in recent years have made FBMC a practically feasible approach.

In the literature, two types of implementation for the FBMC modulation exist, each having different hardware complexity and performance. The first one is the PPN implementation [30] which is based on an IFFT and a PPN for the filtering stage, and enables a low complexity implementation of the FBMC transceiver. This implementation is illustrated in Figure 1.6 in Chapter 1, Section 1.2.1.

The second type of implementation is the FS implementation, proposed in [33], with the PF with an overlapping factor equal to 4 considered for FBMC during PHYDYAS project [77]. The original idea was to shift the filtering stage into the frequency domain, in order to enable the use of a low-complexity per-subcarrier equalizer as in OFDM. The hardware complexity is supposed to be higher than the complexity of the PPN implementation, at least for long PFs. In fact, it requires one FFT of size $L = KM$ per FBMC symbol, where K is the overlapping factor of the PF, and M is the total number of available subcarriers. However, in the short PF case ($K = 1$), the size of the FFT is same as for the PPN implementation.

The rest of the section provides a mathematical background of the PPN-FBMC transceiver and the FS-FBMC receiver.

2.1.1 PolyPhase Network FBMC transceiver

If M is the total number of available subcarriers and $a_n(m)$ the PAM symbol at subcarrier index m and time slot n, then the baseband signal $s(k)$ can be mathematically decomposed as follows:

$$s(k) = \sum_{n=-\infty}^{+\infty} g(k - n\frac{M}{2})\, x_n(k), \tag{2.1}$$

$$x_n(k) = \sum_{m=0}^{M-1} (-1)^{nm} a_n(m)\phi_n(m)e^{i2\pi\frac{km}{M}}, \tag{2.2}$$

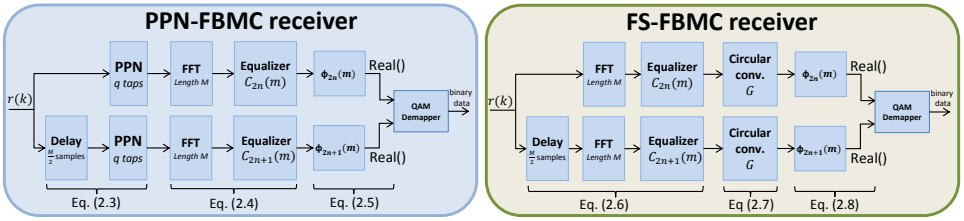

Figure 2.1 — System description of the PPN and FS implementations of the FBMC receivers.

with $i^2 = -1$. To keep the orthogonality in the real field, $\phi_n(m)$ must be a quadrature phase rotation term. In the literature, it is generally defined as $\phi_n(m) = i^{n+m}$, as in [28]. The impulse response of the PF is g, with $g(l) = 0$ when $l \notin [0, L-1]$, where L is the length of the PF. In practice, the PPN-FBMC transmitter is implemented using an IFFT of size M followed by a PolyPhase Network. When a short PF is used ($K = 1$), this latter can be seen as a windowing operation: the outputs of the IFFT are simply multiplied by the PF impulse response g. Consequently, the complexity overhead introduced by the PPN is limited. Note that, due to the OQAM scheme, the obtained FBMC symbol overlaps with both the previous and next symbols on half of the symbol length. Therefore, for practical implementation, 2 FBMC symbols may be generated in parallel. It is however possible to avoid the use of two IFFT blocks at the transmitter side through the use of the pruned FFT algorithm. This leads to a reduced-complexity implementation presented in [32].

Receiver side implementation applies dual operations with respect to the ones performed by the constituent blocks of the transmitter. The IFFT must be replaced by an FFT, and the operations order must be reversed: PPN (windowing if $K = 1$), FFT then OQAM demapper, as shown in Figure 2.1. If r is the received signal and $\hat{a}_n(m)$ are the recovered PAM symbols, then we have:

$$u_n(m) = \sum_{l=0}^{K-1} g(k + lM)\, r\left(k + \frac{M}{2}(2l + n)\right). \tag{2.3}$$

$$U_n(m) = C_n(m) \sum_{k=0}^{M-1} u_n(m) e^{i2\pi \frac{km}{M}}. \tag{2.4}$$

$$\hat{a}_n(m) = \Re\left(\phi_n^*(m) U_n(m)\right). \tag{2.5}$$

where $*$ represents the complex conjugate operation, and $C_n(m)$ is the ZF equalizer coefficient to compensate the impairments introduced by the channel. Note that, contrary to transmitter side, doubling the FFT processing cannot be avoided using the pruned FFT algorithm. The main reason is that the equalization term $C_n(m)$ introduces complex valued coefficients.

2.1.2 Frequency-Spread FBMC receiver

The FS-FBMC implementation is generally considered at the receiver side, since it enables a low-complexity and efficient equalization scheme [78] [79]. It remains perfectly

compatible with the PPN implementation at the transmitter side. The received symbols are expressed as follows:

$$X_n(m) = C_n(m) \sum_{k=0}^{L-1} r(k + n\frac{M}{2}) e^{-i\frac{2\pi}{L}km} \tag{2.6}$$

$$Y_n(m) = \sum_{l=-\frac{L}{2}}^{\frac{L}{2}-1} G(l) X_n(m-l) \tag{2.7}$$

$$\hat{a}_n(m) = \Re\Big(Y_n(Km)\phi_n^*(m)\Big) \tag{2.8}$$

where G is the frequency response of the PF. The FS-FBMC receiver first applies an IFFT of size L on the part of the r signal containing the FBMC symbol to demodulate in order to obtain the X_n signal in frequency domain (2.6). Then, it introduces a filtering stage in frequency domain, as described in (2.7): the frequency response of the PF G is convoluted with the X_n signal, for instance using a Finite Impulse Response (FIR) filter. Finally, the recovered PAM symbols are obtained by extracting the real part of quadrature phase rotated and down-sampled Y_n samples (2.8).

These operations are summarized and illustrated in Figure 2.1. The FS-FBMC implementation seems highly complex, however G has a lot of zero coefficients due to its frequency localization. Therefore, it can be truncated down to N_G coefficients. Then, by defining $\Delta = (N_G - 1)/2$ (N_G is considered an odd number), (2.7) becomes

$$Y_n(m)(k) = \sum_{l=-\Delta}^{\Delta-1} G(l) X_n(m-l).$$

2.2 Design of a novel short prototype filter

Previous section has clearly indicated the interest for the development of short filters for FBMC modulation. Therefore, a section is dedicated to the study of such filters. Indeed, after a short description of the two already existing short filters in the literature, we present a new short filter design that shows significant advantages in terms of performance and complexity.

2.2.1 MMB4 long prototype filter

A specific design procedure for FBMC PFs was introduced by K. W. Martin in 1998 [80] and improved later by M. Bellanger [81] and S. Mirabbasi [82]. The particularity of this procedure concerns the direct design of the PF in frequency domain. The frequency domain coefficients of the PF are adjusted so that a high stopband attenuation is obtained and Nyquist criteria is approximately met. Therefore, the signal transmitted through a FBMC scheme employing this PF cannot be perfectly recovered at the receiver side. However, the level of the resulting interference can be considered negligible, hence the near perfect reconstruction property of the PF. If K is the overlapping factor of the PF,

Table 2.1 — Obtained k_l coefficients for different overlapping factors.

Coefficients	$K = 3$	$K = 4$	$K = 6$	$K = 8$
k_0	$+1$	$+1$	$+1$	$+1$
k_1	-0.91143783	-0.97195983	-0.99722723	-0.99988389
k_2	$+0.41143783$	$+0.70710681$	$+0.94136732$	$+0.99315513$
k_3		-0.23514695	-0.70710681	-0.92708081
k_4			$+0.3373834$	$+0.70710681$
k_5			-0.07441672	-0.37486154
k_6				$+0.11680273$
k_7				-0.01523841

and M is the maximum number of subcarriers, then the frequency response G of the PF is expressed as:

$$G(l) = \begin{cases} k_{|l|} & l \in [\![-(K-1), K-1]\!] \\ 0 & l \notin [\![-(K-1), K-1]\!] \end{cases} \tag{2.9}$$

where k_l are the coefficients to design. The impulse response g of the PF can be obtained by applying an IFFT on the coefficients of the frequency response G. After simplifications and neglecting the normalization term in $1/M$, the following analytical expression is obtained for g:

$$g(k) = k_0 + 2\sum_{l=1}^{K-1} k_l \cos\Big(\frac{2l\pi k}{M}\Big). \tag{2.10}$$

In addition, the following relation between the coefficients k_l must be ensured to obtain a high stopband attenuation [81]:

$$k_0 + \sum_{k=1}^{K-1} k_1 = 0.$$

In addition, the Nyquist criteria is almost respected if [81]:

$$\begin{cases} k_0 = 1 \\ k_l^2 + k_{K-l}^2 = 1 \quad l \in [\![1, K-1]\!] \end{cases} \tag{2.11}$$

The above system of equations can be easily solved for $K = 3$ and $K = 4$. For K values higher than 4, the exact coefficients values have not been derived. Instead, an optimization problem must be solved, as described in [80]. The obtained filter coefficients for different overlapping factor values are presented in Table 2.1.

The PF obtained with $K = 4$ was extensively used in the PHYDYAS European research project [77], and in the literature in general, to study the FBMC/OQAM waveform. In this manuscript, this PF is referred to as Martin–Mirabassi–Bellanger 4 (MMB4), from the name of the authors having contributed to its design. This choice of K is due to the high SIR level of ≈ 70 dB [83] [80], depending on the chosen waveform parameters, enabling almost orthogonal transmission. In addition, it has a very low OOBPL, since only 1 subcarrier acting as guard-band is required to isolate two users occupying adjacent frequency resources [84] [69]. Lastly, having a simple closed-form ex-

Table 2.2 — X_i coefficients of the analytical expression of the TFL1 PF.

l	X_l	l	X_l
0	4.1284847578	4	$-2.1107642825\,10^{1}$
1	1.9727736832	5	$-6.6774831778\,10^{-3}$
2	$1.2781855004\,10^{-1}$	6	$-1.0150558822\,10^{2}$
3	$-1.4505800309\,10^{2}$	7	$1.9143799092\,10^{-2}$

pression is an interesting feature, since it simplifies its implementation without requiring specific skills in PF design.

2.2.2 TFL1 and QMF1 short prototype filters

The Time Frequency Localization 1 (TFL1) PF was the first attempt to specifically design a time and frequency localized short PF for the FBMC modulation [85]. It is the most known short PF in the literature. Indeed, it is already integrated into a proof-of-concept hardware platforms [86]. The analytical expression of the TFL1 PF [87] is given by:

$$g(k) = \frac{\pi}{2}(1-x) + \gamma_0 t + 2t(t^2-1)(\beta_1 + 4\beta_2 t^2),$$

where $x = \frac{2k+1}{M}$ with $k \in [0, \frac{M}{2} - 1]$, $t = 2x - 1$ and

$$\begin{aligned}
\gamma_0(k) &= \frac{1}{X_0 + X_1 \frac{M}{2}} \\
\beta_1(k) &= X_2 + \frac{1}{X_3 + X_4 \frac{M}{2}} \\
\beta_2(k) &= X_5 + \frac{1}{X_6 + X_7 \frac{M}{2}},
\end{aligned}$$

X_l being defined in Table 2.2. The second half of the PF coefficients are constructed by symmetry: $g(k) = g(M-k-1)$ for $k \in [\frac{M}{2}, M-1]$.

Regarding the Quadrature Mirror Filter 1 (QMF1) PF [55], it was applied to FBMC leading to a variant denoted by Lapped-OFDM modulation presented in [88]. The analytical expression of the QMF1 PF is given below:

$$g(k) = \sin\left(\frac{\pi k}{M}\right). \tag{2.12}$$

2.2.3 Proposed NPR1 short prototype filter

This sub-section describes a novel short PF representing one of the major contributions of this manuscript. The main design procedure of the proposed PF starts by inverting the time and frequency axes of the Filter-Bank (FB) impulse response of the MMB4 PF. The coefficients of this FB impulse response are given in [83] and presented in Table 2.3. It can be seen that the FB impulse response of the MMB4 FB is highly localized in frequency since interference is limited only to one adjacent subcarrier (indexes $p = -1$ and $p = 1$)

Table 2.3 — Filter-bank impulse response of the MMB4 filter.

q \ p	-1	0	1
$-\frac{3M}{2}$	$i\,0.043$	-0.067	$-i\,0.043$
$-M$	-0.125	0	-0.125
$-\frac{M}{2}$	$-i\,0.206$	0.564	$i\,0.206$
0	0.239	1	0.239
$\frac{M}{2}$	$i\,0.206$	0.564	$-i\,0.206$
M	-0.125	0	-0.125
$\frac{3M}{2}$	$-i, 0.043$	-0.067	$i\,0.043$

in the frequency plane. Inverting the time (q) and frequency (p) axes will generate a PF highly localized in time, since the obtained FB impulse response coefficients have values only at the adjacent FBMC symbols ($q = -M/2$ and $q = M/2$). Therefore, a PF with an overlapping factor of 1 is sufficient to obtain these coefficients. Consequently, the PF coefficients can be deduced from a given FB impulse response.

By definition, the FB impulse response is composed of the values obtained at the output of the receiver $U_n(m)$ from (2.4) by setting $a_0(0) = 1$ and $a_n(m) = 0$ when $(n, m) \neq (0, 0)$. In this case, we have $r(k) = g(k)$, and $Y_n(m)$ in (2.4) becomes:

$$U_n(m) = \sum_{k=0}^{M-1} g(k)g(k + n\frac{M}{2})\, e^{-i\frac{2\pi km}{M}}. \tag{2.13}$$

Furthermore, we have $U_n(m) = F_{g_{MMB4}}(n, m)$, where $F_{g_{MMB4}}(p, q)$ is the FB impulse response coefficients of the MMB4 PF presented in Table 2.3. Particularly, for $n = 0$, we have:

$$U_0(m) = \sum_{k=0}^{M-1} g(k)^2\, e^{-i\frac{2\pi km}{M}}. \tag{2.14}$$

Thus, g can be deduced as follows:

$$g(k) = \sqrt{\sum_{l=-K_{MMB4}}^{K_{MMB4}-1} F_{g_{MMB4}}(0, l\frac{M}{2})\, e^{i\frac{2\pi kl}{M}}} \tag{2.15}$$

with $K_{MMB4} = 4$ is the overlapping factor the MMB4 PF. Then, the design procedure introduces simplifications to obtain a simpler analytical expression, by taking advantage of the real valued and symmetrical $F_{g_{MMB4}}$ coefficients:

$$g(k) = \sqrt{1 - 2\sum_{l=0}^{2} P_g(l)\cos\Big(\frac{2\pi k(2l+1)}{M}\Big)} \tag{2.16}$$

$$P_g(0) = 0.564447$$

$$P_g(1) = -0.066754$$

$$P_g(2) = 0.002300$$

We call the resulting proposed short PF with overlapping factor equal to 1 as Near

Perfect Reconstruction 1 (NPR1) due to its nature, similar to the MMB4 PF. To analytically calculate the residual interference, the recovered PAM symbols $\hat{a}_n(m)$ must be expressed by taking into account the transmitted $a_n(m)$ symbols and the effect of the PF at the transmitter. Thus, by setting $r(k) = s(k)$ and by integrating equations (2.1), (2.3) and (2.4) into (2.5), we have

$$\hat{a}_n(m) = \Re\left[\phi_n^*(m) \sum_{k=0}^{M-1} g(k) \times \sum_{n'=-\infty}^{+\infty} g\Big(k + (n-n')\frac{M}{2}\Big) x_{n'}\Big(k + n\frac{M}{2}\Big) e^{-i2\pi\frac{km}{M}}\right] \tag{2.17}$$

Due to the time localization of the PF, we have $(n - n') = q \in [\![-Q, Q]\!]$, Q being the number of FBMC symbols acting as interference after (or before) the FBMC symbol currently demodulated. Typically, we have $Q = 1$ for short PFs, since the impulse response of g is equal to zero after M samples. Then, we have:

$$\hat{a}_n(m) = \Re\left[\phi_n^*(m) \sum_{q=-Q}^{Q} \sum_{k=0}^{M-1} g(k) g\Big(k + q\frac{M}{2}\Big) z_{n-q}(k) e^{-i2\pi\frac{km}{M}}\right]$$

with

$$\begin{aligned} z_n(k) &= x_n\Big(k + n\frac{M}{2}\Big) \\ &= \sum_{m=0}^{M-1} a_n(m)\phi_n(m) e^{i2\pi\frac{km}{M}}. \end{aligned}$$

In (2.17), the term corresponding to the FFT of $g(k)g\Big(k + qM/2\Big) \times z_{n-q}(k)$ can be rewritten by a circular convolution operation denoted by $\circledast$, as follows:

$$\hat{a}_n(m) = \Re\left[\phi_n^*(m) \sum_{q=-Q}^{Q} \Big(F_g(m,q) \circledast Z_{n-q}(m)\Big)\right],$$

with

$$\Big(F_g(m,q) \circledast Z_{n-q}(m)\Big) = \sum_{p=-\frac{M}{2}}^{\frac{M}{2}-1} F_g(p, q\frac{M}{2}) Z_{n-q}(m-p),$$

where $F_g(p,q)$ and $Z_n(m-p)$ are the results of the application of a FFT to the terms $g(k)g(k+q)$ and $z_{n-q}(k)$, respectively expressed as:

$$F_g(p,q) = \sum_{k=0}^{M-1} g(k)g(k+q) e^{-i2\pi\frac{pk}{M}}, \tag{2.18}$$

and,

$$Z_n(m) = a_n(m)\phi_n(m).$$

Finally, the expression of the recovered PAM symbol $\hat{a}_n(m)$ becomes:

$$\begin{aligned}\hat{a}_n(m) &= \Re\left[\sum_{(p,q)\in\Omega} \phi_n^*(m)\phi_{n-q}(m-p)F_g(p,q\frac{M}{2}) \times a_{n-q}(m-p)\right], \\ &= \Re\left[\sum_{(p,q)\in\Omega} i^{-q-p}F_g(p,q\frac{M}{2})a_{n-q}(m-p)\right]\end{aligned}$$

with $\Omega = [\![-M/2, M/2-1]\!] \times [\![-Q, Q]\!]$. In fact, $F_g(p,q)$ is the FB impulse response of g, and for the NPR1 PF, we have $F_{g_{NPR1}}(p,q) = F_{g_{MMB4}}(q,p)$. If $a_n(m)$ symbols are independent and identically distributed random variables and $\mathbb{E}(a_n(m)) = 0$, then the residual interference of the PF can be evaluated as follows:

$$\begin{aligned}\text{SIR}_{\text{NPR}} &= \frac{\mathbb{E}\Big(\Re\Big(F_g(0,0)a_n(m)\Big)^2\Big)}{\mathbb{E}\Big((F_g(0,0)a_n(m) - \hat{a}_n(m))^2\Big)} \\ &= \frac{\Re\Big(F_g(0,0)\Big)^2}{\sum_{(p,q)\in\Omega^0} \Re\Big[i^{p+q}F_g(p,q\frac{M}{2})\Big]^2}\end{aligned} \tag{2.19}$$

with $\Omega^0 = \Omega \setminus \{(0,0)\}$. For $M = 512$, and using the coefficients presented in [80] to design the MMB4 PF and the related FB impulse response, we have $F_g(0,0) = 1$ and the obtained SIR is 73 dB for the proposed NPR1 PF. This SIR has the same order of magnitude as the SIR of the MMB4 PF ($\approx$ 70 dB [83] [80]), confirming the near perfect reconstruction nature of the proposed short filter.

2.3 Performance evaluation and comparisons

This section evaluates and compares the performance of the proposed NPR1 short PF with respect to SoTA ones. It provides a comparison of different FBMC short PFs, including the proposed one, in terms of spectral usage and SIR when applying a truncated FS implementation. Their robustness against several types of channel impairments is also evaluated and compared with OFDM, for both PPN and FS implementations. These impairments include timing synchronization errors, carrier frequency offset and the use of a multipath channel.

2.3.1 Comparison of out-of-band power leakage

One of the main advantages of FBMC over OFDM resides in its spectrum shape with low OOBPL. Consequently, a shorter guard-band can be used to fit the adjacent channel leakage ratio (ACLR) constraints and to support relaxed synchronization communication services. In general, long PFs have lower OOBPL when compared to short PFs on one side, but lose the other advantages of short PFs provided in the Section 1.3 of Chapter 1 on the other side.

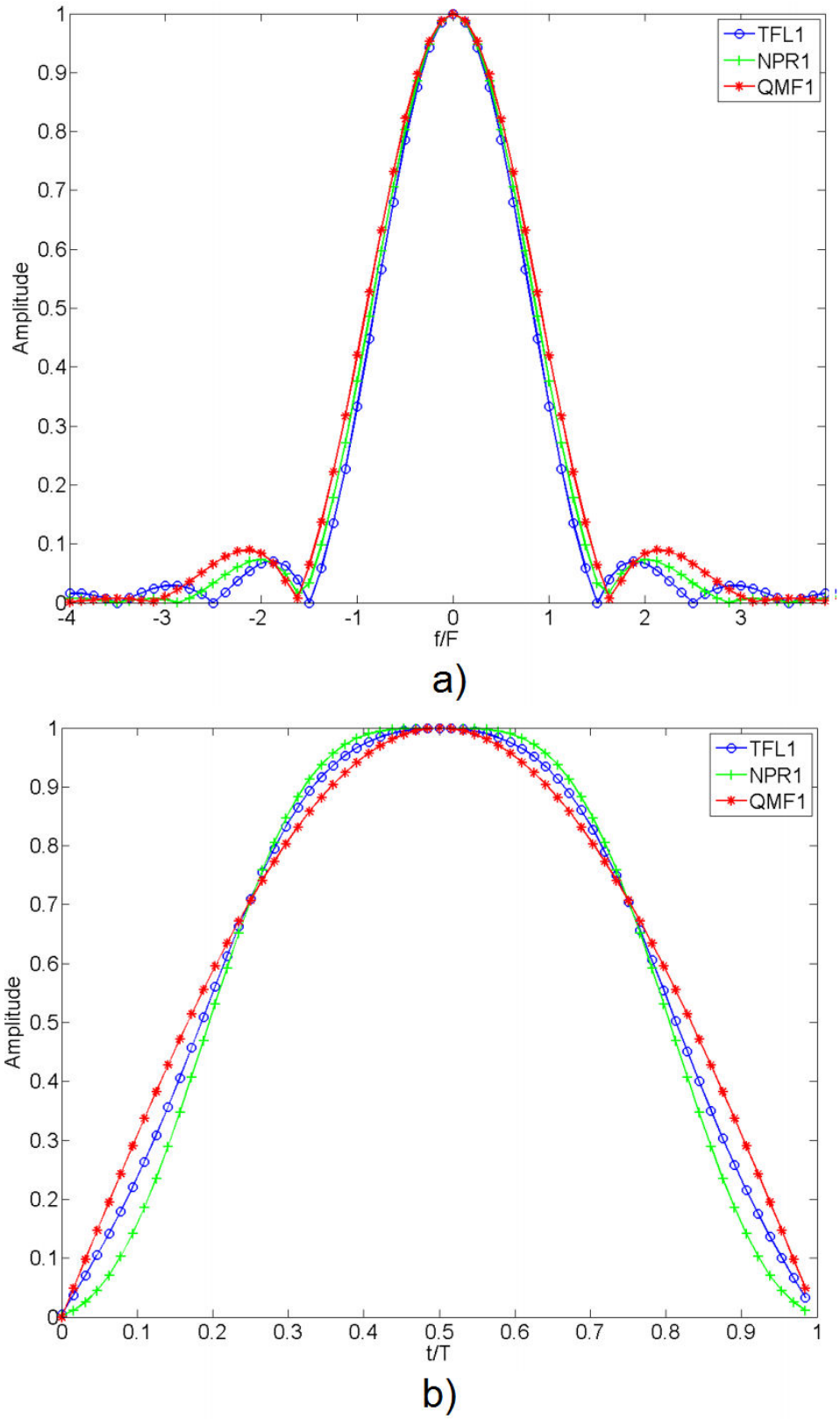

Figure 2.2 — Frequency response a) and impulse response b) of the TFL1, QMF1 and NPR1 PFs.

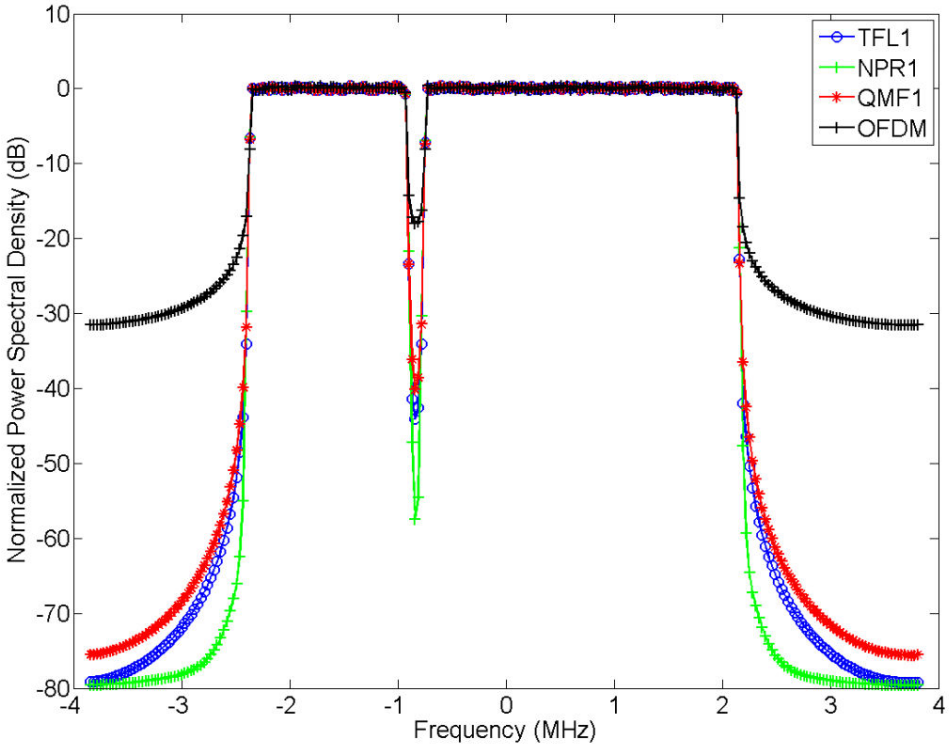

Figure 2.3 — PSD evaluation of FBMC using short PFs in a 4.5 MHz bandwidth.

However, depending on the chosen short PF, the spectral characteristics may vary. The frequency response of the QMF1 PF, depicted in Figure 2.2a, has the secondary lobes with the highest amplitude, followed by TFL1 then NPR1 PF. This explains the reasons behind the differences in the OOBPL depicted in Figure 2.3. Indeed, this figure shows the power spectral density of OFDM and FBMC with different short PFs, on a 4.5 MHz bandwidth. Simulation parameters correspond to a 4G/LTE setting were a notch of 12 subcarriers, or 1 Ressource Block (RB), was inserted in the spectrum to evalute the capacity to support fragmented spectrum for asynchronous communication services.

As expected, the OOBPL is extremely low for FBMC: a gap of 59 dB can be observed between OFDM and FBMC at the extreme edges of the bandwidth, independently from the used PF. For NPR1 case, the OOBPL quickly decreases when compared to the other PFs, since it has the lowest secondary lobes (Figure 2.2a). Inside the notch, a gap of 40 dB can be observed between OFDM and FBMC with NPR1 PF, and a difference of 17 dB between this PF and QMF1. These results demonstrate that, despite using a short PF, the OOBPL is still very low for FBMC when compared to OFDM, even in a fragmented band. In conclusion, NPR1 represents the most suitable short PF to respect high ACLR constraints.

2.3.2 Truncation impact on the frequency response of the filter

The frequency response of the PF can be truncated to reduce the complexity of the FS-FBMC receiver. By truncating the frequency response of the PF at the receiver side, interference may appear due to a non perfect reconstruction, resulting in performance

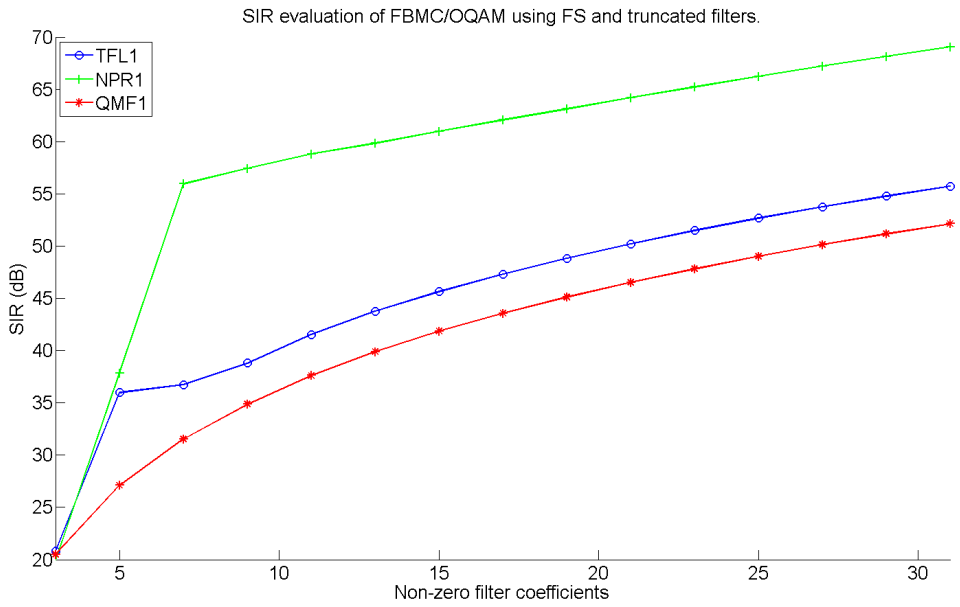

Figure 2.4 — Evaluation of the impact of N_G (number of non-zero filter coefficients) on the SIR for different PFs.

degradation. However, if N_G, the number of non-zero coefficients, is too high, the resulting FS implementation will require important hardware complexity. A compromise between complexity and performance must be devised.

Equation (2.19) can be adapted to evaluate the residual interference introduced by the truncation. In this case, the PF impulse response g is replaced by the truncated one $\tilde{g}$ in (2.17), where $\tilde{g}$ is expressed as follows:

$$\tilde{g}(k) = \sum_{l=-\Delta}^{\Delta} G(l) e^{i2\pi \frac{kl}{M}}. \tag{2.20}$$

The values of $\tilde{g}$ are obtained by computing an IFFT of size M on the N_G non-zero coefficients of G. Then, using similar mathematical development as described in Subsection 2.2.3 from (2.17), the analytic expression of the SIR is:

$$\mathrm{SIR}_{\mathrm{trunc}} = \frac{\Re\Big(F_{g,\tilde{g}}(0,0)\Big)^2}{\sum_{(p,q)\in\Omega^0} \Re\Big[i^{p+q} F_{g,\tilde{g}}(p, q\frac{M}{2})\Big]^2} \tag{2.21}$$

where $F_{g,\tilde{g}}(p,q)$ is the FB impulse response using the PF g at the transmitter side and the PF $\tilde{g}$ at the receiver side. It is expressed as follows:

$$F_{g,\tilde{g}}(p,q) = \sum_{k=0}^{M-1} g(k+q)\tilde{g}(k) e^{-i2\pi \frac{pk}{M}}. \tag{2.22}$$

The obtained numerical values of the SIR are presented in Figure 2.4 for different PFs and corresponding N_G values. The analytical results of (2.21) have also been confirmed

Table 2.4 — N_G values needed to reach target SIR for different PFs.

SIR (dB)	TFL1	NPR1	QMF1
50	23	7	29
55	31	7	41
60	45	15	59
65	65	23	83
70	91	35	115

by simulations. Table 2.4 summarizes the needed number of non-zero coefficients for a SIR target ranging between 50 and 70 dB, depending on the used PF.

The 70 dB target SIR may be interesting to consider as it corresponds to the nearly perfect reconstruction case of the MMB4 PF, but it requires a large number of coefficients (35 for NPR1). In practice, a SIR due to truncation of 55 dB may be sufficient since channel impairments already degrade the resulting SIR, as illustrated in the next subsections. For the rest of the chapter, N_G is chosen so that each PF has the same SIR of 55 dB, enabling a fair comparison. Therefore, we have:

- $N_G = 31$ for TFL1.
- $N_G = 7$ for NPR1.
- $N_G = 41$ for QMF1.

The TFL1 and QMF1 PFs require more than 30 non-zero coefficients to obtain this SIR target for a FS implementation. Such high number of coefficients may not be acceptable if a low complexity receiver is targeted. For the NPR1 PF, only 7 coefficients are required for the NPR1 to achieve a SIR up to 55 dB, making it better suited for the FS implementation.

2.3.3 Robustness against timing offset

Timing offset impairment occurs when the transmitter and receiver baseband samples are not perfectly aligned in time. It is always the case in practice, since the channel introduces a propagation delay. Therefore, timing synchronization algorithms must be employed. In 4G/LTE uplink case, the timing synchronization is realized using time advance mechanism [89] to compensate the propagation delay of each UE located at different geographical distance from the base station. However, new highly demanding scenarios like massive machine communications are considered in 5G. To reduce energy consumption and to improve spectral usage, time advance mechanism should be avoided and relaxed synchronization should be supported, where the propagation delay of each UE is not compensated. Therefore, synchronization errors appear, which causes two types of impairments:

1. Linear phase rotation for each subcarrier due to the additional delay. This effect can be totally compensated after channel estimation and equalization. Indeed, if l_d is the time offset in number of samples, then the frequency domain compensation term is expressed as $C_{TO}(m) = e^{-i\frac{2\pi m l_d}{M}}$.

2. ISI and ICI due to PF misalignment between the transmitter and the receiver.

It is considered, in this paper, that the OFDM signal is synchronized ($l_d = 0$) at the middle of its cyclic prefix. If $-\frac{L_{CP}}{2} < l_d < \frac{L_{CP}}{2}$, where L_{CP} is the length of the CP, then orthogonality is perfectly restored, since a circular shift in time domain represents a linear phase rotation in frequency domain. In 4G/LTE, $\frac{L_{CP}}{M} = 7\%$ for OFDM. Thus, orthogonality is still guaranteed if $|\frac{l_d}{M}| < 3.5\%$, where $|.|$ represents the absolute value operator.

Due to the absence of CP in a FBMC system, timing offset will result in unavoidable performance degradation. However, depending on the PPN or FS implementation, results are different due to the application of different timing offset compensation techniques. For the FS implementation, the compensation step lies between the FFT and the FS filtering stage, whereas in the PPN case, it is performed after the PPN and the FFT.

For the PPN-FBMC case, the SIR expression in (2.17) can be adapted to obtain the expression of the recovered PAM symbol when a timing offset of l_d samples is applied, as follows:

$$\begin{aligned}\hat{a}_n(m) &= \Re\left[C_{TO}(m)\phi_n^*(m)\sum_{q=-Q}^{Q}\sum_{k=0}^{M-1} g(k)g\Big(k+q\frac{M}{2}+l_d\Big)x_{n-q}\Big(k+n\frac{M}{2}+l_d\Big)e^{-i2\pi\frac{km}{M}}\right] \\ &= \Re\left[\sum_{(p,q)\in\Omega} i^{-q-p}F_g(p,q\frac{M}{2}+l_d)a_{n-q}(m-p)e^{-i2\pi\frac{pl_d}{M}}\right], \end{aligned} \tag{2.23}$$

and the expression of the SIR becomes:

$$\mathrm{SIR}_{\mathrm{PPN}}(l_d) = \frac{\Re\Big(F_g(0,l_d)\Big)^2}{\sum_{(p,q)\in\Omega^0}\Re\Big[i^{p+q}F_g(p,q\frac{M}{2}+ld)e^{-i2\pi\frac{pl_d}{M}}\Big]^2} \tag{2.24}$$

Note that the number of FBMC symbols acting as interference denoted by Q must be set to 2. Indeed, when a timing offset is considered, the FBMC symbols at $q = -M$ and $q = M$ are now acting as interference. Therefore, the obtained numerical values are similar to that obtained by simulation in Figure 2.5. Concerning the FS-FBMC receiver, it has been evaluated in [90], where the following expression is obtained:

$$\mathrm{SIR}_{\mathrm{FS}}(l_d) = \frac{1}{\Big(\frac{\sigma_{INT}}{\sigma_a}\Big)^2 + 2\sum_{l=0}^{l_d-1} g^2(l)}, \tag{2.25}$$

where σ_{INT}^2 is the power of the residual interference when $l_d = 0$. In our case, the residual interference comes from the NPR nature of the PF and the truncation applied on the filter coefficients. Therefore, we have:

$$\Big(\frac{\sigma_{INT}}{\sigma_a}\Big)^2 = \sum_{(p,q)\in\Omega^0}\Re\Big[i^{p+q}F_{g,\tilde{g}(k)}(p,q)\Big]^2$$

Figure 2.5 shows SIR values for each considered short PF using the FS-FBMC receiver. The N_G parameters used for the PFs are those defined in Sub-section 2.3.2. It is clear

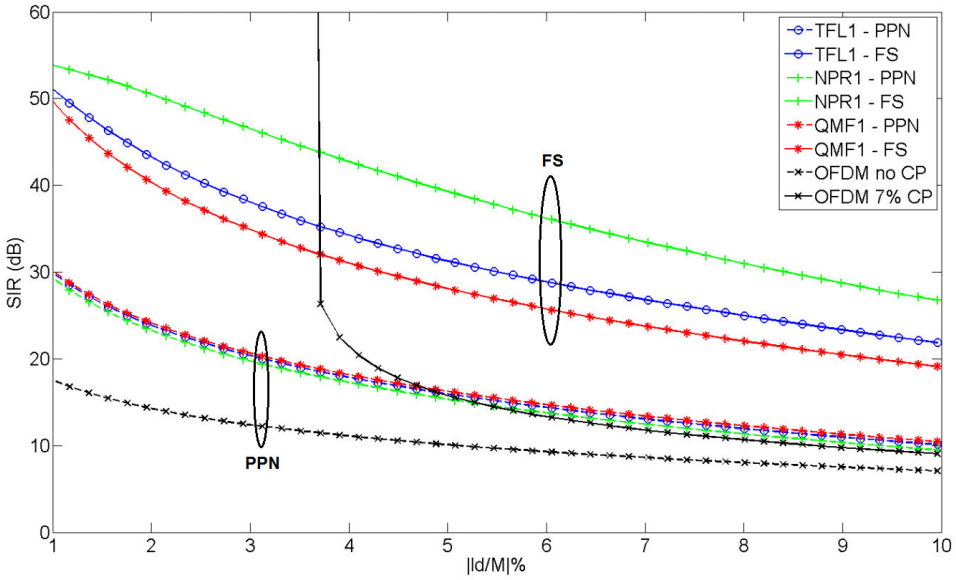

Figure 2.5 — Timing offset evaluation in terms of measured SIR for OFDM and FBMC with the considered short PFs. The effect of different implementations is also evaluated.

that independently from the used PF, the FS implementation outperforms the PPN one, a result that was already demonstrated for the case of the MMB4 PF [79] and the QMF1 PF [88]. When using the PPN implementation, the timing offset error compensation is done in frequency domain, thus after the filtering stage. This lowers the compensation efficiency, causing ICI and ISI as mentioned above. In case of the FS implementation, the compensation is more efficient since the filtering stage is performed in frequency domain, after compensation of the timing offset error. This explains the gap in performance between PPN and FS implementations.

A gain of more than 10 dB can be observed with NPR1 PF when compared to QMF1 PF for timing offset inferior to 5%, and 8 dB when compared to TFL1 PF. Around 3 dB of difference is visible between TFL1 and QMF1 PFs. From (2.25), it is clear that the NPR1 achieves a higher SIR than the other PFs. Figure 2.2 shows the impulse response of each PF. It can be observed that the amplitude of the NPR1 impulse response is lower at its edges. Therefore, the term $\sum_{l=0}^{l_d-1} g^2(l)$ has the lowest value for NPR1, confirming its higher robustness against time offset error than the other PFs.

Concerning OFDM, it is clearly outperformed by FS-FBMC implementation when $|\frac{l_d}{M}| > 3.5\%$. A gap of at least 20 dB can be observed between FBMC with NPR1 PF and OFDM. For lower timing offset impairments, FBMC still exhibits acceptable performance since the SIR remains superior to 40 dB for the NPR1 PF.

These results, validated by simulation, point out that the proposed NPR1 is the most interesting PF to combat timing offset impairment due to imperfect timing synchronization. This is particularly interesting to fulfill the relaxed synchronization requirement foreseen in specific 5G communication scenarios like massive machine communications.

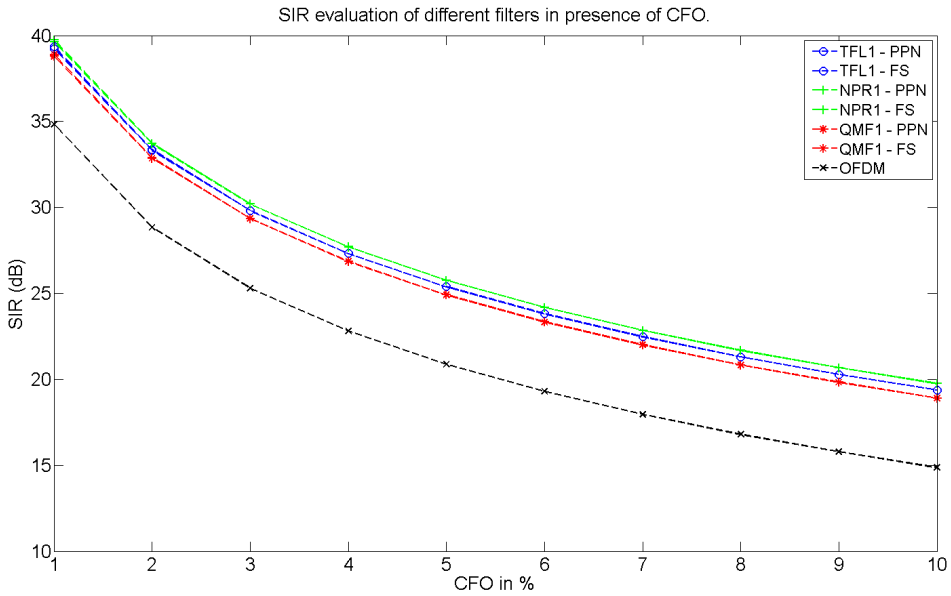

Figure 2.6 — SIR evaluation in presence of CFO.

2.3.4 Robustness against frequency offset

Frequency offset impairment is a common issue in communication systems, and it is the consequence of the transmitter and/or receiver being in a situation of mobility (Doppler Shift/Spread). It also appears when there is a frequency misalignment in local oscillators of the transmitter and the receiver. Mathematically, it corresponds to a linear phase rotation of the received baseband samples. Thus, the received signal r is expressed as

$$r(k) = s(k)e^{-i\frac{2\pi k r}{M}}. \tag{2.26}$$

where $r \in]-\frac{1}{2}, \frac{1}{2}]$ is the CFO value relative to the subcarrier spacing expressed as a percentage. In 4G/LTE downlink case, the CFO is estimated and is compensated in time domain by multiplying the received baseband samples by $e^{i\frac{2\pi k r}{M}}$. However, in 4G/LTE uplink (and related 5G scenarios), it is not possible to compensate it directly in time domain since all baseband signals of all the users overlap. In fact, it generates two types of impairments after demodulation:

1. Common Phase Error (CPE). All the subcarriers in a given symbol experience a phase rotation. The rotation angle is incremented at each received symbol. It can be easily compensated in frequency domain if the CFO is estimated, since the CPE term to compensate is $C_{CPE}(n) = e^{i\pi nr}$.
2. ICI due to misalignment of the transmitter and receiver PFs in frequency domain, also resulting in inter-user interference in 4G/LTE uplink case of related 5G scenarios.

The second described impairment represents a major issue, particularly for OFDM due to its particularly low frequency localization. FBMC is naturally more robust against this type of ICI, especially when using a short PF [28]. Therefore, it is expected that

FBMC provides a higher robustness against CFO than OFDM. This is confirmed in Figure 2.6, which shows the SIR performance in presence of CFO with all the considered PFs, obtained both by numerical and simulation results. The SIR expression can be obtained by adapting equation (2.17), as follows

$$\begin{aligned}\hat{a}_n(m) &= \Re\left[C_{CPE}(n)e^{i\pi nr}\phi_n^*(m)\sum_{q=-Q}^{Q}\sum_{k=0}^{M-1}g(k)g\Big(k+q\frac{M}{2}\Big)x_{n-q}\Big(k+n\frac{M}{2}+l_d\Big)e^{-i2\pi\frac{k(m+r)}{M}}\right]\\ &= \Re\left[\sum_{(p,q)}i^{-q-p}F_g(p+r,q\frac{M}{2})\times\ a_{n-q}(m-p)\right].\end{aligned}$$

Assuming that the interference introduced by the truncation is negligible, the expression of the SIR for both FS-FBMC and PPN-FBMC receivers is

$$\mathrm{SIR}_{\mathrm{CFO}}(r) = \frac{\Re\Big(F_g(r,0)\Big)^2}{\sum_{(p,q)\in\Omega^0}\Re\Big[i^{p+q}F_g(r,q\frac{M}{2})e^{inr}\Big]^2}.$$

Up to 5 dB of SIR can be observed between OFDM and FBMC with the NPR1 PF. This later is also the PF having the highest robustness against CFO. When compared to the TFL1 PF, a difference of ≈ 0.4 dB is observed, and almost 0.9 dB when compared to the QMF1 PF. For this particular channel impairment, PPN-FBMC and FS-FBMC receivers have similar performance. This can be explained by the fact that the compensation term C_{CPE} only depends on the FBMC symbol index. Therefore, it can be integrated before and after the filtering stage without any mathematical difference. The only difference comes from the interference introduced by the filter truncation in FS-FBMC, however the impact on the SIR is negligible. Recently, a low computational complexity Frequency Domain Compensation (FDC) algorithm was proposed for FBMC [91], enabling to greatly reduce the ICI caused by the CFO. This FDC technique represents an interesting advantage for FBMC since it greatly relaxes the frequency synchronization constraint, enabling the support of higher speeds in a mobility situation and enabling the use of a low-cost oscillator for the UEs (particularly the sensors for massive machine communications). This technique is only applicable with the FS-FBMC receiver, since it integrate the Linear Phase Rotation (LPR) term of the CFO into the PF coefficient in frequency domain. Indeed, in presence of CFO and assuming $K = 1$, (2.7) can be rewritten as

$$\begin{aligned}Y_n(m) &= C_{CPE}(n)e^{-i\pi nr}\sum_{k=0}^{M-1}g(k)e^{-i2\pi\frac{kr}{M}}s(k+n\frac{M}{2})e^{-i2\pi\frac{km}{M}}\\ &= \sum_{k=0}^{M-1}g(k)e^{-i2\pi\frac{kr}{M}}s(k+n\frac{M}{2})e^{-i2\pi\frac{km}{M}}.\end{aligned} \tag{2.27}$$

The LPR term introduced by the CFO can be eliminated by replacing $g(k)$ by $g_r(k) =$

$g(k)e^{i2\pi\frac{kr}{M}}$ in the above equation, which becomes

$$\begin{aligned} Y_n(m) &= \sum_{k=0}^{M-1} g_r(k)e^{-i2\pi\frac{kr}{M}} s(k+n\frac{M}{2})e^{-i2\pi\frac{km}{M}} \\ &\approx \sum_{l=-\Delta_r}^{\Delta_r} G_r(l) \sum_{k=0}^{M-1} s(k+n\frac{M}{2})e^{-i2\pi\frac{kr}{M}} e^{-i2\pi\frac{k(m-l)}{M}} \end{aligned} \tag{2.28}$$

where $\Delta_r = (N_{G,r}-1)/2$, $N_{G,r}$ being the number of significant coefficients to represents the frequency shifted response of the PF G_r. The latter is expressed as

$$G_r(l) = \sum_{k=0}^{L-1} g_r(k)\, e^{-2i\pi\frac{km}{M}} \tag{2.29}$$

Assuming that the CFO is perfectly estimated, it can be theoretically compensated if $\Delta_r = M/2-1$, but it leads to a considerable complexity increase. Thus, the G_r must be truncated down to a reasonable number of coefficients. Then, interference is introduced, which can be evaluated by adapting equation (2.17) as follows

$$\begin{aligned} \hat{a}_n(m) &= \Re\left[\phi_n^*(m) \sum_{q=-Q}^{Q} \sum_{k=0}^{M-1} \left(g_r(k) g\Big(k+q\frac{M}{2}\Big) x_{n-q}\Big(k+n\frac{M}{2}+l_d\Big) e^{-i2\pi\frac{k(m+r)}{M}} \right)\right] \\ &= \Re\left[\sum_{(p,q)\in\Omega} i^{-q-p} F_{g,g_r}(p+r, q\frac{M}{2}) a_{n-q}(m-p)\right] \end{aligned}$$

with

$$F_{g,g_r}(p,q) = \sum_{k=0}^{M-1} g(k+q)g_r(k)e^{-i2\pi\frac{pk}{M}}. \tag{2.30}$$

Figure 2.7 shows the obtained SIR numerical values for $r \in [0, \frac{1}{2}]$. For this particular case, the number of significant PF coefficients is fixed to $\Delta_r = 3$ for all the PFs. The NPR1 PF achieves better SIR than the 2 other PFs when $r < 0.35$. As evaluated in Subsection 2.3.2, the number of non-zero coefficient $N_{G,r} = 7$ is insufficient to obtain a SIR value higher than 50 dB. Surprisingly, the FDC technique reduces the interference level when the CFO is increased for the QMF1 and the TFL1 PFs. Particularly, the QMF1 PF has an infinite SIR when $r = 1/2$, for at least $N_{FDC} = 2$ non-zero coefficients. Indeed, the analytical expression of the frequency shifted QMF1 PF becomes

$$\begin{aligned} G_{\frac{1}{2}}(k) &= \sum_{k=0}^{M-1} \sin\Big(\frac{\pi k}{M}\Big) e^{i2\pi\frac{kr}{M}} \\ &= \frac{1}{2i} \sum_{k=0}^{M-1} (1-e^{-i\frac{2\pi k}{M}}) e^{-i\frac{2\pi}{L}ki} \\ &= \frac{M}{2i}\Big(\delta(k) - \delta(M-1-k)\Big) \end{aligned} \tag{2.31}$$

$$\tag{2.32}$$

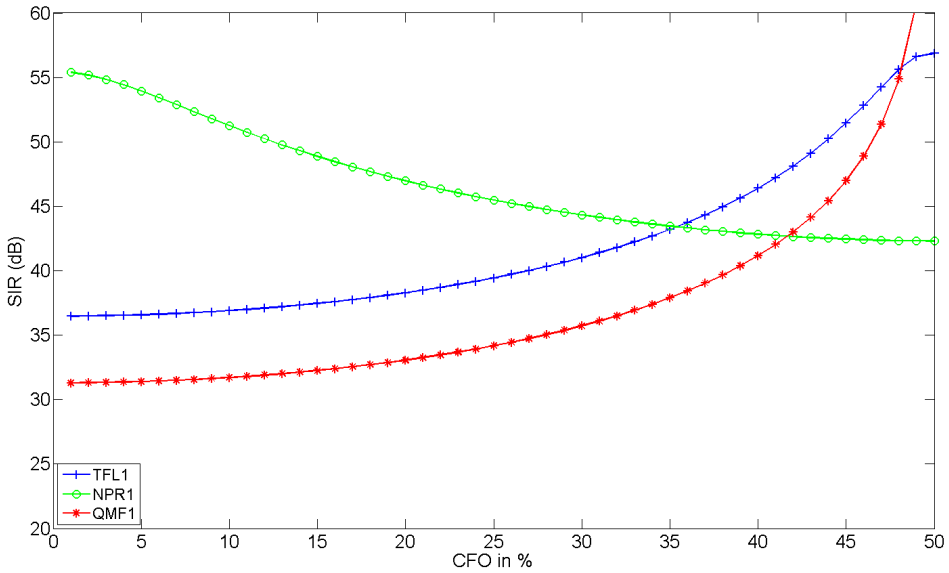

Figure 2.7 — SIR evaluation in presence of CFO when the FDC technique is applied for each PF (assuming $\Delta_r = 3$).

In fact, applying a frequency shift change the values of PF frequency domain coefficients. For a given SIR target, the number of non-zero coefficients obtained after truncation depends on the frequency shift value r. From Figure 2.7, it can be deduced that the optimal frequency shift is $r = 0$ for the NPR1 PF and $r = 1/2$ for the TFL1 and QMF1 PFs. For these latter, it can be interesting to always apply a frequency offset of $1/2$ at the receiver side, and compensate it in frequency domain. In this case, (2.6) and (2.7) becomes

$$X_n(m) = C_n(m) \sum_{k=0}^{L-1} r(k + n\frac{M}{2}) e^{-i\frac{2\pi k r}{M}} e^{-i\frac{2\pi}{L}km} \tag{2.33}$$

$$Y_n(m) = \sum_{l=-\Delta_{\frac{1}{2}}}^{\Delta_{\frac{1}{2}}} G_{\frac{1}{2}}(l) X_n(m-l). \tag{2.34}$$

This new technique applied to FS-FBMC receiver is referred as Half Frequency Shift (HFS) technique in this document. For a fair comparison between each considered FBMC PFs, different $N_{G_{r=0}}$ (NPR1) and $N_{G_{r=\frac{1}{2}}}$ (QMF1 and TFL1) values must be considered. However, we choose to introduce an upper limit at 8 for a reasonable hardware complexity. Figure 2.8 illustrates the evolution of the SIR in the presence of CFO, for FBMC applying different filters and N_{G_r} values with an FDC implementation. When N_{G_r} increases, the gain in performance of the QMF1 filter becomes more interesting, however it remains lower than the one obtained with TFL1 and NPR1 filters, even when $N_G = 8$. More than 8 dB of difference can be observed between NPR1 and QMF1 when the CFO becomes larger than 10%. When considering the TFL1 filter, the slight increase in performance between $N_G = 6$ and $N_G = 8$ may not justify the resulting increase in complexity. The NPR1 filter remains the most robust filter against CFO, even when compared to the TFL1 filter with $N_G = 8$: a gain of more than 3 dB can be observed when the CFO

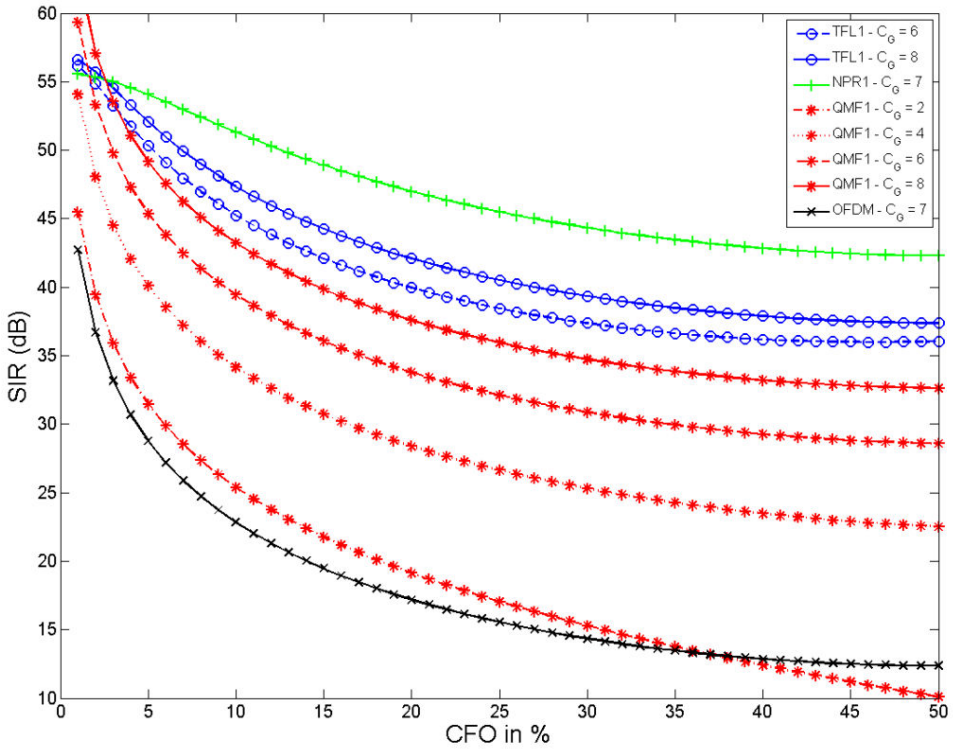

Figure 2.8 — SIR evaluation with different filters and N_G values in presence of CFO, after compensation.

is larger than 10%.

Furthermore, FDC technique can also be applied to OFDM, since this latter can be considered as a particular case of FBMC where the PF has a rectangular shape. However, FDC with OFDM does not lead to large performance gains. With $N_G = 8$, it has comparable results with QMF1 using 2 non-zero coefficients ($N_G = 2$). The gain in performance compared to the overhead in hardware complexity can be considered as questionable in the case of OFDM.

2.3.5 Performance comparison over multipath channels

In the context of the 4G/LTE standard, three multipath fading channel models are defined [92]:

- Extended Pedestrian A (EPA) model: $\tau = 410$ ns,
- Extended Vehicular A (EVA) model: $\tau = 2510$ ns,
- Extended Typical Urban (ETU) model: $\tau = 5000$ ns,

where τ corresponds to the delay spread of the multipath channel. The delay and power profiles of each channel model are detailed in [92]. In the 4G/LTE standard, an OFDM symbol duration is always equal to 66. µs without CP, and the subcarrier spacing is always equal to 15 kHz.

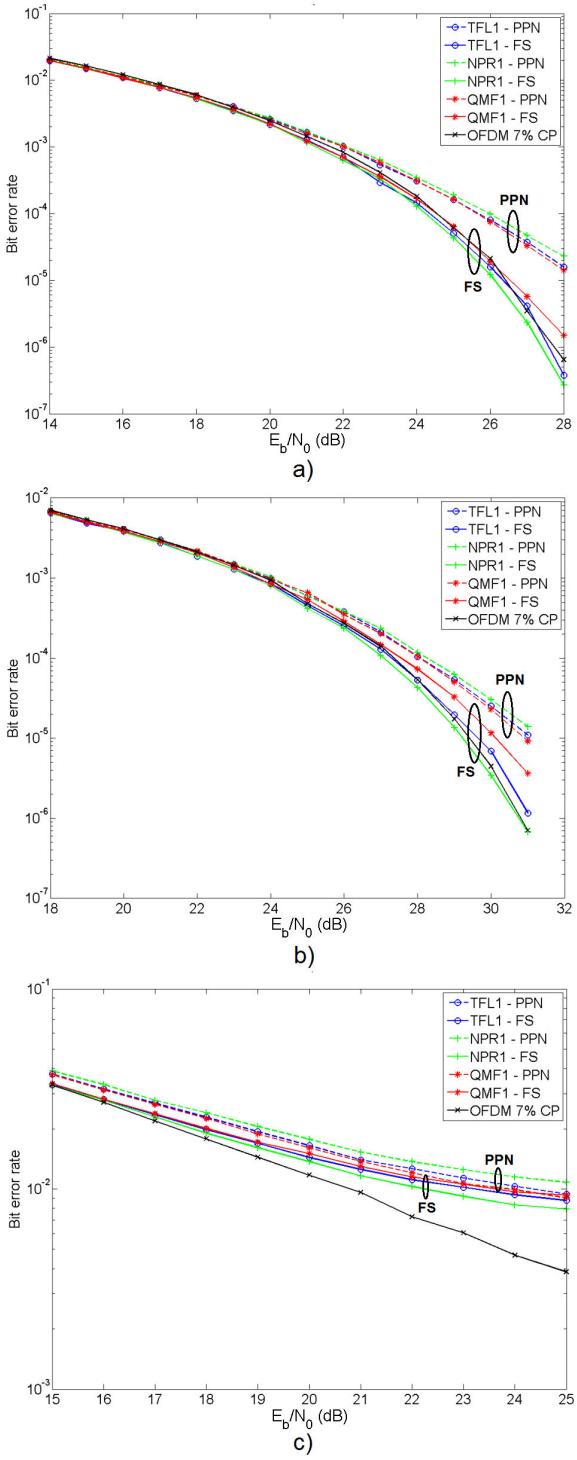

Figure 2.9 — BER evaluation of OFDM and FBMC with different PFs and implementations for a) EPA static channel, b) EVA static channel, c) ETU static channel.

This sub-section aims at evaluating the effect of these channels on the error rate performance of uncoded FBMC using different short PFs, with PPN and FS implementations. LTE parameters are considered for an IFFT length of 512 and a 16-QAM constellation. Thus, $L_{CP} = 36$ for OFDM, and 300 actives carriers are used, corresponding to 25 RBs. However, the frame structure of 4G/LTE is not exatly respected, since

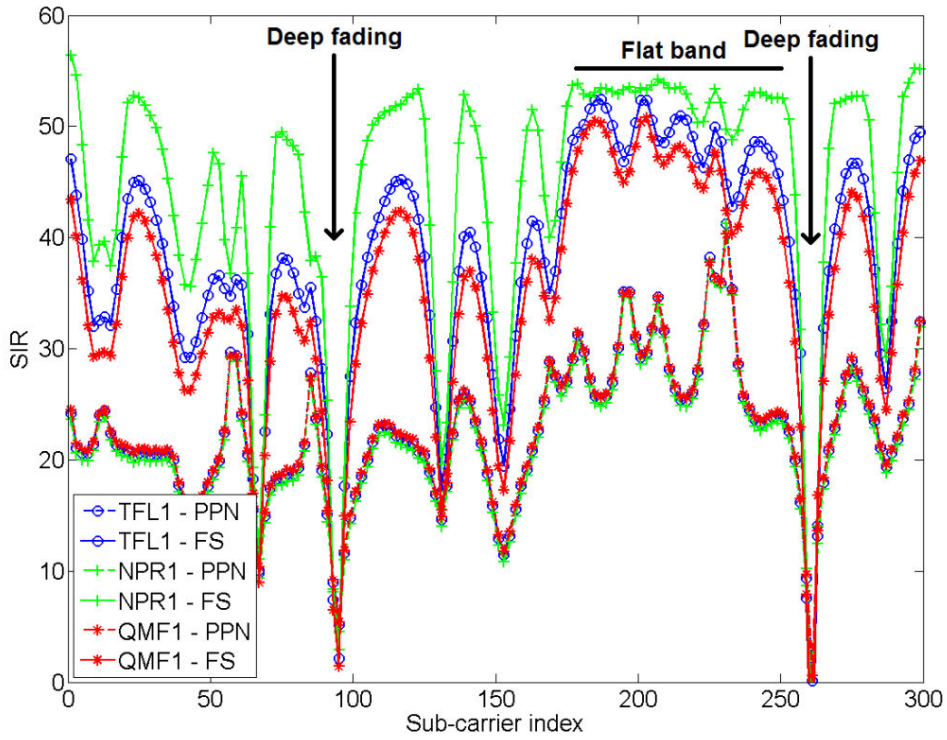

Figure 2.10 — SIR depending on the subcarrier index for FS-FBMC and PPN-FBMC with different short PFs, for an ETU channel.

Demodulation Reference Signal (DRS) [14] are not transmitted, and the Channel State Information (CSI) is considered to be perfectly known. Note that the CSI needs to be estimated in practice by sending, for instance, coded auxiliary pilots [93].

For a fair comparison, the same equalization technique is used for OFDM and FBMC. The equalization step is realized after the computation of the FFT, in frequency domain. The output samples of the FFT are simply divided by the frequency response of the channel, realizing the classical low-complexity and per-subcarrier ZF equalizer.

Static (no Doppler shift/spread) multipath channels with AWGN are considered to only evaluate the multipath and fading effect on the performance of OFDM and FBMC demodulators in terms of Bit Error Rate (BER). Figure 2.9a shows the BER performance when using EPA channel models, considering PPN and FS based FBMC with different PFs. As expected, the FS implementation outperforms the PPN one for all the considered PFs, particularly at higher SNR values where a difference of at least one decade of BER can be observed at $E_b/N_0 = 28$ dB. Furthermore, FS implementation with TFL1 and QMF1 PFs shows comparable performance to OFDM with CP. FS implementation with NPR1 offers slightly better results than OFDM at moderate Eb/No values ($E_b/N_0 > 20$ dB), due to the absence of CP and its robustness against all the different types of timing impairments.

Similar conclusions can be made for a channel with a longer delay spread like EVA, as shown in Figure 2.9b. However, an exception should be made for the QMF1 PF, since it exhibits a performance level inferior to OFDM. On the other hand, with the NPR1 PF, FBMC remains superior to OFDM even for an EVA channel.

Due to the absence of a CP, FBMC seems to be more sensitive to long delay spread channels as it is the case for the static ETU channel model. Indeed, OFDM with CP outperforms FBMC on this type of channels when $E_b/N_0 > 17$ dB, as shown in Figure 2.9c. At low E_b/N_0 values, the FS implementation is close to OFDM, and offers better results than the PPN implementation. NPR1 is again the most interesting short PF when using a FS implementation.

In fact, when deep fading occurs, the received signal is highly degraded, as shown in Figure 2.10, which represents the SIR per subcarrier with a randomly generated ETU channel, for different PFs and implementations. In the case of a flat fading in band, almost no interference occurs in FS implementation case (> 40 dB SIR). It is however not the case for the PPN implementation, where a gap of at most 30 dB can be observed when compared to FS implementation, confirming the superiority of the FS implementation. Finally, the delay spread of the ETU channel model being approximately two times longer than the delay spread of the EVA channel model, one straightforward solution is to double the duration of the FBMC symbol.

2.4 Summary

In this chapter, a novel short PF suitable to address several 5G air interface requirements is proposed. Due to its near perfect reconstruction nature, it is referred to as NPR1 PF. In the presence of timing offset due to imperfect synchronization, the NPR1 filter combined with the FS implementation exhibits a gain of more than 8 dB of SIR when compared to TFL1 and QMF1 short filters, and outperforms OFDM where a gap of 20 dB of SIR can be observed. The NPR1 filter is also the most robust filter to combat CFO, especially when the FDC technique is used. When compared to state-of-the-art filters, a gain of more than 3 dB of SIR is observed for NPR1 filter when the CFO is larger than 10%, at comparable hardware complexity. In this context, a frequency shift technique is proposed enabling a significant reduction in the complexity of the FS implementation of short filters.

In the case of 4G/LTE multipath channel, the NPR1 PF is even better than OFDM for the EPA channel model, despite the absence of CP. In the case of ETU channel model, the NPR1 PF shows improved performance when compared to other FBMC filters. However, due to the absence of a CP, long delay spread channels compromise the performance of FBMC modulations even when using a FS implementation for the receiver.

Finally, the robustness against CFO and Doppler shift being improved, low-cost Local Oscillator (LO)s can be employed and higher speeds can be reached in a mobility situation, as required by the upcoming 5G standard.

CHAPTER

3 Novel FBMC/OQAM receiver techniques for short filters

Several key advantages of using short PFs for FBMC have been highlighted in the previous two chapters. However, due to the absence of a CP, long delay spread channels compromise the performance of FBMC modulations even when using a FS implementation for the receiver. Furthermore, although FBMC using short PFs is sufficiently robust against timing offset to support relaxed synchronization, it does not support asynchronous communications when employing a typical FS or PPN based receiver.

In this chapter, an original FBMC receiver technique that addresses these issues is proposed. The main idea is to employ a time-domain equalizer based on an OS algorithm before the FBMC demodulation. A first version of this receiver, referred to as OS-FBMC, is presented in the next section after a short review of existing FBMC/OQAM equalization techniques. Both the time-domain equalizer and the FBMC receiver are merged in a unique structure due to the frequency localization of the PF, enabling to greatly reduce the computational complexity.

Then, several additional complexity reduction techniques are devised and another block-based receiver is proposed, referred to as OSB-FBMC. In this receiver, FBMC symbols are transmitted in blocks and demodulated all at once in the frequency domain, which further reduces the complexity.

The chapter ends by in-depth analysis of the complexity, latency, data rate, and robustness against timing offset and multipath channel impairments of the proposed FBMC receivers. Performance results are compared with OFDM and with a FBMC/OQAM system using reference long PF.

3.1 Overlap-Save FBMC receiver technique

3.1.1 FBMC/OQAM equalization techniques

As shown in the previous chapter, when using short PFs both the PPN-FBMC and the FS-FBMC receivers fail to compensate the effect of the multipath-channel with long delay spread if a simple one-tap ZF equalizer is employed. Therefore, a more advanced equalization technique must be investigated. For instance, a non-linear equalizer can be employed, such as the well known Decision Feedback Equalizer (DFE) [94].

The principle, illustrated in Figure 3.1, can be summarized with the following steps:

1. The received signal Y is first equalized by a typical linear equalizer.
2. A hard decision is made to estimate the transmitted symbol value d.
3. An interference term J is computed from the previously estimated symbol values.
4. This interference term is then subtracted from the linear equalizer output.
5. The hard decision is again applied, and updated estimations of symbol values are obtained.

A first DFE-based technique for FBMC is proposed in [95], and is referred to as Equalization with Interference Cancellation (EIC). According to [95], the equalized data symbol $\tilde{a}_n(m)$ at the subcarrier m and the FBMC symbol n, using the EIC technique, is expressed as

$$\tilde{a}_n(m) = \Re \frac{Y_n(m) - \hat{J}_n(m)}{\int_0^\tau h(\tau) e^{-i2\pi m F_0 \tau} A_g(-\tau, 0) d\tau}, \tag{3.1}$$

where $\hat{J}_n(m)$ is the estimated interference term, $Y_n(m)$ is the received signal at the output of the Analysis Filter Bank (AFB) and $A_g(\tau, \mu)$ is the ambiguity function of the PF g defined as

$$A_g(\tau, \mu) = \int_{-\infty}^{+\infty} g(t + \tau/2) g(t - \tau/2) e^{i2\pi\tau t} dt. \tag{3.2}$$

The estimated interference term is obtained by summing the estimated data symbol values $d_{n+q}(m+p)$, each weighted by a $i^{p+q+pq+2pn} B_m(q,p)$ coefficient, located at the time q and frequency p neighbouring the data symbol being estimated. In other words, we have

$$\hat{J}_n(m) = \sum_{(p,q) \in \Omega^*_{1,1}} d_{n+q}(m+p) i^{p+q+pq+2pn} B_m(q,p) \tag{3.3}$$

where $\Omega^*_{1,1} = [\![-1,1]\!] \times [\![-1,1]\!] \setminus (0,0)$ (except the (0,0) element) if the PF is well localized in both the time and frequency axes. The weight $B_m(q,p)$ is given by

$$B_m(q,p) = \sum_{k=0}^{L_{DS}-1} h(k) A_g\big[-q\frac{M}{2} - k, pF_0\big] e^{i2\pi \frac{(2m+p)k}{2M}}. \tag{3.4}$$

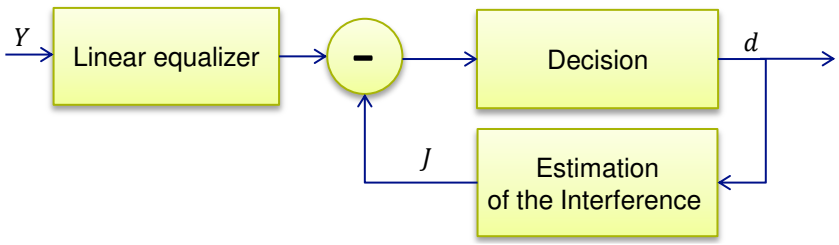

Figure 3.1 — Principle of the DFE technique.

Note that the estimated data symbol values $d_n(m)$ are obtained by making a hard decision on the symbol obtained at the output of a simple one-tap ZF equalizer (the linear equalizer of Figure 3.1). The computation of the weight term $B_m(q,p)$ is assumed to be done off-line according to [95]. Indeed, it is calculated when the channel is estimated using the symbol carrying the pilots, and not for each received FBMC symbol. In this case, these weights must be stored into a memory, which increases the hardware complexity. Furthermore, the off-line assumption only holds if the channel does not vary in time. In this case, the estimated interference term must be calculated for each received symbol, by taking into account the evolution of the CIR values. Therefore, the complexity is greatly increased.

In addition, the complexity introduced by the computation of the interference term $\hat{J}_m(n)$ is not negligible. If the PF is well localized, we have $q \in [\![-1,1]\!]$, $p \in [\![-1,1]\!]$ and $(p,q) \neq (0,0)$. Therefore, 8 complex multiplications are required to compute only one subcarrier, when a Single-Input Single-Output (SISO) transmission is considered. For MIMO, inter-antenna interference must also be considered in the computation of the interference term. In this case, the DFE technique becomes largely more complex. If short PFs have to be considered, the range of p must be extended since this type of PFs is generally less frequency localized than long PFs.

Last, a common issue with the DFE is that error propagation can appear, which limits achieved performance. Indeed, the estimation of the interference term may not be accurate if an error occurs during the first hard decision step. Therefore, an additional interference error term is introduced, and the hard decision is more prone to make a decision error in the next iteration. This is for instance observed in [96], which presents a DFE-based technique for a 2 by 2 spatial multiplexing MIMO technique for FBMC.

More advanced DFE techniques have been proposed in the literature. For instance, the DFE proposed in [97] was designed to minimize the MSE. However, their excessive complexity largely hinders their appeal for a practical FBMC system. Furthermore, no DFE technique is known to support asynchronous communications.

Alternatively, replacing the one-tap equalizer with a multi-tap equalizer can be an interesting solution. However, it is shown in [90] that the FS-FBMC receiver with the MMB4 PF and using a simple one-tap linear equalizer outperforms the PPN-FBMC receiver (with the same PF) using a 7-tap linear equalizer when facing timing offset and multipath channels. Being less robust against this type of channels when compared with long PFs, it is unlikely that short PFs achieve the same performance level as long PFs using this multi-tap equalizer.

However, a recent contribution has proposed a time-domain based equalizer for a FBMC variant having an overlapping factor of 1 [6]. Using this equalizer, the robustness against multipath channel has been greatly improved. Furthermore, this is the first time that a FBMC system using such a low overlapping factor has been proved to support asynchronous communication.

3.1.2 Time-domain equalizer based on Overlap-Save technique for FBMC

In [6], the authors have proposed a time-domain equalizer for a variant of a FBMC, referred to as FBMC/PAM, where the FBMC system has an overlapping factor $K = 1$. This equalizer can be seen as equivalent to the Overlap-Save OS algorithm [98]. In addition, it can be adapted for any FBMC scheme.

The principle of the OS algorithm is to perform a fast convolution between a signal r and a set of coefficients c. For a typical linear convolution, the number of operations scales in $\mathcal{O}(L_r L_c)$, where L_r is the number of samples composing the signal r and L_c is the number of coefficients c. However, in the case of the OS algorithm, the number of operations follows a logarithmic scale since multiples FFT-based operations are performed. Indeed, one iteration of this algorithm can be summarized by the following steps:

Step 1) Isolate N samples from the signal r to convolute with c, where the value of N is a design choice with $N > L_c$.
Step 2) Apply a FFT of size N on the isolated signal, to obtain its frequency domain representation.
Step 3) Multiply the FFT output number m by $C(m)$, where C is the FFT of size N of the coefficients c.
Step 4) Performs an IFFT of size N.
Step 5) Keep L samples, L being a design choice with $L < N$, and discard the $N - L$ remaining samples.

The obtained L samples are concatenated in each iteration until obtaining the complete convoluted signal. Each algorithm iteration is applied on N isolated samples from the signal r, shifted by L samples on each iteration. In fact, performing steps 2) to 4) is equivalent to perform a circular convolution of size N between the isolated signal and the coefficients c. Then, step 5) keeps the part of the signal where the result of the circular convolution is approximatively equal to the result of the linear convolution. Therefore, the higher the N/L ratio is, the better is the approximation. However, the complexity is in turn greatly impacted, and a trade-off between approximation errors and complexity must be considered. Note that this algorithm name comes from the fact that between 2 algorithm iterations, the FFT processing windows overlap by $N - L$ samples, which also represents the number of samples stored (saved) for the next iteration.

The combined OS-based time-domain equalizer and FBMC receiver is shown in Figure 3.2. First, an FFT of size $N = N_{UF}\, L$ is applied on the N samples from the received time-domain samples containing the FBMC symbol to demodulate, where in this chapter N_{UF} is an integer number referred to as the up-sampling factor used for the OS

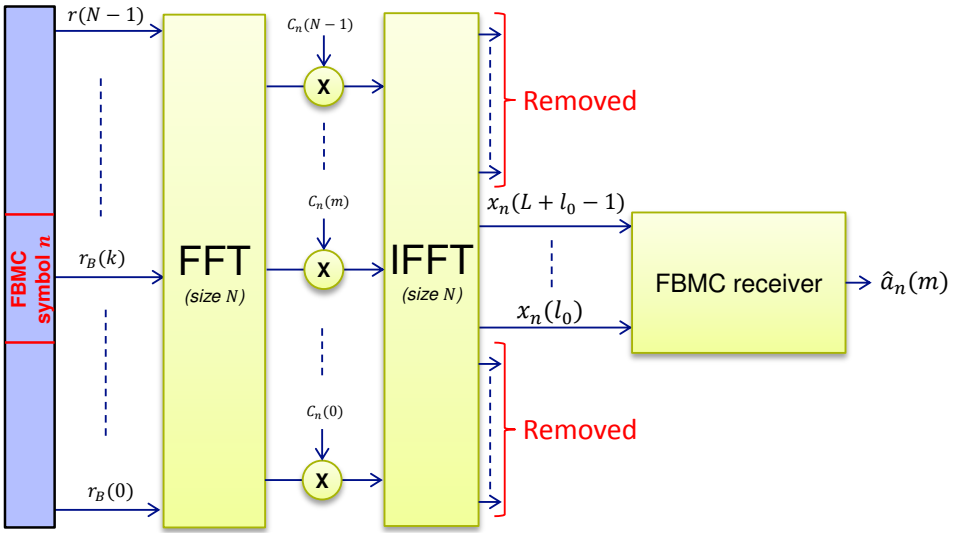

Figure 3.2 — Time-domain equalizer before the FBMC/OQAM receiver.

technique. Then, the one-tap equalizer coefficients are applied to obtain the frequency domain equalized signal X_n

$$X_n(m) = C_n(m) \sum_{k=0}^{N-1} r(k + n\frac{M}{2}) e^{-i\frac{2\pi km}{N}}, \tag{3.5}$$

where $C_n(m)$ is the equalizer coefficient at the FBMC symbol n and the subcarrier m. The equalizer coefficients typically used in OFDM can be employed here. For instance, we have $C_n(m) = 1/H_n(m)$ if the ZF equalizer is used, where $H_n(m)$ is the frequency response of the channel. Alternatively, MMSE equalizer coefficients can be considered to minimize the mean squared error introduced by the noise. In this case, we have

$$C_n(m) = \frac{H_n^*(m)}{||H_n(m)||^2 + \eta}, \tag{3.6}$$

where $||H_n(m)||^2 = H_n(m)H_n^*(m)$ and η is the inverse of the SNR when additive white Gaussian noise is considered. However, the computation of the MMSE equalizer coefficients requires to first estimate the SNR, which adds complexity and it is subject to approximation errors which may limit the obtained performance. Note that more advanced equalizer techniques can be employed, such as a multi-tap equalizer. However, the idea here is to keep the simplicity of the OFDM equalizer technique.

Next, an IFFT of size N is applied to obtain N time-domain samples, from which L samples are extracted, the remaining ones being discarded. The kept x_n samples correspond to the outputs l_0 to $l_0 + L - 1$ of the IFFT. Note that l_0 is also the sample index corresponding to the location of the first sample of the current FBMC symbol to demodulate. Therefore, for $k \in [\![0, L-1]\!]$, the signal x_n is expressed as follows

$$x_n(k) = \sum_{m=0}^{N-1} X_n(m) e^{i\frac{2m\pi(k+l_0)}{N}}, \tag{3.7}$$

The time-domain equalized samples must now be demodulated by a FBMC receiver, for instance based on the FS-FBMC technique presented in Section 2.1.2. This OS time-domain equalizer technique offers improved robustness against a channel with large delay spread. As noted in [6], interference occurs at the edge of the IFFT since the channel impairment is compensated by a circular convolution whereas the received signal has no cyclostationary property due to the FBMC overlapping structure. If only the samples located at the middle of the IFFT output are kept ($l_0 = (N-L)/2 = (N_{UF}-1)L/2$), the remaining interference level is indeed limited. Thus, increasing the size of both FFT/IFFT in Figure 3.2 can reduce the residual interference at the cost of a non-negligible increase in the computational complexity. Indeed, it requires the use of 2 FFTs and 1 IFFT of large size for each processed FBMC symbol, instead of only 1 FFT for a typical FBMC receiver. However, it is possible to highly reduce the computational complexity by taking advantage of the frequency localization of the PF. In fact, the FS-FBMC receiver structure can be merged with the time-domain equalizer leading to the reduced complexity OS-FBMC receiver detailed in the next section.

3.1.3 Proposed Overlap-Save FBMC receiver

The first step leading to the proposed receiver consists of dividing the IFFT of size N into N_{UF} IFFTs of size L. Such division is possible thanks to the decimation in time decomposition of the IFFT algorithm. Then, the output samples x_n of the OS time-domain equalizer can be expressed as follows

$$x_n(k) = \sum_{l=0}^{N_{UF}-1} \sum_{m=0}^{L-1} X_n(N_{UF}m + l) e^{i\frac{2\pi(N_{UF}m+l)(k+l_0)}{N}}, \tag{3.8}$$

which can be rewritten as

$$x_n(k) = \sum_{l=0}^{N_{UF}-1} e^{i\frac{\pi l}{N_{UF}}} x_n(k,l) z_l(k), \tag{3.9}$$

where $z_l(k) = e^{i\frac{2\pi l(k-L/2)}{N}}$ is a LPR term and the signal $x_n(k,l)$ is expressed as follows:

$$x_n(k,l) = \sum_{m=0}^{L-1} X_n(N_{UF}m + l) e^{i\frac{2\pi(N_{UF}m+l)l_0}{N}} e^{j\frac{2\pi km}{L}}. \tag{3.10}$$

Instead of directly processing the x_n signal by the single AFB of the FS-FBMC receiver, each $x_n(k,l)z_l(k)$ signal can be processed separately by a corresponding AFB. Therefore, the AFB is expanded $N_{UF}-1$ times, and the output samples of each AFB $Y_n(m,l)$ are summed together:

$$Y_n(m) = \sum_{l=0}^{N_{UF}-1} Y_n(m,l), m \in [\![0, M-1]\!]. \tag{3.11}$$

where Y_n is the output of the summed AFBs referred to as OS-AFB. Then, the LPR term z_l can be seen as a CFO with an amount of $\frac{l}{KN_{UF}}$ of the subcarrier spacing. By

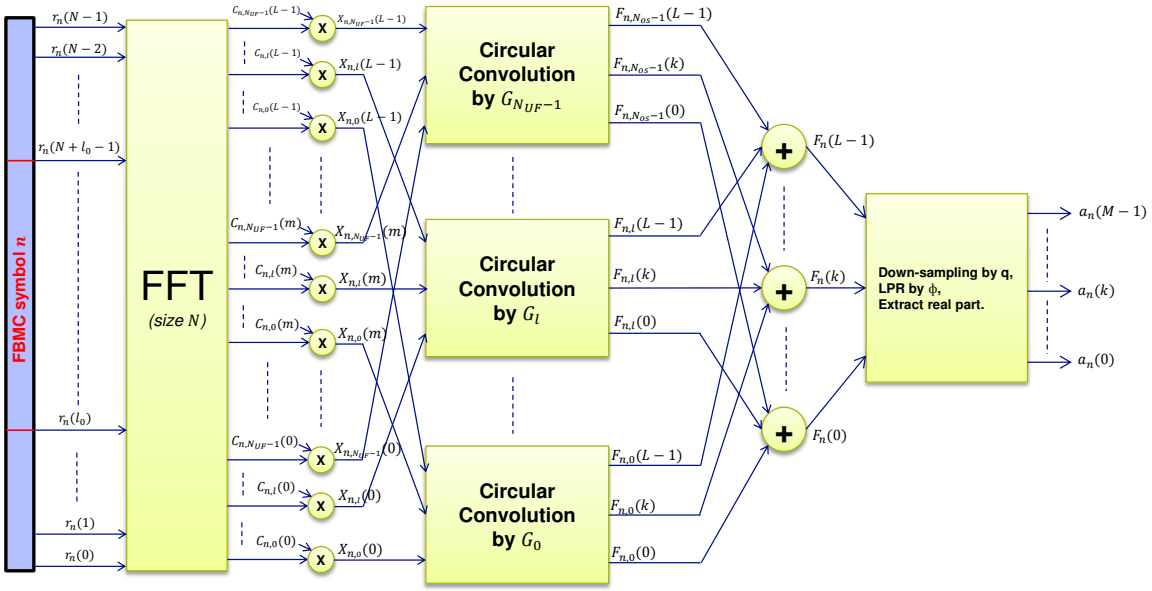

Figure 3.3 — Proposed OS-FBMC receiver.

using the FDC technique proposed in [91], the PF of each AFB can be adapted to directly incorporate the corresponding CFO. In our case, the FDC technique is used inversely to generate the required CFOs. Therefore, the filtering stage output of the AFB number l is expressed as follows:

$$Y_n(m,l) = \sum_{p=-\Delta}^{\Delta} e^{i\frac{\pi l}{N_{UF}}} G_l(p) \sum_{k=0}^{L-1} x_n(k,l) e^{-i\frac{2\pi(Km-p)k}{L}}, \tag{3.12}$$

where $\Delta = (N_G - 1)/2$, N_G is the number of the frequency response coefficients after truncation, and G_l is the frequency shifted response of the PF g as follows

$$G_l(p) = \sum_{k=0}^{L-1} g(k) z_l(k) e^{-i\frac{2\pi pk}{L}}. \tag{3.13}$$

Noting that each time-domain signal x_n is obtained by an IFFT of size L (3.10) followed by an FFT of the same size, both transforms can be simplified, and the output of the OS-AFB filtering stage becomes

$$Y_n(m) = \sum_{l=0}^{N_{UF}-1} \sum_{p=-\Delta}^{\Delta} G_l(p) X_n(Km-p,l), \tag{3.14}$$

with

$$X_n(m,l) = C_n(m,l) \sum_{k=0}^{N-1} r(k + n\frac{M}{2}) e^{-i\frac{2\pi k(N_{UF}m+l)}{N}}, \tag{3.15}$$

where $C_n(m,l) = C_n(N_{UF}m+l)e^{i\frac{\pi l}{N_{UF}}}e^{i\frac{2\pi(N_{UF}m+l)l_0}{N}}$. Assuming $l_0 = \frac{N-L}{2}$ and $q = 1$, the LPR terms in $C_n(m,l)$ become equal to $(-1)^{(N_{UF}-1)m+l}$, which can be processed without using any multiplication. Finally, only 1 FFT of size N is now required to demodulate one FBMC symbol, followed by the single-tap linear equalizer stage and N_{UF} stages of circular convolution by the frequency shifted responses of the PF, as illustrated in Figure 3.3. Similarly to a typical FS-FBMC receiver, the transmitted data symbol can be recovered after extracting the real part of the down-sampled (by K) and linear phase rotated (ϕ_n) filtering stage outputs.

This novel FBMC receiver enables to trade-off complexity for performance by the tuning parameter N_{UF}. The complexity mainly comes both from the FFT size and from the stages of circular convolution. While a convolution operation is generally considered highly complex, the number of the PF coefficients is limited in frequency domain (due to its frequency localization). The next subsection proposes techniques targeting complexity reduction.

3.2 Complexity reduction of the OS-FBMC receiver

3.2.1 Complexity reduction of the filtering stage

The complexity of the circular convolution stages mainly depends on the number of significant coefficients required for G_l. Thanks to the frequency localization of the PF, the number of required coefficients is limited. For instance, it is shown in Figure 2.8 that a SIR of 42 dB is obtained to compensate the worst CFO case when the NPR1 filter is used with $\Delta = 3$. SIR lower than 37 dB is obtained for other short PFs. Therefore, NPR1 seems to be the most adapted filter to limit the complexity of the proposed OS-FBMC receiver. Furthermore, it can be shown that G_l are real valued, reducing the complexity of the filter stage. Indeed, G_l can be expressed as follows

$$G_l(p) = \sum_{m=0}^{L-1} G(p-m)Z_l(m) \tag{3.16}$$

where Z_l is the FFT (size L) of the LPR term z_l, and is expressed as

$$Z_l(m) = z_l(0) + z_l\Big(\frac{L}{2}\Big) + \sum_{k=1}^{\frac{L}{2}-1} z_l(k)e^{-i\frac{2k\pi m}{L}} + z_l^*(k)e^{i\frac{2k\pi m}{L}}.$$

The terms $z_l(k)e^{-i\frac{2k\pi m}{L}} + z_l(k)^*e^{i\frac{2k\pi m}{L}}$ in the summation and $z_l(\frac{L}{2})$ being real valued, we have $\Im(Z_l(m)) = \Im(z_l(0))$. Then, the imaginary part of G_l becomes

$$\begin{aligned}\Im\Big(G_l(p)\Big) &= \Im\Big(z_l(0)\Big)\sum_{m=0}^{L-1} G(p-m) \\ &= \Im\Big(z_l(0)\Big)g(0).\end{aligned}$$

Defining $|.|$ as the absolute value operator, we have $|\Im(z_l(0))| < 1$, and $|g(0)| \approx 0$ since it corresponds to the first sample of the PF ramp-up part. Therefore, only the real part of G_l can be used for each circular convolution.

Furthermore, the G_l coefficients dispose of symmetrical properties which enable to further reduce the number of required multiplication operations. When $l > 0$, we have $G_l(p) = -G_{N_{UF}-l}(1-p), p \in [\![0, \Delta]\!]$. Indeed, $-G_{N_{UF}-l}(1-p)$ can be expressed as follows:

$$-G_{N_{UF}-l}(1-p) = -\sum_{k=0}^{L-1} g(k) z_{N_{UF}-l}(k) e^{-i\frac{2\pi k}{L}} e^{i\frac{2\pi pk}{L}}.$$

Furthermore, we have $z_{N_{UF}-l} = -z_l^* e^{j\frac{2\pi k}{L}}$, and the above equation becomes:

$$-G_{N_{UF}-l}(1-p) = \sum_{k=0}^{L-1} g(k) z_l^* e^{i\frac{2\pi pk}{L}},$$

which corresponds to the result of an IFFT (size L) of $g(k)z_l^*(k)$. Then, a known relation between a FFT and an IFFT can be exploited. If both the inputs and outputs of an IFFT are conjugated, then it is equivalent of directly processing the FFT of the non-conjugated inputs: $\text{FFT}(x) = \text{IFFT}(x^*)^*$. Since $g(k)$ and $G_l(k)$ are real valued, this property can be employed, which proves that the above symmetrical relation is obtained. Therefore, only $\Delta + 1$ real multiplications are required per processed sample for each circular convolution, greatly limiting the computational complexity of this filtering stage. The main complexity issue comes from the FFT processing, which is addressed in Section 3.2.3 by proposing an alternative OS-FBMC receiver technique.

3.2.2 Impact of the truncation on the receiver performance

The truncation of the G_l coefficients in (3.12) may introduce undesirable interference. If N_G, the number of non-truncated coefficients, is sufficiently high, the introduced interference is negligible. However, the complexity overhead of the filtering stage may become unacceptable. Thus, it is important to evaluate the resulting SIR level to devise a compromise between complexity and approximation errors.

To analytically evaluate the SIR, the relation between the transmitted $a_n(m)$ symbols and the recovered $\hat{a}_n(m)$ symbols must be established. If we assume that the FBMC symbol to demodulate is located at the middle of the received r samples, then it implies that $l_0 = M(N_{UF} - 1)/2$. In this case, the equalizer coefficients become $C_n(m, l) = (-1)^l(-1)^{(N_{UF}-1)m}$ if $K = 1$, and the equalized signal in frequency domain can be expressed as

$$\begin{aligned} X_n(m,l) &= (-1)^l(-1)^{(N_{UF}-1)m} \sum_{k=0}^{N-1} r(k + n\frac{M}{2}) e^{-2i\pi\frac{k(N_{UF}m+l)}{N}} \\ &= (-1)^l(-1)^{(N_{UF}-1)m} \sum_{u=0}^{N_{UF}-1} \sum_{k=0}^{M-1} r\Big(k + \frac{M}{2}(2u+n)\Big) e^{-i\frac{2\pi kl}{N_{UF}M}} e^{-i\frac{2\pi ul}{N_{UF}}} e^{-i\frac{2\pi km}{M}} \end{aligned} \tag{3.17}$$

Then, the LPR term $(-1)^{(N_{UF}-1)m}$ can be transposed in time domain as follows

$$X_n(m,l) = (-1)^l \sum_{u=0}^{N_{UF}-1} \sum_{k=0}^{M-1} r\Big(\mathrm{CS}(k) + \frac{M}{2}(2u+n)\Big) e^{-i\frac{2\pi \mathrm{CS}(k) l}{N_{UF} M}} e^{-i\frac{2\pi u l}{N_{UF}}} e^{-i\frac{2\pi k m}{M}}$$

with CS a circular shift operation defined as

$$\begin{cases} \mathrm{CS}(k) = \mathrm{mod}_M(k + \frac{M}{2}) & \mathrm{mod}_2(N_{UF}) = 0, \\ \mathrm{CS}(k) = k & \mathrm{mod}_2(N_{UF}) = 1, \end{cases}$$

By transposing the filtering stage in time domain, the AFB output number l can be expressed as

$$Y_n(m,l) = \sum_{u=0}^{N_{UF}-1} \sum_{k=0}^{M-1} \tilde{g}_l(k) r\Big(\mathrm{CS}(k) + \frac{M}{2}(2u+n)\Big) e^{-i\frac{2\pi u l}{N_{UF}}} e^{-i\frac{2\pi k m}{M}} \tag{3.18}$$

where $\tilde{g}_l(k)$ is the impulse response of the PF with its frequency response truncated down to $N_G = 2\Delta + 1$ coefficients. It is expressed as

$$\tilde{g}_l(k) = (-1)^l e^{-i\frac{2\pi k l}{N_{UF} M}} \sum_{m=-\Delta}^{\Delta} \Re\Big(G_l(m)\Big) e^{i2\pi\frac{km}{M}}$$

Since the first sample of the FBMC symbol to demodulate is $r(l_0)$, then we have $r(k) = s(k - l_0)$, s being the transmitted FBMC signal. The latter is expressed as

$$\begin{aligned} s\Big(\mathrm{CS}(k) + \frac{M}{2}(2u+n) - l_0\Big) = \sum_{n'=-\infty}^{+\infty} \Bigg(& g\Big(\mathrm{CS}(k) + \frac{M}{2}(2u+n-n') - l_0\Big) \\ & \times v_{n'}\Big(\mathrm{CS}(k) + \frac{M}{2}(2u+n) - l_0\Big) \end{aligned} \tag{3.19}$$

with $v_n(k)$ is the time-domain FBMC symbol number n before the filtering, expressed as follows

$$v_n(k) = \sum_{m=0}^{M-1} (-1)^{nm} \phi_n(m) a_n(m) e^{i\frac{2\pi k m}{M}}.$$

Furthermore, we have

$$v_n\Big(\mathrm{CS}(k) + \frac{M}{2}(2u+n) - l_0\Big) = \sum_{m=0}^{M-1} \phi_n(m) a_n(m) e^{i\frac{2\pi k m}{M}}$$

By combining (3.18) and (3.19), we have

$$Y_n(m,l) = \sum_{u=0}^{N_{UF}-1} \sum_{(p,q)\in\Omega} \tilde{F}_{l,u}(p,q) \phi_{n-q}(m-p) a_{n-q}(m-p) \tag{3.20}$$

with

$$\tilde{F}_{l,u}(p,q) = \sum_{k=0}^{M-1} \tilde{g}_l(k) g\Big(\mathrm{CS}(k) + \frac{M}{2}(2u+q) - l_0\Big) e^{-i\frac{2\pi ul}{N_{UF}}} e^{-i\frac{2\pi kp}{M}} \tag{3.21}$$

where Ω is defined so that $\tilde{F}_{l,u}(p,q) \approx 0$ when $(p,q) \notin \Omega$ for any u and l values in $[\![0, N_{UF}-1]\!]$. It can be defined as $\Omega = [\![-M/2, M/2-1]\!] \times [\![-N_{UF}, N_{UF}]\!]$. Indeed, if $q \geq N_{UF}+1$, we have

$$\begin{aligned} \mathrm{CS}(k) + \frac{M}{2}(2u+q) - l_0 &\geq \mathrm{CS}(k) + \frac{M}{2}(N_{UF}+1+2u) - l_0 \\ &\geq \frac{M}{2}(N_{UF}+1) - l_0 \\ &\geq M, \end{aligned} \tag{3.22}$$

and $g\Big(\mathrm{CS}(k) + \frac{M}{2}(2u+q) - l_0\Big) = 0$ when $\mathrm{CS}(k) + \frac{M}{2}(2u+q) - l_0 \geq M$. Therefore, $\tilde{F}_{l,u}(p,q) = 0$ when $q \geq N_{UF}+1$. Through similar development, we also have $\tilde{F}_{l,u}(p,q) = 0$ when $q \leq N_{UF}+1$. Finally, the recovered PAM symbols are expressed as

$$\begin{aligned} \hat{a}_n(m) &= \Re\Big(\phi_n^*(m) \sum_{l=0}^{N_{UF}-1} Y_n(m,l)\Big) \\ &= \Re\Big(\sum_{(l,u)\in\Psi} \sum_{(p,q)\in\Omega} i^{-p-q} \tilde{F}_{l,u}(p,q) a_{n-q}(m-p)\Big) \qquad (3.23) \\ &= A_0 a_n(m) + J_n(m), \qquad (3.24) \end{aligned}$$

where $\Omega^0 = \Omega \setminus (0,0)$, $\Psi = [\![0, N_{UF}]\!]^2$ and $J_n(m)$ is the interference term introduced by the truncation of the PF expressed as

$$\hat{J}_n(m) = \sum_{(l,u)\in\Psi} \sum_{(p,q)\in\Omega^0} \Re\Big(i^{-p-q} \tilde{F}_{l,u}(p,q) a_{n-q}(m-p)\Big), \tag{3.25}$$

and A_0 is the amplitude difference introduced by the filtering stage on the transmitted PAM symbol $a_n(m)$

$$A_0 = \sum_{(l,u)\in\Psi} \Re\Big(\tilde{F}_{l,u}(0,0)\Big). \tag{3.26}$$

The SIR introduced by the truncation of the PF coefficients, referred to as SIR_Δ, is the ratio between the variance of the useful signal $A_0 a_n(m)$ and the variance of the interference term $J_n(m)$. Assuming that $a_n(m)$ terms represent independent and identically distributed random variables with $\mathbb{E}(a_n(m)) = 0$, we have $\mathbb{E}(J_n(m)) = 0$ and the SIR_Δ

Table 3.1 — Obtained SIR values in dB when considering different Δ and N_{UF} values for the NPR1 PF.

Δ \ N_{UF}	2	4	8
2	27.6	26	25.5
3	45.2	45.6	45.5
4	51.8	51.9	51.9

Table 3.2 — Obtained SIR values in dB for different short PFs and Δ values, assuming $N_{UF} = 4$.

Δ \ PF	TFL1	QMF1	NPR1
2	29.6	29.1	26
3	39	33.9	45.6
4	40.9	37.3	51.9

is expressed as

$$\begin{aligned} \mathrm{SIR}_{\Delta} &= \frac{\mathbb{E}\Big(A_0^2 a_n^2(m)\Big)}{\mathbb{E}\Big(J_n(m)\Big)} \\ &= \frac{A_0^2}{\sum_{(l,u)\in\Psi}\sum_{(p,q)\in\Omega^0}\Re\Big(i^{-p-q}\tilde{F}_{l,u}(p,q)\Big)^2}. \end{aligned} \tag{3.27}$$

Numerical results are presented in Table 3.1 for different Δ and N_{UF} values when the NPR1 PF is used. It can be observed that the N_{UF} value has a slight impact on the SIR for a given Δ value. When $\Delta = 3$, the difference in the SIR is at most of 0.4 dB and 0.1 dB when $\Delta = 4$. On the other hand, the choice of Δ has an important impact on the SIR. For instance, increasing Δ from 2 to 3 enables to improve the SIR by almost 10 dB for any N_{UF} value.

Table 3.2 shows the obtained SIR values when considering different short PFs, assuming $N_{UF} = 4$. When $\Delta = 3$ and 4, the NPR1 PF achieves a higher SIR level than the other short PFs. For instance, when $\Delta = 3$, the NPR1 PF outperforms both the QMF1 and the NPR1 PF by respectively 11.7 dB and 6.6 dB. For the particular case of $\Delta = 2$, the obtained SIR level is not tolerable in 4G/LTE for all the considered PFs. In fact, 3GPP tolerates an Error Vector Magnitude (EVM) of 3.5% [92], corresponding to a SIR of ≈ 30 dB for the highest constellation order (256-QAM). The best SIR level is obtained for the TFL1 PF (39.6 dB), but it is inferior to the 3GPP requirement. Therefore, having $\Delta = 3$ and the NPR1 PF offers the best compromise between the complexity and the approximation errors compliant with the 4G/LTE context.

3.2.3 Overlap-Save-Block FBMC receiver

In [88], it is shown that the Lapped-OFDM transceiver (an FBMC variant with a short PF) presents improved performance against multipath channel and timing synchroniza-

tion errors when a half data-rate mode is considered. This can be explained by the fact that there is then no symbol overlapping, and that the ramp-up and ramp-down of the filter shape naturally acts as a pseudo-guard interval. Therefore, the cyclostationary property of the signal is partially restored. Consequently, after FFT, a simple one-tap equalizer can be used since the ISI is limited. However, the data rate is highly reduced in this half-data rate mode.

To restore the data rate while nonetheless improving the robustness against multipath and timing synchronization interference, we propose to jointly consider a block of N_s FBMC symbols. Since the first FBMC symbol adds KM samples in the block, and each following FBMC symbol adds $M/2$ samples, then the total number of samples in the block L_B is equal to

$$L_B = \frac{M}{2}(N_s + 2K - 1)$$

with $\alpha = 1/(2K-1)$. The ideal number of FBMC symbols to achieve maximum data rate is $N_{ideal} = 2L_B/M$. Therefore, the data rate loss is

$$\begin{aligned} DR_{loss} &= 1 - \frac{N_s}{N_{ideal}} \\ &= 1 - \frac{N_s}{N_s + 2K - 1} \\ &= \frac{1}{N_s\alpha + 1} \end{aligned} \tag{3.28}$$

Note that half-data rate Lapped-OFDM symbol can be equivalently seen as a block composed of $N_s = 1$ FBMC symbol using a short filter ($K = 1$), effectively corresponding to a spectral efficiency loss of 1/2.

If equalization is performed on the whole block of length L_B samples, we obtain the benefits of the ramp-up and ramp-down at both ends of the block. In its basic form, this approach yields the receiver shown in Figure 3.4. At the output of this equalizer, standard FBMC receivers are used to process each FBMC symbol in the block.

This structure is similar to the time-domain OS-equalizer followed by the FBMC receiver presented in Section 3.1.2 and in Figure 3.2. The major difference resides in the fact that each FFT output is kept and processed by N_s FBMC receivers. The IFFT and FFT are computed only once to process a block of N_s FBMC symbols. The sample indexes $nM/2$ to $nM/2 + M - 1$ at the output of the FFT correspond to the FBMC symbol number n which is demodulated by the FBMC receiver number n.

Letting $r_b(k) = r(k + bL_B)$ for $k \in [\![0, L_B - 1]\!]$ be the part of the received signal corresponding to the block with index b, the frequency-domain equalized signal can be expressed as

$$X_b(m) = C_b(m) \sum_{k=0}^{L_B-1} r_b(k) e^{-i\frac{2\pi km}{L_B}}, \tag{3.29}$$

where $C_b(m)$ are the equalizer coefficients for block b, and the sum corresponds to a FFT of size L_B. L_B may not necessarily be a power of 2. This can complicate the hardware implementation of the FFT. Therefore, it is possible to append $L_{ZP} = N - L_B$ zeros

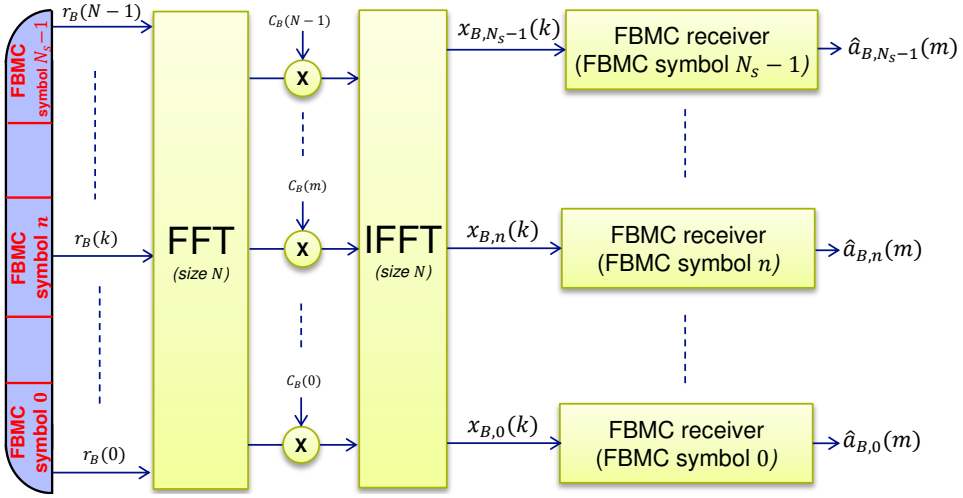

Figure 3.4 — OS equalizer applied to a block of FBMC symbols.

after the received block, where N is a power of 2 greater or equal to L_B. Then, $X_b(m)$ becomes

$$X_b(m) = C_b(m) \sum_{k=0}^{N-1} \tilde{r}_b(k) e^{-i\frac{2\pi km}{N}}, \tag{3.30}$$

where $\tilde{r}_b(k) = r_b(k)$ when $k \in [\![0, L_B - 1]\!]$, otherwise $\tilde{r}_b(k) = 0$. At the output of the equalizer, the samples $x_{b,n}(k)$ corresponding to the FBMC symbol n in the block b are obtained by taking the samples with indices $nM/2$ to $nM/2 + M - 1$ of the equalizer IFFT. It is expressed as follows, for $k \in [\![0, M-1]\!]$

$$x_{b,n}(k) = \sum_{m=0}^{N-1} X_b(m) e^{i\frac{2\pi m}{N}(k+n\frac{M}{2})}, \tag{3.31}$$

Finally, the real or imaginary component $\hat{a}_{b,n}(m)$ of the transmitted QAM symbols is recovered through a standard FBMC receiver.

Equation (3.30) and the IFFT operation in (3.31) are evaluated once to recover N_s symbols. However, this comes with a severe drawback: the receiver is highly sensitive against time variations of the channel (Doppler shift or spread). This issue can be easily resolved by taking into account the variation of the channel in the equalizer coefficients. Instead of (3.30), we then have distinct frequency-domain representations for each FBMC symbol n:

$$X_{b,n}(m) = C_{b,n}(m) \sum_{k=0}^{N-1} \tilde{r}_b(k) e^{-i\frac{2\pi km}{N}}, \tag{3.32}$$

where $C_{b,n}(m)$ is the equalizer coefficient corresponding to FBMC symbol n. However, this solution conflicts with the main idea of the OSB-FBMC, since one IFFT of size N must now be computed for each FBMC symbol. Thankfully, a large complexity reduction can be obtained by exploiting the frequency localization of the PF, through similar development to the one described in Section 3.1.3. Then, if $\hat{a}_{b,n}(m)$ is the recovered

PAM symbol at the block b and FBMC symbol n, we have

$$\hat{a}_{b,n}(m) = \Re\Big(\phi_n^*(m) \sum_{l=0}^{\mathbb{N}_{UF}-1} \sum_{p=-\Delta}^{\Delta} G_l(p) X_{b,n}(Km-p,l)\Big), \tag{3.33}$$

with

$$X_{b,n}(m,l) = C_{b,n}(m,l) \sum_{k=0}^{N-1} \tilde{r}_b(k) e^{-i2\pi k \frac{(m\mathbb{N}_{UF}+l)}{N}}, \tag{3.34}$$

where

$$C_{b,n}(m,l) = C_{b,n}(m\mathbb{N}_{UF}+l)(-1)^{mn} e^{i\pi \frac{l(n+1)}{N_{UF}}}, \tag{3.35}$$

and N_{UF} is chosen so that it is the lowest possible integer value considering that the FFT size must be superior or equal to the block size

$$N_{UF} = \lceil 1 + \frac{N_s - 1}{2K} \rceil. \tag{3.36}$$

In fact, this receiver can be seen as an OS-FBMC receiver where the FFT is applied on a block of N_s FBMC symbols. Therefore, this block-based receiver is referred to as OSB-FBMC in this document.

3.3 Performance evaluation and comparisons

In this section, the performance of FS-FBMC and multiple OS-based receivers using the NPR1 short PF are evaluated. They are compared to OFDM and FS-FBMC with MMB4 PF under several performance metrics, including:

- frame length, data rate and latency,
- timing offset impairment in case of relaxed synchronization and asynchronous communication,
- robustness against a doubly dispersive channel,
- computational complexity.

For clarity, the following notations are adopted in this section:

- FS_1-FBMC and FS_4-FBMC respectively refer to the FS-FBMC receiver with the NPR1 and MMB4 PFs,
- $\text{OS}_{N_{UF}}$-FBMC refers to the OS-FBMC receiver with an up-sampling factor N_{UF},
- OSB_{N_s}-FBMC refers to the OSB-FBMC receiver with a block composed of N_s FBMC symbols.

The FS_4-FBMC system is chosen for comparison since it represents one of the most efficient FBMC receivers found in the literature. In [90], it is shown that the FS_4-FBMC receiver using a simple one-tap linear equalizer outperforms the PPN-FBMC receiver using a 7-tap linear equalizer when facing a timing offset. Indeed, the obtained SIR

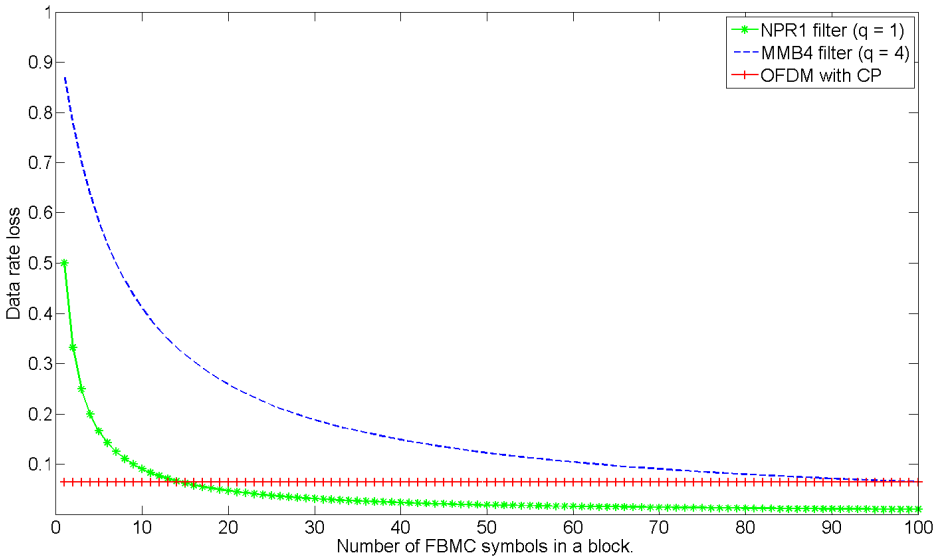

Figure 3.5 — Data rate loss for FBMC with the NPR1 and MMB4 PFs.

level is superior to 50 dB for any timing offset value, implying that the FS_4-FBMC can support asynchronous communication [75]. Furthermore, the FS_4-FBMC receiver also offers similar BER performance in a multipath environment when compared to the 7-tap equalizer. Therefore, showing best performance, this FBMC receiver represents the best candidate to evaluate the robustness of the proposed OS-FBMC receivers.

3.3.1 Frame length, data rate and latency

This section aims to define the number of FBMC symbols N_s in each frame for the compared FBMC-based systems. In fact, the frame length impacts the data rate, as detailed in Section (3.2.3). The analytical expression of the data rate loss is given in (3.28), and the obtained numerical values are shown in Figure 3.5 for the NPR1 and MMB4 PFs.

In OFDM, the data rate is reduced, due to the insertion of the CP of length L_{CP}, by

$$DR_{\text{loss}}(\text{OFDM}) = \frac{1}{\beta + 1}, \tag{3.37}$$

with $\beta = N/L_{CP} \approx 14.22$ in 4G/LTE, which corresponds to a data rate loss of ≈ 6.6 %. For most FBMC receivers, the frame length is chosen so that the obtained data rate loss is equivalent to OFDM in 4G/LTE. For the NPR1 PF, we have $N_s = 14$ to achieve a data rate loss of 6.6%, which corresponds to a frame composed of $L_B = 7.5M$ samples. In this case, we have $N_{UF} = 8$ if the OSB-FBMC receiver is chosen. Additionally, $M/2$ zero valued samples must be padded at the end of each received frame. It is interesting to note that it exactly corresponds to the duration of 1 RB, composed of 7 OFDM symbols including CP. Therefore, NPR1 PF can be a strong candidate if short frames are to be considered. As for the MMB4 PF, the target data rate loss similar to OFDM is

reached when $N_s = 100$. The frame duration is therefore more than 6 times larger than OFDM and FBMC with NPR1 PF, making it not adapted for communication scenarios requiring a short frame duration. For the OSB-FBMC receiver, a second configuration with $N_{UF} = 4$ is considered to evaluate the effect of the block size on the robustness against different channel impairments. In this setup, we have $N_s = 7$, which corresponds to a data rate loss of 12.5%.

From the chosen frame length, the minimal achievable latency can be estimated by assuming that all the samples in a frame must be received to recover the data. For OFDM, one RB is composed of $7.5M$ time-domain samples. The frequency sampling being F_s and $M/F_s = 66.67$ µs, the achievable latency is therefore of 0.5 ms. Using the NPR1 PF, the same latency is achieved for the FS_1-FBMC and the OSB_{14}-FBMC receivers. However, the $\text{OS}_{N_{UF}}$-FBMC receiver requires $M\,(N_{UF} - 1)/2$ additional samples to process the last FBMC symbol in the frame. When $N_{UF} = 2$, the latency is increased by 6.7 % when compared to the other FBMC receivers. Concerning the MMB4 PF, the latency is 6 times larger than OFDM. This is clearly one of the most critical issue of this PF, and is one of the main reasons explaining that typical state-of-the art FBMC systems are not suitable for low latency applications.

3.3.2 Robustness against timing offset

Timing offset impairment occurs when the processing window of the receiver is not aligned in time with the transmitted signal. It is always the case in practice, since the channel introduces a propagation delay. Two scenarios can be considered:

- Relaxed synchronization scenario: scheduled users transmit simultaneously. However, since each user is located at a different geographical distance from the base station, the corresponding signal is affected by a different propagation delay. Therefore, received user-signals are not perfectly aligned at the base station. In 4G/LTE, timing synchronization is realized using time advance mechanism to compensate the propagation delay of each user. However, new highly demanding scenarios like MMC are considered in 5G. To reduce energy consumption, time advance mechanism should be avoided. Therefore, the receiver must be able to compensate for the introduced timing offset.
- Asynchronous communication scenario: in this case, each user transmits at an independent time reference. No time synchronization is performed among all the scheduled users. Therefore, the time misalignment between users may vary between -50% to 50% of the symbol duration. Such scenario is considered for device-to-device communication and MMC.

To compensate the timing offset, the equalizer coefficients $C_n(m) = C_{TO}(m)$ are set to

$$C_{\text{TO}}(m) = e^{-i\frac{2\pi l_d m}{N'}} \tag{3.38}$$

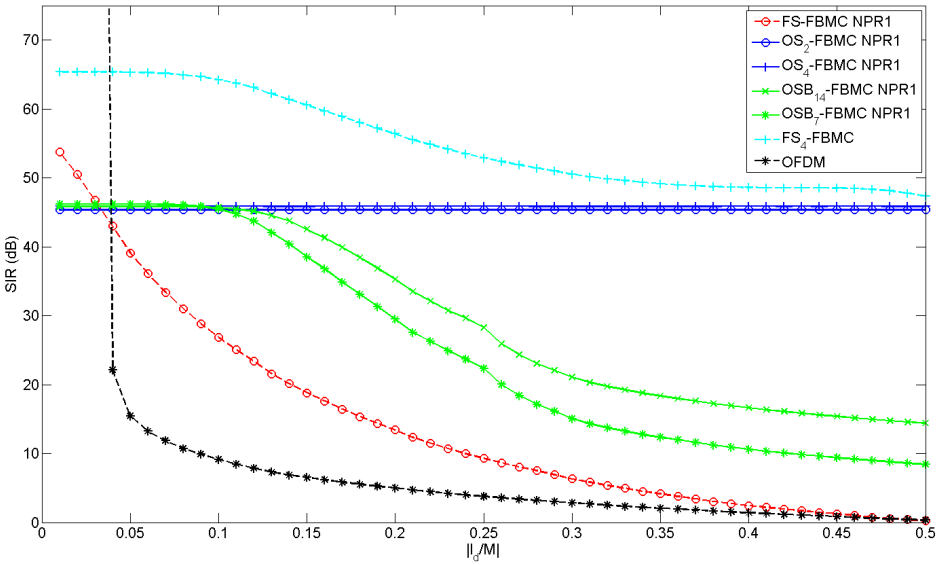

Figure 3.6 — Timing offset evaluation in terms of SIR for different FBMC receivers.

where l_d is the timing offset in number of shifted samples and $N = M$ for OFDM, $N' = KM$ for the FS-FBMC receivers and $N' = N$ for the OS_2-FBMC and OSB_{14}-FBMC receivers. The frequency response of the NPR1 PF is truncated down to $N_G = 7$ ($\Delta = 3$) coefficients for the circular convolution operations.

Figure 3.6 shows the SIR obtained by simulating the effect of the timing offset on all the considered receivers. The FS_1-FBMC receiver is outperformed by all the other FBMC receivers when $|l_d/M| \geq 4\%$. For a SIR target of 30 dB, the later can tolerate a timing offset up to 8%, while the OSB_{14}-FBMC can reach 21% (19% for the OSB_7-FBMC receiver). Furthermore, the OS_2-FBMC and the FS_4-FBMC receivers can support any timing offset values, making them adequate for asynchronous communication.

Concerning the OSB-FBMC receivers, the SIR achieves a constant value up to a timing offset of 13% of the symbol duration, showing that the introduced interference is limited. For higher timing offset values, the SIR gradually decreases, showing that it is not as robust as the OS_2-FBMC receiver. Note that the OSB_{14}-FBMC receiver is more robust than the OSB_7-FBMC receiver for high timing offset values ($> 13\%$). This implies that the block size has an impact on the robustness against timing offset. Finally, OFDM is free from any interference when $|l_d| < L_{CP}/2$, but it is clearly outperformed by any FBMC receiver for higher timing offset values. The rest of this section provides in-depth analysis of the timing offset effect on each considered FBMC receiver.

3.3.2.1 OS-FBMC receivers

As shown in Figure 3.6, the OS_2-FBMC and OS_4-FBMC receivers are insensitive to timing offset impairment. In fact, this statement can be generalized for any $N_{UF} \geq 2$ and any PF. The particular case of $N_{UF} = 1$ corresponds to the case of the typical FS-FBMC receiver and remains sensitive to the timing offset, even for the MMB4 PF, as shown in Figure 3.6. This robustness to timing offset of $OS_{N_{UF} \geq 2}$-FBMC can be proved

by considering the OS time-domain equalizer presented in Section 3.1.3. In presence of timing offset, (3.5) becomes

$$\begin{aligned} X_n(m) &= C_{TO}(m) \sum_{k=0}^{N-1} r(k+n\frac{M}{2}+l_d)e^{-i\frac{2\pi km}{N}} \\ &= \sum_{k=0}^{N-1} r(k+n\frac{M}{2}+l_d)e^{-i\frac{2\pi (k+l_d)m}{N}} \\ &= \sum_{k=l_d}^{N+l_d-1} r(k+n\frac{M}{2})e^{-i\frac{2\pi km}{N}}. \end{aligned} \tag{3.39}$$

If $l_d \geq 0$, (3.39) becomes

$$X_n(m) = \sum_{k=0}^{N-1} r(k+n\frac{M}{2})e^{-i\frac{2\pi km}{N}} + \sum_{k=0}^{l_d-1} \Big(r(k+N+n\frac{M}{2}) - r(k+n\frac{M}{2})\Big)e^{-i\frac{2\pi km}{N}} \tag{3.40}$$

Then, the output samples of the OS time-domain equalizer (3.7) become, for $k \in [\![0, L-1]\!]$

$$x_n(k) = r(k+l_0+n\frac{M}{2}) + \Pi_{l_d}(k+l_0)\Big(r(k+N+l_0+n\frac{M}{2}) - r(k+l_0+n\frac{M}{2})\Big), \tag{3.41}$$

where $\Pi_{l_d}(k)$ is the rectangular window of length l_d defined as: $R_{ld}(k) = 1, k \in [\![0, l_d-1]\!]$ else 0. When $l_d < l_0 = (N_{UF}-1)L$, (3.41) gives $x_n(k) = r(k+l_0+nM/2)$ since $R_{l_d}(k+l_0) = 0$. This corresponds to the samples of the FBMC symbol to demodulate which are free from any interference. Through similar developments, the same conclusion is obtained when $-l_0 < l_d < 0$. The lowest value of l_0 being $l_0 = M/2$ (obtained for $K = 1$, $N_{UF} = 2$), this confirms that the $\text{OS}_{N_{UF}}$-FBMC receiver is insensitive to timing offset lower than 50 % of the symbol duration. Note that this statement also holds for timing offsets larger than $M/2$ samples. Indeed, this value is superior to the OQAM delay. Therefore, the data can be recovered at the next ($l_d > 0$) or the previous ($l_d < 0$) FBMC symbol.

3.3.2.2 OSB-FBMC receivers

For this proposed receiver, the interference is only introduced at the first or last FBMC symbol in the block if $0 < l_d < M/2$. Indeed, the OSB-FBMC receiver can be seen as a particular case of the OS-FBMC receiver where the FFT processes the same set of input samples r for each FBMC symbol to demodulate in a given block. The first sample of the FBMC symbol number n is expected to be located at $r(l_n) = r(nM/2)$. As demonstrated above, if $|l_d| < l_n$, then the timing offset does not introduce any interference for FBMC

symbol indexes $n \in [\![1, N_s - 1]\!]$. When $n = 0$, (3.34) becomes

$$\begin{aligned} X_{b,0}(m) &= C_{TO}(m) \sum_{k=0}^{N-1} \Pi_{L_B}(k) r_b(k + l_d) e^{-i\frac{2\pi km}{N}} \\ &= \sum_{k=l_d}^{L_B+l_d-1} r_b(k) e^{-i\frac{2\pi km}{N}} \\ &= \sum_{k=0}^{L_B-1} r_b(k) e^{-i\frac{2\pi km}{N}} + \sum_{k=L_B}^{L_B+l_d-1} r_b(k) e^{-i\frac{2\pi km}{N}} - \sum_{k=0}^{l_d-1} r_b(k) e^{-i\frac{2\pi km}{N}} \end{aligned} \tag{3.42}$$

First, let's consider that $L_B = N$ ($L_{ZP} = 0$). Then, (3.31) becomes

$$x_{b,0}(k) = r_b(k) + I_b(k),$$

with the time-domain interference term $I_b(k)$ being

$$I_b(k) = \Pi_{l_d}(k)\Big(r_b(k + N) - r_b(k))\Big), \tag{3.43}$$

When $L_{ZP} \neq 0$, we have $L_{ZP} \geq M/2 > l_d$. Indeed, we have

$$\begin{aligned} L_{ZP} &= N - L_{block} \\ &= KN_{UF}M - \frac{M}{2}(N_s + 2K - 1) \\ &= \frac{M}{2}(2K(N_{UF} - 1) - N_s + 1) \end{aligned} \tag{3.44}$$

Furthermore, we have $N/L = N_{UF} > L_B/L$, implying that $K(N_{UF} - 1) - N_s + 1$ in (3.44) is a positive number. Therefore, we have $N > L_B + l_d$. In this case, (3.43) becomes, for $k \in [\![0, L - 1]\!]$

$$\begin{aligned} I_b(k) &= \Pi_{l_d}(k - L_B) r_B(k) - \Pi_{l_d}(k) r_b(k), \\ &= -\Pi_{l_d}(k) r_b(k), \end{aligned}$$

Since $l_d < M/2$, $\Pi_{l_d}(k)r(k)$ corresponds to the first l_d samples of the transmitted block to demodulate (indexed b). It contains the samples of the first FBMC symbol of block b. In (3.43), $\Pi_{l_d}(k)r(k + N)$ corresponds to the first l_d samples of the next transmitted block (indexed $b + 1$) containing the first FBMC symbol of block $b + 1$. Therefore, the interference term becomes

$$I_b(k) = \Pi_{l_d}(k) g(k) \sum_{m=0}^{M-1} \phi_0(m)\Big(\gamma a_{b+1,0}(m) - a_{b,0}(m)\Big) e^{i\frac{2\pi km}{N}},$$

with $\gamma = 0$ if $L_{ZP} = 0$, else $\gamma = 1$, $a_{b,0}(m)$ is the transmitted PAM symbol at the first FBMC symbol of the block number b. At the output of the AFB, the interference term

becomes

$$\begin{aligned} J_b(m) &= \sum_{k=0}^{M-1} g(k) I_{l_d}(k) e^{-i\frac{2\pi km}{N}} \\ &= \sum_{p=-\frac{M}{2}}^{\frac{M}{2}-1} F_{g,ld}(p)\phi_0(m-p)\Big(\gamma a_{b+1,0}(m-p) - a_{b,0}(m-p)\Big), \end{aligned} \tag{3.45}$$

with

$$F_{g,ld}(p) = \sum_{k=0}^{M-1} \Pi_{l_d}(k) g^2(k) e^{-i\frac{2\pi km}{N}}. \tag{3.46}$$

Then, after the OQAM specific processing, the interference term $U_b(m)$ at the output of the FBMC receiver is expressed as

$$\begin{aligned} U_b(m) &= \Re\Big(J_b(m)\phi_0^*(m)\Big) \\ &= \Re\Bigg(\sum_{p=-\frac{M}{2}}^{\frac{M}{2}-1} i^{-p} F_{g,ld}(p)\Big(\gamma a_{b+1,0}(m-p) - a_{b,0}(m-p)\Big)\Bigg), \end{aligned} \tag{3.47}$$

It is worth noting that the above expression is obtained by considering that the effect of the filter coefficient truncation is negligible. Indeed, the interference term introduced by the timing offset is normally affected by this truncation. Finally, the recovered PAM symbol of block b and FBMC symbol $n \in [\![0, N_s - 1]\!]$ is expressed as

$$\hat{a}_{b,n}(m) \approx a_{b,n}(m) + e_{b,n}(m) + U_b(m)\delta(n)$$

where $e_{b,n}(m)$ is the interference introduced by the filter coefficient truncation when $l_d = 0$, and δ is the dirac function ($\delta(0) = 1$, else 0). If $a_n(m)$ are independent and identically distributed random variables of mean $\mathbb{E}(a_{b,n}(m)) = 0$ and of variance σ_a^2, then the SIR expression can be

$$\begin{aligned} \mathrm{SIR}_{\mathrm{OSB}}(l_d) &\approx \frac{\mathbb{E}\Big(a_{b,n}^2(m)\Big)}{\frac{1}{N_s}\sum_{n=0}^{N_s-1}\mathbb{E}\Bigg(\Big(a_{b,n}(m) - \hat{a}_{b,n}(m)\Big)^2\Bigg)} \\ &\approx \frac{\sigma_a^2}{\mathbb{E}\Big(e_{b,n}^2(m)\Big) + \frac{1}{N_s}\mathbb{E}\Big(U_b^2(m)\Big)}, \end{aligned} \tag{3.48}$$

with

$$\mathbb{E}\Big(U_b^2(m)\Big) = 2^\gamma \sigma_a^2 \sum_{p=-\frac{M}{2}}^{\frac{M}{2}-1} \Re\Big(i^{-p} F_{g,ld}(p)\Big)^2.$$

Similar SIR expression is obtained when $-M/2 < l_d < 0$. Figure 3.7 shows the obtained SIR values numerically from (3.48) and by simulation for different block sizes.

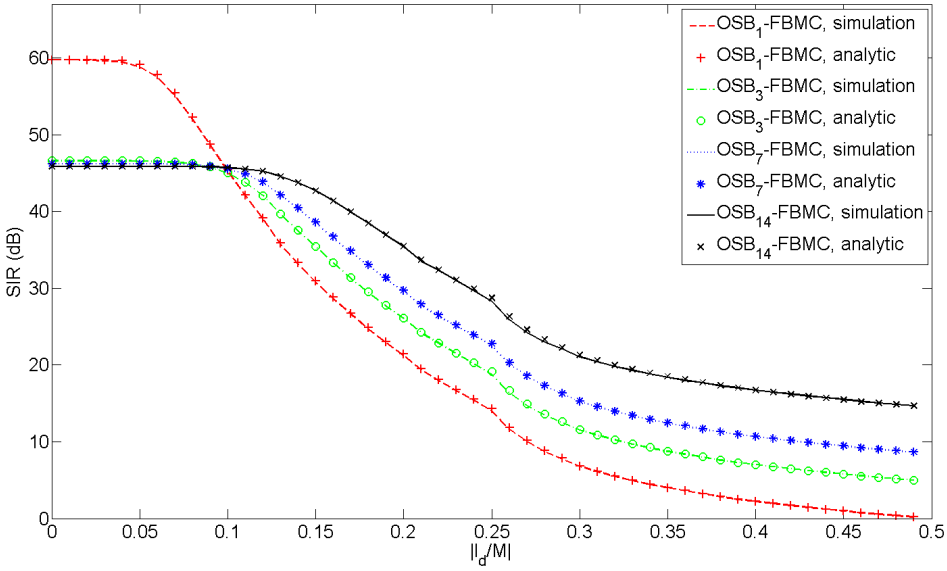

Figure 3.7 — OSB-FBMC: evaluation of the SIR for different block sizes.

As expected, higher robustness against timing offset is achieved when the block size is increased. Particularly, for high timing offset values, doubling the block size increases the SIR by 3 dB. It is also interesting to note that the zero-padding operation can asymptotically increase the SIR by 3 dB.

3.3.2.3 FS-FBMC receivers

The highest SIR values are obtained with the MMB4 PF using a typical FS-FBMC receiver. In this case, the obtained SIR does not fall below 53 dB (at $l_d/M = 25$ %). This high robustness against timing offset can be explained by analyzing the analytical expression of the SIR, evaluated in [90]

$$\mathrm{SIR}_{\mathrm{MMB4}}(l_d) = \frac{1}{3\times 10^{-7} + \frac{1}{8M}\sum_{l=0}^{l_d-1} g_{MMB4}^2(l)}. \tag{3.49}$$

Due to its near-perfect reconstruction nature, the MMB4 PF introduces a residual interference level of $10\log(\mathrm{SIR}_{\mathrm{MMB4}}(0)) \approx 65$ dB. The interference level introduced by the timing offset is determined by the term $\sum_{l=0}^{l_d-1} g_{MMB4}^2(l)$ in (3.49). Since the power level of the MMB4 impulse response is almost null at its first $M/2$ samples ($g_{MMB4}(l) \approx 0$ when $l < M/2$), the interference is therefore limited. This also explains why there is such a performance gap between the NPR1 and the MMB4 PF when using the FS-FBMC receiver.

To outperform the MMB4 PF with FS-FBMC, the OS-FBMC with NPR1 PF requires at least $N_G = 21$ filter coefficients, for a resulting SIR level of 65 dB. The complexity is however greatly increased. Furthermore, when hardware implementation is considered, quantization errors are introduced. Other channel impairments, like CFO, and imperfect channel estimation also greatly reduce the SIR. In 4G/LTE standard, 3GPP tolerates an EVM of 3.5 % [92], corresponding to a SIR of ≈ 30 dB for the high-

est constellation order (256-QAM). Therefore, the proposed OS-FBMC still has a SIR margin of 15 dB when $N_G = 7$ coefficients are chosen.

3.3.3 Performance comparison over multipath channels

To evaluate the robustness against multipath channel with Doppler spread, three multipath fading channel models are considered:

- EPA model: $\tau = 410$ ns, $\mu = 5$ Hz,
- EVA model: $\tau = 2510$ ns, $\mu = 70$ Hz,
- ETU model: $\tau = 5000$ ns, $\mu = 300$ Hz,

where τ corresponds to the delay spread of the multipath channel and μ the extent of the difference in observed frequency or Doppler frequency. These channel models correspond to the three typical ones proposed in 4G/LTE. The delay and power profiles of each channel model are detailed in [92].

To compensate the effect of the channel, the equalizer coefficients are set to

$$C_{\mathrm{n}}(m) = \frac{1}{\sum_{l=0}^{N'-1} h_{\mathrm{idx}(n)}(l) e^{-i2\pi \frac{kl}{N'}}} \tag{3.50}$$

where $\mathrm{idx}(n)$ is the sample index corresponding to the middle of the OFDM or FBMC symbol number n, and is expressed as

$$\mathrm{idx}(n) = \begin{cases} (n+1)L_{CP} + (n+\frac{1}{2})M & \text{for OFDM} \\ \frac{M}{2}(n+q) & \text{for FS-FBMC} \\ \frac{M}{2}(n+q) & \text{for OS-FBMC} \\ \frac{M}{2}(n+q) + bL_B & \text{for OSB-FBMC.} \end{cases} \tag{3.51}$$

Figure 3.8 shows the BER in presence of AWGN for the three considered channel models, assuming perfect knowledge of the CSI. These results are obtained by simulation, with the channels generated by the comm.RayleighChannel MATLAB function from the Communications System Toolbox. The 5 MHz bandwidth configuration of 4G/LTE is considered for all considered waveforms, with 300 allocated subcarriers and a 16-QAM constellation.

The results for the EPA 5 Hz channel are presented in Figure 3.8 a). Similar BER levels are obtained for the OFDM, the OS_4-FBMC, the OSB-FBMC and the FS_4-FBMC receivers. The OS_2-FBMC performs slightly worse than the other OS-based configurations, while the FS_1-FBMC receiver offers the worst BER performance when we have $E_b/N_0 > 25$ dB. Similar observations can be made for the EVA 70 Hz channel model, presented in Figure 3.8 b). In this case, the OS_4-FBMC, FS_4-FBMC and the OSB-based FBMC receivers have a slight performance degradation at high E_b/N_0 values (> 25 dB) when compared to OFDM.

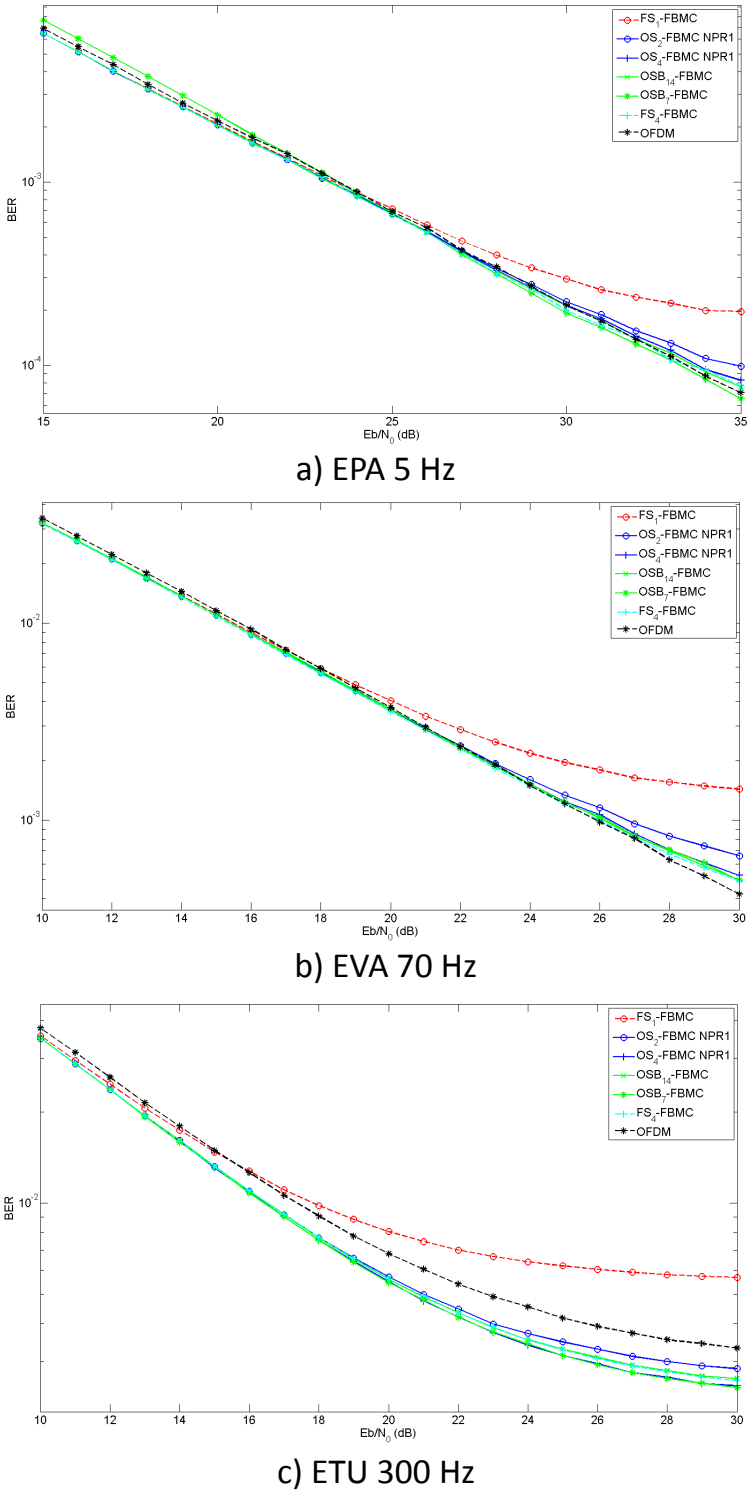

Figure 3.8 — BER evaluation of each receiver for a) the EPA 5 Hz channel, b) the EVA 70 Hz channel and c) the ETU 300 Hz channel.

For the ETU 300 Hz channel model case shown in Figure 3.8 c), the FS_1-FBMC is again outperformed by the other receivers. Particularly, the BER at $E_b/N_0 = 30$ dB is almost 2 times higher than OFDM. However, all the proposed receivers achieve

Table 3.3 — Analytical complexity for each FBMC receiver.

Receiver	FFT	Equalization	LPR	Filtering
OFDM	$C_{RM}(FFT_M)/2$	$3N_c/N_s$	0	0
FS_1-FBMC	$C_{RM}(FFT_M)$	$3N_c + 6\Delta$	0	$N_c(\Delta+1)$
FS_4-FBMC	$C_{RM}(FFT_{4M})$	$12N_c + 18$	0	$6N_c$
$OS_{N_{UF}}$-FBMC	$C_{RM}(FFT_{N_{UF}M})$	$3N_{UF}(N_c + 2\Delta)$	0	$N_{UF}N_c(\Delta+1)$
OSB_{N_s}-FBMC	$C_{RM}(FFT_{N_{UF}M})/N_s$	$3N_{UF}(N_c + 2\Delta)$	(3.52)	$N_{UF}N_c(\Delta+1)$

lower BER than OFDM, demonstrating the high robustness of FBMC against doubly dispersive channel. It is worth noting that the delay spread (5 µs) of the channel is slightly higher than the CP duration (4.7 µs). Although it represents a difference of 6%, it is sufficient to introduce an error floor higher than any of the proposed OS-FBMC receivers which do not rely on any CP. Concerning these latter, the OS_2-FBMC receiver is the one having the worst BER. However, the OS_4 FBMC and OSB-FBMC receivers achieve a similar BER than the FS_4-FBMC. This shows that short PFs can reach similar robustness against doubly dispersive channels when compared to long PF like MMB4.

3.3.4 Computational complexity comparison

In this subsection, the computational complexity of the proposed OS-FBMC techniques are compared to FS-FBMC using short and long filters in terms of number of required Real-valued Multiplications (RMs) to demodulate one FBMC symbol. We denote by $C_{RM}(x)$ the number of RMs required for the operation x. It is assumed that one Complex Multiplier (CM) requires $C_{RM}(CM) = 3$ RMs by using the following known development:

$$(a + jb)(c + jd) = c(a + b) - b(c + d) + j(c(a + b) + a(d - c)).$$

In addition, the choice of the IFFT computation algorithm is another critical aspect when considering complexity, since this choice has a a significant impact on the required number of RMs. A well known and efficient IFFT computation algorithm is the split radix IFFT [99], which can be used when the IFFT size is a power of 2 ($N = 2^n$). The computational complexity of the split radix IFFT of size N, referred to as $C_{RM}(FFT_N)$, is given by [100]

$$C_{RM}(FFT_N) = Nlog_2(N) - 3N + 4$$

The analytical expressions of the complexity of the considered receivers are given in Table 3.3. The complexity of the OFDM receiver is scaled to take into account that 2 FBMC symbols must be processed to recover the transmitted QAM symbols, whereas only 1 OFDM symbol is processed to recover the same amount of QAM symbols for the OFDM case. For the OSB-FBMC receiver, several multiplications can be avoided when processing the LPR term in (3.35). Indeed, when $\mathrm{mod}_{N_{UF}/2}\Big(l(n+1)\Big) = 0$, we have $\exp[i(\pi l(n+1))/N_{UF}] \in \{-1, 1, i, -i\}$. Therefore, the required number of multiplications

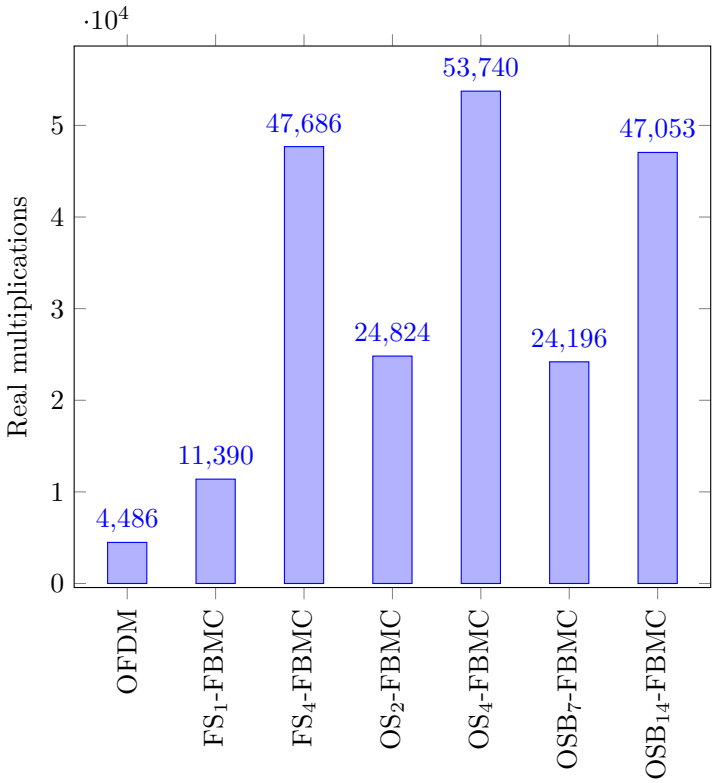

Figure 3.9 — Required number of real multiplications per processed FBMC symbol for each receiver.

to compute this LPR term is

$$C_{RM}(\text{LPR}_{\text{OSB}}) = \frac{3N_c}{Ns} \sum_{(l,n)\in\Lambda} \left\lceil \frac{\text{mod}_{\frac{N_{UF}}{2}}\Big(l(n+1)\Big)}{N_{UF}} \right\rceil, \tag{3.52}$$

with $\Lambda = [\![0, N_{UF}-1]\!] \times [\![0, N_s-1]\!]$. Figure 3.9 shows the required number of real multiplications per processed FBMC symbol for each receiver. It is assumed that $M = 1024$, $N_c = 600$ and $\Delta = 3$. It appears that the proposed OS$_2$-FBMC receiver is almost 50% less complex than the FS$_4$-FBMC receiver. Therefore, asynchronous communication can be supported with lower complexity at the receiver side. Furthermore, the use of short PF like NPR1 enables to also reduce the complexity at the transmitter side. The OS$_4$-FBMC receiver is 13% more complex than the FS$_4$-FBMC receiver, but this complexity increase concerns only the receiver and can be considered acceptable in uplink MMC scenario. It can be explained by the slightly more complex filtering stage in the OS$_4$-FBMC receiver when compared to the one in the FS$_4$-FBMC receiver.

While having the same N_{UF} value, the OSB$_7$-FBMC receiver is 55% less complex than the OS$_4$-FBMC receiver. Even with higher N_{UF} value, the OSB$_7$-FBMC receiver has almost the same complexity as OS$_2$-FBMC receiver and the OSB$_{14}$-FBMC receiver is 12% less complex than the OS$_4$-FBMC receiver. This complexity reduction can be explained by the fact than only 1 FFT of size N_{UF} is needed to process several FBMC

symbols. Technically, OSB_1-FBMC is 50% less complex than the FS_1-FBMC receiver and has a complexity comparable to OFDM. However, the achieved data rate is highly impacted. This points out the drawback of this receiver: there is a trade-off between complexity and data rate. Note that the block-type structure used by the OSB-FBMC receiver can be advantageous when the MIMO block-Alamouti, proposed in [101], is considered.

Finally, OFDM and FS_1-FBMC receivers are the least complex receivers, but have limited performance as shown in the previous sub-section.

3.3.5 Strengths and weaknesses of the FBMC transceivers

This sub-section summarizes the strengths and weaknesses of the considered FBMC and OFDM systems, presented in Table 3.4. The suitability of the FBMC receivers for relaxed synchronization and asynchronous communication has been investigated in Sub-section 3.3.2. It is shown that using the proposed OS-FBMC receivers, asynchronous communication can also be supported for a short PF. This is one of the major contributions of this chapter, since asynchronous communication is currently only considered for MMB4 PFs in the literature.

It is also considered that long PFs have better robustness against multipath channels with a long delay spread when compared to short PFs. However, Section 3.3.3 shows that OS-FBMC receivers can achieve the same performance level as the FS_4-FBMC receiver. Furthermore, OS-FBMC receivers outperform OFDM when the delay spread of the channel is larger than the CP length.

It is known that FBMC systems show improved robustness against CFO than OFDM for any PF, as investigated in [28]. In [28], it is also shown that a short PF has a higher robustness against CFO than a long PF. The robustness against CFO is evaluated in Section 2.3.4 for the FS_1-FBMC receiver, and shows that the NPR1 PF outperforms the other short PFs by at least ≈ 0.4 dB. Therefore, the NPR1 PF is currently the PF having the highest robustness against CFO. It is worth noting that the proposed OS-FBMC receivers do not alter the interference introduced by the CFO. In fact, the time-domain equalizer in Figure 3.2 only compensates for the CPE term. Therefore, the resulting SIR level remains unchanged.

Latency is considered to be one of the major weaknesses of FBMC, as pointed out in [84] and [20]. However, the corresponding analyses do not take into account the PF choice, assuming that a long PF such as MMB4 represents the only option for FBMC. We show in Sub-section 3.3.1 that short PFs can achieve the same latency as OFDM at comparable data rate if the FS_1-FBMC or the OSB-FBMC receivers are used. The latency is slightly increased when using the OS-FBMC receivers, but not as much as the MMB4 PF. For the latter PF, the latency is indeed a major issue, since the frame duration must be 6 times larger than OFDM if the same data rate is targeted.

The strengths of the FBMC systems come at the price of a higher computational complexity at the receiver side, as evaluated in sub-section 3.3.4. At comparable spectral efficiencies, the FBMC receiver having the lowest complexity is the FS_1-FBMC receiver,

which is still 1.5 times more complex than OFDM. The complexity is further increased for the OS-FBMC receivers. However, this complexity increase may be considered reasonable if this receiver is implemented at the BS. In this context, the complexity of the transmitter is more critical due to the limited hardware resources at the UE. Furthermore, the complexity analysis conducted here only concerns the FBMC receiver with its equalizer. Other signal processing techniques having demanding computational complexity such as channel estimation or FEC decoding must be considered for an overall evaluation.

At the transmitter side, it is advised to use the PPN implementation for FBMC, as it is in general less complex than the FS-FBMC transmitter. In addition, the truncated PF coefficients used in the FS filter stage may impact the spectral confinement. Furthermore, it is shown in [32] that the computational complexity of the PPN-FBMC transmitter can be halved by using a pruned FFT algorithm. This reduction is confirmed in Chapter 5, Section 5.2, through a real hardware implementation. Therefore, the complexity increase with respect to OFDM is lower at the transmitter side.

The analysis of the PAPR is addressed in Chapter 1, Section 1.3.3 for FBMC. Without any pre-coder for PAPR reduction, the FBMC signal using a short PF has similar PAPR level when compared to the long PF. In fact, the PF choice has almost no impact on the signal PAPR. When compared to OFDM, the PAPR is however slightly increased. This is due to the presence of a ramp-up and a ramp-down transition at the beginning and at the end of the FBMC frame. When the pre-coder is employed, significant peak-power reduction is achieved. For FBMC, the efficiency of the pre-coding technique depends on the PF choice, as shown in Chapter 1, Section 1.3.3. A long PF has a higher PAPR than a short PF, although the same pre-coder is employed. Such result was observed in [56], where multiple PAPR reduction techniques were tested for different PFs.

This pre-coding makes the use of block-type pilot structure mandatory in 4G/LTE uplink communication. However, the channel estimation is a challenging task because of the OQAM scheme. In Section 1.3.4 of Chapter 1, it is shown that an efficient channel estimation can still be obtained if the pilots are exempt from any source of interference generated from the data. This assumes that FBMC symbol acting as guard-interval must be inserted between the pilots and the data, introducing a data rate loss. However, the data rate loss is minimal for short PFs, where only 1 FBMC symbol as guard-interval is necessary to perfectly isolate the pilots. If the OSB-FBMC receiver is considered, the pilots can be inserted between two successive blocks of FBMC symbols.

To complete the above analysis, the compatibility with MIMO diversity techniques is evaluated in the section.

Table 3.4 — Comparison of different FBMC systems.

FBMC receiver	OFDM	FS_1-FBMC	FS_4-FBMC	OS-FBMC	OSB-FBMC
Support of relaxed synchronization	−−	+	++	++	+
Support of asynchronous communication	−−	−−	++	++	−−
Robustness against the doubly dispersive channel	++/−−	−	++	++/+	++
Robustness against CFO (non-compensated)	−−	+	−	++	++
Latency	++	++	−−	+	++
Spectrum shape	−−	+	++	+	+
Transmitter complexity	++	++	−	++	++
Receiver complexity	++	+	−−	−−	−/−−
Compatibility with MIMO Block-Alamouti	/	+	−−	+	++
PAPR	++	+	+	+	+
PAPR with precoding techniques	++	+	−	+	+
Block-type-pilot support	++	+	−−	+	+

3.3.6 Support of MIMO Alamouti

The use of a MIMO Alamouti code for diversity is challenging because of the lack of orthogonality in the complex plane between neighbouring OQAM symbols [102]. Straightforward approaches require the use of interference cancellation techniques, such as [103]. Nonetheless, as shown in [101] for the 2×1 antenna configuration, Alamouti coding can be combined with FBMC by applying the Alamouti code structure over entire blocks of FBMC symbols. This technique was later extended to support the 2×2 antenna configuration [104].

In the block Alamouti code, two blocks of N_s FBMC symbols are transmitted using two antennas and two time slots. Let $d_n^{(i)}(m) = \phi_n(m)a_n(m)$ be a sequence of FBMC symbols indexed by n, with index $i \in \{1, 2\}$ used to distinguish the two information blocks. The code is formed by transmitting, in the first time slot, $d_n^{(1)}$ on antenna 1 and $d_n^{(2)}$ on antenna 2, and in the second time slot, $-{d_{N_s-1-n}^{(2)}}^*$ on antenna 1 and ${d_{N_s-1-n}^{(1)}}^*$ on antenna 2. Note that the FBMC symbols are time reversed in the second time slot. Therefore, the formation of the code is simple as in the OFDM case.

The block Alamouti scheme can also be used in the frequency dimension as proposed in [105]. In this case, groups of subcarriers must be defined. However, the main issue of this technique is that it assumes that the channel frequency response is flat for 2 groups of subcarriers, which is not guaranteed for all the 4G/LTE channel models, especially if the group size is large. Furthermore, short PFs are less localized in frequency than long PFs used in [105], and may require 1 or 2 additional guard-band subcarriers to suppress interference in successive groups of subcarriers, thus reducing the data rate. For this reason, the use of such MIMO block-coding technique in time domain is preferred for short PFs.

At the receiver side, a Maximum Ratio Combining (MRC) technique is typically employed for detection. Since blocks constituted from several FBMC symbols are transmitted, the OSB-FBMC receiver seems to represent the best suitable receiver type solution. Then, the MRC equalizer can be integrated after the FFT and before the N_{UF} filtering stages. If $R_{u,v}$ is the FFT of the received FBMC block signal in time slot u received by antenna v, we have

$$\begin{bmatrix} R_{1,1} \\ R_{1,2} \\ R_{2,1}^* \\ R_{2,2}^* \end{bmatrix} = \boldsymbol{H} \begin{bmatrix} S_1 \\ S_2 \end{bmatrix}, \tag{3.53}$$

with S_u being the outputs of the FFT of the transmitted FBMC block signal at time slot u (zero-padded if necessary). By assuming that the CFR is constant over a pair of FBMC symbols, $\boldsymbol{H}$ is the CFR matrix expressed as

$$\boldsymbol{H} = \begin{bmatrix} \hat{H}_{1,1} & \hat{H}_{1,2} \\ \hat{H}_{2,1} & \hat{H}_{2,2} \\ \hat{H}_{1,2}^* & -\hat{H}_{1,1}^* \\ \hat{H}_{2,2}^* & -\hat{H}_{2,1}^* \end{bmatrix}, \tag{3.54}$$

The corresponding zero-forcing MRC equalization is thus

$$\begin{bmatrix} \hat{S}_1 \\ \hat{S}_2^* \end{bmatrix} = \boldsymbol{H}^+ \begin{bmatrix} R_{1,1} \\ R_{1,2} \\ R_{2,1}^* \\ R_{2,2}^* \end{bmatrix}, \tag{3.55}$$

with $\boldsymbol{H}^+ = \frac{1}{\alpha}\boldsymbol{H}^\dagger$ and $\alpha = \sum_{u,v} |\hat{H}_{u,v}|^2$.

In the presence of high mobility, the constant channel assumption becomes inappropriate. At the cost of higher complexity, it is possible to improve the performance by using a typical zero-forcing equalizer that does not assume a constant channel. The channel matrix then takes the form

$$\boldsymbol{H}(n) = \begin{bmatrix} H_{1,1}(n) & H_{1,2}(n) \\ H_{2,1}(n) & H_{2,2}(n) \\ H_{1,2}^*(N_s-1-n) & -H_{1,1}^*(N_s-1-n) \\ H_{2,2}^*(N_s-1-n) & -H_{2,1}^*(N_s-1-n) \end{bmatrix}, \tag{3.56}$$

and the zero-forcing equalizer is obtained by performing the full computation of the Moore-Penrose pseudo-inverse for each n: $\boldsymbol{H}^+(n) = \left(\boldsymbol{H}^\dagger(n)\boldsymbol{H}(n)\right)^{-1}\boldsymbol{H}^\dagger(n)$.

This Block-Alamouti technique is not adapted for long PFs such as the MMB4, since a large number of FBMC symbols must be transmitted by the block-based structure to avoid significant spectral efficiency loss. Consequently, this greatly increases the latency and the complexity. Furthermore, the constant channel assumption becomes inappropriate even for moderate mobility levels. Therefore, this technique is much more adapted to short PFs.

It is worth noting that other block-based MIMO schemes can be considered. For instance, [106] proposes to apply a Walsh-Hadamard matrix precoding over the FBMC symbols in each block. The complexity of this pre-coding step is relatively low since no multiplications are required [107]. However, this technique is not interference-free, and the level of interference depends on the block length. In addition, the Walsh-Hadamard matrix sizes are limited to power of 2 values. Therefore, this technique does not have the flexibility to support an arbitrary frame length. Alternatively, the MIMO Alamouti technique can be straightforwardly employed for the FFT-FBMC transceiver [108], presented in Chapter 1, Section 1.2.3. The obtained BER performance is comparable to OFDM, however this technique is more computationally complex to implement than the other presented methods in this section, since additional FFTs must be computed at both transmitter and receiver sides.

3.3.7 Final discussions

From the above analysis, it can be inferred that, at comparable receiver complexity, the NPR1 and the MMB4 PFs can both support asynchronous communication and have comparable robustness against multipath channels. However, using the NPR1 PF provides the following advantages when compared to the MMB4 PF:

1. The complexity of the transmitter is reduced.
2. At a comparable data rate, a shorter frame can be employed, greatly reducing the latency.
3. Lower PAPR is achieved when the same PAPR reduction technique is employed.
4. The robustness against Doppler spread and CFO is increased.
5. Efficient use of Block-type MIMO Alamouti.
6. A block-type pilot structure can be efficiently supported.

On the other hand, the advantage of the MMB4 PF resides in its higher spectral confinement. Therefore, the short PFs become a much more interesting option for FBMC.

When compared to OFDM, the FBMC system with the NPR1 PF provides the following advantages:

1. Better spectrum shape; enabling to allocate more subcarriers at the edge of the bandwidth for higher spectral efficiency.
2. Support of relaxed synchronization or asynchronous communication,
3. Higher robustness against CFO,
4. Higher robustness against multipath channels having a large delay spread.

The first advantage enables an increase in the data by at most 10%, which is not negligible. The second advantage is one of the most important features of FBMC. It allows, in uplink communication, to avoid the signalling overhead introduced by complex synchronization mechanisms. Consequently, the energy-consumption is highly reduced. The third advantage is also interesting in uplink, as it allows the UE to use low-cost LO. If the CFO is correctly estimated, it can be perfectly compensated for in frequency domain even if each user is facing a different CFO value. This is particularly appealing for MMC. However, these advantages come at the cost of:

1. Slightly higher PAPR.
2. Larger receiver complexity.
3. Support of limited type of pilot structures (block-based).

The increase in complexity may not be considered as a critical issue in uplink since the receiver is at the BS, where the hardware resources are less limited when compared to UE. In this context, the complexity of the transmitter is more important. The pruned-IFFT based PPN-FBMC transmitter applied to short PFs enables to have a transmitter with a complexity comparable to OFDM.

When pre-coding techniques are employed for PAPR reduction, scattered-pilot or comb-type-pilot cannot be efficiently used. Indeed, for a given OFDM symbol, all the allocated subcarriers are pre-coded, leaving no place for reference signals. For this reason, block-type pilot structure is already employed in 4G/LTE uplink case. Therefore, the third drawback is not penalizing for FBMC in this context.

The only disadvantage is the slight increase in PAPR, which is about 0.3 dB according to Figure 1.10. This constitutes the remaining drawback for FBMC, and further research must be conducted to reduce this slight PAPR gap.

It is also worth noting that FBMC is not directly compatible with the MIMO Alamouti used in OFDM. Instead, a Block-based Alamouti must be employed, as described in Section 3.3.6.

3.4 Summary

In this chapter, two original FBMC receivers (OS-FBMC and OSB-FBMC) are presented in order to improve the system robustness, when using short PFs, against long delay spread channels and timing offset. The main two ideas are (1) to combine a time-domain equalizer based on an OS algorithm with the FBMC demodulation and (2) to design a block-based scheme where FBMC symbols are transmitted in blocks and demodulated all at once in the frequency domain.

One of the most interesting results is that the OS-FBMC receiver can support asynchronous communications when short PFs are employed. While the OSB-FBMC receiver cannot support asynchronous communications, its robustness against timing offset up to 21% of the symbol duration makes it a perfect candidate for relaxed synchronization. In addition, OSB-FBMC receiver is less complex than OS-FBMC receiver (assuming the same FFT size is used), and its block-based structure is perfectly adapted to support MIMO Alamouti scheme.

When facing multipath channel conditions with long delay spread, it is shown that both OS-FBMC and OSB-FBMC receivers achieve similar BER performance compared to the FS-FBMC receiver with the MMB4 long PF.

Considering these additional advantages brought by the proposed contributions in this chapter, FBMC with short PFs become very interesting solution to cope with the new 5G air interface requirements.

CHAPTER

4 Low-complexity transmitter for UF-OFDM

UF-OFDM waveform is another promising multicarrier waveform since it combines the advantages related to OFDM with better spectral properties and with improved robustness against time-frequency misalignment. However, its main drawback resides in the computational complexity of the transmitter reaching up to 200 times that of OFDM if no simplification is applied. While still of high complexity, recent proposed simplification techniques significantly compromise the achieved spectral confinement through signal approximations. In this context, a novel low-complexity UF-OFDM transmitter without any signal quality loss is proposed. For small subband sizes, the complexity becomes comparable to OFDM regardless of the number of allocated subbands. Furthermore, the proposed transmitter architecture is flexible and can be easily adapted to support OFDM modulation.

This chapter is organized as follows. The first section of presents a review on existing recent UF-OFDM transmitter implementations. The high complexity of these techniques is highlighted. The need to explore low complexity techniques without degrading the signal quality leads us to propose a novel UF-OFDM transmitter. The idea and the architecture of this transmitter are detailed. It is also shown that the proposed UF-OFDM transmitter can be easily adapted to support OFDM transmission. Analytical complexity comparison is provided for several configurations, corresponding to the extreme cases where a user occupies all the available bandwidth to achieve high date rates.

4.1 Existing UF-OFDM transmitters

The 5G of mobile communication systems is foreseen to support multiple new services while coexisting with the typical mobile broadband service of 4G/LTE. For internet-of-things applications, massive MMC service is introduced, adding specific requirements such as the support of imperfect synchronization. Other applications, like MCC, may require the support of low-latency communication, which can be achieved by reducing the time transmission interval. Therefore, multiple waveform parameters on the same carrier (often referred to as numerology) may be required to support all types of applications, which raises the issue of their coexistence. To partly answer these new challenges, novel waveforms have been designed and proposed for the upcoming 5G standard.

UF-OFDM is one of the key 5G candidate waveforms and was originally proposed in [34]. The original idea of this waveform consists in grouping multiple allocated subcarriers into subbands, independently filtered in the time domain. Thus, the filtering is realized subband-wise and not subcarrier-wise as in the FBMC [24]. UF-OFDM shows advantages for low-latency communications (MCC services) and enables the use of open-loop synchronization to save bandwidth and energy [36]. In addition, unlike other 5G candidate waveforms such as FBMC, the majority of the techniques employed in OFDM can be reused without significant modifications. For instance, the techniques presented in [109] are applicable to UF-OFDM.

However, the main drawback of the UF-OFDM modulation resides in the complexity of the transmitter. The baseline implementation is estimated to be up to 200 times more computationally complex than OFDM [4]. Some recent techniques have been proposed to reduce the computational complexity [4] [5], are presented in this section.

4.1.1 Baseline UF-OFDM transmitter

The principle of the UF-OFDM modulation is to group the complex samples carrying information into several subbands, each composed of Q subcarriers. These complex samples can be, for instance, symbols from a QAM constellation. A maximum of $K = \lfloor N/Q \rfloor$ subbands carrying Q subcarriers can be used, where N is the total number of subcarriers, and $\lfloor x \rfloor$ represents the largest integer less than or equal to x (floor operator). The secondary lobes (residual power outside the subbands) of each subband are attenuated by independent subband-wise filtering of length L samples. The resulting discrete time signal represents the sum of the signals emanating from the filtered subbands. It forms the UF-OFDM symbol, composed of $N + L - 1$ samples. The baseline UF-OFDM transmitter is represented in Figure 4.1.

Let c be a vector of length BQ containing the complex symbols to be transmitted. To map each symbol in c to the allocated subbands, we first group the symbols into B subsets $c_j(q)$, for $q \in [\![0, Q-1]\!] (= \{0, 1, ..., Q-1\})$, such that $c_j(q) = c(q + Qk)$. In order to support an arbitrary assignment of symbol groups to subbands, we define a bijective function $j = \phi(k)$ that maps the index $k \in \Omega_B$ of an allocated subband to a symbol group j, where Ω_B is the set of the B allocated subband indexes. The segmented samples

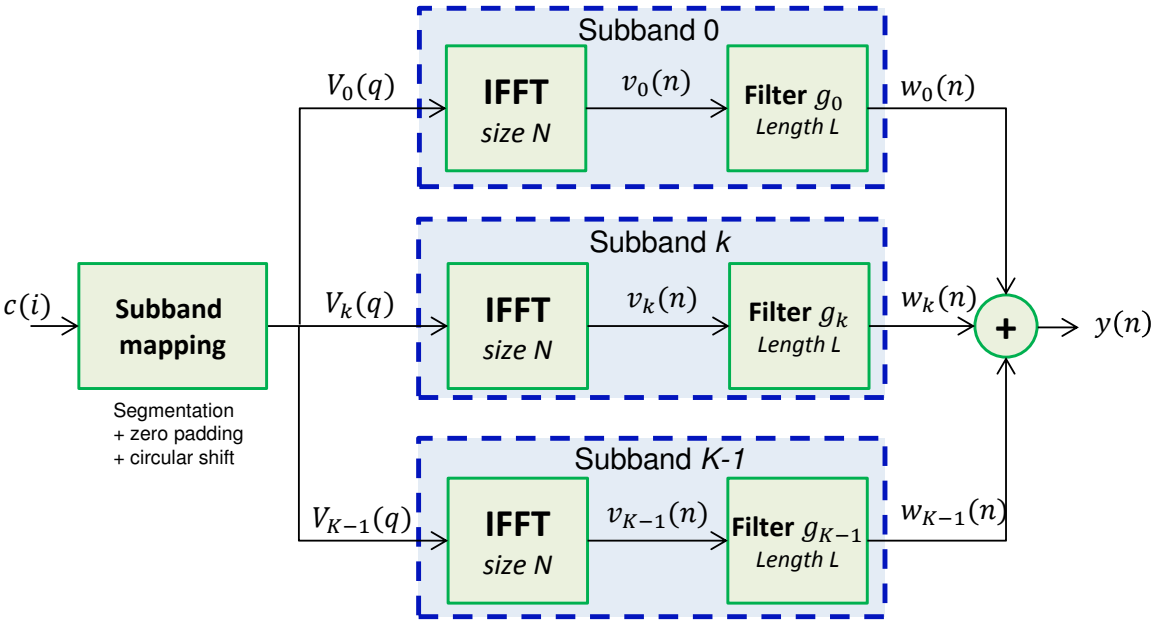

Figure 4.1 — Baseline UF-OFDM transmitter.

$s_k(q)$ for subcarrier index q of subband $k \in [\![0, K-1]\!]$ can then be expressed as

$$s_k(q) = \begin{cases} c_{\phi(k)}(q) & , k \in \Omega_B, \\ 0 & , k \notin \Omega_B. \end{cases} \tag{4.1}$$

In the frequency domain, a total of N subcarriers are defined. Thus, the samples $s_k(q)$ must be zero padded with $N - Q$ zeros

$$s'_k(q) = \begin{cases} s_k(q), & q \in [\![0, Q-1]\!] \\ 0, & q \in [\![Q, N-1]\!], \end{cases},$$

where $s'_k(q)$ represents the zero padded version of s_k. Then, a circular shift of $kQ + k_0$ samples is applied, to move each subband into its respective subband position in the frequency domain. The obtained signal $V_k(q)$ is expressed as

$$V_k(q) = s'_k(\mathrm{mod}_N(q - (kQ + k_0))),$$

where mod_N corresponds to the modulo N operator, $k_0 \in [\![0, Q-1]\!]$ corresponds to the value of the shift in number of subcarriers. This shift at subcarrier level can be used to move each subband to the center of the allocated bandwidth. For each index k, the $V_k(q)$ signal for subband k contains N samples, one for each subcarrier. However, only Q subcarriers, defining the subband number k, carry the information to transmit. The remaining subcarriers are not used (zero padded). Thus, each subband is isolated from the others, and can be processed independently. The subband mapping block represented in Figure 4.1 corresponds to the segmentation, the zero padding and the circular shift operations detailed above.

Next, the $V_k(q)$ samples are transformed to the time domain using an IFFT of size

N for each subband k:

$$v_k(n) = R_N(n) \sum_{q=0}^{N-1} V_k(q) e^{i2\pi \frac{qn}{N}}, n \in [\![0, N+L-2]\!], \tag{4.2}$$

where L is the length of the impulse response of the subband filter and $R_N(n)$ represents the rectangular window of length N: $R_N(n) = 1, n \in [\![0, N-1]\!]$ else 0. This window is introduced to limit the number of useful samples to transmit. It is not required in a practical implementation, since only N samples are usually computed by the IFFT processors, it is only used here for mathematical considerations since the IFFT is a periodic function. Therefore, it is omitted in Figure 4.1.

Then, as shown in Figure 4.1, each subband is filtered separately using a linear convolution by the impulse response of the subband filter g_k:

$$w_k(n) = \sum_{l=0}^{L-1} g_k(l) v_k(n-l), n \in [\![0, N+L-2]\!],$$

where $w_k(n)$ represents the result of the filtering operation. The impulse response of these filters can be obtained from the impulse response of a common filter $f_Q(n)$, that we refer to as the Subband Prototype Filter (SBF), as

$$g_k(n) = f_Q(n) e^{i2\pi \frac{kQn}{N}}, n \in [\![0, L-1]\!].$$

In fact, the impulse response of the subband filter number k corresponds to the impulse response of the SBF, shifted in frequency by kQ subcarriers. This frequency shift aligns the frequency response of the filter to the subband position k. Furthermore, the frequency response of the SBF f_Q is centered around the subcarrier index $Q/2$ if Q is even (or around $(Q-1)/2$ if Q is odd), corresponding to the center of a subband. If $f(n)$ is the impulse response of the SBF, then, for $n \in [\![0, L-1]\!]$, we have

$$f_Q(n) = \begin{cases} \frac{Q}{2} & Q \text{ even}, \\ \frac{Q-1}{2} & Q \text{ odd}. \end{cases} \tag{4.3}$$

In the literature, a typical choice for the SBF is the Dolph-Chebyshev filter [110]. More recently, a specific filter design has been studied to reduce the out-of-band power spectral leakage for UF-OFDM [111] and to improve robustness against frequency/timing-offset errors [112].

Finally, the $N+L-1$ time domain samples of the filtered subbands are summed together to form the UF-OFDM symbol $y(n)$, implicitly sampled at the frequency f_s

$$y(n) = \sum_{k=0}^{K-1} w_k(n), n \in [\![0, N+L-2]\!]. \tag{4.4}$$

In a practical implementation, only the B allocated subbands are considered to calculate the UF-OFDM symbol, since the $B-K$ other subbands correspond to zero-valued

samples in the time domain

$$y(n) = \sum_{k \in \Omega_B} w_k(n), n \in [\![0, N + L - 2]\!].$$

While this solution has an acceptable computational complexity for a limited number of allocated subbands, it becomes computationally expensive when the number of allocated subbands increases. Indeed, the computation of one subband requires the use of an IFFT of size N (complexity in $\mathcal{O}(N \log_2 N)$) and a linear convolution operation (complexity in $\mathcal{O}(L^2 + LN)$)). Therefore, the computation of only one subband already requires a larger number of operations than needed to compute one OFDM symbol (one IFFT of size N), due to the complexity overhead introduced by the linear convolution of the subband filtering stage. These operations have to be repeated for each allocated subband. For $B = 100$, which corresponds to the maximum number of resource blocks ($Q = 12$) that can be allocated in 4G/LTE, the computational complexity exceeds 200 times the computational complexity of the OFDM transmitter [4].

Few techniques with lower computational complexity have been investigated in the literature. Among existing techniques, one applies the subband filtering in the frequency domain instead of the time domain, and a second approximates the UF-OFDM signal by decomposing it into multiple windowed OFDM signals that are then summed. These approaches are reviewed in the following subsections. They reduce the computational complexity of the UF-OFDM transmitter, but at the cost of a degradation of the original signal.

4.1.2 Frequency domain approximation UF-OFDM transmitter

In this approach [4], the filtering stage and the summation of all subbands are computed in the oversampled frequency domain, i.e. before the IFFT. We refer to this technique as Frequency Domain Approximation (FDA) UF-OFDM in this chapter. The IFFT size is multiplied by N_{OS} which corresponds to a chosen oversampling factor. In general, this parameter is set to $N_{OS} = 2$ since this value provides the best compromise between approximation errors and computational complexity [4]. Additionally, the computation of the filtering stage in the frequency domain requires an IFFT of size N_0 and an FFT of size $N_{OS}N_0$ for each subband, where $N_0 \geq Q$ is a design parameter. Note that the computational complexity increases with the value of N_0. However, the impact on the OOBPL is reduced with respect to the baseline solution. Finally, only $N+L-1$ samples, corresponding to the length of one UF-OFDM symbol, are kept after the computation of the IFFT of size $N_{OS}N$.

As for the baseline solution, the complex samples carrying information to transmit $c(j)$ are segmented into B subbands of Q subcarriers. Then, for each subband k, the $s_k(q)$ samples (4.1) are appended with $(N_0Q)/2$ zeros at the extremities (zero padding).

The zero padded samples $a_k(q)$ are expressed as follows:

$$a_k(q) = \begin{cases} 0, & q \in [0, \frac{N_0-Q}{2} - 1] \\ s_k(q - \frac{N_0-Q}{2}), & q \in [\frac{N_0-Q}{2}, \frac{N_0+Q}{2} - 1] \\ 0, & q \in [\frac{N_0+Q}{2}, N_0 - 1] \end{cases}$$

Then, for each subband k, an IFFT of size N_0 is computed:

$$A_k(p) = \sum_{q=0}^{N_0-1} a_k(q) e^{i2\pi \frac{pq}{N_0}}$$

Next, the $A_k(p)$ samples are appended with $(N_{OS} - 1)N_0$ zeros (zero padding) for each subband k to obtain the signal $A'_k(p)$ expressed as follows:

$$A'_k(p) = \begin{cases} A_k(p), & p \in [0, N_0 - 1] \\ 0, & p \in [N_0, N_{OS}N_0 - 1] \end{cases}$$

Then, for each subband k, an FFT of size $2N_0$ is applied on the $A'_k(p)$ samples, and the resulting samples are multiplied by the approximation of the frequency response of the SBF F_{cut} to obtains the $a'_k(p)$ samples:

$$a'_k(p) = F_{cut}(p) \sum_{p=0}^{N_{OS}N_0-1} A'_k(p) e^{-i2\pi \frac{pq}{N_{OS}N_0}}$$

The computation of the F_{cut} coefficients is detailed in [4]. At this stage, each subband is filtered independently. Thus, filtered subbands must be summed together to obtain $x(q)$; the UF-OFDM symbol in the frequency domain. For this purpose, an overlapping summation is performed, expressed as follows:

$$x(q) = \sum_{k=0}^{K-1} a_k^{zp}(mod_{2N}(CS(k))),$$

where a_k^{zp} are the zero padded a'_k samples by $N_{OS}N - N_0$ zeros and $CS(k)$ is the value of the circular shift that should be applied on the $a'_k(p)$ samples for the subband number k, expressed as follows:

$$CS(k) = N_{OS}(kQ + k_0 - \frac{N_0 - Q}{2}).$$

This overlapping summation can be computed by successively using a zero padding operation on the a'_k samples, then by applying a circular shift of $S(k)$ samples on the zero padded samples, and finally by summing the shifted and zero padded samples for each subband k. The UF-OFDM symbol is obtained by using an IFFT of size $N_{OS}N$ and by only keeping the first $N + L - 1$ samples:

$$y(n) \approx \sum_{q=0}^{N_{OS}N-1} x(q) e^{i2\pi \frac{qn}{N_{OS}N}}, n \in [0, N + L - 2]$$

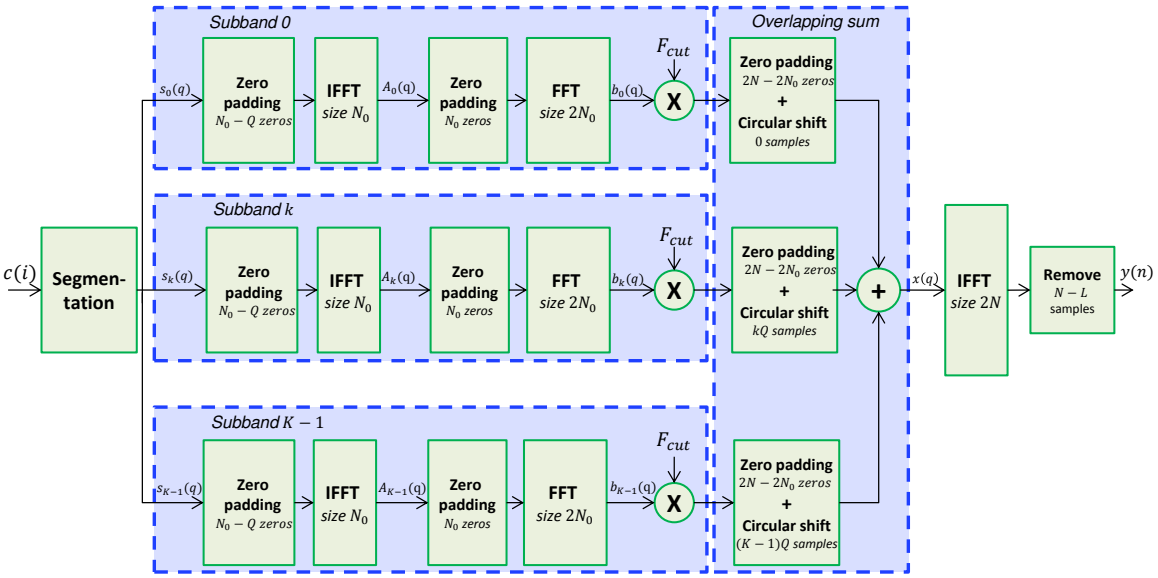

Figure 4.2 — Frequency domain UF-OFDM transmitter.

The above steps defining the FDA UF-OFDM technique are represented in Figure 4.2. Since this technique uses a smaller IFFT size per processed subband than the baseline solution presented in Subsection 4.1.1, the computational complexity is significantly reduced. However, it is still higher than that of OFDM, due to the use of an IFFT of size $N_{OS}N$ instead of N, and due to the additional small IFFT/FFT of size N_0 and $N_{OS}N_0$ for each allocated subband. According to [4], the required number of multipliers and adders can be up to 10 times higher than in the case of OFDM.

4.1.3 Time domain windowed UF-OFDM transmitter

The second simplified UF-OFDM transmitter is based on a time-domain processing without oversampling [5]. We refer to it as Time Domain Windowing (TDW) UF-OFDM in this chapter. It consists of subdividing each subband into small groups of subcarriers, each group being subcarrier-wise filtered by a dedicated filter. This subcarrier-wise filtering can be efficiently implemented by using a windowing operation in the time domain (after IFFT). The impulse response of the common group filter is used as window coefficients. This results in an approximation of the UF-OFDM signal, which is obtained by summing multiple windowed OFDM symbols as

$$y(n) \approx \sum_{j=0}^{N_w-1} w_j(n)u_j(n), n \in [0, N+L-2],$$

where N_w designates the number of subcarrier groups (equal to the number of windows), the $w_i(n)$ samples correspond to the window coefficients of the group number i, and $u_i(n)$ denote the OFDM symbols corresponding to the subcarrier group number i and periodically extended to $N + L - 1$ samples. These OFDM symbols are expressed as

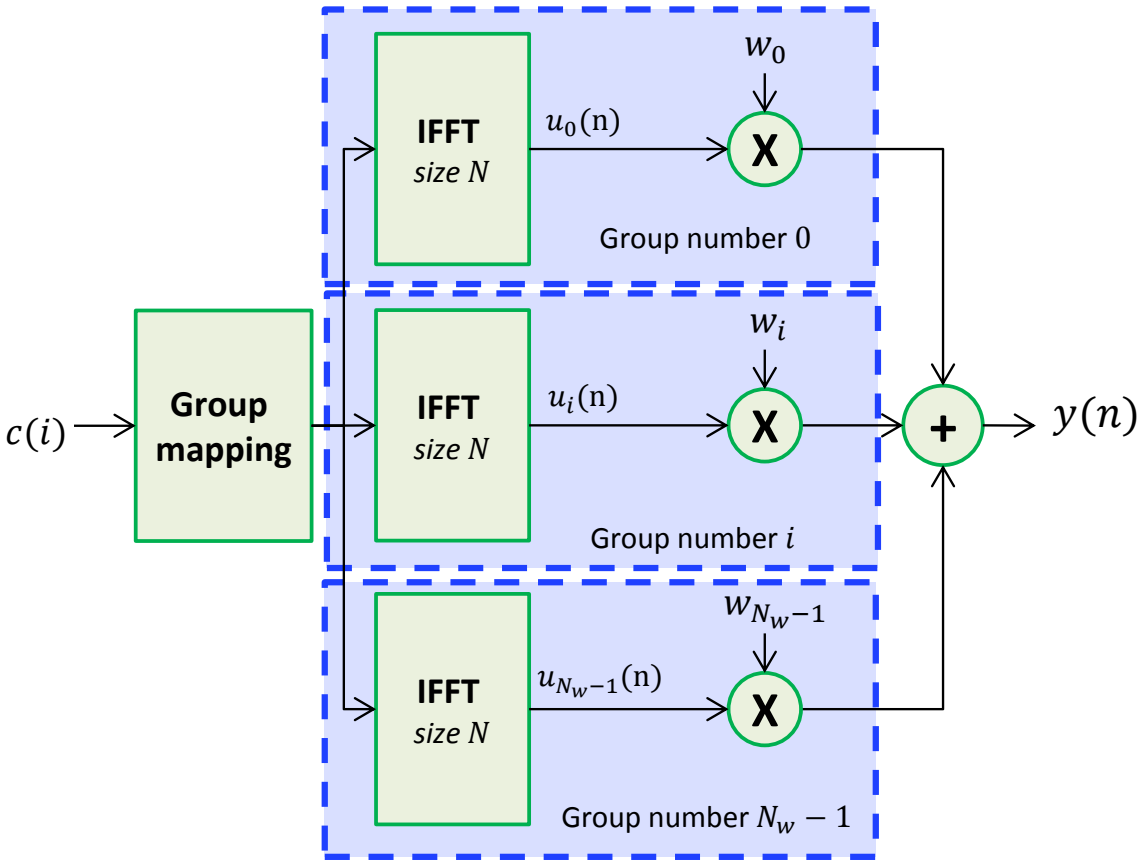

Figure 4.3 — Time domain windowed UF-OFDM transmitter.

follows:

$$u_j(n) = \sum_{k=0}^{K-1} \sum_{q \in \Psi(j)} s_q(k) e^{i2\pi \frac{(kQ+k_0+q)n}{N}},$$

where $\Psi(j)$ corresponds to the set of the subcarrier indexes of the group number j. It is equivalent to the computation of an IFFT of size N with non-zeros valued complex input samples at the subcarrier indexes $\{kQ + k_0 + q\}_{q \in \Psi(i)}$ [5]. Finally, the window coefficients are obtained by the following equation:

$$w_j(n) = \sum_{l=0}^{L-1} (f_Q(l) R_N(n-l) e^{i2\pi \frac{j(n-l)}{N}}),$$

where $R_N(n)$ and f_Q represent respectively the rectangular function of length N and the impulse response of the SBF, as defined in Subsection 4.1.1.

The computational complexity increases linearly with the number of windows being employed (in $\mathcal{O}(N_W N \log_2 N)$) comparable to N_W times the complexity of a typical OFDM transmitter. However, increasing the number of windows decreases the approximation errors and reduces the OOBPL. Similarly to the FDA UF-OFDM technique, a trade-off between approximation errors and computational complexity must be considered.

4.2 Proposed low-complexity UF-OFDM transmitter

For all simplified UF-OFDM transmitters, a compromise must be found between performance and complexity. Thus, a novel UF-OFDM technique that reduces the computational complexity to an acceptable level without altering the original signal is of high interest. The proposed approach achieves this goal by exploiting a specific decomposition into subband and subcarrier processing.

4.2.1 Description of the proposed technique

The proposed technique exploits two main ideas to reduce the computational complexity of the UF-OFDM baseline implementation. First, the required UF-OFDM processing is divided into subband-wise and subcarrier-wise computations in such a way to avoid redundant operations, especially when a high number of subbands is allocated. The second core idea is to divide the UF-OFDM symbol into prefix, core and suffix parts, which are efficiently processed by exploiting the previous decomposition into subband-wise and subcarrier-wise processing. The suffix part is deduced from the core part and the prefix part by a simple subtraction. These two core ideas exploit the UF-OFDM baseline equation. Therefore the resulting signal is not altered when compared to this baseline solution.

By using the circular shift property of the IFFT, (4.2) can be rewritten as

$$\begin{aligned} v_k(n) &= R_N(n) e^{i2\pi \frac{(kQ+k_0)n}{N}} \sum_{q=0}^{N-1} s'_k(q) e^{i2\pi \frac{qn}{N}} \\ &= e^{i2\pi \frac{k_0 n}{N}} R_N(n) \sum_{q=0}^{Q-1} s_k(q) e^{i2\pi \frac{(q+kQ)n}{N}}. \end{aligned} \tag{4.5}$$

To simplify the development of the following equations, the number of shifted subcarriers is assumed to be equal to zero ($k_0 = 0$). This constraint does not alter the following demonstration, since the frequency shifted UF-OFDM symbol can be recovered by applying a simple linear phase rotation to the unshifted UF-OFDM symbol. Thus, expression (4.4) of the UF-OFDM symbol combined with (4.5) becomes, for $n \in [\![0, N+L-1]\!]$,

$$\begin{aligned} y(n) = \sum_{k=0}^{K-1} \sum_{l=0}^{L-1} \Big(& f_Q(l) e^{i2\pi \frac{kQl}{N}} R_N(n-l) \\ & \times \sum_{q=0}^{Q-1} s_k(q) e^{i2\pi \frac{q+kQ}{N}(n-l)} \Big). \end{aligned}$$

It is possible to simplify this equation by rearranging the order of the three summations

as

$$y(n) = \sum_{q=0}^{Q-1} \sum_{l=0}^{L-1} \Big(f_Q(l) R_N(n-l) \sum_{k=0}^{K-1} s_k(q) e^{i2\pi \frac{q(n-l)+kQ(n-l)+kQl}{N}} \Big)$$
$$= \sum_{q=0}^{Q-1} \Big(f_q(n) \sum_{k=0}^{K-1} s_k(q) e^{i2\pi \frac{kQn}{N}} \Big), \tag{4.6}$$

with

$$f_q(n) = \sum_{l=0}^{L-1} f_Q(l) R_N(n-l) e^{i2\pi \frac{q(n-l)}{N}}. \tag{4.7}$$

These equations are further developed, by assuming that the total number of subcarriers across all the subbands (N) can be decomposed into an integer number of subbands ($\mathrm{mod}_Q(N) = 0$). Then we have $K = N/Q$, and (4.6) can be rewritten as

$$y(n) = \sum_{q=0}^{Q-1} f_q(n) x_q(n), \tag{4.8}$$

with

$$x_q(n) = \sum_{k=0}^{K-1} s_k(q) e^{i2\pi \frac{kn}{K}}, \tag{4.9}$$

where $x_q(n)$ corresponds to the IFFT of size K of the samples related to the subcarrier number q of each of the K subbands. Then, by exploiting the fact that the IFFT of size K is a periodic function of K samples, the first N samples of the UF-OFDM symbol ($y(n)$) can be decomposed into Q fragments of K samples ($N = K \times Q$). The fragmented symbol $y_p(n') = y(n' + pK)$, for $n' \in [\![0, K-1]\!]$ and $p \in [\![0, Q-1]\!]$, its expression can be written as

$$y_p(n') = \sum_{q=0}^{Q-1} f_q(n' + pK) x_q(n'). \tag{4.10}$$

Thus, it is possible to separate the processing of each subband (for a given subcarrier index) and the processing of each subcarrier (for a given subband index), as illustrated in Figure 4.4. The subband processing consists of calculating the $x_q(n')$ samples from (4.9) using an IFFT of size K. This processing must be repeated for all the Q subcarrier indexes, and K samples are generated per subband processing to obtain a total of N samples. Then, the UF-OFDM symbol is generated by the subcarrier processing that computes the $y_p(n')$ samples (for each subcarrier index q) from the subband processing according to (4.10). This separation between subband processing and subcarrier processing is the first core idea of the proposed technique and enables to reduce the computational complexity to process the first N samples of the UF-OFDM symbol. Indeed, the required number of operations scales in $\mathcal{O}(N\log_2(K))$ which is less computationally demanding than the processing of one IFFT of size N (in $\mathcal{O}(N\log_2(N))$). Furthermore, the computational complexity does not depend anymore on the number of allocated subbands B. However, the corresponding overhead introduced by the subcarrier processing (complexity in $\mathcal{O}(Q(N+L))$) is not negligible.

In fact, it is possible to further simplify the subcarrier processing by decomposing

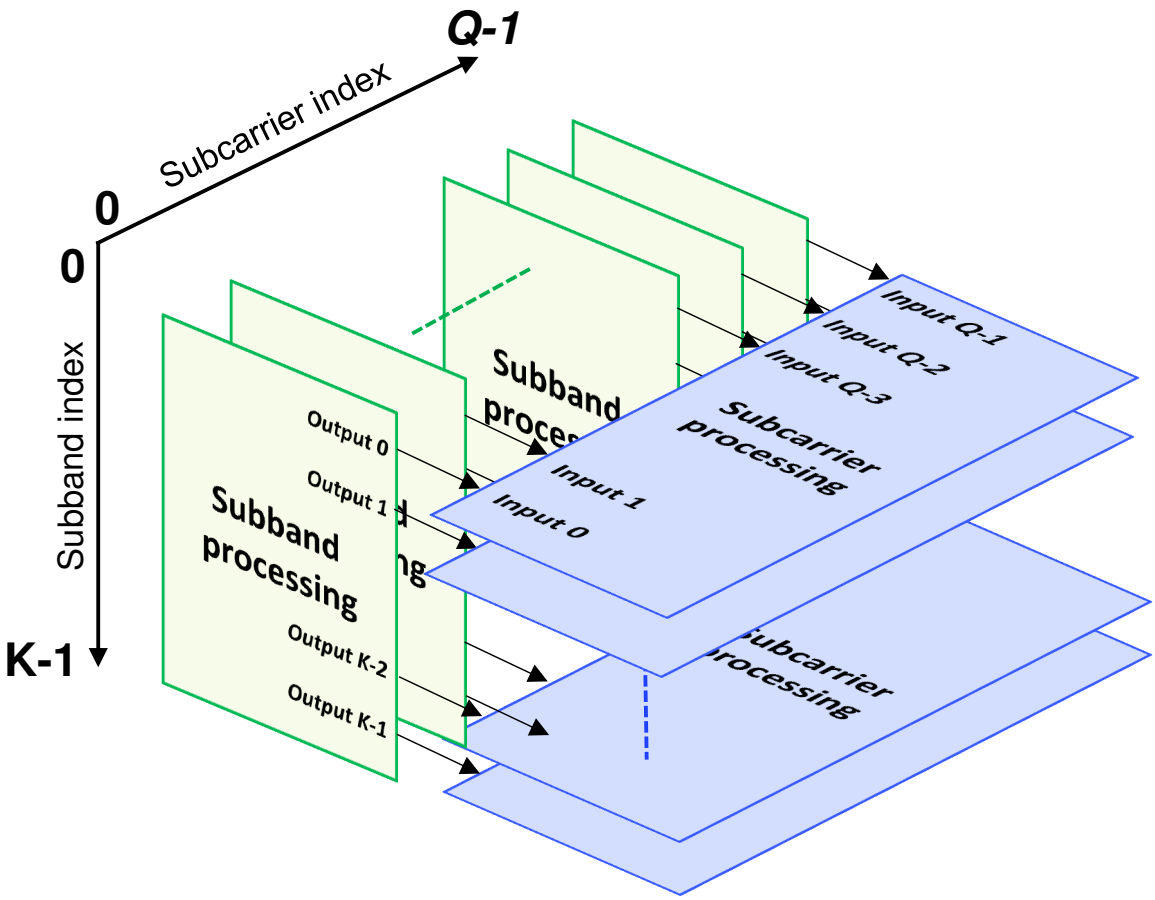

Figure 4.4 — Separation of the subband processing and the subcarrier processing.

the UF-OFDM symbol into 3 distinct parts, as shown in Figure 4.5:

- The first part of the UF-OFDM symbol corresponds to the first L samples processed by the linear convolution operation (subband filtering). This part of the UF-OFDM symbol has a signal envelope that corresponds to the shape of the first half of the impulse response of the SBF. We refer to this part as the prefix part of the UF-OFDM symbol.
- The second part of the UF-OFDM symbol, which we call the core part, is composed of $N - L$ samples and corresponds to the samples in the interval $n \in [\![L, N-1]\!]$. This part of the symbol can be seen as the result of a circular convolution applied to the output of the IFFTs of size N of the UF-OFDM baseline solution.
- Finally, the last part of the UF-OFDM symbol corresponds to the last $L-1$ samples processed by the linear convolution operation. This part of the UF-OFDM symbol has a signal envelope that corresponds to the shape of the second half of the impulse response of the SBF. We refer to this part as the suffix part of the UF-OFDM symbol.

The core part of the UF-OFDM symbol can be efficiently computed by noting that

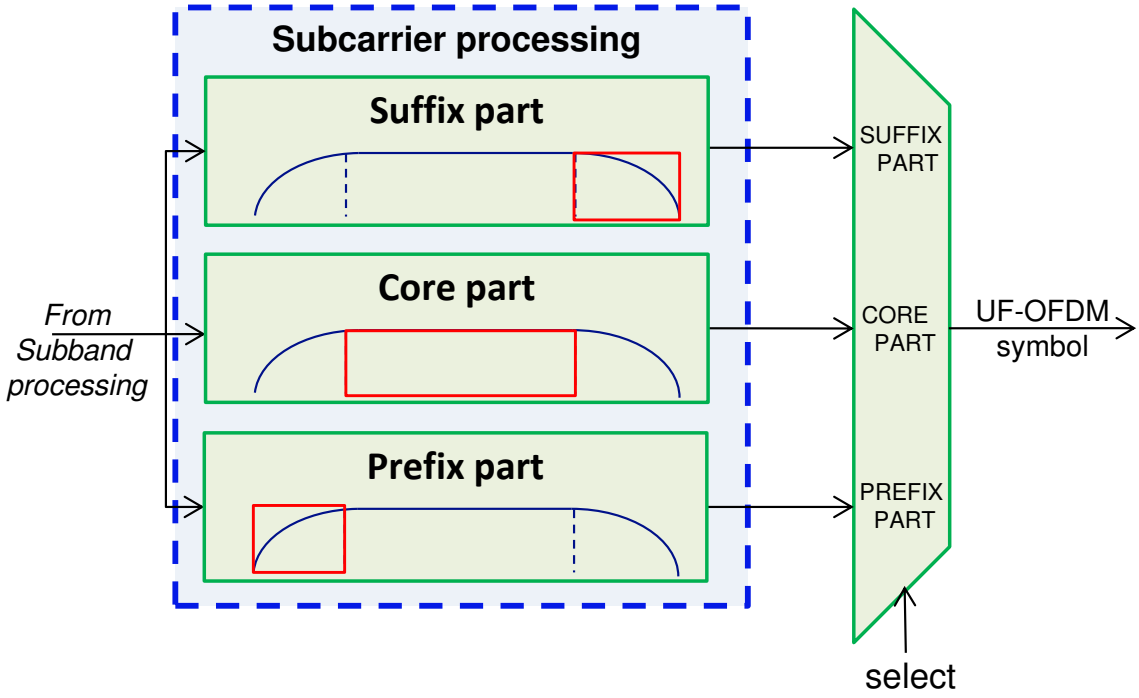

Figure 4.5 — Decomposition of the subcarrier processing into a prefix, core, and suffix parts.

(4.7) can be simplified when $n \in [\![L, N-1]\!]$ as

$$f_q(n) = e^{i2\pi \frac{qn}{N}} \sum_{l=0}^{L-1} f_Q(l) e^{-i2\pi \frac{ql}{N}}.$$

Furthermore, these coefficients can be segmented as follows:

$$f_q(n' + pK) = e^{i2\pi \frac{qp}{Q}} F_q(n'),\ (n' + pK) \in [\![L, N-1]\!], \tag{4.11}$$

with

$$F_q(n') = e^{i2\pi \frac{qn'}{N}} \sum_{l=0}^{L-1} f_Q(l) e^{-i2\pi \frac{ql}{N}}. \tag{4.12}$$

The coefficients $F_q(n')$ can be obtained by applying an FFT of size N on the impulse response of the SBF $f_Q(l)$. From the result of this FFT, only the first Q coefficients are useful (since $q \in [\![0, Q-1]\!]$). Then, a linear phase rotation is applied (the exponential term) for each subcarrier index q. In total, $Q \times K = N$ coefficients are generated. These coefficients constitute the filter core coefficients. By combining the equation of the segmented samples (4.10) with the equation of the segmented filter coefficients (4.11), we obtain

$$y_p(n') = \sum_{q=0}^{Q-1} z_q(n') e^{i2\pi \frac{qp}{Q}}, (n' + pK) \in [\![L, N-1]\!], \tag{4.13}$$

with

$$z_q(n') = F_q(n') x_q(n'). \tag{4.14}$$

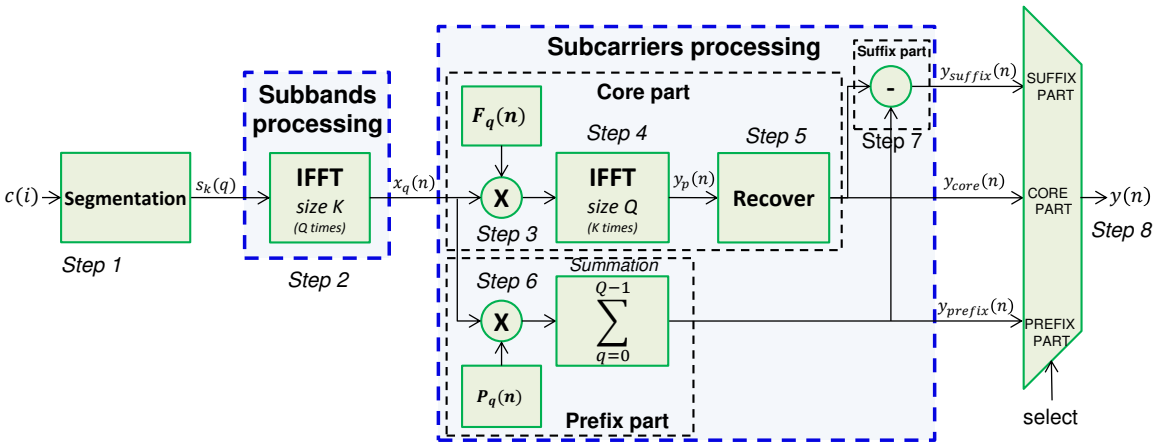

Figure 4.6 — Proposed low-complexity UF-OFDM transmitter.

The $z_q(n')$ samples are obtained after multiplication of the $x_q(n')$ samples by the filter core coefficients $F_q(n')$ defined in (4.12), and can be seen as a windowing operation. Then, the n'-th samples of each of the Q fragments are calculated using an IFFT of size Q of the windowed samples $z_q(n')$ across the Q subcarriers. With the proposed separation between subband and subcarrier processing, it is then possible to efficiently compute the core part of the UF-OFDM symbol by using K IFFTs of size Q, reducing the computational complexity to $\mathcal{O}(N\log_2(Q))$. As shown in Figure 4.4, the Q input samples of the subcarrier processing number $n' \in [\![0, K-1]\!]$ corresponds to the output samples number n' of the Q subbands processing. Thus, for the subcarrier processing, the order in which the subcarrier and subband samples are processed is interleaved when compared to the subband processing. Each subcarrier processing requires one windowing stage and one IFFT of size Q to generate Q samples of the segmented core part. Then, the core part is recovered using the following equation:

$$y_{\text{core}}(n) = y_{\lfloor n/K \rfloor}(\text{mod}_K(n)). \tag{4.15}$$

After the computation of the core part ($n \in [\![L, N-1]\!]$), the prefix ($n \in [\![0, L-1]\!]$) and suffix ($n \in [\![N, N+L-2]\!]$) parts of the UF-OFDM symbol must be calculated. When $n_p \in [\![0, L-1]\!]$, n_p being the sample index of the prefix part, (4.7) becomes

$$\begin{aligned} f_q(n_p) &= e^{i2\pi \frac{qn_p}{N}} \sum_{l=0}^{n_p} f_Q(l) e^{-i2\pi \frac{ql}{N}} \\ &= P_q(n_p). \end{aligned} \tag{4.16}$$

The $P_q(n_p)$ coefficients constitute the prefix tail coefficients. An efficient way to calculate these coefficients is by exploiting the following

$$\begin{aligned} P_q(n_p+1) &= e^{i2\pi \frac{q(n_p+1)}{N}} \sum_{l=0}^{n_p+1} f_Q(l) e^{-i2\pi \frac{ql}{N}} \\ &= f_Q(n_p+1) + P_q(n_p) e^{i2\pi \frac{qn_p}{N}}. \end{aligned}$$

Thus, the prefix tail coefficient number $n_p + 1$ can be recursively calculated by adding the sample number $n_p + 1$ of the impulse response of the SBF to the previously calculated prefix tail coefficients (number n_p), after multiplication by a linear phase rotation term. This efficient way to compute the prefix tail coefficients is interesting if there is a requirement to generate these filters in real time, for instance to support multiple types of filter coefficients and/or filter lengths. Otherwise, such coefficients can be simply pre-computed and stored in a LUT. Then, the prefix part of the UF-OFDM symbol $y_{\text{prefix}}(n_p)$ can be deduced from equation (4.8)

$$y_{\text{prefix}}(n_p) = \sum_{q=0}^{Q-1} P_q(n_p) x_q(n_p), n_p \in [\![0, L-1]\!]. \tag{4.17}$$

The samples corresponding to the prefix part of the UF-OFDM symbol are obtained by:

- Multiplying the $x_q(n_p)$ samples by the prefix tail coefficients $P_q(n_p)$, which can be seen as a windowing operation.
- Summing over the subcarrier index q all the Q windowed samples for each sample n of the prefix part.

The generation of the prefix part can be included in the subcarrier processing of Figure 4.4 since the interconnections between the subband and the subcarrier processing are unchanged. The sample number n of the prefix part is generated from the output number n of each of the Q subband processing blocks. For the suffix part of the UF-OFDM symbol, we have $n_s \in [\![N, N+L-2]\!]$, and in that case (4.7) becomes

$$\begin{aligned} f_q(n_s) &= e^{i2\pi \frac{qn}{N}} \sum_{l=n_s-N+1}^{L-1} f_Q(l) e^{-i2\pi \frac{ql}{N}}, \\ &= S_q(n_s). \end{aligned}$$

The coefficients $S_q(n_s)$ denote the suffix tail coefficients. These coefficients can be deduced by subtracting the filter core coefficients from the prefix tail coefficients as follows:

$$\begin{aligned} S_q(n_s) &= e^{i2\pi \frac{qn}{N}} \Big(\sum_{l=0}^{L-1} f_Q(l) e^{-i2\pi \frac{ql}{N}} - \sum_{l=0}^{n_s-N} f_Q(l) e^{-i2\pi \frac{ql}{N}} \Big), \\ &= F_q(n_s) - P_q(n_s - N). \end{aligned}$$

Then, the suffix part of the UF-OFDM symbol can be deduced from (4.8):

$$y(n_s) = \sum_{q=0}^{Q-1} \Big(F_q(n_s) - P_q(n_s - N) \Big) x_q(n_s),\ n_s \in [\![N, N+L-2]\!].$$

Due to the periodicity of $x_q(n_s)$ and $F_q(n_s)$, the above equation is equivalent to:

$$y(n_s) = \sum_{q=0}^{Q-1} \Big(F_q(n_s - N) - P_q(n_s - N) \Big) x_q(n_s - N).$$

Thus, the suffix part $y_{\text{suffix}}(n_s)$ can be expressed as follows for $n_s \in [\![0, L-2]\!]$:

$$\begin{aligned} y_{\text{suffix}}(n_s) &= y(n_s + N) \\ &= \sum_{q=0}^{Q-1} \Big(F_q(n_s) - P_q(n_s) \Big) x_q(n_s) \\ &= y_{\text{core}}(n_s) - y_{\text{prefix}}(n_s), \end{aligned} \tag{4.18}$$

where the support of $y_{\text{core}}(n)$ is extended to $n \in [\![0, N-1]\!]$ instead of $[\![L, N-1]\!]$ as in (4.13). The samples in the interval $n \in [\![0, L-1]\!]$ are only generated to compute the suffix part of the UF-OFDM symbol. This shows that the suffix part of the UF-OFDM symbol can be simply deduced by subtracting the core part of the UF-OFDM symbol from its prefix part, avoiding additional computational complexity overhead. Finally, the complete UF-OFDM symbol is obtained by the concatenation of the prefix part, the core part and the suffix part

$$y(n) = \begin{cases} y_{\text{prefix}}(n), & n \in [\![0, L-1]\!] \\ y_{\text{core}}(n), & n \in [\![L, N-1]\!] \\ y_{\text{suffix}}(n-N), & n \in [\![N, N+L-2]\!] \end{cases} \tag{4.19}$$

The proposed UF-OFDM transmitter is illustrated in detail in Figure 4.6 and can be summarized by the 8 steps:

Step 1) Segment the complex source symbols c into B subbands of Q subcarriers.

Step 2) Compute the IFFT of size K of the segmented samples (from step 1) corresponding to the qth subcarrier of each of the K subbands. This IFFT has to be computed Q times, for each subcarrier $q \in [\![0, Q-1]\!]$ to obtain the $x_q(n)$ samples.

Step 3) Multiply the $x_q(n')$ samples (from step 2) by the SBF coefficients $F_q(n')$ to obtain the windowed samples $z_q(n')$.

Step 4) Compute the IFFT of size Q of the windowed sample $z_q(n')$ for the n-th sample index of each of the Q subcarriers. This IFFT has to be computed K times, for each sample, to obtain the fragmented samples $y_p(n')$.

Step 5) Recover the core part of the UF-OFDM symbol from the fragmented samples $y_p(n')$.

Step 6) Calculate the prefix part of the UF-OFDM symbol by multiplying the $x_q(n_p)$ samples by the prefix tail coefficients $P_q(n_p)$, and by summing them over each subcarrier index $q \in [\![0, Q-1]\!]$.

Step 7) Calculate the suffix part of the UF-OFDM symbol ($y_{\text{suffix}}(n_s)$) by subtracting the samples of the core part ($y_{\text{core}}(n_s)$) from the samples of the prefix part ($y_{\text{prefix}}(n_s)$) for $n_s \in [\![0, L-2]\!]$.

Step 8) Concatenate the prefix part, the core part and the suffix part to obtain the UF-OFDM symbol.

Note that the generation of the prefix and the core parts being independent, step 4/5 and step 6 can be processed in any order. Only the generation of the suffix part (step 7) requires to first compute the prefix part and the core part of the UF-OFDM symbol.

The proposed UF-OFDM technique generates the UF-OFDM symbol without frequency shift, since it was assumed to be equal to 0 to simplify the development of the equations. When the frequency shift by (k_0 subcarriers) is taken into account, the equation of the frequency shifted UF-OFDM symbol is given by

$$y'(n) = e^{i2\pi\frac{k_0 n}{N}} y(n), n \in [\![0, N+L-2]\!].$$

This additional linear phase rotation would increase the complexity of the transmitter by adding $N+L-1$ complex multipliers. It is however possible to calculate the frequency shifted UF-OFDM symbol more efficiently. Indeed, for the prefix part of the UF-OFDM symbol ($y_{\text{prefix}}(n)$), the linear phase rotation term can be included in the prefix tail coefficients:

$$P_q(n_p) = e^{i2\pi\frac{(q+k_0)n_p}{N}} \sum_{l=0}^{n_p} f_Q(l) e^{-i2\pi\frac{ql}{N}}.$$

Concerning the core part of the UF-OFDM symbol $y_{\text{core}}(n)$, the fragmented samples $y_p(n')$ can be expressed as follows:

$$y_p(n') = e^{i2\pi\frac{k_0 p}{Q}} \sum_{l=0}^{Q-1} (z_q(n') e^{i2\pi\frac{k_0 n'}{N}} e^{i2\pi\frac{qp}{Q}}).$$

The term $\exp[i2\pi(k_0 n')/N]$ can be included in the core filter coefficients $F_q(n)$ and the term $\exp[i2\pi(k_0 p)/Q]$ is equivalent to a circular shift of k_0 samples applied to the inputs of the IFFT of size Q (on the windowed samples $z_q(n)$)

$$y_p(n') = \sum_{q=0}^{Q-1} z_{q-k_0}(n') e^{i2\pi\frac{qp}{Q}},$$

with the filter core coefficients given by

$$F_q(n') = e^{i2\pi\frac{(q+k_0)n'}{N}} \sum_{l=0}^{L-1} (f_Q(l) e^{-i2\pi\frac{ql}{N}}).$$

Therefore, the frequency shift of k_0 subcarriers does not introduce any computational complexity overhead.

4.2.2 Adaptation for any subband size

The proposed technique detailed in Subsection 4.2.1 assumes that the total number of subcarriers across all the subbands N can be divided into an integer number of subbands ($\text{mod}_Q(N) = 0$). However, in the particular case of 4G/LTE system, the minimum allocation size, called a RB, corresponds to 12 subcarriers (frequency) and 7 OFDM symbols (time). Thus, the subband size Q must be equal to a multiple of 12, whereas

the IFFT size in 4G/LTE is defined to be a power of 2 in most cases. The only exception concerns the numerology related to the 15 MHz bandwidth case, where the IFFT size is equal to 1536 and the proposed technique can be directly applied for this case since $\mathrm{mod}_{12}(1536) = 0$.

One straightforward solution is to adapt the subband size to satisfy both the simplification constraints and the LTE allocation size. Such condition is satisfied if $Q = 4$, implying that each allocated RB is divided into 3 subbands. However, the spectral confinement and system performance would be negatively affected for such values.

A second solution is to consider a power of 2 subband size, allocate the complex sample carrying information to the center of the corresponding allocated subbands, and pad with zero-valued samples the edge of the first and last allocated subbands to complete the subband allocation. As an example, if 1 RB must be allocated, then $Q = 16$ and $B = 1$ can be chosen, and $(Q - 12)/2 = 2$ zeros must be inserted at each edge of the allocated subbands. More generally, if P corresponds to the minimum allocation size (in number of subcarriers) supported by the communication system ($P = 12$ in 4G/LTE) and N_P is the number of allocated P subcarriers, then, if the subband size Q is kept unvaried, we have:

$$B = \left\lceil \frac{N_P \times P}{Q} \right\rceil,$$

$$N_{ZP} = \frac{B \times Q - N_P \times P}{2},$$

where N_{ZP} corresponds to the number of zero valued samples which must be padded at each edge of the allocated subbands. If the number of allocated subbands B is equal to 1, any subband size superior to P can be used and leads to the same spectral confinement as the baseline solution with $Q = P$, since the SBF coefficients ($f(n)$) do not depend on the subband size Q. However, for a higher number of allocated subbands, the presence of zero-padded samples at the edges of the allocated subbands can impact the spectral confinement and the performance of the system. Thankfully, this solution can be used without performance degradation when $N_{ZP} = 0$, namely when $\mathrm{mod}_Q(N_P \times P) = 0$, but this does not cover all the 4G/LTE RB allocation possibilities. A third solution is to increase, at the transmitter side, the total number of subcarriers and the frequency sampling by a factor β such that:

$$\mathrm{mod}_P(\beta N) = 0, 1 \leq \beta < 2$$

with $\beta = 1.5$ to support 4G/LTE numerology. The subcarrier spacing being equal to the ratio between the frequency sampling and the total number of subcarriers ($\Delta f = f_s/N$), it remains unchanged (15 kHz for 4G/LTE). The subband size is now a multiple of P, satisfying the condition to employ the proposed technique. Note that this solution does not require changing the frequency sampling and the total number of subcarriers at the receiver side, since it is an oversampling technique. Thus, such solution is transparent for the receiver and is totally compatible with 4G/LTE numerology. Using an IFFT size which is not a power of 2 can be seen as a drawback, but as mentioned in the beginning of this subsection, 4G/LTE numerology requires the support of an IFFT of size 1536 ($= \beta \times 2^{10}$), and the FFT precoder of the Single Carrier (SC) OFDM modulation used

in 4G/LTE uplink already requires a size which is a multiple of 12 (more precisely, FFT of size $N = 2^a 3^b 5^c \leq 1200$). Furthermore, if Q ($\neq 2^n$) can be decomposed into a product between a power of 2 integer number (Q_N) and any integer number R ($Q = Q_N \times R$), then it is possible to calculate an IFFT of size Q from R IFFTs of size Q_N as follows:

$$\begin{aligned} x(n) &= \sum_{k=0}^{RQ_N-1} X(k) e^{i2\pi \frac{kn}{RQ_N}} \\ &= \sum_{k=0}^{R-1} e^{i2\pi \frac{kn}{R}} \sum_{l=0}^{Q_N-1} X(kQ_N + l) e^{i2\pi \frac{ln}{Q_N}}. \end{aligned} \tag{4.20}$$

As an example, if the subband size is set to the 4G/LTE RB size composed of 12 subcarriers, then the IFFT of the subcarrier processing part can be calculated using 3 IFFTs of size 4. The main issue with this solution is that the computational complexity is increased due to the oversampling.

4.2.3 Flexibility to support OFDM modulation

With the increasing number of scenarios supported in 5G, some applications may require the reuse of the classical OFDM modulation of 4G/LTE in addition to the support of novel multicarrier waveforms such as UF-OFDM. This implies that the transmitter should be able to switch between UF-OFDM and OFDM modulations without major modifications to the computation core, to avoid the duplication of the processing units when considering hardware implementation issues.

In fact, the signal decomposition presented in Sub-section 4.2.1 can be applied for OFDM. Indeed, the OFDM symbol with the extension of a CP of length L can be generated as

$$y(n) = \sum_{k=0}^{N-1} c(k) e^{i2\pi \frac{kn}{N}}, n \in [\![-L, N-1]\!].$$

The signal $y(n)$ can be decomposed into virtual (non-filtered) subbands as

$$\begin{aligned} y(n) &= \sum_{q=0}^{Q-1} \sum_{k=0}^{K-1} c(q + Qk) e^{j2\pi \frac{(q+Qk)n}{N}} \\ &= \sum_{q=0}^{Q-1} e^{j2\pi \frac{qn}{N}} \sum_{k=0}^{K-1} s_k(q) e^{j2\pi \frac{kn}{K}} \\ &= \sum_{q=0}^{Q-1} x_q(n) e^{i2\pi \frac{qn}{K}}. \end{aligned} \tag{4.21}$$

Similarly to an UF-OFDM symbol, the OFDM symbol can be segmented as

$$y_p(n') = \sum_{q=0}^{Q-1} F'_q(n') x_q(n') e^{i2\pi \frac{qp}{Q}},$$

with

$$F'_q(n') = e^{j2\pi \frac{qn'}{N}},$$

Therefore, the OFDM symbol without the cyclic prefix can be generated by using the equation of the UF-OFDM core part and changing the filter core coefficients to $F'_q(n')$. The cyclic prefix part can be generated by using (4.17) (step 6 of the method), and is given by

$$y_{\text{prefix}}(n_p) = y(n_p - L) = \sum_{q=0}^{Q-1} x_q(n_p - L)P'_q(n_p), n_p \in [\![0, L-1]\!],$$

with

$$P'_q(n_p) = e^{j2\pi \frac{q(n_p - L))}{N}}.$$

The prefix tail coefficients of the UF-OFDM modulation (4.16) must be replaced by the $P'_q(n)$ coefficients defined above. An alternative way to generate the cyclic prefix is simply by copying the last L samples of the core part. This can be done during the recover step (step 5) since it is a concatenation operation. The cyclic prefix can be inserted at the same time, without any complexity increase. Note that, for the two proposed cyclic-prefix insertion methods, the cyclic prefix length in OFDM mode can be different from the filter length in UF-OFDM mode. The related processing unit just has to be adapted to process the corresponding length.

4.3 Computational complexity analysis and comparisons

4.3.1 Complexity analysis

We evaluate the computational complexity of the proposed technique in terms of the number of Real Addition (RA)s and Real Multiplication (RM)s required to compute one UF-OFDM symbol, and compare it with state-of-the-art approaches for UF-OFDM modulation. We distinguish RAs and RMs because their impact on implementation complexity can differ depending on the type of implementation. For instance, when considering a dedicated hardware implementation, a RM requires more hardware resources (more logic gates) than a RA.

For complex-valued operations, it is necessary to define the number of RMs and RAs required to compute one complex multiplication (CM). We denote by $C_{\text{RM}}(x)$ and $C_{\text{RA}}(x)$ respectively the number of RMs and RAs required for the operation x. Typically, a complex multiplication requires $C_{\text{RM}}(\text{CM}) = 4$ RMs and $C_{\text{RA}}(\text{CM}) = 2$ RAs. But a complex multiplication can be also be counted as $C_{\text{RM}}(\text{CM}) = 3$ RMs and $C_{\text{RA}}(\text{CM}) = 5$ RAs by using the following development:

$$(a + jb)(c + jd) = c(a + b) - b(c + d) + j(c(a + b) + a(d - c)).$$

Furthermore, if a complex sample is multiplied by pre-computed complex coefficients (for instance, filter coefficients), 2 RAs can be removed and $C_{RA}(\text{complexMultiplier}) = 3$.

Indeed, if $c+jd$ is the pre-computed complex coefficient, then $c+d$ and $d-c$ can also be pre-computed instead of directly calculated. Since all the complex multiplications of the UF-OFDM techniques involve a pre-computed coefficient, only 3 RAs are required for any complex multiplication. Thus, $C_{\mathrm{RM}}(\mathrm{CM}) = 3$ RMs and $C_{\mathrm{RA}}(\mathrm{CM}) = 3$ are considered in this section.

In addition, the choice of the IFFT computation technique is another critical aspect when considering complexity, since this choice has a significant impact on the required number of RMs and RAs. A well-known and efficient IFFT computation technique is the split radix IFFT [99], which can be used when the IFFT size is a power of 2 ($N = 2^n$). The computational complexity of the split radix IFFT of size N, refered as $C_{\mathrm{RA/RM}}(\mathrm{IFFT}_N)$, is given by [100]

$$C_{\mathrm{RM}}(\mathrm{IFFT}_N) = N\log_2(N) - 3N + 4,$$

$$C_{\mathrm{RA}}(\mathrm{IFFT}_N) = 3N\log_2(N) - 3N + 4.$$

The computational complexity of the baseline UF-OFDM technique is not considered in this section due to its relatively high complexity when compared to the other presented techniques. This baseline solution is generally presented for understanding and illustrating the UF-OFDM modulation and its specific per-subband filtering. On the other hand, computational complexity analysis of the FD UF-OFDM, the TDW UF-OFDM and the proposed UF-OFDM techniques are derived in the rest of this subsection.

4.3.1.1 FDA UF-OFDM

As explained in Subsection 4.1.2, the FDA UF-OFDM technique employs multiple small IFFTs of size proportional to N_0 in the oversampled frequency domain (by an oversampling factor N_{OS}) to efficiently process the subband filter. In this section, the oversampling factor N_{OS} is fixed to 2 since this value provides a good trade-off between the signal approximation error and the computational complexity. Thus, the computational complexity of the FDA UF-OFDM technique is given by

$$\begin{aligned} C_{\mathrm{RM}}(\text{FD UF-OFDM}) =& B\Big(C_{RM}(\mathrm{FFT}_{N_0}) + C_{\mathrm{RM}}(\mathrm{IFFT}_{2N_0}) \\ &+ 6N_0\Big) + C_{RM}(\mathrm{IFFT}_{2N}), \end{aligned}$$

$$\begin{aligned} C_{\mathrm{RA}}(\text{FD UF-OFDM}) =& B\Big(C_{\mathrm{RA}}(\mathrm{FFT}_{N_0}) + C_{\mathrm{RA}}(\mathrm{IFFT}_{2N_0}) \\ &+ 6N_0\Big) + C_{\mathrm{RA}}(\mathrm{IFFT}_{2N}) \\ &+ 4(B-1)N_0. \end{aligned}$$

Table 4.1 — Choice of N_0 depending on the subband size for the FD UF-OFDM technique.

Subband size	N_0	Normalized Mean Square Error (NMSE) (dB)
12	64	-25.8
16	64	-25.6
48	128	-29.3
64	128	-28

Due to the IFFT of size $2N$, the FDA UF-OFDM is in any case more computational complex than an OFDM transmitter which only requires an IFFT of size N. Furthermore, the complexity is dependent on the number of allocated subbands and the chosen small IFFT size N_0. For each allocated subband, one FFT of size N_0, one IFFT of size $2N_0$ and $2N_0$ complex multiplications (subband filtering) have to be computed. Thus, the computational complexity increases linearly with the number of allocated subbands. Additionally, when the subband size changes, the choice of N_0 must be reconsidered such that the approximation errors are kept within an acceptable level. The choice of $N_0 = 64$ determined in [111] is applicable for $Q = 12$. However, for other subband sizes, no analysis has been performed in the literature. In order to fairly evaluate the computational complexity, the NMSE of the approximated UF-OFDM symbol has been evaluated for the subband size of 12, 16, 48 and 64 subcarriers for different N_0 values. Table 4.1 shows the N_0 values corresponding to each of these subband sizes for an NMSE inferior to -25 dB, assuming a Dolph-Chebyshev filter [110] with a sidelobe level of 70 dB. This value was chosen to obtain an NMSE level comparable to the one obtained for the case where $Q = 12$ and $N_0 = 64$, to keep an acceptable approximation error. It can be seen from Table 4.1 that the N_0 value is only doubled if the subband size is multiplied by 4. This implies that the computational complexity does not increase linearly with the subband size, contrary to the number of allocated subbands. Thus, it is preferable to use few subbands of large size instead of multiple subbands of short size when considering this technique.

4.3.1.2 TDW UF-OFDM

The complexity of this method mainly depends on the number of windows N_w. A TDW UF-OFDM transmitter using N_w windows will be denoted by TDW_{N_w} UF-OFDM in this section. According to [5], the computational complexity of this technique in terms of number of required RMs and RAs is

$$C_{\text{RM}}(\text{TDW}_{N_w}\ \text{UF-OFDM}) = N_w\Big(C_{RM}(\text{IFFT}_N) + 3(N + L - 1)\Big),$$

$$\begin{aligned} C_{\mathrm{RA}}(\mathrm{TDW}_{N_w}\ \text{UF-OFDM}) =& N_w\Big(C_{RA}(\mathrm{IFFT}_N) \\ &+ 3(N+L-1)\Big) \\ &+ (N_w-1)(N+L-1). \end{aligned}$$

Contrary to the FDA UF-OFDM technique, the computational complexity does not increase with the number of allocated subbands B. However, it increases linearly with the number of windows N_w. When only 1 window is used ($N_w = 1$), the computational complexity is close to the one of an IFFT of size N. Thus, the computational complexity is at least N_w times larger than the computational complexity required to compute an OFDM symbol. In the original paper [5], the number of windows N_w considered was set to:

- $N_w = 1$ for the lowest computational complexity, but at the cost of higher approximation errors leading to lower spectral confinement.
- $N_w = 3$ for a good compromise between computational complexity and approximation errors.

In this section, TDW_1 UF-OFDM and TDW_3 UF-OFDM techniques are considered, since $N_w > 3$ leads to a high computational complexity largely undermining the interest of using this technique.

4.3.1.3 Proposed UF-OFDM

Table 4.2 shows the number of required RMs and RAs per step (see Subsection 4.2.1 for the details of each step) to compute one UF-OFDM symbol using the proposed technique, assuming $\mathrm{mod}_Q(N) = 0$. The total computational complexity in number of RMs and RAs to calculate one UF-OFDM symbol is given by

$$C_{\mathrm{RM/RA}}(\text{UF-OFDM}) = \sum_{i=1}^{8} C_{\mathrm{RM/RA}}(\mathrm{step}_i),$$

$$C_{\mathrm{RM}}(\text{UF-OFDM}) = C_{\mathrm{RM}}(\mathrm{IFFT}_N) + 4(Q+K-1) + 3N\frac{L}{K},$$

$$\begin{aligned} C_{\mathrm{RA}}(\text{UF-OFDM}) =& C_{\mathrm{RA}}(\mathrm{IFFT}_N) + 4(Q+K-1) + 3N\frac{L}{K} \\ &+ 2L - 1. \end{aligned}$$

Similarly to the TDW UF-OFDM technique, the computational complexity does not depend on B, the number of allocated subbands. Furthermore, the computational

Table 4.2 — Number of required RMs and RAs for the proposed UF-OFDM technique.

Step	Operation	C_{RM}	C_{RA}
1	Segmentation	0	0
2	IFFTs of size K	$Q \times C_{\mathrm{RM}}(\mathrm{IFFT}_K)$	$Q \times C_{\mathrm{RA}}(\mathrm{IFFT}_K)$
3	Core windowing	$3Q \times K = 3N$	$3Q \times K = 3N$
4	IFFTs of size Q	$K \times C_{\mathrm{RM}}(\mathrm{IFFT}_Q)$	$K \times C_{\mathrm{RA}}(\mathrm{IFFT}_Q)$
5	Reconstruction	0	0
6	Prefix calculation	$Q \times 3L$	$Q \times 3L$
7	Suffix calculation	0	$2(L-1)$
8	Concatenation	0	0

complexity is equivalent to the one required to compute an OFDM symbol (IFFT of size N) plus an overhead term. This overhead term depends on the ratio between the filter length L and the total number of subbands K ($\alpha = L/K$). In other words, the proposed technique has a computational complexity almost equivalent to OFDM for short subband sizes (for any number of allocated subbands), and the complexity increases with the subband size Q.

When an arbitrary subband size is considered, the oversampling techniques presented in Subsection 4.2.2 can be used at the cost of an increase in the computational complexity, as the total number of subcarriers must be multiplied by a factor β (= 1.5 for 4G/LTE). Since the IFFT of the subcarrier processing part is no longer a power of 2, the split radix FFT technique cannot be directly applied, except if this IFFT is computed using (4.20). This mostly requires R IFFT of size Q_N and $(R-1)RQ_N$ complex multiplications by the $\exp[j2\pi(kn)/R]$ terms (for $k \in [\![1, R-1]\!]$). The computational complexity related to the multiplication by the exponential terms can be greatly reduced by noting that $\exp[j2\pi(kn)/R] = 1$ when $\mathrm{mod}_R(n) = 0$, for any $k \in [\![1, R-1]\!]$ values. Thus, $Q/R = Q_N$ complex multiplications can be avoided for the set of k values. In this case, the computation complexity of an IFFT of size $Q = R \times Q_N$ becomes

$$\begin{aligned} C_{\mathrm{RM}}(\mathrm{IFFT}_{R,Q_N}) =& RC_{\mathrm{RM}}(\mathrm{IFFT}_{Q_N}) \\ &+ 3Q_N(R-1)^2, \end{aligned}$$

$$\begin{aligned} C_{\mathrm{RA}}(\mathrm{IFFT}_{R,Q_N}) =& RC_{\mathrm{RA}}(\mathrm{IFFT}_{QN}) \\ &+ 3Q_N(R-1)^2 + 2(R-1)RQ_N. \end{aligned}$$

In this section, only the oversampled solution is considered, since it enables the support of any subband size without any restriction, while being less computationally complex than the solution based on multiple intermediate UF-OFDM symbols.

Table 4.3 — Analytical expression of the complexity for each considered UF-OFDM transmitter.

Transmitter	C_{RM}	C_{RA}
OFDM	$N\log_2(N) - 3N + 4$	$3N\log_2(N) - 3N + 4$
FDA UF-OFDM	$B\Big(3N_0\log_2(N_0) - N_0 + 8\Big)$ $+ 2N\log_2(2N) - 6N + 4$	$B\Big(9N_0\log_2(N_0) + 7N_0 + 8\Big)$ $+ 6N\log_2(2N) - 6N - 4N_0 + 4$
TDW_{N_w} UF-OFDM	$N_w\Big(N\log_N + 3L + 1\Big)$	$N_w\Big(3N\log_N + N + 4L\Big) - N - L + 1$
Proposed UF-OFDM ($\mathrm{mod}_Q(N) = 0$)	$N\log_2(N) - 3N + 4(Q + K) + 3N\frac{L}{K}$	$3N\log_2(N) - 3N + 4(Q + K) + 3N\frac{L}{K} + 2L - 1$
Proposed UF-OFDM ($\mathrm{mod}_Q(N) \neq 0$)	$\beta N\Big(\log_2(\frac{\beta N}{R}) + 3\Big(\frac{(R-1)^2}{R} + \frac{\beta L}{K} - 1\Big)\Big)$ $+ 4(Q + KR)$	$\beta N\Big(3(\log_2(\frac{\beta N}{R}) + 3\beta\frac{L}{K} + 5R + \frac{3}{R} - 11\Big)$ $+ 4(Q + KR) + 2(\beta L - 1)$

Table 4.4 — Selected configurations for complexity comparison.

	Number of subband allocated B	Subband size Q
Configuration A	1	16
Configuration B	1	64
Configuration C	37	16
Configuration D	9	64
Configuration E	50	12
Configuration F	12	48

4.3.2 Complexity comparison

The computational complexity of the FDA UF-OFDM, TDW UF-OFDM and the proposed UF-OFDM are compared with respect to OFDM using the following ratio:

$$\text{Ratio-to-OFDM}_{\text{RM/RA}} = \frac{C_{\text{RM/RA}}(\text{UF-OFDM})}{C_{\text{RM/RA}}(\text{OFDM})},$$

where the required numbers of RMs and RAs $C_{\text{RM/RA}}(\text{UF-OFDM})$ correspond to the analytical evaluations provided in the previous subsection for each technique and summarized in Table 4.3. Note that $C_{\text{RM/RA}}(\text{OFDM}) = C_{\text{RM/RA}}(\text{IFFT}_N)$ since an OFDM transmitter only requires an IFFT of size N. Several representative sets of subband sizes and number of allocated subbands must be considered to fairly compare the different UF-OFDM techniques. For this purpose, 6 different configurations are considered. They are detailed in Table 4.4. For all these configurations, the total number of subcarriers is fixed to 1024 and the length of the SBF is equal to $L = 73$ samples. Short and large subband sizes are considered to evaluate their impact on the complexity. In addition, subband sizes compatible with a 4G/LTE system are considered for configuration E and F. Configuration A and B represent the cases where only 1 subband is allocated, which is adequate for low data rate services like massive machine communications. Configurations C to F represent the cases where multiple subbands are allocated: the number of allocated subbands is determined such that the entire bandwidth that can be allocated in 4G/LTE is occupied (at most 600 active subcarriers from the total 1024 subcarriers). This corresponds to the extreme cases where a user occupies the totality of the available bandwidth to achieve high date rates.

The computational complexity results are illustrated in Figure 4.7a for configuration A. The proposed UF-OFDM technique requires almost the same number of RMs and RAs when compared to the TDW_1 UF-OFDM technique, and only 53% more RMs and 14% more RAs when compared to OFDM. Furthermore, the proposed technique requires 37% less RM and 51% less RAs than the FDA UF-OFDM technique. The TDW_3 UF-OFDM technique has the highest computational complexity for this configuration, and is therefore the least interesting technique. When considering configuration B, the proposed UF-OFDM technique requires 13% more RMs when compared to the FDA UF-OFDM technique, as shown in Figure 4.7b. However, the number of RAs being reduced by 40%, the proposed UF-OFDM technique is still less complex than the FDA UF-OFDM technique if the total number of operations is considered (28% less number of RMs and

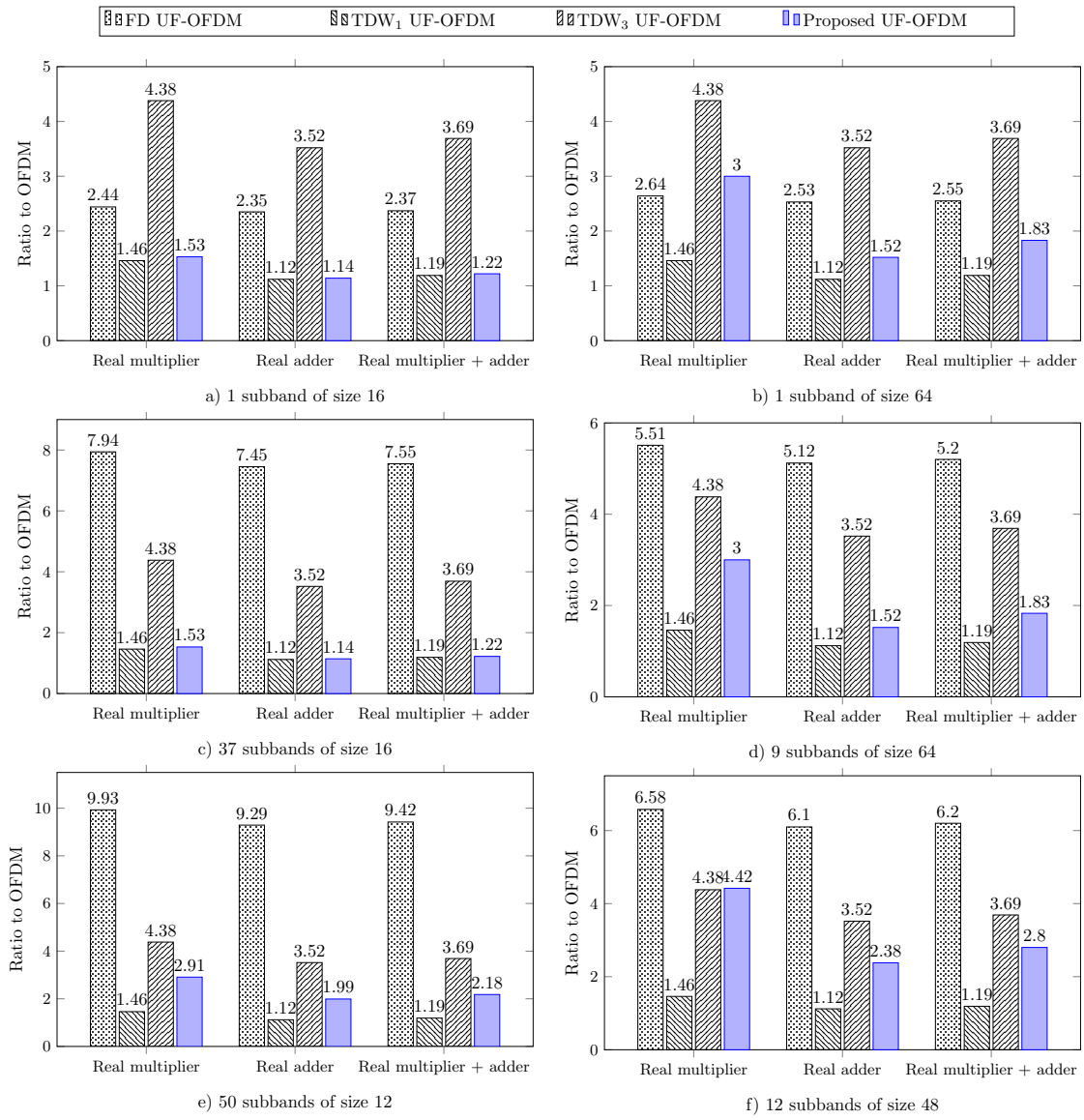

Figure 4.7 — Computational complexity of the FDA UF-OFDM, TDW UF-OFDM and proposed UF-OFDM for different subband configurations.

RAs).

Concerning the TDW$_1$ UF-OFDM technique, its complexity reduction comes at the price of an accuracy loss. Thus, the effect of the approximation errors must be considered for a fair comparison. For this purpose, the power spectral densities of the considered UF-OFDM techniques are presented in Figure 1.12 for the following parameters:

- allocation of 1 subband of 48 subcarriers,
- use of 1024 subcarriers in total, for a sampling frequency of 15.36 MHz as defined in 4G/LTE,
- application of the Dolph-Chebyshev filter with a sidelobe level of 70 dB.

The OOBPL located outside the allocated subband is higher in the case of the FDA

UF-OFDM technique by around 5 dB when compared to the proposed technique. As mentioned in [111], this part of the spectrum is not as important as the OOBPL located at each edge of the allocated subband. Indeed, in a practical system, such low OOBPL is rarely achieved due to the imperfection of the front end components, for instance due to the non-linearity of the power amplifier. Therefore, the approximation errors introduced by the FDA UF-OFDM technique do not degrade much the spectral confinement. When considering the TDW UF-OFDM technique, the number of windows has a great impact on the signal approximation and the resulting OOBPL. This is illustrated in Figure 1.12, which shows the PSD of each UF-OFDM transmitter, assuming that the subbands are normalized: the distortion caused by the subband filter is compensated by readjusting the power of each subcarrier. It can be seen that the use of only 1 window greatly degrades the OOBPL at the edges of the allocated subband. When 3 windows are used, the spectral confinement is improved, but not as much as with the proposed technique: at -40 dB, the frequency difference between the TDW_3 UF-OFDM and the proposed UF-OFDM techniques is around 50 kHz, which is not negligible since it corresponds to more than 3 subcarriers. Thus, a larger guard interval may be required between users to offer the same spectral isolation as the proposed UF-OFDM technique, leading to a data rate loss. A larger number of windows can be employed to reduce the approximation errors, at the cost of an increased computational complexity. Concerning the TDW_1 UF-OFDM technique, the original signal is highly degraded along with the OOBPL. In fact, the TDW_1 UF-OFDM is closer to windowed-OFDM than UF-OFDM.

When considering a subband size of 12 subcarriers for configuration A and a subband of size of 48 subcarriers for configuration B, the same complexity results are obtained. Indeed, Subsection 4.2.2 shows that the proposed technique is compatible with any subband size when $B = 1$: the active carriers can be allocated at the middle of the subband, and zero-valued samples can be padded at its extremities. Thus, the proposed UF-OFDM technique is the most interesting technique for $B = 1$, since it has the lowest computational complexity while preserving the signal quality.

Concerning configuration C, the proposed UF-OFDM technique is employed without any oversampling since the total number of subcarriers can be divided into an integer number of subbands. Figure 4.7c shows that the proposed technique has a lower complexity than the FDA UF-OFDM and the TDW_3 UF-OFDM techniques. Particularly, the FDA UF-OFDM technique requires 4.18 times more RMs and 5.51 times more RA than the proposed UF-OFDM technique. Thus, the FDA UF-OFDM loses its appeal when a large number of subbands is employed. When considering a larger subband size with configuration D (Figure 4.7d), the proposed UF-OFDM still has a lower complexity than the other techniques, with the exception of the TDW_1 UF-OFDM, which has an unacceptable spectral confinement.

Next, configuration E and configuration F concern the cases where multiple subbands are allocated, but the subband size is not a multiple of the total number of subcarriers ($\text{mod}_Q(N) > 0$). In this context, the oversampling technique described in Subsection 4.2.2 must be employed for the proposed technique. While the complexity is increased when the oversampling technique is employed, our proposal still offers reduced complexity when compared to the FDA UF-OFDM and to the TDW UF-OFDM techniques, as

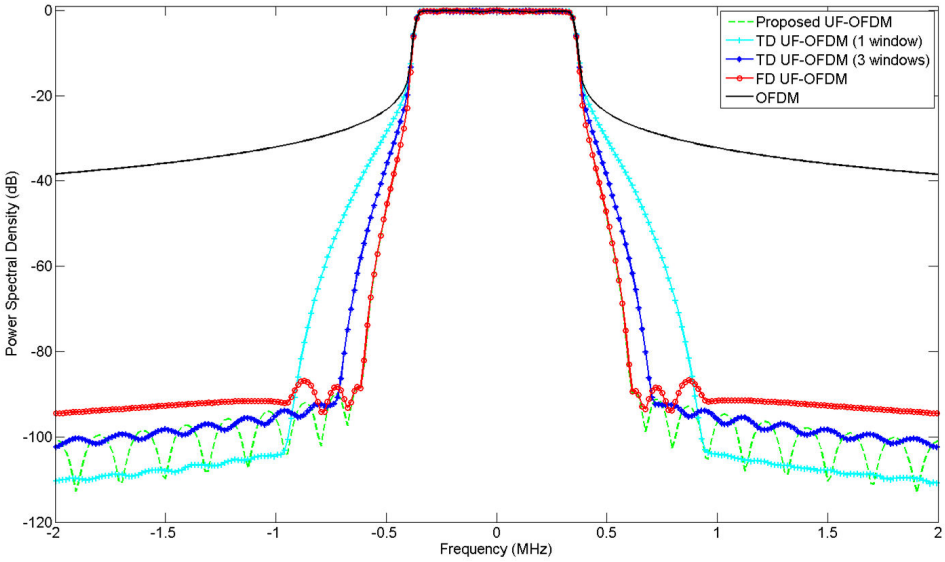

Figure 4.8 — Power spectral density of the UF-OFDM techniques.

shown in Figure 4.7e and in Figure 4.7f.

Therefore, for all the considered configurations, the proposed technique offers significant reductions in computational complexity while preserving the signal accuracy. Note also that the complexity is close to OFDM for a subband size $Q = 16$, regardless of the number of allocated subbands. Finally, our proposed transmitter architecture can be easily adapted to generate an OFDM symbol as demonstrated in Section 4.2.3, which is more difficult for techniques like FDA UF-OFDM where the IFFT size must be doubled (assuming $N_{OS} = 2$). This is particularly interesting from a hardware implementation perspective, where resources must be shared to reduce the hardware complexity.

Finally, the proposed technique assumes that each subband contains the same number of subcarriers. Therefore, the use of different subband sizes on the same carrier is not directly supported. In fact, for downlink communication, multiple communication services using different numerologies are considered in 5G. For instance, narrow subbands can be employed for mMTC, whereas wider subbands can be used for broadband communication. For the uplink, the user equipment being configured for a particular application, the subband size should be kept constant. Note that the TDW UF-OFDM technique suffers from the same drawback, and only the FDA UF-OFDM transmitter can support multiple subband sizes in the same bandwidth. For the latter, the stage of IFFT/FFT (of size N_0) can simply be adapted for a given subband configuration, since subbands are processed separately and independently. In our case, the support of multiple subband sizes can be done by duplicating the transmitter. Assuming that the whole bandwidth is allocated and both subband sizes of 16 and 64 subcarriers must be supported, the proposed transmitter remains 18% to 43% less complex (in number of RM) than the FDA UF-OFDM transmitter, despite the replication. These values are obtained by considering the lowest and highest complexities of the FDA UF-OFDM transmitter, which correspond to 9 subbands of size 64 and 37 subbands of size 16 respectively. If subbands of size 12 and 48 are considered, the complexity of the proposed transmitter

is comparable to the FDA UF-OFDM transmitter (between 26% less and 11% more complex).

4.4 Summary

A novel UF-OFDM technique with low computational complexity is proposed. One of the main features of this novel technique is that, contrary to the ones proposed in the literature, it does not introduce any approximation of the original signal. Additionally, appropriate solutions have been detailed to support any subband size as defined in 4G/LTE numerology. Comparisons were performed with the techniques presented in the literature using different sets of subband allocations and subband sizes. The results show that the proposed UF-OFDM technique provides significant computational complexity reduction in most cases. Finally, power spectral density comparisons were conducted showing that the proposed technique preserves the spectral confinement of UF-OFDM, contrary to the recently proposed TDW UF-OFDM technique. This demonstrates, for the first time, the possibility to design a low-complexity UF-OFDM transmitter without any signal degradation, making the UF-OFDM particularly appealing for adoption in upcoming wireless applications and standards.

CHAPTER

5 Hardware implementation and on-board prototyping

Several technical contributions are emerging nowadays to fulfill the new requirements foreseen in the 5G standard. Among these contributions, different variants of waveform design are proposed for the new radio air interface as alternative to OFDM adopted in 4G. However, in order to prove the feasibility and the benefits of the proposed waveforms, practical hardware implementations are necessary. In this context, novel pipelined hardware architectures are proposed for the UF-OFDM and the FBMC/OQAM transceivers in this chapter, targeting low complexity. The performance of these transceivers are then evaluated through a flexible and efficient hardware platform for proof-of-concept. This latter constitutes a complete hardware/software development environment, with digital processing, radio frequency boards, and all associated interfaces for control, communication, and display. Furthermore, the proposed platform allows the support of several communication scenarios as foreseen in 5G.

This chapter is organized as follows. The first section presents the hardware architecture of the OFDM and UF-OFDM transceivers, while the second section focuses on the hardware architecture of the FBMC/OQAM transceivers. Indeed a novel pipelined FBMC transmitter with reduced complexity is presented. The last section is dedicated to the description of the proposed proof-of-concept 5G platform. The performance of the UF-OFDM, OFDM and FBMC waveforms are presented for the MMC, MCC and V2X related scenarios.

5.1 Hardware architecture of OFDM and UF-OFDM

5.1.1 OFDM transmitter

The first unit of the OFDM modulator architecture is the QAM mapper which is typically implemented through a LUT.

The second unit is the IFFT, the core element of the OFDM architecture. The R2^{2}SDF architecture [113] was chosen for the IFFT block thanks to its low complexity, its minimum memory requirement and its pipelined structure. The R2^{2}SDF exploits the fact that an IFFT of size M can be recursively decomposed into four IFFT of length $M/4$, and can be implemented by $\log_4(M)$ stages of elementary IFFT of length 4 (when M is a power of 4), called radix-4 butterfly. Instead of computing all butterflies iteratively stage by stage, all stages are computed at the same time, in a pipeline way. For this purpose, a feedback buffer is attached to each of the $\log_4(M)$ radix-4. At each clock cycle, one sample is processed at each stage, then put into the buffer or sent to the next stage. The R2^{2}SDF also optimizes the radix-4 by decomposing it into two pipelined radix-2 butterflies (hence the name R2^2), each having two adders and one buffer. With such a decomposition, the hardware complexity of this architecture amounts to $\log_4(M) - 1$ multipliers, $4\log_4(M)$ adders, and total memory size equal to $M - 1$. It is worth noting that the recursive structure of the R2^{2}SDF is interesting for flexibility. Indeed, the IFFT size can by dynamically reduced by bypassing the first stages, using multiplexers, without any changes in the control interface of the R2^2 processing units.

The devised architecture for the IFFT uses the Decimation In Frequency (DIF) decomposition which results in output sample indexes interleaved in *bit reversal* order. Thus, to avoid additional memory usage and latency overhead, both the insertion of the cyclic prefix and the reordering operation are done jointly. IFFT output samples are alternatively read and written in a memory unit of depth M, in bit reversed and normal order, with the L_{CP} last samples read first to generate the cyclic prefix between subsequent blocks. The resulting OFDM modulator architecture is fully pipelined, enabling continuous stream processing of one complex sample per clock cycle.

5.1.2 UF-OFDM transmitter

The hardware architecture of the proposed UF-OFDM transmitter in chapter 4 is devised. As a reminder, the following parameters are considered for the UF-OFDM modulation:

- M is the total number of subcarrier, as in OFDM,
- Q is the number of subcarriers in a subband,
- K is the total number of subband,
- L is the subband filter length.

This architecture is illustrated in Figure 5.1. First, A QAM/Pilot mapper, similar to the one used in the OFDM transmitter, maps the incoming bits into QAM symbols

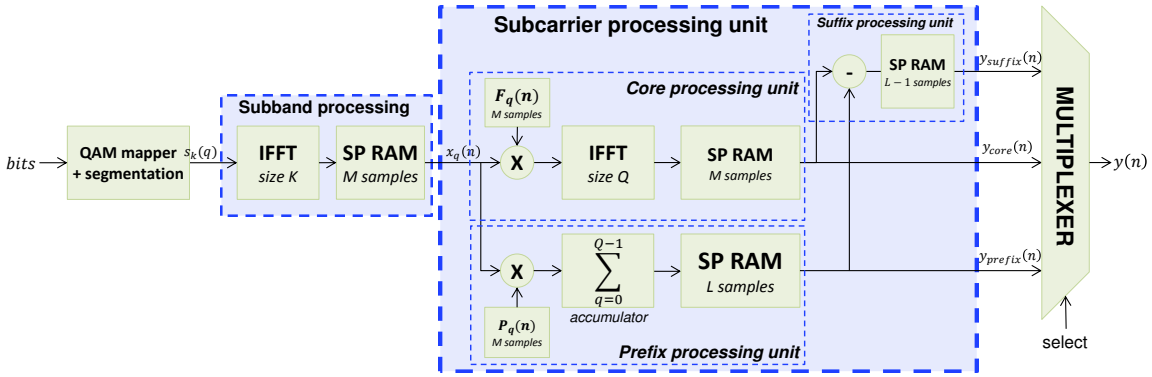

Figure 5.1 — Architecture of the UF-OFDM transmitter

and inserts the pilot samples. If a subcarrier is not allocated, a zero valued sample is generated at the output of the QAM/Pilot mapper unit instead. A Single-Port Random-Access Memory (SP-RAM) stores the QAM symbols, then they are segmented into subbands and subcarriers, and serially transmitted, grouped by sequences of length M. Therefore, the first Q samples of the sequence contains the Q subcarrier values of the first subband, the next group of Q samples corresponds to the subcarriers values of the second subband, and so one. If a subcarrier is not assigned to a pilot or a QAM symbol because it is not allocated, a zero valued sample is instead transmitted. Therefore, the SP-RAM only stores the allocated QAM/pilot, implying that a memory depth of N_{AC} samples is sufficient, where $N_{AC} < M$ is the maximum number of allocated subcarriers. Note that an idle time of $L-1$ clock-cycles is inserted between the two sequences of M samples so that the next processing units have the time to process and insert the suffix part.

The next subband processing unit contains one IFFT of size K followed by a SP-RAM. During the processing of one UF-OFDM symbol, the IFFT receives at its input a sequence of $Q \times K = M$ serial samples, during M clock-cycles. Due its pipeline behaviour, Q IFFTs of size K are performed, and a sequence of M samples are obtained in serial at its output. Note that each group of Q samples at the output of the IFFT processor are obtained in bit reversed order because of the Decimation In Frequency (DIF) nature of the IFFT processor. Therefore, the function of the SP RAM is to reorder the obtained samples in natural order. At the same time, this memory interleaves the samples for the next subcarrier processing unit. Therefore, the first K samples of the obtained sequence contain the K subband sample values of the first subcarrier, the next group of K samples corresponds to the subband sample values of the second subcarrier, and so one. These reordering and interleaving operations are realized with an address generator, composed of one counter and one block of combinational logic.

The subband processing is followed by the subcarrier processing unit, composed of core, prefix and suffix processing units. As their names imply, these processing units generate the corresponding part of the UF-OFDM symbol. The core and prefix processing units work on the input samples in parallel, since the processing of the prefix and core part can be done independently. However, the output of these two processing units are connected to the suffix processing unit since the suffix part of the UF-OFDM is deduced

from the core and the prefix parts.

The core processing unit is composed of 1 complex multiplier, 1 IFFT of size Q and 1 SP RAM of depth N complex samples. The complex multiplier processes the windowing operation by the core filter coefficients, which are stored in a LUT. The SP RAM has the same functionality as the SP RAM of the subbands processing: it stores, reorders and assembles the complex samples to obtain the core part of the UF-OFDM symbol. The prefix processing unit is composed of 1 complex multiplier (windowing), an accumulator (composed of an adder and a register) and a SP RAM (storing and reordering) are used to generate the prefix part of the UF-OFDM. Finally, the suffix processing unit is composed of one complex subtractor and a SP RAM to store the suffix part of the UF-OFDM. The complete UF-OFDM symbol is obtained by multiplexing the prefix samples during the first L clock-cycles, the core samples during the next $N-L$ clock-cycles, and finally the suffix samples during the last $L-1$ clock-cycles.

5.1.3 OFDM and UF-OFDM receivers

The UF-OFDM receiver applies the following steps [37] to recover the transmitted signal:

1. Isolate the $M+L-1$ samples constituting the received UF-OFDM symbol.
2. Extract the last $L-1$ samples, add them to the first $L-1$ samples so that M samples are obtained.
3. Apply an FFT of size M to obtain the frequency domain signal.
4. Equalize the frequency domain signal per subcarrier, assuming that channel estimation was performed previously.

If the distortion caused by the subband filter is taken into account in the equalizer coefficients, then the transmitted QAM symbols can be reconstructed without interference. Indeed, after step 3), the frequency domain sample $Y(k)$ at the subcarrier index k is expressed as

$$Y(m) = \sum_{n=0}^{M-1} \tilde{y}(n) e^{-2i\pi \frac{mn}{M}} \tag{5.1}$$

with $\tilde{y}$ the signal obtained after step 2), expressed as

$$\tilde{y}(n) = \begin{cases} y(n) + y(N+n) & n \in [\![0, L-2]\!] \\ y(n) & n \in [\![L-1, M-1]\!] \end{cases} \tag{5.2}$$

Furthermore, the above expression can be rewritten as a function of the y_{prefix}, y_{core} and y_{suffix} symbol parts defined in Section 4.2.1, Chapter 4. For $n \in [\![0, L-2]\!]$, we have

$$y(n) + y(N+n) = y_{prefix}(n) + y_{suffix}(n) = y_{core}(n). \tag{5.3}$$

In addition, $y(L-1) = y_{suffix}(L-1) = y_{core}(L-1)$, and $y(m) = y_{core}(m)$ when $min[\![L, M-1]\!]$. Therefore, the obtained samples after step 2) correspond to the core of the UF-OFDM symbol, and we have $\tilde{y}(m) = y_{core}(m)$. This is the part of the symbol where the effect of the subband filter can be equivalently seen as a circular convolution.

Therefore, in frequency domain, the distortion caused by this filter corresponds to a subcarrier-wise attenuation and phase rotation. In fact, if $Y_k(q) = Y(pK + q)$ is the received frequency domain sample at the subcarrier $kin[\![0, Q-1]\!]$ and subband number $kin[\![0, K-1]\!]$, then we have

$$Y_p(q) = \frac{s_k(q)}{F_Q(q)}. \tag{5.4}$$

where $s_k(q)$ is the transmitted QAM symbol at the subcarrier q and the subband k, and F_Q is the frequency response of the subband filter f_q, expressed as

$$F_Q(q) = \sum_{l=0}^{L-1} f_Q(l) e^{-i2\pi \frac{ql}{M}}. \tag{5.5}$$

Note that this distortion can be estimated using a typical channel estimation technique with block-type pilots. The compensation terms are therefore included in the equalizer coefficients, implying that no additional processing is required. Therefore, the structure of UF-OFDM receiver is similar the OFDM one, since the 2 last steps defined above correspond to the main steps performed by a typical OFDM receiver. The difference is that the cyclic-prefix is removed in the case of OFDM, while the suffix part is removed after being added to the prefix part for UF-OFDM. The processing unit which remove the CP must be adapted to support the UF-OFDM, and the remaining processing unit of the receiver remains unchanged for UF-OFDM. Optionally, an optional windowing operation can be applied on the time-domain samples, between step 2) and step 3). Its usage is however highly recommended since it improves the performance of the UF-OFDM receiver when relaxed synchronization is considered [36].

The receiver presented in [37] has however a drawback. The last $L-1$ samples must be first recovered before being processing by the FFT. If Analog-to-Digital Converter (ADC) outputs the sample in serial, the N previous samples of the received symbol must be stored in memory, increasing the complexity. Instead, we propose to extract the first $L-1$ samples of the prefix part and to add them to the suffix part of the UF-OFDM symbol, which only requires a SP-RAM of depth $L-1$ samples. The obtained time domain signal is then circularly shifted by $L-1$ samples when compared to the signal $\tilde{y}$ obtained from the original solution. This corresponds, in frequency domain, to a multiplication of the LPR terms $exp[2i\pi m(L-1)/M]$. Similarly to the filter distortion coefficients, the LPR coefficients can be estimated and included in the equalizer coefficients.

The obtained hardware architecture of the UF-OFDM receiver is shown in Figure 5.2. The processing unit specific to UF-OFDM, located before the FFT, comprises:

- a SP-RAM to store the prefix part of the UF-OFDM symbol,
- two real multipliers to perform the windowing operation,
- one complex adder to add the prefix and the suffix parts of the symbol,
- a multiplexer which selects between the input of the unit (path number 1) and the output of the complex adder (path number 2).

When the prefix part of a UF-OFDM symbol is received, during $L-1$ clock-cycles, the input samples are stored into the RAM of depth $L-1$. No valid samples are available at

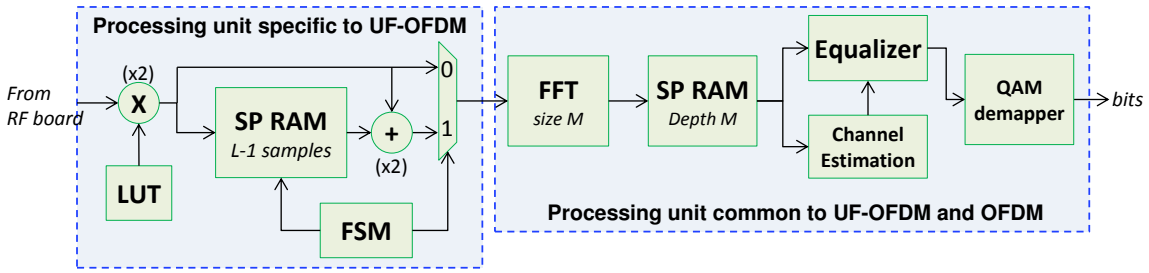

Figure 5.2 — Hardware architecture of the OFDM and UF-OFDM receivers

the output, therefore the FFT must be set to an idle state. During the next $N - L + 1$ clock-cycles, the core part of the symbol is received. Then, the multiplexer selects the path number 1 so that the samples can be directly processed by the FFT. Finally, the prefix part previously stored is read from the SP-RAM during the last $L-1$ clock-cycles. The above cycle is repeated for each UF-OFDM symbol to process.

5.2 Hardware architecture of FBMC/OQAM transmitter

5.2.1 FBMC transmitter based on pruned IFFT algorithm

A novel pruned IFFT based algorithm was proposed in [32] to divide the computational complexity of the FBMC/OQAM transmitter by a factor of almost two. The main idea is to exploit the relation between the IFFT_M outputs to only calculate half of them, then deduce the remaining samples. Such relation exists thanks to the real valued $a_n(m)$ samples. They introduce redundancy in the computation of the complex valued IFFT, and the outputs are symmetrical in case of real valued inputs. In fact, the relation depends on the length of the prototype filter. For $L = qM$, if $u_n(m)$ is the output of IFFT_M at index m, OQAM symbol n, then, for $0 \leq m \leq \frac{M}{4} - 1$:

$$\begin{aligned} u_n(2m+1) &= (-1)^n u_n^*(\frac{M}{2} - 2(m+1)), \\ u_n(2m+1+\frac{M}{2}) &= (-1)^n u_n^*(M - 2(m+1)), \end{aligned} \tag{5.6}$$

The output sample relation for a DIF IFFT_8 is illustrated in Figure 5.3 as an example. This decomposition is obtained by a stage of radix-2 butterfly connected to two $\text{IFFT}_{\frac{M}{2}}$ identified as $\text{IFFT}^{even}_{\frac{M}{2}}$ and $\text{IFFT}^{odd}_{\frac{M}{2}}$. Thanks to the relation (5.6) between even and odd index samples at the output of IFFT_M, there is no need to calculate $\text{IFFT}^{even}_{\frac{M}{2}}$ or $\text{IFFT}^{odd}_{\frac{M}{2}}$. Still, there is a need to compute this pruned IFFT twice, one for real and one for imaginary OQAM symbols (x_{2n} and x_{2n+1}). However, the computational complexity is practically divided by two compared to classic IFFT_M. The stage of addition before the $\text{IFFT}^{even}_{\frac{M}{2}}$ behaves like a natural down-sampler (M inputs for $\frac{M}{2}$ outputs). Thus, only one $\text{IFFT}^{even}_{\frac{M}{2}}$ can be used if the previous blocks before the additions are doubled

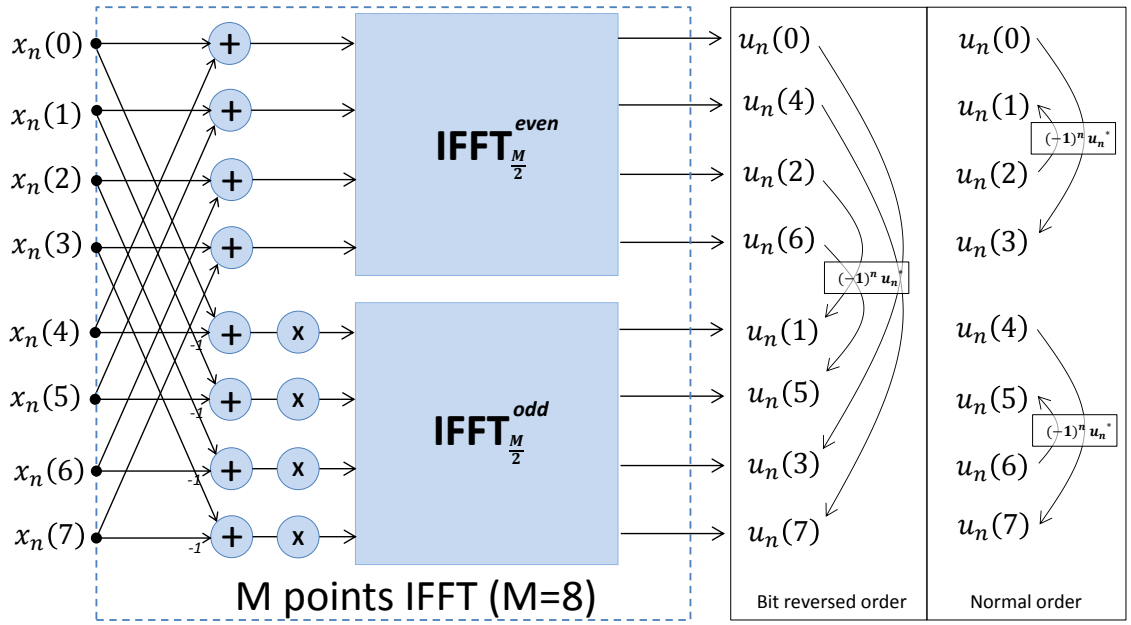

Figure 5.3 — Relation between IFFT output in case of FBMC/OQAM

(parallelized), without changing the clock frequency rate. Therefore, instead of sending real ($a_{2n}(m)$) and imaginary ($a_{2n+1}(m)$) terms of the QAM component at the same time, two real or imaginary terms ($a_n(m)$ and $a_n(m + \frac{M}{2})$) must be sent. At the output of $\text{IFFT}^{even}_{\frac{M}{2}}$, the odd samples can be reconstructed and once again parallelized for the two PPNs. The resulting architecture is shown in Figure 5.4. The following subsections detail how to adapt the design of remaining hardware units to the pruned IFFT.

5.2.2 Hardware architecture

5.2.2.1 OQAM mapper

A new scheme is proposed to parallelize the output of the OQAM mapper unit, and the resulting hardware design is presented in Figure 5.5. In a typical design, the real parts of $c_n(m)$ ($= c_n^R(m) = a_{2n}(m)$) are directly sent to the next unit whereas imaginary parts ($= c_n^I(m) = a_{2n+1}(m)$) are delayed. In the proposed architecture, $a_n(m)$ and $a_n(m + \frac{M}{2})$ must be sent in parallel. The OQAM translation and parallelization are done according to a scheme based on two-buffer strategy with First In First Out (FIFO) memories:

1. For the $\frac{M}{2}$ first clock cycles, $c_n^R(m)$ and $c_n^I(m)$ are sent to two FIFOs, respectively named FIFO_1 and FIFO_2.

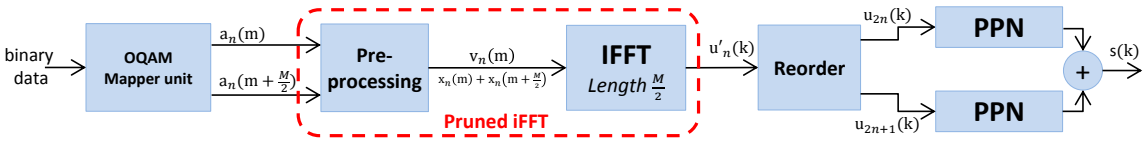

Figure 5.4 — Optimized FBMC/OQAM hardware architecture using pruned IFFT algorithm

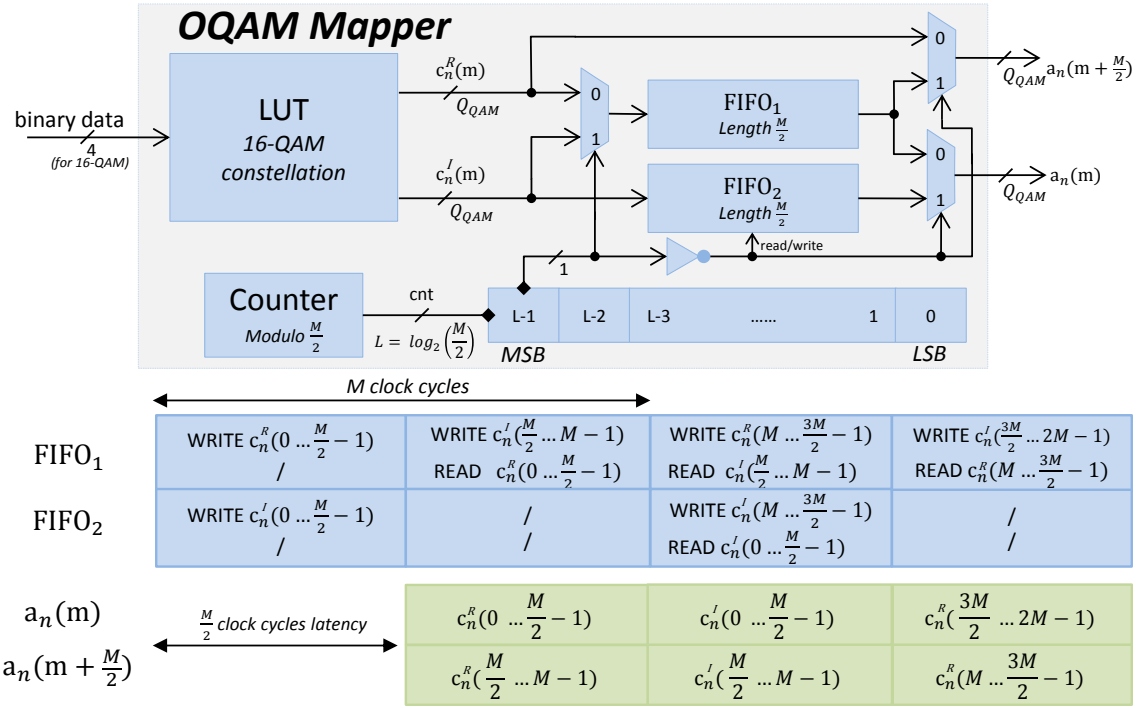

Figure 5.5 — OQAM mapper architecture with FIFO read/write timing

2. During the following $\frac{M}{2}$ clock cycles, $c_n^R(m+\frac{M}{2})$ samples are sent directly to the output of the OQAM mapper, whereas $c_n^R(m)$ samples are read from FIFO_1. Thus, $a_{2n}(m)$ and $a_{2n}(m+\frac{M}{2})$ are generated in parallel. Meanwhile, $c_n^I(m)$ samples are kept inside FIFO_2, and $c_n^I(m+\frac{M}{2})$ samples are sent to FIFO_1.
3. To finish the cycle, $c_n^I(m+\frac{M}{2})$ and $c_n^I(m)$ come respectively from FIFO_1 and FIFO_2, generating $a_{2n+1}(m+\frac{M}{2})$ and $a_{2n+1}(m)$ in parallel. At the same time, samples of the next block $c_{n+1}^R(m)$ and $c_{n+1}^I(m)$ are respectively sent to FIFO_1 and FIFO_2, as during the first step.

The FIFO read/write timing is detailed in Figure 5.5.

5.2.2.2 Pre-processing unit

By parallelizing the pre-processing stage, the number of complex multipliers is normally doubled. However, we propose to reformulate the equation by factorizing the exponential term to have only one pre-processing unit. If $v_n(m)$ is the input index m of $\text{IFFT}_{M/2}^{even}$, then:

$$\begin{aligned} v_n(m) = (-1)^{q(m+\frac{M}{2})}\, e^{\frac{i\pi(m+\frac{M}{2})}{M}}\, a_n(m+\frac{M}{2})\, i^{n+m+\frac{M}{2}} \\ + (-1)^{qm}\, e^{\frac{i\pi m}{M}}\, a_n(m)\, i^{n+m} \end{aligned} \tag{5.7}$$

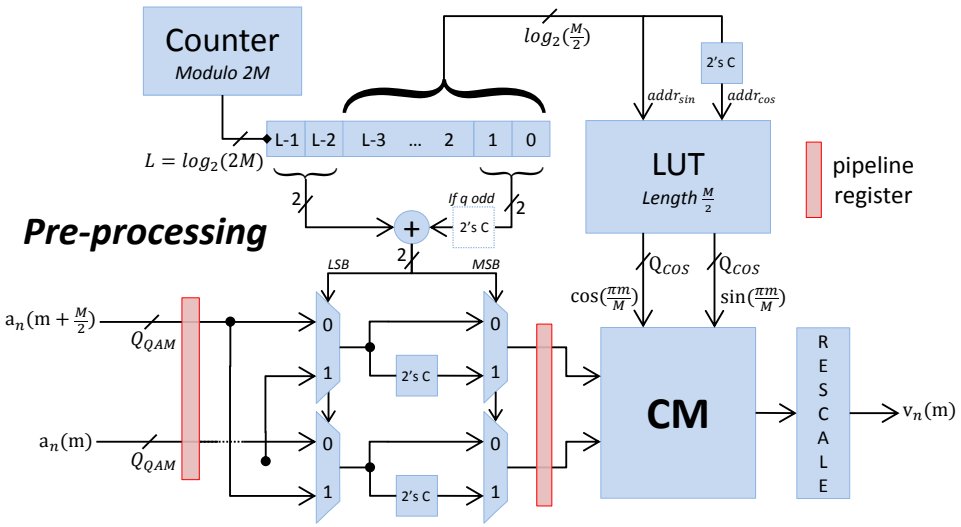

Figure 5.6 — Proposed pre-processing unit architecture

If we assume that M is a power of 2, which is often the case in practice, then the equation above can be rewritten as:

$$v_n(m) = (-1)^{qm}\, i^{n+m}\, e^{\frac{i\pi m}{M}} (a_n(m) + i a_n(m + \frac{M}{2})) \tag{5.8}$$

The term $(-1)^{qm}\, i^{n+m}$ only needs sign inversion (two's complement (2's C) logic) and multiplexers (for real and imaginary part swapping), controlled by a main counter. The exponential term requires Complex Multiplier (CM) with a LUT of depth $\frac{M}{2} \times Q_{COS}$, where Q_{COS} is the number of bits used to quantize the cosinus and sinus coefficients. Figure 5.6 shows the resulting hardware architecture.

5.2.2.3 Reorder unit

This component has 3 functions:

- Reorder the sample index to be in "normal" order instead of bit reversed order. The reorder unit of OFDM covers the same functionality.
- Reconstruct the odd samples from the calculated even samples.
- Adapt the data flow in order to have 2 parallelized time-domain sample sequences for the next 2 PPNs.

In order to reduce the total amount of memory and latency, these 3 operations have to be computed at the same time. The basic idea is to write the coming samples into one or more Random Access Memories (RAM), then read them in the desired order by generating appropriate addresses. This address mapping must ensure that there is no address conflict (writing before reading). A 3-RAMs based design is proposed, where

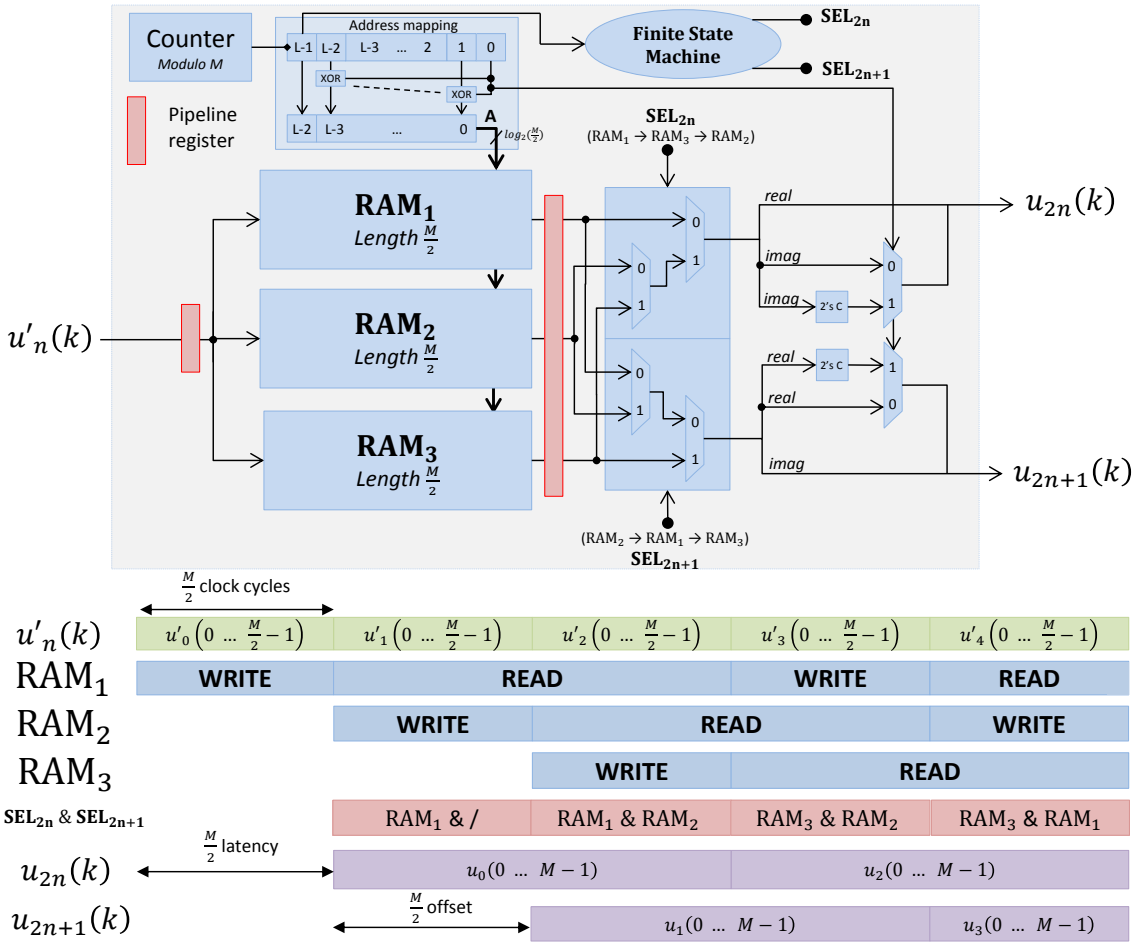

Figure 5.7 — Reorder unit architecture and associated data flow based on 3-RAMs design

read and write operations are computed at separate times. RAM_1, RAM_2 and RAM_3 have each a depth of $\frac{M}{2}$ complex samples. The applied scheme is the following:

- For the $\frac{M}{2}$ first clock cycles, samples from IFFT are written into RAM_1.
- In the next $\frac{M}{2}$ clock cycles, samples from IFFT are written into RAM_2, and the first $\frac{M}{2}$ reconstructed data are read from RAM_1.
- During the following $\frac{M}{2}$ clock cycles, samples from IFFT are written into RAM_3, while RAM_1 and RAM_2 are read. Since all the data in RAM_1 are reconstructed, its content can be rewritten in the next $\frac{M}{2}$ clock cycles.

Figure 5.7 provides the resulting hardware design and summarizes graphically the above scheme in the form of a data flow.

To generate the addresses, the idea was to simplify the problem by decomposing the required steps: first, the writing operation rearranges the output samples of the $\text{IFFT}_{\frac{M}{2}}$ in bit reversal order, then the reading operation recovers the odd samples. For the write address, all the bits of the counter have to be bit reversed. In fact, the read order represents the counter value, noted C (from 0 to $M-1$). A is the address index, from 0 to $\frac{M}{2}-1$. For C even, we have $A = C >> 2$, where $>>$ represents a right

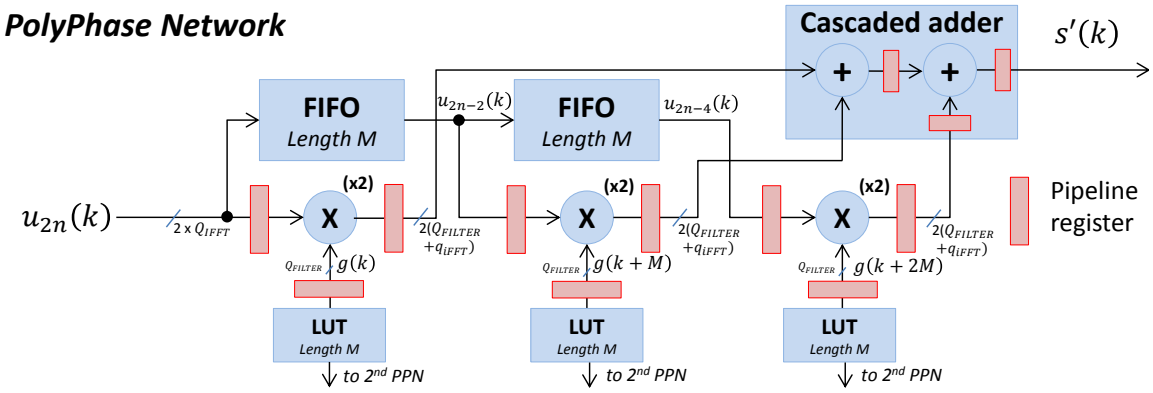

Figure 5.8 — Hardware architecture of the PolyPhase Networks

shift operation, since the even samples are already calculated and reordered. The index relation between odd and even samples are given in (5.6). Thus we have, for C odd:

$$A = \frac{M}{4} - 1 - (C >> 2), 0 \leq C < \frac{M}{2} \tag{5.9}$$

$$A = \frac{M}{4} + (\frac{M}{4} - 1 - (C >> 2)), \frac{M}{2} \leq C < M. \tag{5.10}$$

The address mapping applying these equations can be implemented using only XOR gates. The mapping to the main counter signal is shown in Figure 5.7.

5.2.2.4 PolyPhase Network unit

The last unit of the FBMC/OQAM modulator is the PPN filter. Figure 5.8 illustrates the devised architecture for a filter length $L = 3M$. The proposed architecture is derived from [31] with adaptation to the OQAM component structure. One PPN is composed of:

- $2(K-1)$ single port RAM of size $\frac{M}{2} \times Q_{IFFT}$, where Q_{IFFT} is the quantization length of the output of the pruned IFFT (real or imaginary part). Note that for a one tap PPN ($L = M$, NPR1 filter), the FIFOs are not needed.
- K LUTs of size $M \times Q_{FILTER}$, where Q_{FILTER} represents the quantization length of the filter coefficients. To reduce the hardware complexity, they are shared between the two PPN units.
- $2K$ real multipliers: q taps per PPN, each tap having only 2 multipliers since the filter coefficients are real valued.
- $2(K-1)$ real adders: 2 for each tap (complex adders), except for the last one. It is possible to reduce the number of adders by adopting a tree-like organization.

Table 5.1 — Complexity comparison based on analytical study

Operation	**OFDM**	**FBMC (typical)**	**FBMC (proposed)**
Adders	$10\lceil log_4(M)\rceil - 2$	$20\lceil log_4(M)\rceil + 4q - 6$	$10\lceil log_4(\frac{M}{2})\rceil + 4q - 4$
Multipliers	$4\lceil log_4(M)\rceil - 4$	$8\lceil log_4(M)\rceil + 4q - 4$	$4\lceil log_4(\frac{M}{2})\rceil + 4q$
LUTs depth	$\approx M + \frac{M}{4} + \frac{M}{16}$	$\approx qM + 3M + \frac{M}{8} + \frac{M}{32}$	$\approx qM + M + \frac{M}{8} + \frac{M}{32}$
RAM depth	$2M$	$2qM + 2M + \frac{M}{4}$	$2qM + \frac{M}{2}$
RAM R/W per clock cycle	$log_2(M) - 1$	$2log_2(M) + 2q - 1$	$log_2(\frac{M}{2}) + 2q$

$\lceil x \rceil$ is the smallest integer not less than x.

5.2.3 Implementation results

In this section, implementation results are presented and compared with OFDM. As stated previously, identical architectural choices have been made for the common blocks of all three transmitters in order to perform fair comparisons. 4G/LTE system parameters are adopted for this comparison.

5.2.3.1 Analytical hardware complexity comparison

Table 5.1 summarizes the results of an analytical study of the complexity in terms of number of adders and multipliers, depth of memories, and number of RAM read/write (R/W) accesses per clock cycle. These results can be found using the detailed architecture description provided above. Identical quantization is considered for the three considered transmitters.

The table illustrates a significant reduction in the number of multipliers for the proposal with respect to the typical FBMC/OQAM architecture. This number becomes comparable to that of OFDM for short prototype filters (with $K = 1$). In addition, for this type of filter, the PPN unit does not require any memory which leads to a total memory depth comparable to OFDM. Adopting a pruned IFFT architecture allows to divide by two the memory requirement with respect to the typical FBMC/OQAM transmitter.

Regarding the depth of the LUTs, in case of OFDM this corresponds to the twiddle factor coefficients. Since the number of coefficients is divided by 4 at each IFFT stage, only the three first terms are counted in the table. The contribution of the QAM constellation LUT is simplified (it is typically negligible). In case of FBMC, coefficients related to the pre-processing unit and PPN filters are included. For short PFs, concerning multipliers and RAM requirements, the proposed architecture allows significant complexity reduction compared to the typical FBMC architecture.

Finally, these analytical results illustrate how the complexity of the FBMC/OQAM transmitter increases significantly with the length of the PF.

5.2.3.2 Synthesis results on FPGA

The architectures of the three transmitters have been described in VHSIC (Very High Speed Integrated Circuit) Hardware Description Language (VHDL) and synthesized tar-

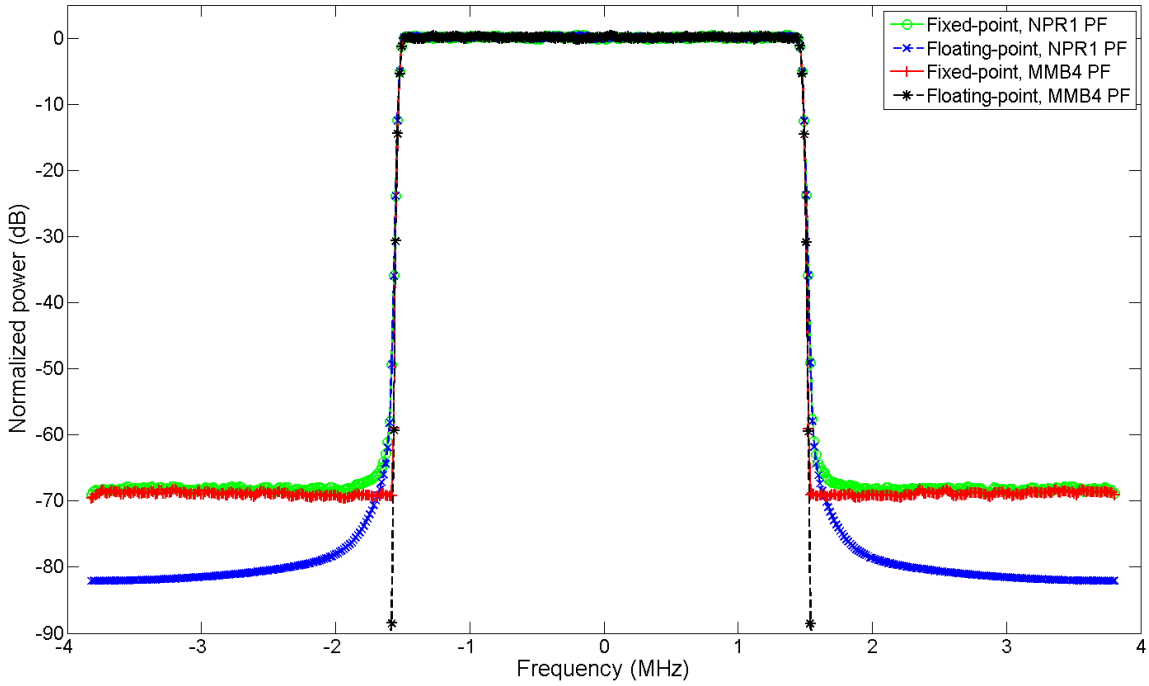

Figure 5.9 — Power Spectral Density of FBMC with fixed-point and floating-point precision, when considering the NPR1 and the MMB4 PFs.

geting the XC7z020-1 Xilinx Zynq SoC device. Obtained results are summarized in Table 5.2. These results correspond to an IFFT size of $M = 512$ and two different prototype filters (NPR1 and MMB4). The LUTs include, in addition to the synthesized combinational logic, the different coefficients related to the pre-processing unit, the twiddle factors, and the PPN filters. Note that, all memories and FIFOs used in all the developed transmitters are RAM-based, however they are synthetized as LUTs (distributed RAM) rather than block RAMs for more accurate comparisons.

Quantization issues have been studied through MATLAB simulation in order to propose efficient fixed-point software model while preserving signal accuracy. The number of quantization bits, the fixed-point representation, the applied shift for re-scaling after multiplication, and the type of approximation (floor or round) have been specified for each unit. Round approximation is chosen due to its reduced impact on the spectrum shape and the quantization errors. In order to obtain a power spectral density without significant quantization error, the following fixed-point representation has been devised enabling less than -70 dB Signal-to-Quantization-Noise Ratio (SQNR) for all specified constellation sizes in LTE (4, 16 and 64-QAM):

- All samples at input and output of each unit have 16-bit quantization. This also applies for each stage of the IFFT.
- All coefficients in LUTs are quantized and stored with a precision of 12 bits.
- Round approximation is chosen for precision purpose.

The resulting power spectral density of FBMC using fixed-point and floating-point precision is shown in Figure 5.9, using typical 4G/LTE parameters. The OOBPL is indeed increased by the quantization for both the NPR1 PF and MMB4 PF.

As expected, with NPR1, the proposed FBMC architecture is almost two times less complex than the typical FBMC implementation in terms of number of registers and LUTs. Its complexity is comparable to OFDM in terms of registers, LUTs (10% more), and memory requirements (15% more). As for the number of multipliers, they are increased by 25% due to the one tap PPN unit. This complexity becomes relatively negligible when the IFFT size is increased.

The overall complexity is greatly increased in the case of the 4-tap MMB4 prototype filter. It requires more than twice the memory needed for OFDM. This highlights the fact that the PPN unit is the real problem concerning the memory requirement when the prototype filter has a length larger than one tap. In addition, each multiplier requires an input pipeline register for real and imaginary samples (16×16). Still, even with this high filter length, the proposed design outperforms typical FBMC implementation.

Regarding latency, the $\text{IFFT}_{\frac{M}{2}}$ and the reordering unit of the proposed modulator only process half of the required samples, reducing the latency to approximately $\frac{M}{2}$ clock cycles for both. On the other side, the proposed OQAM mapper unit increases the latency by $\frac{M}{2}$ clock cycles. Therefore, the proposed architecture presents an overall latency reduction of 25% when compared to OFDM and to the typical FBMC architecture.

Regarding processing speed, all designed architectures have the same critical path which corresponds to the propagation delay related to one real multiplier Digital Signal Processor (DSP). Therefore, they all reach the same maximum clock frequency of 220 MHz when targeting XC7z020-1 device. Furthermore, all designed architectures are fully pipelined allowing to process one baseband sample per clock cycle, thus reaching a maximum of 220 Msamples/s.

The power consumption has been measured using the on-board current sense resistor of $10m\Omega$. Several measures have been conducted by activating or deactivating the specific transmitter blocks to deduce the related dynamic power consumption for each transmitter. With $K = 1$, results of the proposed architecture indicate an increase of 27% in dynamic power consumption compared to OFDM. This is due to the additional required memory accesses (Table 5.1) in the OQAM mapper and the reorder stage. The 4 multipliers in the PPN unit also contribute to this increase. On the other hand, compared to the typical FBMC/OQAM implementation, the proposed architecture achieves a reduction of 43% in dynamic power consumption.

Synthesis results with short filter and the largest value of M ($M = 2048$) in LTE show that the proposed architecture requires 7677 LUTs (6911 for OFDM), 3748 LUTs as RAM (3160 for OFDM), and 24 multipliers (20 for OFDM). When compared with results of Table 5.2 for $M = 512$, these values scale in compliance with the results of the analytical study provided in Table 5.1.

Table 5.2 — FPGA-based implementation results with $M = 512$ and NPR1/MMB4 prototype filters, for a maximum clock speed of 220 MHz

Unit	**Transmitter architecture**	**Registers**	**LUTs**	**RAM** (as LUTs)	**DSP multiplier**	**Power** (mW)	**Latency** (clock cycles)
QAM mapper	OFDM	20	109	16	0	1	1
	FBMC/OQAM (typical)	51	254	104	0	6	1
	FBMC/OQAM (proposed)	108	300	192	0	6	257
Pre-processing	FBMC/OQAM (typical)	172	546	0	4	11	4
	FBMC/OQAM (proposed)	106	426	0	4	11	4
IFFTs	OFDM	2833	3343	544	16	97	549
	FBMC/OQAM (typical)	5666	6686	1088	32	194	549
	FBMC/OQAM (proposed)	2218	2534	348	12	88	278
Reorder	OFDM	111	141	352	0	12	514
	FBMC/OQAM (typical)	222	282	704	0	24	514
	FBMC/OQAM (proposed)	180	420	528	0	20	258
PPN NPR1	FBMC/OQAM (typical and proposed)	135	300	0	4	11	5
PPN MMB4	FBMC/OQAM (typical and proposed)	1095	1846	2112	16	124	8
TOTAL	OFDM	3006	3599	912	16	109	1064
	FBMC/OQAM NPR1 (typical)	5687	7385	1632	40	246	1073
	FBMC/OQAM NPR1 (proposed)	**2828**	**4011**	**1068**	**20**	**139**	**802**
	FBMC/OQAM MMB4 (typical)	6641	8952	3744	52	359	1076
	FBMC/OQAM MMB4 (proposed)	**3788**	**5585**	**3180**	**32**	**252**	**805**

5.3 Hardware architecture of the FBMC/OQAM receiver

The FS-FBMC receiver is known to be more complex than the PPN-FBMC receiver. This is mainly due to the required convolution operation with N_G coefficients, compared to the simple windowing operation of the PPN-based implementation when short PFs are used. However, additional complexity reduction is possible for the FS-based receiver thanks to the properties of the PF. After detailing the proposed complexity reduction, a hardware architecture is proposed for the FS filter stage, its complexity is evaluated and compared to the PPN filter stage.

5.3.0.1 Complexity reduction of the FS filtering stage

When a short PF is considered ($K = 1$), the FFT size becomes equal to M, and there is no down-sampling step after the filter stage. Therefore, the complexity overhead comes from the circular convolution operation, which depends on the number of filter coefficients N_G after truncation. A circular convolution typically requires N_G CMs and $2(N_G - 1)$ RAs per sample. However, these resources can be reduced by exploiting the properties of the PF and the OQAM scheme. First, if $g(k) = g(N - k)$ and $\Im(g) = 0$, verified for the NPR1 PF (2.16), then we have:

$$\begin{aligned} G(l) &= \sum_{k=0}^{M/2-1} g(k)e^{i\frac{2\pi}{M}kl} + g(M-k)e^{i\frac{2\pi}{M}(N-k)l} \\ &= \sum_{k=0}^{M/2-1} 2g(k)\Re(e^{i\frac{2\pi}{M}kl}). \end{aligned} \tag{5.11}$$

This expression shows that G is real valued. Therefore, the filter stage requires now only $2N_G$ RMs per sample. Furthermore, $G(-l)$ can be expressed as follows:

$$\begin{aligned} G(-l) &= \Big(\sum_{k=0}^{M-1} g(k)e^{-i\frac{2\pi}{M}kl}\Big)^* \\ &= G(l). \end{aligned} \tag{5.12}$$

Consequently, the output of the filter stage $Y_n(m)$ becomes

$$\begin{aligned} Y_n(m) &= G(0)X_n(m) + \sum_{l=1}^{\Delta+1} G(l)\Big(X_n(m-l) + X_n(m+l)\Big) \\ &= \sum_{l=0}^{\Delta+1} G(l)X_n(m,l), \end{aligned} \tag{5.13}$$

where $X_n(m,l) = X_n(m-l) + X_n(m+l)$ if $l > 0$ and $X_n(m,0) = X_n(m)$. One RM can be removed by re-scaling the PF coefficients by $G'(l) = G(l)/G(0)$. Then, equation

(5.13) becomes:

$$Y_n(m) = \sum_{l=0}^{\Delta+1} G'(l) X'_n(m,l). \tag{5.14}$$

with $X'_n(m,l) = G(0)X_n(m,l)$. This scaling factor $G(0)$ can be integrated without complexity increase in the equalizer coefficients. Alternatively, it can be taken into account in the decision stage (QAM demapper). The re-scaled PF coefficients $G'(l)$ can be computed during design time, and stored in a LUT. At this step, the filter stage requires 2Δ RMs per sample. This number can be further reduced since half of the circular convolution outputs are discarded due to the OQAM scheme. In this case, we have:

$$\begin{aligned}
\hat{a}'_{2n}(2m) &= (-1)^{(n+m)} \sum_{l=0}^{\Delta+1} G'(l) \Re\Big(X'_{2n}(2m,l)\Big), \\
\hat{a}'_{2n}(2m+1) &= (-1)^{(n+m+1)} \sum_{l=0}^{\Delta+1} G'(l) \Im\Big(X'_{2n}(2m+1,l)\Big), \\
\hat{a}'_{2n+1}(2m) &= (-1)^{(n+m+1)} \sum_{l=0}^{\Delta+1} G'(l) \Im\Big(X'_{2n+1}(2m,l)\Big), \\
\hat{a}'_{2n+1}(2m+1) &= (-1)^{(n+m+1)} \sum_{l=0}^{\Delta+1} G'(l) \Re\Big(X'_{2n+1}(2m,l)\Big),
\end{aligned} \tag{5.15}$$

where $\hat{a}'_n(m)$ being the re-scaled $\hat{a}_n(m)$ signal. Therefore, there is no need to process $\Im\Big(X'_n(m,l)\Big)$ or $\Re\Big(X'_n(m,l)\Big)$ depending on the parity of n and m. Only Δ RMs and 2Δ RAs per sample are now required. Additionally, only the outputs corresponding to the allocated subcarrier indexes can be considered. If the number of allocated subcarriers is denoted by N_c, this gives ΔN_c RMs required per FBMC symbols.

Regarding the PPN stage, it requires $2M$ RMs per FBMC symbol for short PFs. Thus, when considering only multiplication operations, the complexity ratio between FS and PPN filter stages is given by $R_{RM} = \alpha\Delta/2$, with $\alpha = N_c/M \approx 0.586$ in 4G/LTE. For QMF1 ($\Delta = 20$) and TFL1 ($\Delta = 15$) PFs, the complexity RMs is multiplied by 5.86 and 4.395 respectively. This confirms that these PFs are not suitable for the FS implementation. However, for NPR1 PF ($\Delta = 3$), the FS filter stage is 12% less complex than the PPN stage.

It is worth noting that the PPN stage requires a LUT memory of depth M to store the PF coefficients. Furthermore, the FS filter stage still requires $2\Delta N_c$ additions per FBMC symbols. When targeting hardware implementation, registers must also be considered to store the input signal $X'_n(k)$ due to the iterative processing of the circulation convolution operation. Finally, this operation uses constant filter coefficients which do not change during the processing iterations. This particularity can be taken into account to further reduce the complexity when considering hardware implementation.

Therefore, the above ratio may not be accurate enough to reflect the comparative hardware complexity since it only considers the number of multipliers. For an accurate

comparison, we propose a detailed hardware architecture for the FS filter stage.

5.3.1 Proposed hardware architecture for the FS filtering stage

The circular convolution operation can be efficiently implemented in hardware using a typical FIR filter architecture. Such architecture can take one input and generate one output per clock cycle in pipelined manner. If a Multiplier-less Constant Multiplication (MCM) is used, multiplier-less FIR architecture can be designed for fixed-point precision. If G_Q are the PF coefficients quantized on Q-bit to be multiplied by a Q-bit input X_Q, then:

$$G_Q \times X_Q = \sum_{k=0}^{Q-1} c_k 2^k X_Q, \tag{5.16}$$

where $c_k \in \{-1, 0, 1\}$ denotes the symbol number k of the Canonical Signed Digit (CSD) representation of G_Q [114]. Therefore, only adders and registers are required for this architecture. It is advantageous to consider it if the same set of coefficients has to be re-used for each processed sample, which is the case for the FS filter stage. Since an adder requires less hardware resources (logic gates) than a multiplier, an important hardware complexity reduction is expected.

As a baseline solution, (5.14) can be directly implemented using one FIR filter for the computation of the real part, and another FIR filter for the computation of the imaginary part. It is however not an optimal choice if a low-complexity implementation is targeted, since half of the generated samples by both FIR filters are discarded due to the OQAM scheme, as shown in (5.15). However, this equation cannot be directly implemented using a typical FIR filter. In fact, the content of the corresponding registers must be switched between the real and imaginary parts of the stored $X'_n(m)$ samples. Therefore, we propose a novel architecture adapted for the FS filter stage.

In the following, only even FBMC symbol indexes are considered ($\hat{a}'_{2n}(m)$ and $X'_{2n}(m)$). Similar demonstration can be applied for the odd indexed symbols. Index $2m$ of (5.15) can be rewritten as follows:

$$\begin{aligned}\hat{a}'_{2n}(2m) =& (-1)^{(n+m)} \Big(\sum_{l=0}^{\lfloor \frac{\Delta+1}{2} \rfloor} G_{even}(l) \Re\Big(X'_{2n}(2m, 2l) \Big) \\ &+ \sum_{l=0}^{\lfloor \frac{\Delta+1}{2} \rfloor} G_{odd}(l) \Re\Big(X'_{2n}(2m, 2l+1) \Big) \Big),\end{aligned} \tag{5.17}$$

where $G_{even}(l) = G(2l)$ and $G_{odd}(l) = G(2l+1)$. Similarly, index $2m+1$ of (5.15) becomes

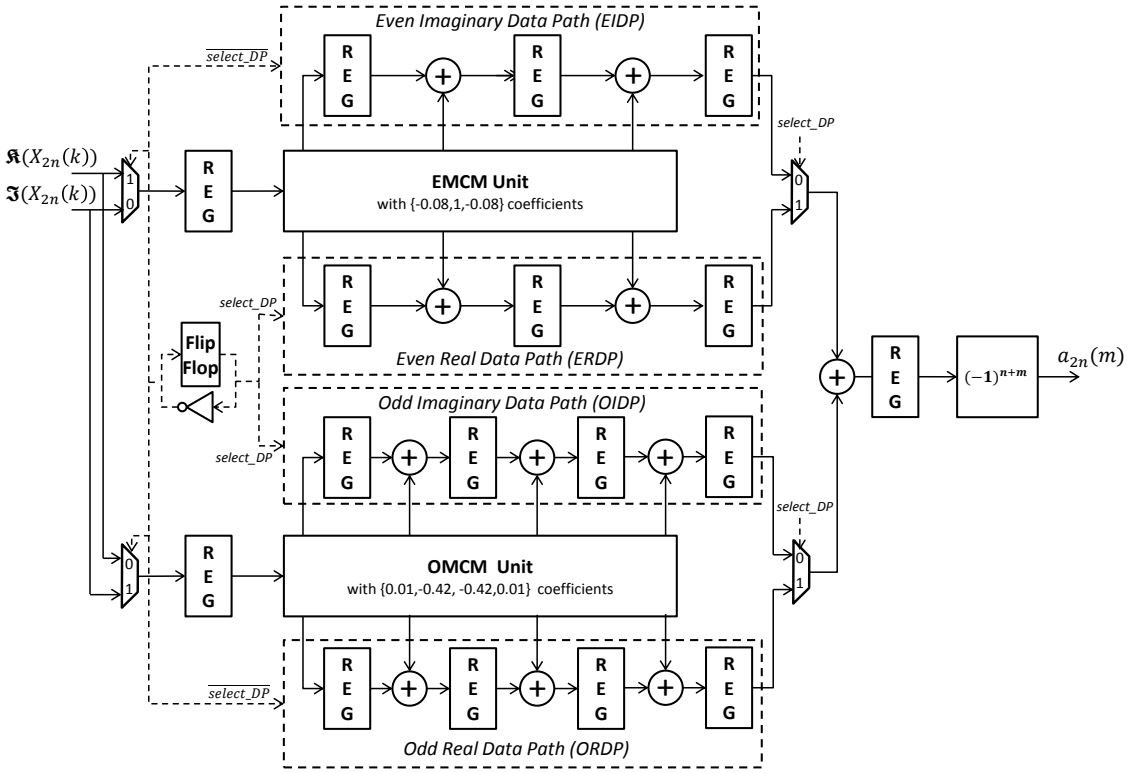

Figure 5.10 — Proposed FS filter stage architecture for NPR1 filter.

$$\begin{aligned}\hat{a}'_{2n}(2m+1) =&(-1)^{(n+m+1)}\Big(\\ &\sum_{l=0}^{\lfloor\frac{\Delta+1}{2}\rfloor} G_{even}(l)\Im\Big(X'_{2n}(2m+1,2l)\Big) \\ &+\sum_{l=0}^{\lfloor\frac{\Delta+1}{2}\rfloor} G_{odd}(l)\Im\Big(X'_{2n}(2m+1,2l+1)\Big)\Big). \end{aligned} \tag{5.18}$$

The above equations show that the FS filter stage can be separated into two FIR filters, each respectively holding even and odd indexes of the PF coefficients. Indeed, for each received $X'_{2n}(2m)$ sample, its real part is processed by the even-indexed FIR filter, while its imaginary part is processed by the odd-indexed FIR filter. Conversely, the real part of $X'_{2n}(2m+1)$ is processed by the odd-indexed FIR filter, and its imaginary part by the even-indexed FIR filter. Therefore, 2 FIR filters are required, similarly to the baseline solution. However, the number of required coefficients per FIR filter is divided by 2, reducing the complexity. The obtained architecture using the NPR1 filter is presented in Figure 5.10.

The Even Multiplierless Constant Multiplication (EMCM) unit executes the multiplications by the even-indexed filter coefficients, while the Odd Multiplierless Constant Multiplication (OMCM) unit executes the multiplications by the odd-indexed filter coefficients. Therefore, the applied scheduling by the designed architecture follows two

phases, repeated continuously. Each phase takes one clock cycle.

In the first phase, the real part of $X'_{2n}(2m)$ is sent to the EMCM unit while its imaginary part is sent to the OMCM unit. Meanwhile:

- the registers of the Even Real Data Path (ERDP) (Figure 5.10), belonging to the even-indexed FIR filter, are enabled by the *select_DP* control signal,
- the registers of the Odd Imaginary Data Path (OIDP), belonging to the odd-indexed FIR filter, are also enabled,
- the registers of the Even Imaginary Data Path (EIDP) and the Odd Real Data Path (ORDP) are both disabled.

Finally, the outputs of the ERDP and the ORDP are summed together. Eventually, sign inversion is performed, depending on the $(-1)^{n+m}$ term value of equation (5.15).

At the second phase, the real part of $X'_{2n}(2m)$ is sent to the OMCM unit while its imaginary part is sent to the EMCM unit. The registers which were disabled (respectively enabled) are now enabled (respectively disabled) by the $\overline{select\_DP}$ control signal. The outputs of the EIDP and the OIDP are selected and summed together, followed by a possible sign inversion depending on the $(-1)^{n+m+1}$ term value.

5.3.2 Hardware complexity comparison

The proposed FS filter stage architecture, in addition to the baseline architecture, were described in VHDL/Verilog and synthesized targeting the XC7z020 Xilinx Zynq SoC device. All the MCM units are generated using the SPIRAL code generator [115]. The results, summarized in Table 5.3, include:

- the PPN unit detailed in Section 5.2,
- the baseline FS filter directly derived from equation (5.14),
- the proposed FS filter presented in the previous sub-section.

The architecture of the PPN unit in Section 5.2 is adapted to process 2 FBMC symbols in parallel (OQAM scheme). To enable a fair comparison, we have considered 2 FS filter stages in parallel, in such a way that the same processing speed is achieved. Furthermore, the same quantization chosen in Section 5.2.3.2 is considered:

- the samples at the input and the output of each unit use 16-bit quantization,
- all filter coefficients are quantized on 12-bits.

Only the NPR1 PF is considered in this section. The QMF1 and TFL1 PFs are less adapted for FS implementation since they require, at least, 4 times more filter coefficients (see Section 2.3.2 of Chapter 2).

The baseline solution of the FS filter stage requires 11.5% less LUTs than the PPN unit. This confirms that one MCM is less complex than 2 multipliers. On the other hand,

Table 5.3 — Required hardware resources for each considered receiver.

Filter stage	LUTs	Flip Flops	Total	Frequency
PPN unit	1460	135	1595	220 MHz
Baseline FS filter stage	1292	512	1804	186 MHz
Proposed FS filter stage	902	520	1422	218 MHz

the FS filter stage uses 2.85 times more flip-flops due to the FIR filter registers. If we consider that LUTs and flip-flops have similar complexities, then the baseline FS filter stage requires 13 % more hardware resources than the PPN unit. It also achieves a clock frequency speed of 186 MHz, 15 % less than the PPN unit.

Concerning the proposed architecture, it requires 38% less LUTs than the PPN unit and 30% less LUTs than the baseline solution. The number of required flip-flops is almost unchanged when compared to the baseline solution. However, the proposed architecture is less complex than the PPN implementation since it requires 11% less in total hardware resources. It also achieves a clock frequency speed of 218 MHz, which is 17% higher than the baseline solution.

Section 2.3 shows that the FS-FBMC receiver offers improved robustness when compared to PPN-FBMC against timing offset and multipath impairments. Furthermore, hardware complexity evaluation conducted in this section shows that the proposed FS filtering stage (using the proposed NPR1 PF) has a lower complexity than the PPN implementation. This concludes that the FS-FBMC receiver represents a more advantageous solution than the PPN-FBMC receiver when using the proposed short NPR1 filter.

5.4 5G platform for on-board prototyping

On board validation is a crucial step to fully validate any proposed algorithm or hardware architecture. This is particularly the case when multiple techniques are competing to meet specific application needs, as it is the case in waveform design for the new radio air interface in the upcoming 5G of mobile communication systems. The 5G standard is foreseen to support multiple new services while coexisting with the typical mobile broadband service of 4G/LTE. For internet-of-things applications, MMC service is introduced, adding specific requirements such as the support of relaxed synchronization. Other applications, like MCC, require the support of low-latency communication.

5.4.1 Platform description

The developed platform environment is presented in Figure 5.11 where one board (Xilinx ZedBoard) emulates a user equipment (UE) at the transmitter side, and a second board (Xilinx ZC706 evaluation board) is used to emulate the BS at the receiver side. These two digital processing boards are based on the recent Zynq-7000 System on Chip (SoC) which integrates a dual-core ARM Cortex A9 processor and a reconfigurable logic fabric (Field-Programmable Gate Array (FPGA)). Both boards are extended by a RF board

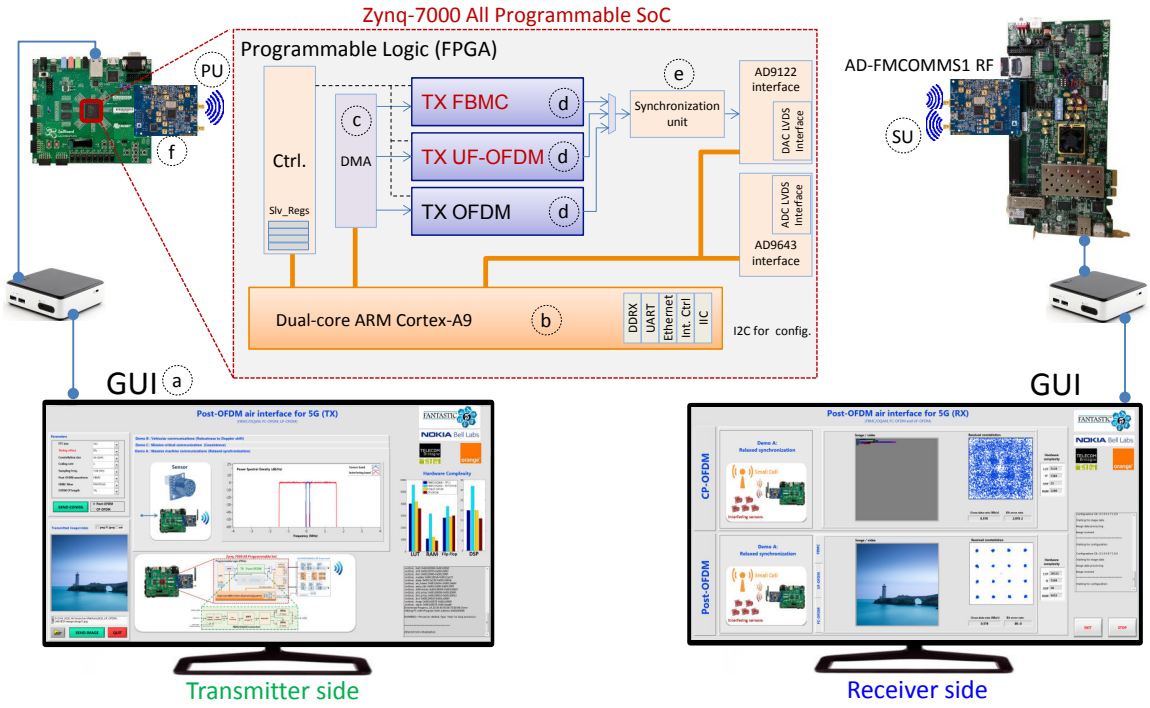

Figure 5.11 — Demonstration setup with front-end interface.

(Analog Devices AD-FMCOMMS1-EBZ) to enable radio transmissions. Each of these RF boards integrates one transmitter and one receiver interfaces. The transmit interface of the BS is optionally used to emulate a multi-user environment for demonstration purpose. On-board control and communication interfaces are ensured by the embedded dual-core Cortex A9 processor. The considered modulation techniques are implemented in hardware on the FPGA part of the Zynq-7000 SoC.

In addition to these boards, two host computers are used for control and display results purpose. They run two dedicated LabVIEW Graphical User Interfaces (Graphical User interface (GUI)). The GUI at the transmitter side is used to select the target scenario, the waveform parameters, and the image file to transmit. In addition, it displays the power spectral density corresponding to the selected waveform parameters. At the receiver side, the GUI displays relevant performance metrics, such as BER, received constellation and received image data. Furthermore, both GUIs display metrics related to the hardware complexity and throughput.

As illustrated in Figure 5.11 ⓐ multiple parameters can be selected using the GUI at the transmitter side (TX): target scenario, QAM constellation, type of waveform, type of filter for FBMC, etc. The user can also select between several images to transmit. Once selected, the following elements are sent by the GUI:

- control data: waveform and demonstration parameters,
- image data: payload transmitted to the receiver side for evaluating the quality of the transmission.

These elements are sent via an Ethernet link to the Cortex A9 processor, using Transmission Control Protocol/Internet Protocol (TCP/IP) Application Programming

Interface (API) in LabVIEW and lightweight IP library from ARM. The hardware related to the digital baseband is integrated between a Direct Memory Access (DMA) block and the AD9122 interface block on the FPGA, as presented in Figure 5.11. The AD9122 interface adapts the modulator output signals, including clocks, to the 16 bits DAC of the AD-FMCOMMS1-EBZ board with Low Voltage Differential Signal (LVDS). The DMA ensures the transfer of the data from a Double Data Rate (DDR) memory, embedded in the ZedBoard, to the QAM mapper input. The Advanced eXtensible Interface (AXI) bus of the ARM processor is used to configure the slave registers (on the FPGA) which hold the scenario and waveform configuration. Therefore, the ARM processor supports the following tasks:

1. receive data (control or image) through the Ethernet interface,
2. parse and interpret the transmitted command from the GUI,
3. configure, via an AXI bus, the slave registers which hold the scenario and waveform configuration,
4. store the image data into the DDR memory,
5. activate the DMA which transfers the content of the image data stored in the DDR memory to the processing unit of the waveform (FPGA part).

For transmitting the control data, the ARM ⓑ executes sequentially the first three tasks defined above. For transmitting the image data, tasks 1), 4) then 5) are executed. When the data are transferred via the DMA ⓒ, they are processed by the unit in the FPGA ⓓ related to the selected waveform. Then, the output waveform samples are sent to a synchronization unit ⓔ. This latter inserts an impulse signal before these samples. At the same time, it transmits a synchronization signal (denoted by *sync*) through a wire directly connected to the receiver board. This signal enables, at the receiver side, to correct the timing offset introduced by the channel.

Lastly, the output waveform samples are sent to the RF board for digital to analog conversion, amplification, and modulation ⓕ.

The control interface at receiver side (RX) is similar to that at transmitter side. The received signal by the RF board is demodulated by the selected waveform receiver. The obtained binary data are sent to the DMA, which writes them into the on-board DDR memory. The content of the memory is read by the dual-core ARM processor, then the image data are transmitted to the host computer through the Ethernet link. Lastly, the GUI displays the key performance metrics, such as the received image, the constellation points, the BER, and the hardware complexity of the selected waveform.

In the FPGA part of the Zynq SoC, time and frequency synchronization must be achieved to recover the transmitted signal. The timing synchronization is realized by measuring the time separating the reception of the *sync* signal and the impulse signal inserted by the TX synchronization unit. When the *sync* signal is received, a counter starts and the number of clock cycles is counted until the impulse signal is received. Thus, the latency induced by the propagation channel is estimated. The *sync* signal is then delayed accordingly by a configurable shift register and set as a validation signal for the waveform receivers.

Table 5.4 — Waveform parameters

Parameter	**Value**	
	Config. 1	**Config. 2**
FFT size	512	256
Sampling rate	7.68 MHz	
Constellation	16-QAM	
CP length	36	18
Filter length (UF-OFDM)	37	19
Filter type (UF-OFDM)	Dolph-chebyshev, sidelobe level of 70 dB	
Prototype filter (FBMC)	NPR1 or MMB4	
Equalizer	Zero forcing	
Channel estimation	Least square	

The frequency offset induced by the frequency difference between the LO of both boards should be canceled properly. This issue is resolved by synchronizing both LOs with a common clock. The reference common clock is that of the transmitter, which is connected using a coaxial cable.

The transmit interface of the RX board is used to emulate a multi-user environment. The transmitted signal is referred to as Secondary User (SU) signal. The signal transmitted by the TX board is referred to as Primary User (PU) signal. For the considered PoC scenarios, the timing offset between the received PU and SU signals must be controlled. Since the latency of the digital processing is known, it is then possible to apply a delay before transmitting the SU signal to control the desired timing offset.

5.4.2 Demonstration results

This section presents the results obtained for MMC, MCC and V2X scenarios. The considered waveform parameters are summarized in Table 5.4. Two configurations are demonstrated:

- config. 1 corresponds to a typical 4G/LTE numerology,
- config. 2 corresponds to a set of parameters where the symbol duration is halved when compared to config. 1.

5.4.2.1 MMC scenario

The first considered demonstration concerns MMC scenario, where MBB users may coexist with MMC-type users such as sensors. Under power and signalling overhead constraints, perfect timing synchronization may not be easily ensured since the closed-loop synchronization based on TA mechanism in 4G/LTE must be avoided. Therefore, open-loop synchronization is considered: the sensors wake-up from sleep mode and directly transmit the required few bits of information to the BS and switch to sleep mode again. It is still assumed that the time reference of the BS is recovered. Since users are located at different distances from the BS, the propagation delay may differ and interference is

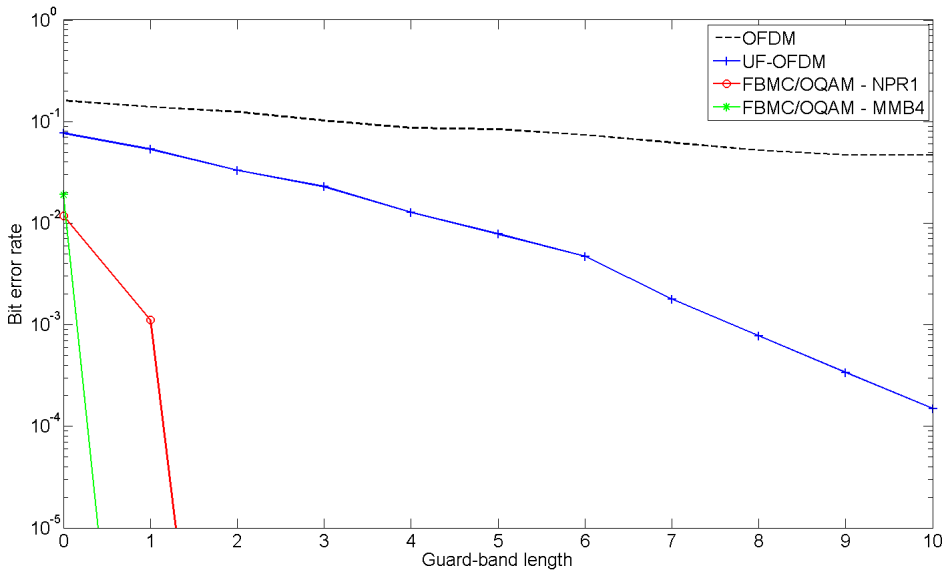

Figure 5.12 — Measured BER for MMC demonstration.

introduced between two users occupying adjacent spectrum resources. The key aspect of this scenario is to assess the behaviour of the candidate waveforms in the context of open-loop synchronization foreseen in MMC.

The platform setup emulates a situation where a large number of sensors send short packets of information to the BS. The TX board acts as a sensor (the PU) by sending small-size image files to the BS at low data rate. It is assumed that the PU uses 1 Resource Block (RB) and is synchronized with the BS. The SU of the RX board emulates multiple interfering sensors. Eight RBs are allocated for the SU, and G subcarriers are introduced as a guard-band with respect to PU. Furthermore, the SU is not perfectly synchronized with the BS. The introduced timing offset is equal to 8% of the OFDM symbol duration. This value is higher than the OFDM CP duration. Therefore, orthogonality is lost between the PU and the SU. Thus, interference occurs at a certain power level depending on the number of used subcarriers as guard-band and the selected waveform.

To evaluate the robustness of each waveform against time synchronization offset, the BER of the PU is measured for different guard-band lengths. The measured results are plotted in Figure 5.12. The waveforms are configured with config. 1 presented in Table 5.4. The best results are obtained with FBMC/OQAM using MMB4 filter, where a BER of zero is achieved for any guard-band length $G > 0$. This comforts the theoretical results obtained in [20], and can be explained by the high frequency localization of the MMB4 filter. Using the short filter NPR1, the BER is degraded for $G = 1$ and $G = 2$ when compared to MMB4, but it still outperforms OFDM and UF-OFDM. While qualified as *short*, the length of the NPR1 filter is still ≈ 13 times higher than the subband filter length (UF-OFDM), providing a higher spectral confinement. Being the only non-filtered waveform and having the lowest spectral confinement, the worst results are obviously obtained for OFDM. OFDM is outperformed by UF-OFDM, with a BER at least 10 times lower when $G \geq 5$.

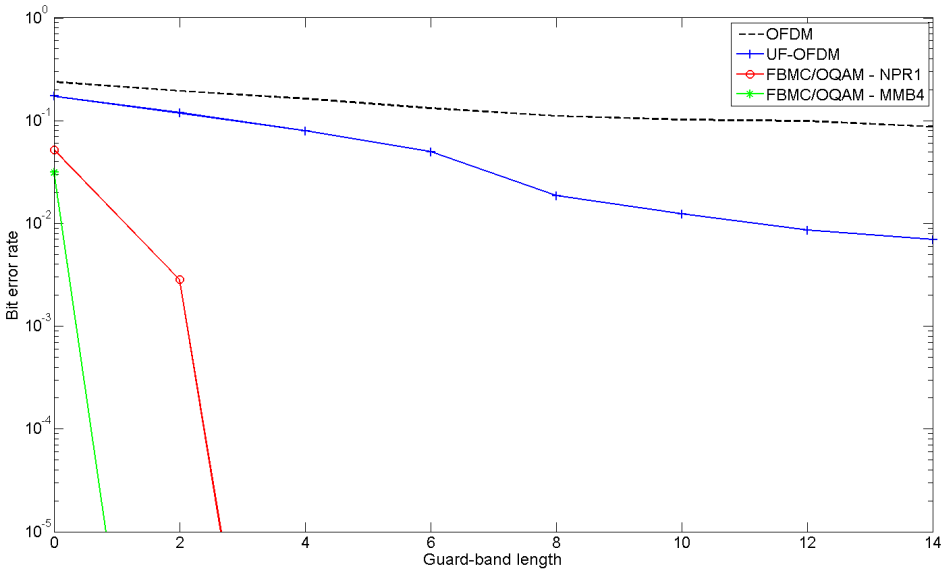

Figure 5.13 — Measured BER for MCC demonstration.

5.4.2.2 MCC scenario

In MCC scenario, low latency and reliability are the most important requirements. It is foreseen in 5G that low latency transmission will be achieved by reducing the TTI, which typically corresponds to the frame duration. In 4G/LTE, the TTI duration is 1 ms, corresponding to the transmission of 14 OFDM symbols. It is the lowest transmission latency which can be achieved in 4G/LTE, assuming negligible propagation delay. However, for 5G services like MCC, the latency requirement has to be lower than 1 ms.

An efficient way to reduce the TTI is to reduce the symbol duration, leads to increasing the subcarrier spacing from 15 kHz (typical LTE setup) to 30 kHz. Thus, the TTI duration is halved (down to 0.5 ms), which in turn reduces the latency. As a consequence, subcarriers acting as guard-band may be inserted to reduce the interference level between two adjacent spectrum resources.

In this scenario, the PU emulates a UE using a typical MBB service with 15 kHz of subcarrier spacing (config. 1). The SU emulates a low latency MCC user with 30 kHz subcarrier spacing (half TTI, config. 2), and acts as an interfering user. The target of this demonstrated scenario is to evaluate the impact of the interference on the BER when different numerologies are mixed in the same carrier. A guard-band of G subcarriers (at 15 kHz) is introduced between the PU and SU spectrum resources. Lastly, it is assumed that the PU and the SU are perfectly synchronized with the BS.

The measured BER for different guard-band lengths are plotted in Figure 5.13. For FBMC/OQAM, only 2 subcarriers for MMB4 filter and 4 subcarriers for NPR1 filter are required as guard-band to isolate the PU and SU from any interference. On the other hand, UF-OFDM outperforms OFDM for any guard-band length.

Concerning latency, UF-OFDM has the same latency as OFDM since both have the same symbol duration. With an improved support for several numerologies when compared to OFDM, UF-OFDM is perfectly adapted to support this scenario. However,

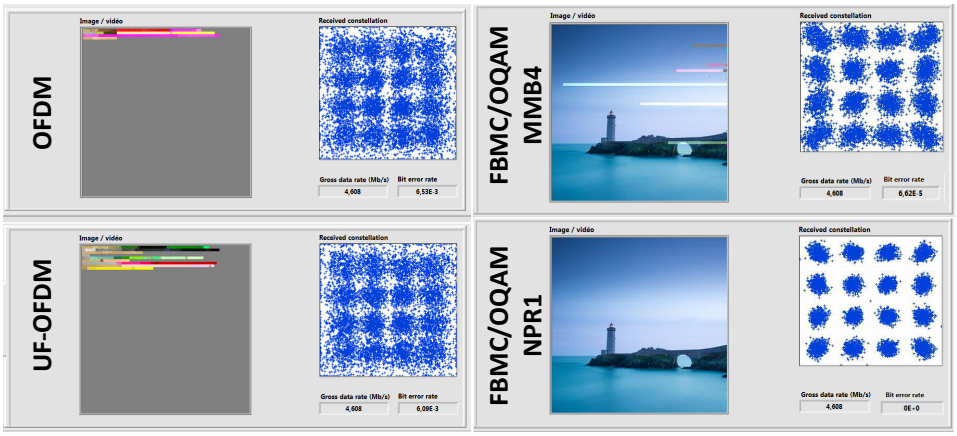

Figure 5.14 — Obtained results for the V2X scenario.

FBMC/OQAM employs a filter with a duration which is K times the duration of one OFDM symbol (= 33.3 μs for config. 2, excluding CP), q being the overlapping factor of the FBMC filter. Additionally, OQAM scheme adds 1/2 OFDM symbol duration as latency to recover the real and imaginary parts of the transmitted QAM symbols. OFDM is penalized with its CP of duration 2.34 μ s. Therefore, demodulating one FBMC/OQAM symbol using MMB4 filter ($K = 4$) adds a latency of 114 μ s when compared to OFDM, which is not negligible. Concerning NPR1 filter ($K = 1$), the additional latency is equal to 14.3 μ s which is 6 times lower than that of MMB4 filter. This may be acceptable for MCC, but UF-ODM waveform is a more appropriate choice since it achieves lower latency.

5.4.2.3 V2X scenario

The third demonstrated scenario concerns V2X communications. This scenario corresponds to the establishment of communication links in mobile environments such as between the classical infrastructure and a moving vehicle, or communication between vehicles. The purpose is to illustrate the robustness of the considered 5G candidate waveforms against Doppler effects compared to OFDM. Such impairments appear in a situation where users are subject to high Doppler, for instance in a high speed vehicle, or in a train. The proof-of-concept implements a situation where a user in a high speed vehicle uploads a compressed image or a streaming video to the BS (uplink communication). The effect of high mobility is emulated directly in hardware by the introduction of a respective carrier-frequency offset. Such an effect is simple to emulate in hardware and corresponds to the case where a direct path is available and dominant in terms of received power. Note that the CFO is assumed to be known at the receiver side. Therefore, the phase rotation is compensated. The image and constellation points are received in a high mobility condition. A speed of 600 km/h is considered, corresponding to 9% CFO considering a carrier frequency of 2.4 GHz. This is compliant with the V2X requirement in 5G specifying at least a speed of 500 km/h. In fact, a speed of 575 km/h for high-speed railway has already been experimented [21].

It can be shown in Figure 5.14 that the received QAM symbols are corrupted by ICI

Table 5.5 — Required hardware resources at transmitter side

Transmitter	**LUTs**(as logic)	**LUTs**(as RAM)	**Flip-flop**	**DSPs**
OFDM	3599	912	3006	16
UF-OFDM	4688	1257	3073	20
FBMC/OQAM (NPR1)	4011	1068	2828	20
FBMC/OQAM (MMB4)	5585	3180	3788	32

for the case of OFDM, UF-OFDM, and FBMC. For both OFDM and UF-OFDM, the displayed image is not recognizable due to the high BER of $\approx 6\,10^{-3}$. Concerning FBMC with the MMB4 filter, the ICI is clearly reduced since the constellation points are less noisy than with OFDM. Some distortions are however present in the received image due to the $\approx 6.6\,10^{-5}$ BER value. When the NPR1 short PF is used, better performance is obtained since the received constellation is less noisy than the MMB4 PF as shown in Figure 5.14. In this case, the compressed image is perfectly recovered with a BER of 0. This demonstrates the improvement in transmission quality that can be offered by the FBMC modulation in a scenario related to high mobility, particularly when using the NPR1 filter.

5.4.3 Hardware complexity comparison

The logic synthesis results have been evaluated for the Zynq-7000 devices in terms of LUTs as logic, LUTs as RAM, Flip Flops and DSP blocks, i.e. number of multipliers. The same quantization chosen in Section 5.2.3.2 is considered.

Same architecture choices have been made for all the considered architectures. The processing units of each transceiver take as inputs and outputs the complex samples (2×16 bits) in serial, at the rate of 1 complex sample per clock cycle. All the architectures have been designed to be clocked at the same frequency rate, and the maximum clock frequency is ≈ 220 MHz. Therefore, the processing speed corresponds to $\approx 220 \times 10^6$ output samples per second for each architecture and for any number of allocated subcarriers, enabling a fair comparison.

Logic synthesis results of the all considered transmitters are summarized in Table 5.5. The complexity of FBMC/OQAM using a NPR1 filter is close to that of OFDM. It only requires 25% more multipliers, 10% more LUTs as logic, and 15% more memory elements (LUTs as RAM). This is due to the pruned IFFT, which removes redundant operations introduced by the OQAM scheme. The filtering unit requires only one processing stage for NPR1 filter, which becomes a simple windowing operation. It is implemented using 4 DSPs without any additional memory. For MMB4 filter, 4 processing stages are required, and the memory requirement is tripled. This highlights the fact that the filtering unit is the real problem concerning the memory requirement when the filter has a duration larger than one OFDM symbol. Therefore, the use of short filters like NPR1 is preferable if a low hardware complexity implementation is primarily targeted.

The UF-OFDM transmitter requires 25% more multipliers, 30% more LUTs as logic, and 38% more memory elements (LUTs as RAM) when compared to OFDM. While it is slightly higher than FBMC/OQAM with NPR1 filter, this complexity increase can

Table 5.6 — Required hardware resources at receiver side

Receiver	**LUTs**(as logic)	**LUTs**(as RAM)	**Flip-flop**	**DSPs**
OFDM	5119	1200	3384	23
UF-OFDM	5393	1265	3531	25
FBMC/OQAM ($K = 1$)	9453	2320	6467	46
FBMC/OQAM ($K = 4$)	10121	4452	7349	58

be considered acceptable given the advantages offered by UF-OFDM for MMC and especially the MCC scenario.

Concerning the receiver side (Table 5.6), UF-OFDM only requires 2 additional DSP multipliers when compared to OFDM. This corresponds to the additional windowing operation, as the remaining receiver processing units are the same as used for OFDM (including channel estimation and equalization). Concerning FBMC/OQAM, the complexity is at least multiplied by 2 when compared to OFDM. The memory requirement of FBMC/OQAM receiver with MMB4 filter is much higher than the other considered waveforms (2.71 times larger than OFDM). Nevertheless, such complexity may be acceptable at the BS which can tolerate complex processing units.

5.5 Summary

A novel low-complexity pipelined implementation for the UF-OFDM and the FBMC/OQAM transmitters are proposed. The latter is based on the use of a pruned IFFT algorithm and on the proposal of novel architectures related to all constituent blocks. Analytical and post-synthesis FPGA results of the proposed transmitter demonstrate significant complexity reduction. For a short prototype filter like NPR1, complexity scales down to 40 to 50% when compared to a typical FBMC design and becomes comparable to OFDM. On-board dynamic power consumption is measured for the corresponding designs. Results with a NPR1 filter indicate an increase of only 27% for the proposed optimized implementation with respect to OFDM. Whereas, this increase reaches up to 126% for the typical FBMC/OQAM implementation.

Concerning the receiver side, an efficient hardware architecture of the FS filter stage is proposed for FBMC. Hardware complexity evaluation shows that the proposed FS-based FBMC receiver, using the NPR1 PF, requires 11% less hardware resources than the PPN-based FBMC receiver. Therefore, combining the proposed NPR1 filter and FS-FBMC receiver architecture provides an original solution that combines complexity reduction and performance improvement with respect to a typical PPN-FBMC receiver.

Last, a flexible and efficient hardware platform for 5G waveform design proof-of-concept is proposed. The proposed platform constitutes a complete hardware/software development environment that can emulate different communication scenarios foreseen in 5G. It integrates digital processing boards based on FPGAs and an embedded dual-core ARM cortex A9 processor, radio frequency boards, and all associated interfaces for control, communication, and display. Measured BER demonstrates how the candidate waveforms clearly outperform OFDM in the considered scenarios, confirming state-of-

the-art theoretical results. Hardware synthesis results show that the required hardware resources for most of the candidate waveforms are close to that of OFDM at the transmitter side. Therefore, with the recently proposed optimizations and hardware PoC, the hardware complexity becomes no longer a discriminating factor for most of the considered 5G candidate waveforms in this work.

Conclusions and perspectives

Research contributions:

While FBMC/OQAM systems using long PFs such as the MMB4 PF have been extensively studied in the literature, FBMC with short PFs provides interesting advantages. For instance, the corresponding lower duration enables: (1) the support of shorter frame lengths, (2) the introduction of efficient block-type pilot structure for channel estimation, and (3) the robustness improvement against CFO or Doppler shift.

In addition, short PFs present the following features when compared to long PFs:

- Lower PAPR using pre-coding techniques.
- Reduced complexity of the transmitter.

Consequently, FBMC system employing short PF can potentially be more energy-efficient.

In this context, a novel short PF for FBMC, referred to as NPR1, is presented in Chapter 1. The original filter design approach is to reverse the time and frequency axes of the filter-bank impulse response generated by the MMB4 long PF, and to deduce the related prototype filter. Indeed, the impulse response of the MMB4 filter is highly localized in frequency since interference is limited only to one adjacent subcarrier in the frequency plane. Therefore, reversing the axis will generate a prototype filter highly localized in time, with an overlapping factor equal to 1. The NPR1 shows improved performance for multiple channel impairments when compared to the other existing short PFs. In presence of timing offset due to imperfect synchronization, the NPR1 PF combined with the FS implementation exhibits a gain of more than 8 dB of SIR when compared to SoTA short PFs (TFL1 and QMF1). It outperforms OFDM, where a gap of 20 dB of SIR can be observed. The NPR1 PF is also the most robust filter to combat CFO. In the case of 4G/LTE multipath channel models, the NPR1 PF is even better than OFDM for the EPA channel model, due to the absence of CP.

In addition, an efficient hardware architecture of the FS filtering stage is proposed in Chapter 5. Hardware complexity evaluation shows that the proposed FS-FBMC receiver, using the NPR1 PF, requires 11% less hardware resources than the PPN-FBMC

receiver. Therefore, combining the proposed NPR1 filter and FS-FBMC receiver architecture provides an original solution that combines complexity reduction and performance improvement with respect to a typical PPN-FBMC receiver.

However, the conventional FS-FBMC receiver architecture fails to efficiently support long delay spread such as encountered in the ETU channel model when short PFs are considered. Furthermore, it cannot support asynchronous communications, unlike the case where it is combined with a long filter such as the MMB4 PF. In order to overcome these two limitations, a novel FBMC receiver adapted for short PFs has been investigated and presented in Chapter 3. This FBMC receiver, referred to as OS-FBMC, consists of merging the structure of a typical FS-FBMC receiver with a time-domain equalizer based on an OS algorithm.

A second FBMC receiver is derived, referred to as OSB-FBMC, where the OS-FBMC is adapted to process a block of transmitted FBMC symbols. Consequently, the FFT is only computed once per block, instead of once per FBMC symbol, enabling to reduce the complexity.

The NPR1 PF appears to be the most adapted PF for these receivers since it achieves the lowest residual interference, due to the filter coefficients truncation. When facing a timing offset, the proposed receivers offer improved SIR performance compared to the conventional FS-FBMC receiver. For a SIR target of 30 dB, the later can tolerate a timing offset up to 8% of the FBMC symbol duration, while the OSB-FBMC can reach up to 21%. Furthermore, the OS-FBMC receiver can support any timing offset value, making it perfectly suited for asynchronous communications. The robustness against multipath channels with Doppler spread is evaluated. It is shown that the OS-FBMC and OSB-FBMC receivers achieve similar BER than the FS-FBMC receiver with a MMB4 PF. This shows that short PFs can reach similar robustness against doubly dispersive channels when compared to long PFs like MMB4, at similar receiver complexity.

Still targeting FBMC, a novel low-complexity pipelined hardware architecture is proposed for the transmitter (Chapter 5). It is based on the use of a pruned IFFT algorithm and on the proposal of novel architectures related to all constituent blocks. For comparison purpose, typical FBMC and OFDM transmitters have been developed with similar architectural choices for the common blocks. Analytical and post-synthesis FPGA results of the proposed transmitter demonstrate significant complexity reduction. For a short PF like NPR1, complexity scales down to 40 to 50% when compared to a typical FBMC design and becomes comparable to OFDM. For longer PF lengths such as MMB4, the PPN unit represents the main bottleneck in terms of hardware complexity. Moreover, on-board dynamic power consumption is measured for the corresponding designs. Results with a short filter indicate an increase of only 27% for the proposed optimized implementation with respect to OFDM. This increase reaches up to 126% for the typical FBMC implementation. In addition, the energy consumption is reduced by 45% when a short PF is used instead of a long PF.

In Chapter 4, another contribution is introduced concerning the proposal of a novel UF-OFDM transmitter. The proposed technique exploits two main ideas in order to reduce the computational complexity of the UF-OFDM baseline implementation. First,

the processing of each subband and each subcarrier is separated, which enables to remove redundant operations. The subband processing requires an IFFT for each subband, which enables to reduce the computational complexity. The second idea of the proposed technique consists of decomposing the UF-OFDM symbol into 3 parts:

- The prefix part, corresponding to the ramp-up transition of the UF-OFDM symbol.
- The suffix part, corresponding to the ramp-down transition of the UF-OFDM symbol.
- The core part, corresponding to the remaining samples of the UF-OFDM symbol.

By using the proposed decomposition into subband and subcarrier processing, it can be shown that the core part of the UF-OFDM symbol can be computed using a windowing operation followed by an IFFT for each decomposed subband. The samples corresponding to the prefix part of the UF-OFDM symbol are obtained by using a windowing operation and an accumulator for each sample of the prefix part. Finally, the suffix part is deduced by subtracting the prefix part from the core part.

When compared to state-of-the-art solutions, a considerable complexity reduction is achieved for several configurations corresponding to the extreme cases where a user occupies the totality of the available bandwidth to achieve high data rates. Particularly, under these extreme conditions, the existing FDA UF-OFDM technique requires up to 4.18 times more RMs and 5.51 times more RAs than the proposed UF-OFDM technique. In addition, the proposed transmitter does not rely on any signal approximation, contrary to the state-of-the-art techniques. Therefore, the spectral confinement of the UF-OFDM signal is preserved.

The last contribution concerns one of the first flexible and efficient hardware platform for 5G waveform design proof-of-concept. The proposed platform constitutes a complete hardware/software development environment that can emulate different communication scenarios foreseen in 5G. It integrates digital processing boards based on FPGAs and an embedded dual-core ARM cortex A9 processor, radio frequency boards, and all associated interfaces for control, communication, and results display. The implemented FBMC/OQAM and UF-OFDM transceivers, in addition to OFDM, have been integrated in the platform. Measured BER demonstrates how the candidate waveforms clearly outperform OFDM in the considered scenarios, confirming state-of-the-art theoretical results. For MMC scenario, the best results are obtained for FBMC/OQAM with the MMB4 filter, closely followed by the NPR1 short filter. The latter is the most adapted waveform for V2X and it is suitable for MCC. UF-OFDM outperforms OFDM for both MMC and MCC scenarios, and it is the most suitable waveform for MCC. Hardware synthesis results show that the required hardware resources for most of the candidate waveforms are close to that of OFDM at the transmitter side. Therefore, with the recently proposed optimizations and hardware proof-of-concept, the hardware complexity becomes no longer a discriminating factor for the considered 5G candidate waveforms.

Perspectives for future work:

5G proof-of-concept platform

The current platform simulates 5G scenarios where Line-of-Sight (LoS) propagation is considered. A possible improvement consists in integrating a dedicated real-time channel emulator in the platform. Initial work towards the development of such an emulator has been already started. It is based on the technique presented in [116], which consists of using an OS algorithm (based on FFTs) to generate in real time and at low memory cost the channel coefficients (Rayleigh sequences correlated with Doppler).

In this thesis, we focused on the hardware implementation of the waveform transmitter, since this is the most critical component in terms of complexity and energy-consumption for uplink communication. At the receiver side, typical FBMC receivers have been implemented. However, in Chapter 3, we have proposed novel OS-FBMC and OSB-FBMC receiver techniques. These receivers use typical processing units such as FFT and FIR filters. Therefore, the design and implementation of an optimized hardware architecture for these receivers are considered in the short term.

Finally, the current platform only supports SISO communication. Since MIMO techniques are widely investigated for 5G, a considerable improvement of the platform could be to integrate the support of this technology. This mostly requires to change the current RF board, which only has one antenna for transmission and a second for reception.

FBMC and MIMO compatibility

It is known that FBMC systems have difficulties to apply MIMO diversity based on Alamouti code due to the lake of complex orthogonality (OQAM scheme). The most efficient (interference-free) techniques apply an Alamouti-based code on a block of FBMC symbols. For this reason, the proposed OSB-FBMC receiver can be easily combined with the FBMC-Alamouti coding proposed in [101]. This code has the major advantage of being simple to implement since it relies on simple conjugate and interleaving operations. Assuming that the channel variation over the block duration is negligible, the complexity of the MRC equalization can be greatly reduced when an OSB-FBMC receiver is considered. In a typical PPN-FBMC receiver, the MRC equalizer must be applied for each allocated subcarrier and each symbol in a block, even though the channel coefficients are the same for each symbol. For the OSB-FBMC receiver, it can be applied for each FFT output corresponding to the frequencies where N_c subcarriers are allocated. Therefore, for a block composed of 7 FBMC symbols with the FFT size set to $4M$ at the receiver side, the MRC equalization is applied on $4N_c$ FFT outputs instead of $7N_c$ for a PPN implementation. Consequently, potential complexity reduction of the MIMO processing can be achieved when using the OSB-FBMC receiver.

However, performance degradation may arise when the communications channel varies in time, which is inherent when considering that the transmission scheme is based on a block of symbols. The channel variation can be taken into account when designing

the channel matrices for the MRC equalization. However, the complexity is greatly increased. Therefore, further investigations must be conducted to find a solution having an interesting compromise between the performance and the complexity. Thereby, we are currently trying to simplify the matrix calculation by introducing realistic assumptions on the channel variation.

As a promising technology for future communication systems, massive MIMO techniques are currently widely investigated in the literature. In a typical massive MIMO scenario, each UE has a few number of antennas (between one and four), while the BS disposes of a larger number of antennas, generally between 32 and 256. This large number of antennas offers diversity gain and can serve multiple users occupying the same time and frequency resources, which increases the channel capacity. Its association with FBMC begins to be investigated [117] [118]. Similarly to the SISO case, BER performance gain is obtained when using a FS-FBMC receiver compared to a typical PPN-FBMC receiver [119]. Most of the current studies focus on a FBMC system using a long PF. There is therefore an opportunity to evaluate how short PFs can perform (in terms of BER, latency, etc.) when compared to long PFs for massive MIMO. Particularly, Time-Division Duplexing (TDD) transmission being privileged for massive MIMO, the reduced frame duration when using a short PF may be advantageous for such application.

PAPR reduction for FBMC with short PFs

One of the remaining issues of FBMC concerns its high PAPR. If we assume that an infinite number of FBMC symbols are successively transmitted, the PAPR of the FBMC signal is the same as the one obtained with OFDM, independently from the chosen PF. In practice, frames have finite duration, and the ramp-up and ramp-down of the FBMC signal, at the beginning and the end of each frame, introduce a slight increase in the PAPR. More concerning, the pre-coding techniques employed in OFDM to reduce the PAPR, such as the FFT pre-coder in SC-OFDM, cannot be applied in a straightforward manner to FBMC due to the OQAM scheme. When adapted to support FBMC, the obtained PAPR reduction is not as significant as in the OFDM case. In fact, the achieved reduction depends on the overlapping factor K, and it is observed that a short PF ($K = 1$) can potentially reach higher PAPR reduction than long PFs ($K = 4$). However, regardless of the filter type, pre-coded FBMC has higher PAPR than pre-coded OFDM. In addition, FBMC is more sensitive to HPA non-linearity than OFDM. Particularly, it was observed that FBMC can suffer from spectral regrowth in this case. The spectral confinement is highly degraded, losing one of the main advantage of FBMC over OFDM. For this reason, it is highly important to investigate solutions to reduce the PAPR favoring further the introduction in real world applications.

In a recent article, a FFT-based pre-coding combined with a low-complexity Selective Mapping (SLM) technique is proposed for FBMC [120]. The SLM technique [121] consists of transmitting the QAM symbols with C different phase rotations or interleaving schemes. From the C resulting modulated signals, the one having the lowest PAPR is chosen. Then, the index of the chosen signal is separately transmitted as a Side Information (SI). This technique is typically highly complex and not efficient in terms of

data rate. However, the proposed SLM in [120] for FBMC only requires a SI of 2 bits per FBMC symbol. Furthermore, the processing is applied in time domain, after FFT, reducing the complexity. The results show that FBMC with the MMB4 can achieve lower PAPR than OFDM. Since the simple use of short PFs generally enables to further reduce the PAPR when compared to long PFs, it can be interesting to investigate how to adapt such technique for short PFs.

Bibliography

[1] F. Schaich, B. Sayrac, S. Elayoubi, I.-P. Belikaidis, M. Caretti, A. Georgakopoulos, X. Gong, E. Kosmatos, H. Lin, P. Demestichas, B. Mouhouche, K. Pedersen, N. Pratas, M. Schellmann, M. Schubert, M. Shaat, and G. Wunder, "Fantastic-5g: flexible air interface for scalable service delivery within wireless communication networks of the 5th generation," *Transactions on Emerging Telecommunications Technologies*, vol. 27, no. 9, pp. 1216–1224, 2016, ett.3050. [Online]. Available: http://dx.doi.org/10.1002/ett.3050

[2] T. Hwang, C. Yang, G. Wu, S. Li, and G. Y. Li, "Ofdm and its wireless applications: A survey," *IEEE Transactions on Vehicular Technology*, vol. 58, no. 4, pp. 1673–1694, May 2009.

[3] S. M. Alamouti, "A simple transmit diversity technique for wireless communications," *IEEE Journal on Selected Areas in Communications*, vol. 16, no. 8, pp. 1451–1458, Oct 1998.

[4] T. Wild and F. Schaich, "A Reduced Complexity Transmitter for UF-OFDM," in *2015 IEEE 81st Vehicular Technology Conference (VTC Spring)*, May 2015, pp. 1–6.

[5] M. Matthe, D. Zhang, F. Schaich, T. Wild, R. Ahmed, and G. Fettweis, "A Reduced Complexity Time-Domain Transmitter for UF-OFDM," in *2016 IEEE 83rd Vehicular Technology Conference (VTC Spring)*, May 2016, pp. 1–5.

[6] D. Mattera, M. Tanda, and M. Bellanger, "Filter bank multicarrier with PAM modulation for future wireless systems," *Signal Processing*, vol. 120, pp. 594–606, Mar. 2016.

[7] S. Weinstein and P. Ebert, "Data transmission by frequency-division multiplexing using the discrete fourier transform," *IEEE Transactions on Communication Technology*, vol. 19, no. 5, pp. 628–634, October 1971.

[8] J. A. C. Bingham, "Multicarrier modulation for data transmission: an idea whose time has come," *IEEE Communications Magazine*, vol. 28, no. 5, pp. 5–14, May 1990.

[9] W. Henkel, G. Taubock, P. Odling, P. O. Borjesson, and N. Petersson, "The cyclic prefix of ofdm/dmt - an analysis," in *2002 International Zurich Seminar on Broadband Communications Access - Transmission - Networking (Cat. No.02TH8599)*, 2002, pp. 22–1–22–3.

[10] J. Zyren, "White Paper Overview of the 3GPP Long Term Evolution Physical Layer."

[11] FANTASTIC-5G, Deliverable D2.1, "Air interface framework and specification of system level simulations," May 2016.

[12] F. Boccardi, R. W. Heath, A. Lozano, T. L. Marzetta, and P. Popovski, "Five disruptive technology directions for 5g," *IEEE Communications Magazine*, vol. 52, no. 2, pp. 74–80, February 2014.

[13] C. Bockelmann, N. Pratas, H. Nikopour, K. Au, T. Svensson, C. Stefanovic, P. Popovski, and A. Dekorsy, "Massive machine-type communications in 5g: physical and mac-layer solutions," *IEEE Communications Magazine*, vol. 54, no. 9, pp. 59–65, September 2016.

[14] 3GPP TS 36.211, "Technical specification group radio access network; physical channels and modulation," http://www.3gpp.org/dynareport/36211.htm.

[15] B. Holfeld, D. Wieruch, T. Wirth, L. Thiele, S. A. Ashraf, J. Huschke, I. Aktas, and J. Ansari, "Wireless communication for factory automation: an opportunity for lte and 5g systems," *IEEE Communications Magazine*, vol. 54, no. 6, pp. 36–43, June 2016.

[16] 3GPP TS 38.913, "Technical specification group radio access network; study on scenarios and requirements for next generation access technologies," http://www.3gpp.org/DynaReport/38913.htm.

[17] K. I. Pedersen, T. E. Kolding, F. Frederiksen, I. Z. Kovacs, D. Laselva, and P. E. Mogensen, "An overview of downlink radio resource management for utran long-term evolution," *IEEE Communications Magazine*, vol. 47, no. 7, pp. 86–93, July 2009.

[18] F. Schaich and T. Wild, "Subcarrier spacing - a neglected degree of freedom?" in *2015 IEEE 16th International Workshop on Signal Processing Advances in Wireless Communications (SPAWC)*, June 2015, pp. 56–60.

[19] A. A. Zaidi, R. Baldemair, H. Tullberg, H. Bjorkegren, L. Sundstrom, J. Medbo, C. Kilinc, and I. D. Silva, "Waveform and numerology to support 5g services and requirements," *IEEE Communications Magazine*, vol. 54, no. 11, pp. 90–98, November 2016.

[20] S. Eldessoki, B. Holfeld, and D. Wieruch, "Impact of Waveforms on Coexistence of Mixed Numerologies in 5G URLLC Networks," in *WSA 2017; 21th International ITG Workshop on Smart Antennas*, March 2017, pp. 1–6.

[21] B. Ai, X. Cheng, T. Kürner, Z. D. Zhong, K. Guan, R. S. He, L. Xiong, D. W. Matolak, D. G. Michelson, and C. Briso-Rodriguez, "Challenges toward wireless communications for high-speed railway," *IEEE Transactions on Intelligent Transportation Systems*, vol. 15, no. 5, pp. 2143–2158, Oct 2014.

[22] NGMN Alliance, "Ngmn 5g white paper, version 1.0," https://www.ngmn.org.

[23] M. Bellanger and J. Daguet, "TDM-FDM Transmultiplexer: Digital Polyphase and FFT," *IEEE Trans. on Commun.*, vol. 22, no. 9, pp. 1199–1205, Sep. 1974.

[24] P. Siohan, C. Siclet, and N. Lacaille, "Analysis and design of OFDM/OQAM systems based on filterbank theory," *IEEE Trans. on Signal Process.*, vol. 50, no. 5, pp. 1170–1183, May 2002.

[25] R. Balian, "Un principe d'incertitude fort en théorie du signal ou en mécanique quantique," *Compt. Rend. Acad. Sci. Ser. II*, vol. 292, no. 20, pp. 1357–1362, 1981.

[26] B. Saltzberg, "Performance of an Efficient Parallel Data Transmission System," *IEEE Trans. on Commun. Technology*, vol. 15, no. 6, pp. 805–811, Dec. 1967.

[27] R. Razavi, P. Xiao, and R. Tafazolli, "Information theoretic analysis of ofdm/oqam with utilized intrinsic interference," *IEEE Signal Processing Letters*, vol. 22, no. 5, pp. 618–622, May 2015.

[28] H. Lin, M. Gharba, and P. Siohan, "Impact of time and carrier frequency offsets on the FBMC/OQAM modulation scheme," *Signal Process.*, vol. 102, pp. 151–162, Sep. 2014.

[29] Y. Medjahdi, M. Terre, D. L. Ruyet, D. Roviras, J. A. Nossek, and L. Baltar, "Inter-cell interference analysis for ofdm/fbmc systems," in *2009 IEEE 10th Workshop on Signal Processing Advances in Wireless Communications*, June 2009, pp. 598–602.

[30] B. Hirosaki, "An Orthogonally Multiplexed QAM System Using the Discrete Fourier Transform," *IEEE Trans. on Commun.*, vol. 29, no. 7, pp. 982–989, Jul. 1981.

[31] D. Dasalukunte, V. O¨wall, and S. Mehmood, "Complexity analysis of IOTA filter architectures in faster-than-Nyquist multicarrier systems," in *Proc. NORCHIP Conf.*, Nov. 2011, pp. 14–15.

[32] Y. Dandach and P. Siohan, "FBMC/OQAM Modulators with Half Complexity," in *2011 IEEE Global Telecommun. Conf. (GLOBECOM 2011)*, Dec. 2011, pp. 1–5.

[33] M. Bellanger, "FS-FBMC: An alternative scheme for filter bank based multicarrier transmission," in *2012 5th Int. Symp. on Commun. Control and Signal Process. (ISCCSP)*, May 2012, pp. 1–4.

[34] V. Vakilian, T. Wild, F. Schaich, S. ten Brink, and J. F. Frigon, "Universal-filtered multi-carrier technique for wireless systems beyond LTE," in *2013 IEEE Globecom Workshops*, Dec 2013, pp. 223–228.

[35] T. Wild, F. Schaich, and Y. Chen, "5G air interface design based on Universal Filtered (UF-)OFDM," in *2014 19th International Conference on Digital Signal Processing*, Aug 2014, pp. 699–704.

[36] F. Schaich and T. Wild, "Relaxed synchronization support of universal filtered multi-carrier including autonomous timing advance," in *2014 11th International Symposium on Wireless Communications Systems (ISWCS)*, Aug 2014, pp. 203–208.

[37] FANTASTIC-5G, Deliverable D3.1, "Preliminary results for multi-service support in link solution adaptation," 2016.

[38] H. Lin, "Flexible Configured OFDM for 5G Air Interface," *IEEE Access*, vol. 3, pp. 1861–1870, 2015.

[39] "Fantastic-5g project," http://fantastic5g.com/.

[40] FANTASTIC-5G, Deliverable D5.1, "Identification of the poc scenarios," 2016.

[41] G. Berardinelli, F. M. L. Tavares, T. B. Sørensen, P. Mogensen, and K. Pajukoski, "Zero-tail dft-spread-ofdm signals," in *2013 IEEE Globecom Workshops (GC Wkshps)*, Dec 2013, pp. 229–234.

[42] H. G. Myung, "Introduction to single carrier fdma," in *2007 15th European Signal Processing Conference*, Sept 2007, pp. 2144–2148.

[43] J. Abdoli, M. Jia, and J. Ma, "Filtered ofdm: A new waveform for future wireless systems," in *2015 IEEE 16th International Workshop on Signal Processing Advances in Wireless Communications (SPAWC)*, June 2015, pp. 66–70.

[44] D. Demmer, R. Gerzaguet, J. B. Doré, D. L. Ruyet, and D. Kténas, "Block-filtered ofdm: A novel waveform for future wireless technologies," in *2017 IEEE International Conference on Communications (ICC)*, May 2017, pp. 1–6.

[45] R. Zakaria and D. L. Ruyet, "A novel fbmc scheme for spatial multiplexing with maximum likelihood detection," in *2010 7th International Symposium on Wireless Communication Systems*, Sept 2010, pp. 461–465.

[46] M. Schellmann *et al.*, "FBMC-based air interface for 5g mobile: Challenges and proposed solutions," in *2014 9th Int. Conf. on Cognitive Radio Oriented Wireless Networks and Commun. (CROWNCOM)*, Jun. 2014, pp. 102–107.

[47] M. Bellanger, "Efficiency of filter bank multicarrier techniques in burst radio transmission," in *2010 IEEE Global Telecommunications Conference GLOBECOM 2010*, Dec 2010, pp. 1–4.

[48] M. Bellanger, M. Renfors, T. Ihalainen, and C. A. F. da Rocha, "Ofdm and fbmc transmission techniques: a compatible high performance proposal for broadband power line communications," in *ISPLC2010*, March 2010, pp. 154–159.

[49] F. Wang, D. Qu, T. Jiang, and B. Farhang-Boroujeny, "Tail shortening by virtual symbols in fbmc-oqam signals," in *2015 IEEE Signal Processing and Signal Processing Education Workshop (SP/SPE)*, Aug 2015, pp. 157–161.

[50] D. Qu, F. Wang, Y. Wang, T. Jiang, and B. Farhang-Boroujeny, "Improving spectral efficiency of fbmc-oqam through virtual symbols," *IEEE Transactions on Wireless Communications*, vol. 16, no. 7, pp. 4204–4215, July 2017.

[51] Y. Dandach and P. Siohan, in *[Wireless Communications and Signal Processing.*

[52] E. Costa, M. Midrio, and S. Pupolin, "Impact of amplifier nonlinearities on ofdm transmission system performance," *IEEE Communications Letters*, vol. 3, no. 2, pp. 37–39, February 1999.

[53] L. Wang and C. Tellambura, "An overview of peak-to-average power ratio reduction techniques for ofdm systems," in *2006 IEEE International Symposium on Signal Processing and Information Technology*, Aug 2006, pp. 840–845.

[54] S. Eldessoki, J. Dommel, K. Hassan, L. Thiele, and R. F. H. Fischer, "Peak-to-average-power reduction for fbmc-based systems," in *WSA 2016; 20th International ITG Workshop on Smart Antennas*, March 2016, pp. 1–6.

[55] H. Malvar, "Modulated QMF filter banks with perfect reconstruction," *Electron. Lett.*, vol. 26, no. 13, pp. 906–907, Jun. 1990.

[56] B. Elmaroud *et al.*, "On the Impact of Prototype Filter Length on the PAPR Reduction of FBMC Signals," *Int. J. of Eng. and Technology*, vol. 6, no. 4, pp. 1951–1960, Aug. 2014.

[57] E. Lahetkangas *et al.*, "Achieving low latency and energy consumption by 5g TDD mode optimization," in *2014 IEEE Int. Conf. on Commun. Workshops (ICC)*, Jun. 2014, pp. 1–6.

[58] M.-H. Hsieh and C.-H. Wei, "Channel estimation for ofdm systems based on comb-type pilot arrangement in frequency selective fading channels," *IEEE Transactions on Consumer Electronics*, vol. 44, no. 1, pp. 217–225, Feb 1998.

[59] S. Coleri, M. Ergen, A. Puri, and A. Bahai, "Channel estimation techniques based on pilot arrangement in ofdm systems," *IEEE Transactions on Broadcasting*, vol. 48, no. 3, pp. 223–229, Sep 2002.

[60] D. Chu, "Polyphase codes with good periodic correlation properties (corresp.)," *IEEE Transactions on Information Theory*, vol. 18, no. 4, pp. 531–532, July 1972.

[61] J. J. van de Beek, O. Edfors, M. Sandell, S. K. Wilson, and P. O. Borjesson, "On channel estimation in ofdm systems," in *1995 IEEE 45th Vehicular Technology Conference. Countdown to the Wireless Twenty-First Century*, vol. 2, Jul 1995, pp. 815–819 vol.2.

[62] O. Edfors, M. Sandell, J. J. van de Beek, S. K. Wilson, and P. O. Borjesson, "Ofdm channel estimation by singular value decomposition," in *Proceedings of Vehicular Technology Conference - VTC*, vol. 2, Apr 1996, pp. 923–927 vol.2.

[63] C. Lele, P. Siohan, R. Legouable, and J. P. Javaudin, "Preamble-based channel estimation techniques for ofdm/oqam over the powerline," in *2007 IEEE International Symposium on Power Line Communications and Its Applications*, March 2007, pp. 59–64.

[64] C. Lele, R. Legouable, and P. Siohan, "Iterative scattered pilot channel estimation in ofdm/oqam," in *2009 IEEE 10th Workshop on Signal Processing Advances in Wireless Communications*, June 2009, pp. 176–180.

[65] C. Lélé, J.-P. Javaudin, R. Legouable, A. Skrzypczak, and P. Siohan, "Channel estimation methods for preamble-based ofdm/oqam modulations," *European Transactions on Telecommunications*, vol. 19, no. 7, pp. 741–750, 2008. [Online]. Available: http://dx.doi.org/10.1002/ett.1332

[66] J. Du and S. Signell, "Novel preamble-based channel estimation for ofdm/oqam systems," in *2009 IEEE International Conference on Communications*, June 2009, pp. 1–6.

[67] C. Lele, P. Siohan, and R. Legouable, "2 dB Better Than CP-OFDM with OFDM/OQAM for Preamble-Based Channel Estimation," in *IEEE Int. Conf. on Commun., 2008. ICC '08*, May 2008, pp. 1302–1306.

[68] E. Kofidis, D. Katselis, A. A. Rontogiannis, and S. Theodoridis, "Preamble-based channel estimation in OFDM/OQAM systems: A review," *CoRR*, vol. abs/1303.2136, 2013. [Online]. Available: http://arxiv.org/abs/1303.2136

[69] Y. Medjahdi, D. L. Ruyet, D. Roviras, H. Shaiek, and R. Zakaria, "On the impact of the prototype filter on fbmc sensitivity to time asynchronism," in *2012 International Symposium on Wireless Communication Systems (ISWCS)*, Aug 2012, pp. 939–943.

[70] Y. Medjahdi, M. Terre, D. L. Ruyet, D. Roviras, and A. Dziri, "The impact of timing synchronization errors on the performance of ofdm/fbmc systems," in *2011 IEEE International Conference on Communications (ICC)*, June 2011, pp. 1–5.

[71] L. G. Baltar, I. Slim, and J. A. Nossek, "Efficient filter bank multicarrier realizations for 5g," in *2015 IEEE International Symposium on Circuits and Systems (ISCAS)*, May 2015, pp. 2608–2611.

[72] S. S. K. C. Bulusu, H. Shaiek, and D. Roviras, "Impact of HPA Non-Linearity on Coexistence of FBMC-OQAM Systems with PMR/PPDR Systems," in *2016 IEEE 83rd Vehicular Technology Conference (VTC Spring)*, May 2016, pp. 1–5.

[73] ——, "Prediction of spectral regrowth for FBMC-OQAM system using cumulants," in *2014 IEEE 10th International Conference on Wireless and Mobile Computing, Networking and Communications (WiMob)*, Oct 2014, pp. 402–406.

[74] D. Roque, C. Siclet, and P. Siohan, "A performance comparison of FBMC modulation schemes with short perfect reconstruction filters," in *2012 19th Int. Conf. on Telecommun. (ICT)*, Apr. 2012, pp. 1–6.

[75] D. Mattera, M. Tanda, and M. Bellanger, "Analysis of an fbmc/oqam scheme for asynchronous access in wireless communications," *EURASIP Journal on Advances in Signal Processing*, vol. 2015, no. 1, p. 23, Mar 2015. [Online]. Available: https://doi.org/10.1186/s13634-015-0191-4

[76] P. Sabeti, H. Saeedi-Sourck, and M. Omidi, "Low-complexity CFO correction of frequency-spreading SMT in uplink of multicarrier multiple access networks," in *2015 23rd Iranian Conference on Electrical Engineering (ICEE)*, May 2015, pp. 410–415.

[77] "Phydyas project," http://www.ict-phydyas.org.

[78] M. Bellanger, "FS-FBMC: A flexible robust scheme for efficient multicarrier broadband wireless access," in *2012 IEEE Globecom Workshops (GC Wkshps)*, Dec. 2012, pp. 192–196.

[79] V. Berg, J.-B. Dore, and D. Noguet, "A flexible FS-FBMC receiver for dynamic access in the TVWS," in *2014 9th Int. Conf. on Cognitive Radio Oriented Wireless Networks and Commun. (CROWNCOM)*, Jun. 2014, pp. 285–290.

[80] K. Martin, "Small side-lobe filter design for multitone data-communication applications," *IEEE Trans. on Circuits and Syst. II: Analog and Digital Signal Process.*, vol. 45, no. 8, pp. 1155–1161, Aug. 1998.

[81] M. G. Bellanger, "Specification and design of a prototype filter for filter bank based multicarrier transmission," in *2001 IEEE International Conference on Acoustics, Speech, and Signal Processing. Proceedings (Cat. No.01CH37221)*, vol. 4, 2001, pp. 2417–2420 vol.4.

[82] S. Mirabbasi and K. Martin, "Overlapped complex-modulated transmultiplexer filters with simplified design and superior stopbands," *IEEE Transactions on Circuits and Systems II: Analog and Digital Signal Processing*, vol. 50, no. 8, pp. 456–469, Aug 2003.

[83] M. Bellanger, "FBMC physical layer: A primer,," PHYDYAS FP7 Project Document, Jan. 2010.

[84] F. Schaich, T. Wild, and Y. Chen, "Waveform Contenders for 5g - Suitability for Short Packet and Low Latency Transmissions," in *Veh. Technology Conf. (VTC Spring), 2014 IEEE 79th*, May 2014, pp. 1–5.

[85] D. Pinchon, P. Siohan, and C. Siclet, "Design techniques for orthogonal Modulated filterbanks based on a compact representation," *IEEE Trans. on Signal Process.*, vol. 52, no. 6, pp. 1682–1692, Jun. 2004.

[86] M. Lanoiselee *et al.*, "Comparative evaluation on real-time hardware platforms of coded OFDM/QAM and OFDM/OQAM systems," in *2012 Int. Symp. on Wireless Commun. Syst. (ISWCS)*, Aug. 2012, pp. 186–190.

[87] D. Pinchon and P. Siohan, "Derivation of analytical expressions for flexible PR low complexity FBMC systems," in *Signal Process. Conf. (EUSIPCO), 2013 proc. of the 21st European*, Sep. 2013, pp. 1–5.

[88] M. Bellanger, D. Mattera, and M. Tanda, "Lapped-OFDM as an Alternative to CP-OFDM For 5g Asynchronous Access and Cognitive Radio," in *Veh. Technology Conf. (VTC Spring), 2015 IEEE 81st*, May 2015, pp. 1–5.

[89] 3GPP TS 36.133, "Technical specification group radio access network; requirements for support of radio resource management," http://www.3gpp.org/dynareport/36133.htm.

[90] D. Mattera, M. Tanda, and M. Bellanger, "Performance analysis of some timing offset equalizers for FBMC/OQAM systems," *Signal Processing*, vol. 108, pp. 167 – 182, 2015.

[91] ——, "Frequency domain CFO compensation for FBMC systems," *Signal Process.*, vol. 114, pp. 183–197, Sep. 2015.

[92] 3GPP TS 36.104, "Technical specification group radio access network; base station (bs) radio transmission and reception," http://www.3gpp.org/dynareport/36104.htm.

[93] W. Cui, D. Qu *et al.*, "Coded auxiliary pilots for channel estimation in fbmc-oqam systems," *IEEE Transactions on Vehicular Technology*, vol. 65, no. 5, pp. 2936–2946, May 2016.

[94] C. A. Belfiore and J. H. Park, "Decision feedback equalization," *Proceedings of the IEEE*, vol. 67, no. 8, pp. 1143–1156, Aug 1979.

[95] H. Lin, C. Lele, and P. Siohan, "Equalization with interference cancellation for hermitian symmetric ofdm/oqam systems," in *2008 IEEE International Symposium on Power Line Communications and Its Applications*, April 2008, pp. 363–368.

[96] E. Kofidis and A. A. Rontogiannis, "Adaptive blast decision-feedback equalizer for mimo-fbmc/oqam systems," in *21st Annual IEEE International Symposium on Personal, Indoor and Mobile Radio Communications*, Sept 2010, pp. 841–846.

[97] L. G. Baltar, D. S. Waldhauser, and J. A. Nossek, "Mmse subchannel decision feedback equalization for filter bank based multicarrier systems," in *2009 IEEE International Symposium on Circuits and Systems*, May 2009, pp. 2802–2805.

[98] F. Harris, *Handbook of Digital Signal Processing.* San Diego: Academic Press, 1987.

[99] P. Duhamel and H. Hollmann, "Split radix FFT algorithm," *Electronics Letters*, vol. 20, pp. 14–16, January 1984.

[100] H. Sorensen, M. Heideman, and C. Burrus, "On computing the split-radix FFT," *IEEE Transactions on Acoustics, Speech, and Signal Processing*, vol. 34, no. 1, pp. 152–156, Feb 1986.

[101] M. Renfors, T. Ihalainen, and T. Stitz, "A block-Alamouti scheme for filter bank based multicarrier transmission," in *Wireless Conf. (EW), 2010 European*, Apr. 2010, pp. 1031–1037.

[102] H. Lin, C. Lele, and P. Siohan, "A pseudo alamouti transceiver design for ofdm/oqam modulation with cyclic prefix," in *2009 IEEE 10th Workshop on Signal Processing Advances in Wireless Communications*, June 2009, pp. 300–304.

[103] R. Zakaria and D. L. Ruyet, "On interference cancellation in alamouti coding scheme for filter bank based multicarrier systems," in *ISWCS 2013; The Tenth International Symposium on Wireless Communication Systems*, Aug 2013, pp. 1–5.

[104] C. Le, S. Moghaddamnia, and J. Peissig, "On the performance of alamouti scheme in 2 x 2 mimo-fbmc systems," in *ICOF 2016; 19th International Conference on OFDM and Frequency Domain Techniques*, Aug 2016, pp. 1–6.

[105] D. Na and K. Choi, "Intrinsic ICI-free Alamouti coded FBMC," *IEEE Communications Letters*, vol. 20, no. 10, pp. 1971–1974, Oct 2016.

[106] C. Lélé, P. Siohan, and R. Legouable, "The alamouti scheme with cdma-ofdm/oqam," *EURASIP Journal on Advances in Signal Processing*, vol. 2010, no. 1, p. 703513, Jan 2010. [Online]. Available: https://doi.org/10.1155/2010/703513

[107] R. Nissel and M. Rupp, "Enabling low-complexity mimo in fbmc-oqam," in *2016 IEEE Globecom Workshops (GC Wkshps)*, Dec 2016, pp. 1–6.

[108] R. Zakaria and D. L. Ruyet, "A novel filter-bank multicarrier scheme to mitigate the intrinsic interference: Application to mimo systems," *IEEE Transactions on Wireless Communications*, vol. 11, no. 3, pp. 1112–1123, March 2012.

[109] T. Hwang *et al.*, "OFDM and Its Wireless Applications: A Survey," *IEEE Trans. on Veh. Technology*, vol. 58, no. 4, pp. 1673–1694, May 2009.

[110] T. W. Parks and C. S. Burrus, *Digital Filter Design.* New York: John Wiley & Sons, 1987, ch. 7.

[111] M. Mukherjee, L. Shu, V. Kumar, P. Kumar, and R. Matam, "Reduced out-of-band radiation-based filter optimization for UFMC systems in 5G," in *2015 International Wireless Communications and Mobile Computing Conference (IWCMC)*, Aug 2015, pp. 1150–1155.

[112] X. Wang, T. Wild, and F. Schaich, "Filter Optimization for Carrier-Frequency and Timing-Offset in Universal Filtered Multi-Carrier Systems," in *2015 IEEE 81st Vehicular Technology Conference (VTC Spring)*, May 2015, pp. 1–6.

[113] H. Shousheng and M. Torkelson, "A new approach to pipeline FFT processor," in *Proc. Int. Parallel Process. Symp. (IPPS)*, Apr. 1996, pp. 766–770.

[114] R. M. Hewlitt and E. S. Swartzlantler, "Canonical signed digit representation for FIR digital filters," in *IEEE Workshop on Signal Processing Systems*, 2000, pp. 416–426.

[115] M. Püschel, J. M. F. Moura, J. Johnson, D. Padua, M. Veloso, B. Singer, J. Xiong, F. Franchetti, A. Gacic, Y. Voronenko, K. Chen, R. W. Johnson, and N. Rizzolo, "SPIRAL: Code generation for DSP transforms," *Proceedings of the IEEE, special issue on "Program Generation, Optimization, and Adaptation"*, vol. 93, no. 2, pp. 232– 275, 2005.

[116] J. Yang, C. A. Nour, and C. Langlais, "Correlated fading channel simulator based on the overlap-save method," *IEEE Transactions on Wireless Communications*, vol. 12, no. 6, pp. 3060–3071, June 2013.

[117] N. E. Tunali, M. Wu, C. Dick, and C. Studer, "Linear large-scale mimo data detection for 5g multi-carrier waveform candidates," in *2015 49th Asilomar Conference on Signals, Systems and Computers*, Nov 2015, pp. 1149–1153.

[118] P. Sabeti, A. Farhang, N. Marchetti, and L. Doyle, "Performance analysis of fbmc-pam in massive mimo," in *2016 IEEE Globecom Workshops (GC Wkshps)*, Dec 2016, pp. 1–7.

[119] A. Aminjavaheri, A. Farhang, N. Marchetti, L. E. Doyle, and B. Farhang-Boroujeny, "Frequency spreading equalization in multicarrier massive mimo," in *2015 IEEE International Conference on Communication Workshop (ICCW)*, June 2015, pp. 1292–1297.

[120] D. Na and K. Choi, "Low papr fbmc," *IEEE Transactions on Wireless Communications*, vol. PP, no. 99, pp. 1–1, 2017.

[121] R. W. Bauml, R. F. H. Fischer, and J. B. Huber, "Reducing the peak-to-average power ratio of multicarrier modulation by selected mapping," *Electronics Letters*, vol. 32, no. 22, pp. 2056–2057, Oct 1996.

Résumé

La 5ème génération de réseaux mobiles (5G), actuellement en cours de standardisation, prévoit de nouveaux scénarios de communication dans l'évolution vers un monde entièrement connecté et communicant. Dans ce contexte, un nombre très important de techniques avancées sont en cours d'exploration pour répondre aux nombreux défis imposés en termes de débit, de latence, de consommation énergétique, et de capacité à faire communiquer entre eux, efficacement, des milliards d'objets très différents. Parmi les techniques les plus prometteuses de la couche physique, de nouvelles formes d'ondes multiporteuses filtrées sont proposées. Bien qu'elles offrent un meilleur confinement spectral et une meilleure localisation en temps et en fréquence par rapport à l'OFDM de la 4G, elles présentent des limitations soit en termes de complexité soit en termes de performance et d'intégration. De plus, ces formes d'ondes sont évaluées d'un point de vue théorique et les résultats ne sont pas toujours validés sur des plateformes matérielles de preuve de concept reproduisant les conditions réelles des scénarios de la 5G.

Dans ce contexte, les travaux de cette thèse proposent plusieurs contributions originales aussi bien au niveau algorithmes de traitement qu'au niveau architectures matérielles. Dans le domaine algorithmique, les travaux réalisés ont mené aux contributions suivantes : (1) Un nouveau filtre prototype court est proposé pour la forme d'onde FBMC/OQAM. Des analyses analytiques, complétées par simulation, montrent que le filtre proposé permet d'améliorer la résistance aux erreurs de synchronisation temporel et de réduire la complexité du récepteur FBMC de type « frequency-spread » comparé aux autres filtres de la littérature, (2) Un nouveau type de récepteur FBMC adapté pour les filtres courts est proposé. Ce récepteur a la particularité d'améliorer sensiblement la résistance aux canaux doublement dispersifs pour des filtres courts, et de supporter les communications asynchrones, (3) Un émetteur UF-OFDM original de complexité significativement réduite par rapport à la littérature est proposé. Contrairement aux techniques existantes, l'émetteur proposé n'introduit aucune approximation dans le signal généré, et préserve ainsi le confinement spectral de la forme d'onde. Dans le domaine de la conception matérielle, les travaux réalisés durant cette thèse ont mené aux contributions suivantes : (4) Une architecture matérielle optimisée des émetteurs FBMC et UF-OFDM de complexité comparable à OFDM, (5) Une architecture matérielle optimisée de l'étage de filtrage du récepteur FBMC « frequency-spread », avec une complexité comparable à celle d'un récepteur « polyphase-network », et (6) Une des premières plateformes matérielles de preuve de concept de la 5G, pouvant évaluer les performances des formes d'ondes pour les différents services de la 5G.

Mots clef : 5G, Formes d'ondes, OFDM, FBMC/OQAM, UF-OFDM, FPGA

Abstract

The 5th generation of mobile communications is foreseen to cope with a high degree of heterogeneity in terms of services: enhanced mobile broadband, massive machine, vehicular and mission critical communications, broadcast services. Consequently, diverse and often contradicting key performance indicators need to be supported, such as high capacity/user-rates, low latency, high mobility, massive number of devices, low cost and low power consumption. 4G is not designed to efficiently meet such a high degree of heterogeneity: the OFDM waveform exhibits several limitations in terms of spectrum usage and robustness to frequency and timing synchronization errors. In order to overcome these limitations and to cope with the new 5G requirements, several research initiatives have been conducted to design new waveforms. Proposed candidates, such as FBMC/OQAM or UF-OFDM, are mainly based on multicarrier modulation with specific filtering scheme used on the top of the OFDM basis. However, most of the proposed new waveforms are often studied and analyzed at the algorithmic level considering mainly the quality of the communication link. Therefore, the investigation of low-complexity implementations and the availability of real hardware prototypes are of high interest for performance validation and proof-of-concept of the diverse proposed communication techniques.

In the above context, this thesis work proposes several original contributions in the algorithm and the hardware design domains. In the algorithm domain, this work leads to the following contributions: (1) A novel short prototype filter for FBMC allowing for near perfect reconstruction and having the same size as one OFDM symbol is proposed. Using the Frequency Spread implementation for the FBMC receiver, analytical studies and simulation results show that the proposed filter exhibits better robustness to several types of channel impairments when compared to state-of-the-art short prototype filters and OFDM modulation. (2) A novel FBMC receiver technique suitable for short filters is proposed. This receiver enables to greatly improve the robustness against double dispersive channels for short filters, and enables the support of asynchronous communications, (3) A novel low-complexity UF-OFDM transmitter without any signal quality loss is proposed. For small subband sizes, the complexity becomes comparable to OFDM regardless of the number of allocated subbands. In the hardware design domain, this thesis work leads to the following contributions: (4) An efficient pipelined hardware architecture of the FBMC/OQAM transmitter capable of supporting several filter lengths and targeting low complexity is proposed and compared to typical FBMC/OQAM and OFDM implementations, (5) An optimized frequency spread based hardware architecture of the filtering stage is proposed for the designed short prototype filter, showing lower complexity than the classical PolyPhase-Network-based implementation, (6) One of the first flexible and efficient hardware platforms for 5G waveform design, allowing the support of several communication scenarios as foreseen in 5G.

Keywords: 5G, Waveform, OFDM, FBMC/OQAM, UF-OFDM, FPGA

IMT Atlantique
Bretagne-Pays de la Loire
École Mines-Télécom

N° d'ordre : 2017IMTA0065

IMT Atlantique Bretagne-Pays de la Loire - www.imt-atlantique.fr

Campus de Brest
Technopôle Brest-Iroise
CS 83818
29238 Brest Cedex 03
T +33 (0)2 29 00 11 11
F +33 (0)2 29 00 10 00

Campus de Nantes
4, rue Alfred Kastler - La Chantrerie
CS 20722
44307 Nantes Cedex 3
T +33 (0)2 51 85 81 00
F +33 (0)2 51 85 81 99

Campus de Rennes
2, rue de la Châtaigneraie
CS 17607
35576 Cesson Sévigné Cedex
T +33 (0)2 99 12 70 00
F +33 (0)2 99 12 70 08